The regulation of peptidoglycan hydrolysis in *Escherichia coli*

Adam C. Lodge (BSc, MRes)

Centre for Bacterial Cell Biology

Institute for Cell and Molecular Biosciences

Thesis submitted for the degree of Doctor of Philosophy

Newcastle University

June 2016

Declaration:

I hereby declare that this thesis is my own work and effort and that it has not been submitted elsewhere for any award. Any contribution made to the project by others is explicitly acknowledged in this thesis.

Adam C. Lodge

Abstract

The bacterial cell envelope heteropolymer, peptidoglycan (PG), is essential for maintaining the osmotic stability and shape of most bacteria. PG biosynthesis is the target of our most successful antibiotics, the β-lactams and glycopeptides. However, the spread of antibiotic resistant strains highlights the need for novel antibiotic targets.

Gram-negative bacteria possess a mainly single layered PG, which is enlarged in growing and dividing bacteria by the coordinated action of PG synthases and hydrolases. PG synthesis in Gram-negative bacteria is regulated from the cytoplasmic membrane (CM), by prokaryotic cytoskeletal elements, and from the outer membrane (OM) by the lipoproteins, LpoA and LpoB. LpoA/B interact with, and are essential for the *in vivo* activity of, the major PG synthases PBP1A and PBP1B, respectively. While the regulation of PG synthesis has been well studied in recent years, the mechanisms of PG hydrolysis regulation in *E. coli* remain poorly understood. *E. coli* possesses ~30 PG hydrolases with relatively few known regulators.

In this work, we have structurally characterised LpoA from *E. coli* using nuclear magnetic resonance (NMR) spectroscopy of the N-terminal domain and use this to further the understanding of the *in vitro* and *in vivo* interaction of LpoA/PBP1A. We also studied PBP1A and LpoA in *Haemophilus influenzae*; in this species LpoA is essential.

In a search for novel LpoA interaction partners we discovered the *in vitro* and *in vivo* interaction with the PG hydrolase, PBP4 and show that PBP4 also interacts with PBP1A. Subsequently, we optimised a process for the rapid identification of *in vitro* interactions and identified >20 interactions between PG synthases, PG hydrolases and other cell envelope proteins. We therefore present a putative PG hydrolysing complex with direct associations to the PG synthesis machinery.

Through direct functional interactions with at least five PG hydrolases, we present the characterisation of the OM-anchored lipoprotein NlpI, of currently unknown cellular function, as a regulator of hydrolase activity. We show the *in vitro* regulation of activity by NlpI and the *in vivo* relevance of these interactions using a β-lactamase induction assay.

This work significantly enhances our understanding of how PG synthesis and hydrolysis are coordinated as multi-enzyme complexes and presents the characterisation of a novel regulator of hydrolase activity, NlpI.

Acknowledgements

I would like to acknowledge Newcastle University, at which I have attended for my Undergraduate degree, my MRes degree and my Ph.D. and the MRC for funding through the latter. I must thank all members of the Centre for Bacterial Cell Biology within the Institute for Cell and Molecular Biosciences, in which it has been a privilege to work.

I must thank the group of Waldemar Vollmer, members past and present, for their support, friendship and tolerance, which has led to four years of the most rewarding and character building experiences. I must thank Jacob Biboy, the source of all knowledge, Daniela Vollmer, without whom the lab would fall apart, and Hamish Yau for being an excellent apprentice and extremely competent scientist in his own right. My wholehearted thanks go to Alex Egan, my mentor throughout my studies and, above all, a good friend. Words of thanks fall short with regard to Waldemar Vollmer whose supervision and guidance has been crucial to my success in this degree and whose passion for science has inspired and motivated from the first day until the last.

I would like to extend my thanks to Manuel Banzhaf, AK Hov, Nassos Typas, Nicholas Jean, Jean-Pierre Simorre, Tanneke den Blaauwen, Andrew Gray, Manjula Reddy, Alexandra Solovyova and Joe Gray for their fruitful and ongoing collaborations.

Without the support of my friends both in and out of science this work would not be possible. From the CBCB, I would like to particularly thank Alex, Hamish, Lauren, Beth, Tom, Flint and Jad, who made the lab a fantastic place to work and whose company in the North Terrace is unparalleled. From elsewhere I must thank Atta, Robson, Emily, Sam, Ben, Nat, Jordan and Will for so many things I would need an extra thesis to include.

Finally, my parents, whom I owe all and dedicate this thesis.

Abbreviations

ABC	ATP-binding cassette
AFM	Atomic force microscopy
Amp	Ampicillin
APS	Ammonium Peroxodisulphate
AUC	Analytical Ultracentrifugation
BSA	Bovine serum albumin
CCCP	Carbonyl cyanide *m*-chlorophenyl hydrazine
CPM	Counts per minute
C-terminal	Carboxy-terminal
CM	Cytoplasmic membrane
D-Ala-D-Ala	D-Alanyl-D-Alanine
Da / kDa	Dalton / Kilodalton
DD-CPase	DD-Carboxypeptidase
DD-EPase	DD-Endopeptidase
D-iGlu	D-isoglutamic acid
dH_2O	Deionised Water
DNA	Deoxyribonucleic acid
DNase	Deoxyribonuclease
DTSSP	3,3'-dithiobis(sulfosuccinimidylpropionate)
DTT	Dithiothreitol
ECL	Enhanced chemiluminescnce
EDC	1-Ethyl-3-(3-dimethylaminopropyl)carbodiimide
EDTA	Ethylenediaminetetraacetic acid
× g	Acceleration due to gravity
Glc*N*Ac	*N*-acetylglucosamine
GTase	Glycosyltransferase
HEPES	(4-(2-hydroxyethyl)-1-piperazineethanesulfonic acid)
His- / -His	Hexahistidine tag (N- / -C terminal)
HPLC	High performance liquid chromatography
IEX	Ion Exchange Chromatography
IMAC	Immobilised Metal-ion Affinity Chromatography
Kan	Kanamycin

L-Ala	L-Alanine
LB	Luria Bertani
m-Dap	*meso*-diaminopimelic acid
MOPS	Potassium morpholinopropane sulfonate
Mur*N*Ac	*N*-acetylmuramic acid
Mur*N*Ac-LAAs	*N*-acetylmuramyl-L-alanine amidases
Na-acetate	Sodium acetate
NADPH	Nicotinamide adenine dinucleotide phosphate
Ni-NTA	$Nickel^{2+}$-nitrilotriacetic acid
NMR	Nuclear Magnetic Resonance
N-terminal	Amino-terminal
ODD	Outer Membrane PBP1A Docking Domain
OM	Outer Membrane
PAGE	Polyacrylamide Gel Electrophoresis
PBP	Penicillin-Binding Protein
PIC	Protease Inhibitor Cocktail
PG	Peptidoglycan
PMF	Proton Motive Force
PMSF	Phenylmethanesulfonylfluoride
rpm	Revolutions Per Minute
RU	Response Units
SAXS	Small Angle X-ray Scattering
SDS	Sodium Dodecyl Sulphate
SeMet	Selenomethionine
SEC	Size Exclusion Chromatography
s-NHS	Sulfo-N-hydroxysuccinimide
SPR	Surface Plasmon Resonance
TBS	Tris-buffered saline
TEMED	Tetramethylethylenediamine
TPase	Transpeptidase
TPR	Tetratricopeptide Repeat
Tris	Tris(hydroxymethyl)aminomethane
UDP	Uridine diphosphate
U-Pr	Undecaprenol pyrophosphate

Index of figures and tables

1 Introduction

1.1 Growth and morphogenesis of *Escherichia coli*

Most bacteria proliferate by binary fission, replicating genetic and proteinaceous material before dividing into two, usually identical, daughter cells [1]. Rod-shaped bacteria, such as the model organisms *Escherichia coli* and *Bacillus subtilis* grow by alternating phases of cell elongation and division. These processes must ensure doubling of cell length, replication and segregation of genetic material, and cell division at the centre of the newly elongated structure, without losing structural integrity [2].

The peptidoglycan (PG) sacculus is the component of the bacterial cell wall crucial for resisting internal osmotic challenges and protection from bursting due to turgor [3,4]. This continuous, macromolecular, net-like structure encompasses the cytoplasmic membrane of the majority of bacteria and maintains cell morphology. Exceptions include the mollicutes, for example the mycoplasma and phytoplasma, which live intracellularly where the internal turgor is the same as the external and do not possess a cell wall, using cytoskeletal elements to maintain cell shape [3-5]. The essentiality of the sacculus necessitates highly coordinated growth and division, but how the cell accomplishes this whilst maintaining morphology and structural integrity is a poorly understood process.

Bacteria can be characterised based on the layers and thickness of the cell envelope, including the PG. The monoderm Gram-positive and diderm Gram-negative bacteria (Gram, 1884) both have a cytoplasmic membrane (CM), composed of phospholipids and proteins, encasing the cytoplasm. The CM is ~7 nm thick and its primary roles are to control the influx and efflux of metabolites and to maintain membrane potential [7,8]. Gram-positive bacteria possess up to 30 layers of extracellular PG, ~10-20 nm thick, with membrane-attached lipoteichoic acids, and wall teichoic acids in the PG layer itself [9]. Gram-positive bacteria can modify the glycan chains of the PG layer as methods of evading the host immune system, for example by *O*-acetylation and *N*-deacetylation, which make the glycan chains poor substrates for lysozyme [10]. *O*-acetylation of the Mur*N*Ac residue at the C6 hydroxyl group has also been observed in Gram-negative bacteria [11]. Gram-negative bacteria possess a single layer of PG, 3-6 nm thick, which lies parallel to the CM surface in a disordered, circumferential fashion, between the CM and an OM [12,13]. In *E. coli*, the pH of this periplasmic space changes depending on the pH of the external environment [14]. This is contrary to within the cytoplasm which is maintained at pH 7.4-7.8 [14]. The OM of Gram-negative bacteria possesses porins and attached lipopolysaccharides (LPS), the O-antigen of which can be modified as a method of evading the host immune system [15].

The PG layer is essential for bacterial viability and exclusive to the prokaryotic domain [5]. PG synthesis is therefore an attractive target for the development of antibiotics, for example the glycopeptides (e.g. vancomycin) and the β-lactams (e.g. penicillin). However, due to wide-spread usage of these PG-targeting antibiotics, bacteria have developed resistance mechanisms to almost every known antibiotic. For example, β-lactams, which target the proteins responsible for PG synthesis and hydrolysis, cause a discoordination of these processes which induces intracellular expression and export of enzymes capable of hydrolysing the attacking β-lactam, termed β-lactamases. This process is discussed in more detail in section 1.6.

The increasing prevalence of resistant bacterial strains highlights the urgency to discover novel antibiotic targets, with the PG layer remaining one of the most promising sources. Characterisation of the proteins involved in PG synthesis and hydrolysis, and the functional or spatio-temporal interactions between these proteins, will help to establish these novel targets.

1.2 The peptidoglycan sacculus

The PG layer is composed of repeating disaccharide subunits forming linear glycan chains connected by short peptides. These glycan chains are formed from β1,4 linked *N*-acetylmuramic acid (Mur*N*Ac) and *N*-acetylglucosamine (Glc*N*Ac) residues [16]. A pentapeptide is attached to the lactoyl group of each Mur*N*Ac residue. In *E. coli* this pentapeptide is comprised of; L-Ala-D-iGlu-*m*-Dap(*meso*-diaminopimelic acid)-D-Ala-D-Ala, however the composition of this peptide stem can vary across species and strains [3]. The characteristic mesh-like composition of the PG layer arises from the cross-linkage of peptides protruding from adjacent glycan chains. The architecture of the PG sacculus has remained largely unknown due to its heterogeneous and non-crystalline nature. However, recently it has been isolated from the Gram-negative model organism *E. coli* and visualised by cryo-electron microscopy (figure 1.1) and atomic force microscopy (AFM) [12, 17, 18]. In *E. coli*, the glycan chains can be separated by HPLC analysis up to 30 disaccharides in length [19], and it is estimated that the average glycan chain length in *E. coli* is 21 disaccharides [20, 21]. This number varies dramatically across species for example in the Gram positives, *Bacillus* species can contain glycan chains that are 50-250 disaccharides in length [22], where *S. aureus* contains, on average, glycan chains that are 16 disaccharides in length [23].

The mechanisms of PG growth during elongation and division are poorly understood [24]. PG synthesis is thought to be facilitated by multi-enzyme complexes of periplasmic and

membrane-bound PG synthases and hydrolases. The activity and spatio-temporal localisation of these proteins is coordinated from the CM by prokaryotic cytoskeletal elements, and associating CM proteins, and from the OM by membrane-anchored lipoproteins. The intracellular prokaryotic actin homolog MreB is essential for rod shape in a number of species and is thought to control insertion of nascent PG throughout the lateral cell wall [25]. MreB forms discrete, dynamic patches which move along the short axis of the cell in a helical and circumferential fashion [26]. The current model suggests that MreB and associated proteins act to spatio-temporally position and/or regulate the PG synthase/hydrolase complexes along the lateral cell wall, supported by the observed helical insertion of lipid II [21,22]. This cell wall synthesis machinery specific for elongation of the cell is termed the elongasome and will be discussed in more detail in section 1.5.1.

The polymerisation of the prokaryotic tubulin homologue FtsZ into the Z ring is essential for cell division [29]. The Z ring recruits a number of other essential division proteins which in turn recruit PG synthases. This complex is termed the divisome and is required for the formation of the septum, daughter cell pole synthesis and cleavage [30]. This will be discussed in more detail in see section 1.5.2.

Gram-negative bacteria are also capable of coordinating PG synthesis from the OM. The OM-anchored lipoproteins, LpoA and LpoB interact with, and are essential for the *in vivo* activity of, the CM-anchored major PG synthases PBP1A and PBP1B, respectively [25,26]. This regulation will be discussed in more detail in section 1.3.4.

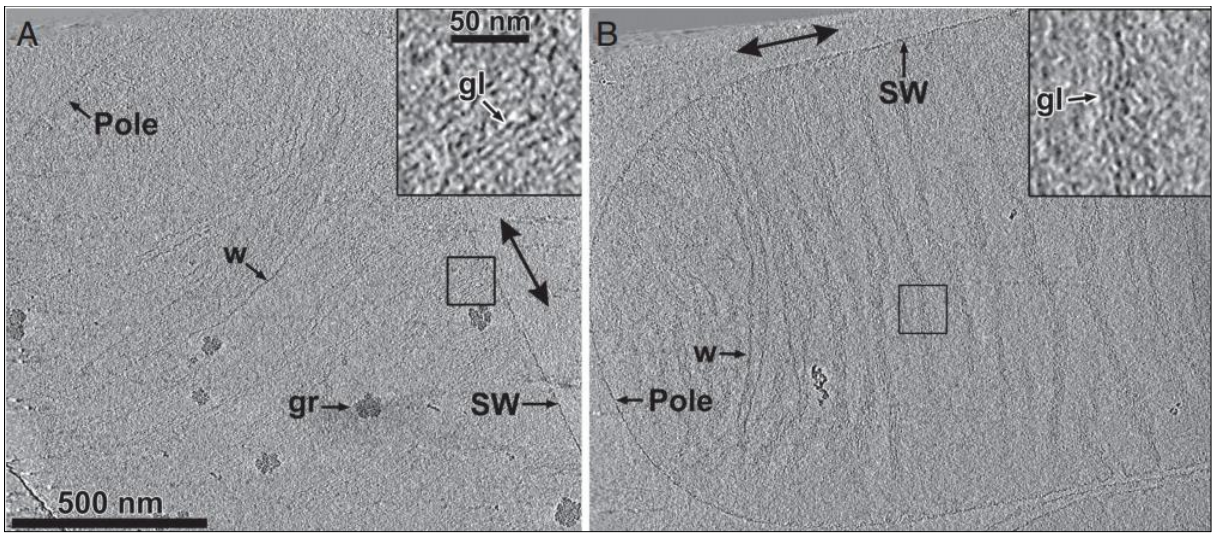

Figure 1.1 The peptidoglycan sacculus [12]

Electron cryotomography slices of an *E. coli* sacculus show the perpendicular orientation of the glycan strands to the polar axis of the cell. SW; Side wall. GR; granule. W; wrinkle.

1.3 Peptidoglycan synthesis in *E. coli*

1.3.1 Synthesis of the peptidoglycan precursor lipid II

Lipid II is the last PG precursor and its synthesis is initiated in the cytoplasm. The sequential action of three enzymes, GlmS, GlmM, and the bifunctional GlmU, complete four activities; glucosamine-6-phosphate synthase, phosphoglucosamine mutase, glucosamine-1-phosphate acetyltransferase, and *N*-acetylglucosamine-1-phosphate uridyltransferase which yield the nucleotide-activated UDP-Glc*N*Ac from fructose-6-phosphate [27-29].

MurA (formerly MurZ) catalyses the transfer of an enolpyruvate moiety from phosphoenolpyruvate (PEP), onto UDP-Glc*N*Ac, to yield UDP-Mur*N*Ac-enolpyruvate. This is reduced by the NADPH-dependent UDP-Mur*N*Ac dehydrogenase MurB, to yield UDP-Mur*N*Ac [35]. The antibiotic fosfomycin targets MurA whose essential activity is the first committed step to PG synthesis [31,32].

The successive activity of four murein (Mur) ligases; MurC, MurD, MurE and MurF, catalyse the addition of L-Ala, D-iGlu, *m*-Dap, and a D-Ala-D-Ala dipeptide, respectively, to the D-lactoyl moiety of UDP-Mur*N*Ac [33,34]. L-Ala is converted to D-Ala by the alanine racemase DadX (and/or Alr) [40]. The D-Ala-D-Ala dipeptide is generated by two D-Ala-D-Ala ligases, DdlA and DdlB [41]. The glutamate racemase MurI is activated by UDP-Mur*N*Ac-L-Ala to catalyse the formation of D-iGlu from its L-enantiomer [42]. *m*-Dap occurs as an intermediate of the lysine biosynthetic pathway [43].

The transferase MraY catalyses the transfer of the phospho-Mur*N*Ac pentapeptide moiety from UDP-Mur*N*Ac-pentapeptide to the membrane acceptor molecule undecaprenol phosphate (Upr-P), creating the CM-linked intermediate, lipid I [44]. MurG catalyses the transfer of Glc*N*Ac from the nucleotide-activated sugar UDP-Glc*N*Ac to lipid I to form the β1,4 linked disaccharide pentapeptide, lipid II (Glc*N*Ac-β1,4-Mur*N*Ac-L-Ala-D-iGlu-*m*-Dap-D-Ala-D-Ala) [40,33]. See figure 1.2 for a schematic of the formation of lipid II and incorporation of lipid II into the pre-existing PG layer.

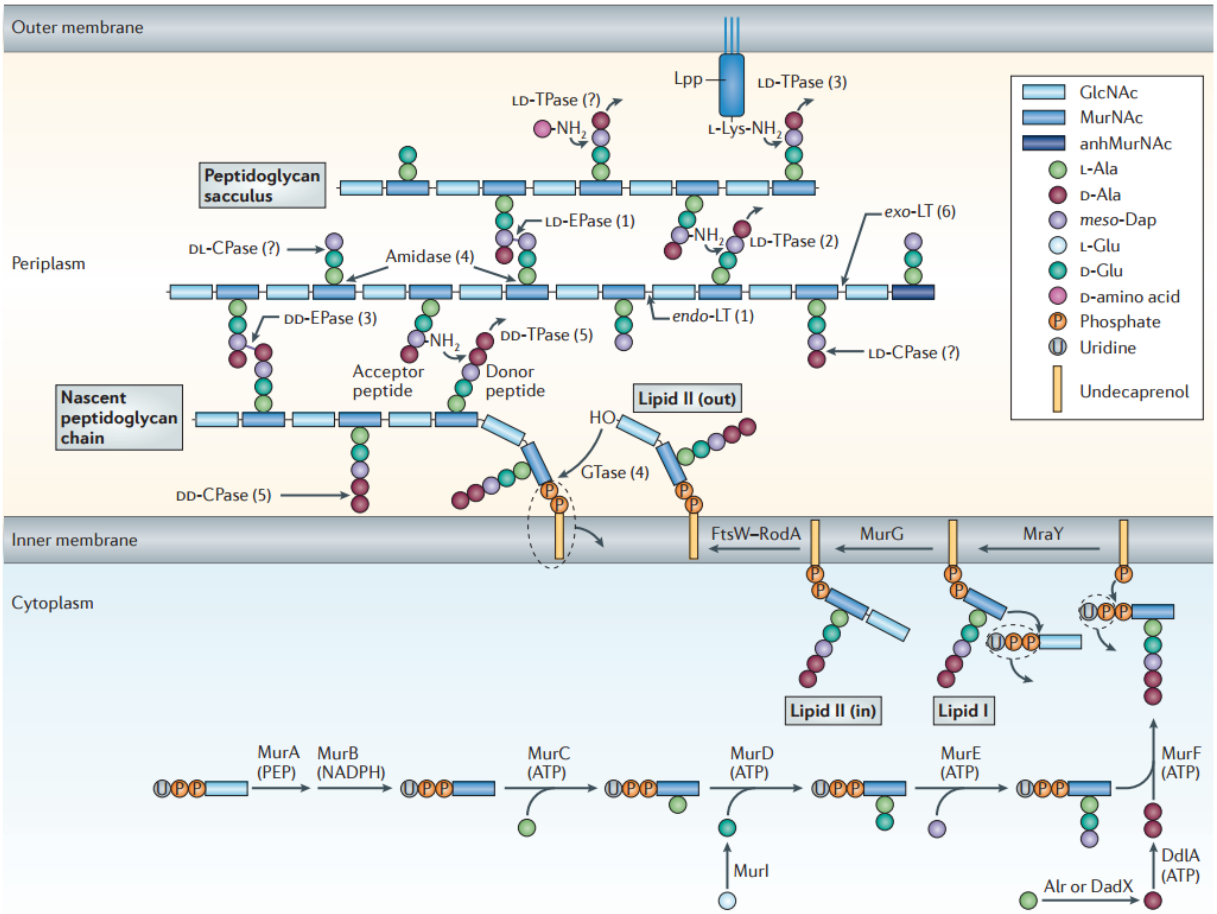

Figure 1.2 Synthesis and hydrolysis of peptidoglycan [46]

The synthesis of the last PG precursor, lipid II, is initiated and completed in the cytoplasm with the sequential activity of MurC, MurD, MurE, and MurF which respectively catalyse the addition of L-Ala, D-iGlu, *m*-Dap, and a D-Ala-D-Ala dipeptide to the D-lactoyl moiety of UDP-Mur*N*Ac. The transferase MraY catalyses the transfer of the phospho-Mur*N*Ac pentapeptide moiety from UDP-Mur*N*Ac-pentapeptide to the membrane acceptor molecule undecaprenol phosphate (Upr-P), creating the CM-linked intermediate, lipid I. MurG catalyses the addition of a Glc*N*Ac residue forming lipid II. Lipid II is 'flipped' into the periplasmic space by integral membrane proteins FtsW/RodA, to be incorporated into the pre-existing PG layer by a process of glycosyltransferase (GTase) reactions and transpeptidation (TPase) reactions. These processes are performed by the PG synthases. The PG hydrolases including endopeptidases (EPase), carboxypeptidases (CPase), lytic transglycosylases (LT) and amidases have specificity for almost every bond of the PG network and cleavage of these bonds allows insertion of nascent material.

1.3.2 Growth of the sacculus

In *E. coli,* lipid II is flipped from the cytoplasmic side of the CM to the periplasmic side by integral CM proteins; either MurJ or FtsW/RodA or both [41,42]. Lipid II undergoes processive polymerisation into glycan chains via glycosyltransferase (GTase) reactions. The pre-existing donor glycan chain is transferred to the next lipid II molecule, the energy required for which is produced by the removal of the Upr-P anchor of the acceptor chain [29-31]. The pentapeptide side chains between adjacent strands are cross-linked by transpeptidase (TPase) reactions between the carboxyl group of the penultimate D-Ala residue of a donor strand and the ε-amino group of the *m*-Dap residue of an acceptor strand. The energy for this cross-linkage is generated from the cleavage of the terminal D-Ala residue of the donor strand [51]. Referred to as DD-peptide bonds these D-Ala-*m*-Dap linkages comprise 93% of cross-links in *E. coli*. A small percentage of peptides are connected by *m*-Dap-*m*-Dap linkages (LD-peptide bonds) [21]. Glycosyltransferase reactions can occur without subsequent transpeptidation, as observed upon application of TPase domain-targeting β-lactams [52].

The bifunctional Class A penicillin-binding proteins (PBPs) PBP1A, PBP1B and PBP1C, monofunctional TPase Class B PBPs, PBP2 and PBP3 and the monofunctional GTase MtgA, carry out these processes for the successful incorporation of nascent PG into the sacculus (see section 1.3.3 for more detail) [51]. Enzymes possessing GTase activity are the target of the phosphoglycolipid antibiotic moenomycin, which mimics the structure of lipid II and binds to the GTase domain of PBPs [53]. β-lactams, such as penicillin, are structurally analogous to the terminal D-Ala-D-Ala dipeptide and covalently bind to the TPase active site to block activity, hence the nomenclature, penicillin-binding proteins [54]. Modifications to the substrates to which these compounds mimic, are a method of acquiring multi-drug resistance [55].

There are a number of models for dynamic PG growth [51,12,13]. Most agree that PG synthases produce glycan chains from the PG precursor lipid II and attach it to the pre-existing sacculus where PG hydrolases generate the space for incorporation of the nascent material. Indeed, if there were only insertion of PG, the cell wall would thicken rather than increase in surface area, whereas the cell is capable of doubling in length whilst maintaining a constant diameter. Intuitively then, there must be coordination between PG hydrolysis and PG synthesis. Höltje's 'three-for-one' model purports that three nascent glycan strands are synthesised and docked beneath one pre-existing glycan strand, before PG hydrolases remove the docking strand allowing for simultaneous insertion of the nascent material [43,51]. This would facilitate safe and coordinated enlargement of the sacculus whilst maintaining rod-

shape (see figure 1.3). The model suggests the presence of multi-enzyme PG-synthesising complexes for the coordination of PG synthesis and hydrolysis. Further, a theory was presented for the bactericidal properties of PG synthase-targeting antibiotics. It was proposed that the inhibition of the PG synthases, by moenomycin and penicillin for example, does not stop the movement of this multi-enzyme complex, leaving the space-making hydrolases free to degrade PG without subsequent insertion of newly synthesised PG, and thus cause cell lysis [52,53]. A single-layered model for PG in Gram-negative bacteria is currently widely accepted. Huang *et al* (2008) used their 'elastic' model to predict that the single layered scenario is most likely, in comparison to the scaffold model which purports that the glycan chains lie vertically [60]. Similarly, Gan *et al*, (2008) used electron cryotomography of the *E. coli* sacculus to reveal the perpendicular orientation of the glycan chains to the polar axis of the cell (see figure 1.1), which supports the single-layered model rather than the vertical glycan strands of the scaffold model [12].

While much of the basic PG-synthesising apparatus in *E. coli,* and described in the following sections, are conserved throughout Gram-negative and Gram-positive bacteria, the myriad of morphologies that exist suggest differing methods of coordinating the processes of PG synthesis and hydrolysis [46]. A broad example of this is the absence of an OM in Gram-positive bacteria, therefore the OM-anchored proteins described in the following sections, such as NlpI and LpoA are not present. However, the redundantly essential endopeptidases of *B. subtilis* CwlO and LytE, are controlled by the CM-bound FtsEX sub complex [61] which likely acts to coordinate hydrolase activity with PG synthesis where, in contrast to, and presented in this work, a number of EPases in *E. coli* that are controlled by an OM-anchored lipoprotein. As the proteins that these OM-anchored proteins interact and regulate are widely conserved throughout walled bacteria, for example PBP1A whose interaction with LpoA is essential *in vivo* for PBP1A activity, it is therefore possible that PBP1A orthologues in other species may undergo regulation by different methods. The mechanisms of controlling hydrolase activity in *E .coli* and described in this project may be conserved throughout Gram-negative bacteria due to the ubiquity of the proteins involved; however other species may have adaptations on these methods to tailor the coordination between PG synthesis and hydrolysis with their size, growth rate and external environments.

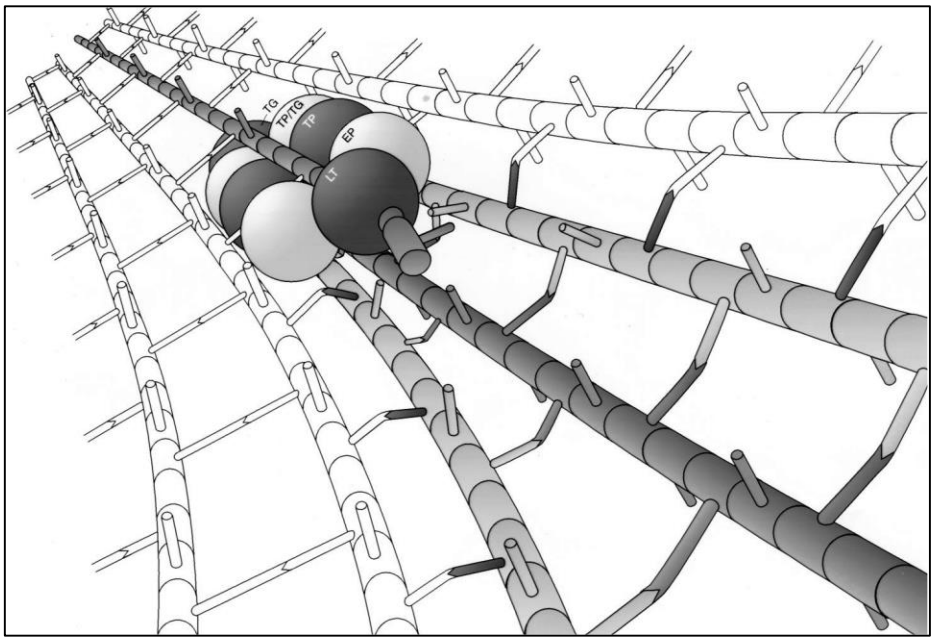

Figure 1.3 The 'three-for-one' model of peptidoglycan growth [50]

Proposed by Höltje (1998) the three-for-one model suggests that a multi-enzyme complex of PG synthases (TPases; transpeptidases, TG/GTase; transglycosylases) and hydrolases (LT; lytic transglycosylases, EP; endopeptidases) act to insert three nascent PG strands (grey strands) using one pre-existing strand as a template. The template docking strand is removed by the action of PG hydrolases.

1.3.3 Peptidoglycan synthases of *E. coli*

Table 1.1 The synthases/regulators of *Escherichia coli* PG synthesis

Protein	Gene	MW (Da)	pI	Localisation	Activities/ Primary role[1]	Interaction partners[1]		Copy number synthesised per generation[2]	
								MOPS	MOPS minimal
PBP1A	*mrcA*	93636	6.1	• CM • Lateral wall • Division site	• GTase • TPase • Cell wall synthesis in cell elongation	• PBP2 • LpoA		554	116
PBP1B	*mrcB*	94292	9.1	• CM • Division site • Lateral wall	• GTase • TPase • Cell wall synthesis in cell division	• PBP3 • LpoB • MltA • MltB • TolA	• Slt • FtsN • CpoB • FtsW	512	139
PBP1C	*pbpC*	85067	9.5	• CM	• GTase • TPase • Unknown	• PBP1B • PBP2 • PBP3	• MltA • MltB	18	11
PBP2	*pbpA/ mrdA*	70857	8.8	• CM • Lateral wall • Division site	• TPase • Essential for cell elongation	• PBP1A • MreC	• MltA • MltB • Slt	324	76
PBP3	*ftsI*	63877	9.6	• CM • Division site	• TPase • Essential for cell division	• PBP1B • FtsW • Slt • ZapA	• FtsQ • FtsL • FtsK • MltB • Slt	349	144
MtgA	*mtgA*	27369	10.4	• CM • Division site	• GTase • Unknown	• PBP3 • FtsW • FtsN		47	22
LpoA	*lpoA*	72873	5.3	• OM • Lateral wall	• Regulation of PBP1A activity	• PBP1A		513	250
LpoB	*lpoB*	22516	6.4	• OM • Division site	• Regulation of PBP1B activity	• PBP1B		1490	954
CpoB	*ybgF*	25932	8	• SP • Division site	• Regulation of PBP1B activity	• PBP1B • TolA		5262	1511

[1]See text for detailed discussions and references [2]Figures obtained from [62]

CM, cytoplasmic membrane; OM, outer membrane; SP, soluble periplasmic

MOPS, potassium morpholinopropane sulfonate

1.3.3.1 The bifunctional penicillin-binding proteins

In *E. coli* there are three families of enzymes responsible for PG synthesis; the bi-functional Class A PBPs (PBP1A, PBP1B and PBP1C), the monofunctional TPase Class B PBPs (PBP2 and PBP3), and a monofunctional GTase (MtgA) (table 1.1).

The major PG synthases of *E. coli* are the bifunctional Class A PBPs; PBP1A (*mrcA*) and PBP1B (*mrcB*). Cells with single deletions in these genes grow normally, but a double deletion is synthetically lethal, indicating these proteins are redundantly essential for cell growth [55,56]. Both proteins are CM-anchored via a single transmembrane region, possess a small non-catalytic domain and have two enzymatic domains (GTase and TPase) that are linked by a short β-rich region [44,56,49]. PBP1A and PBP1B, as well as PBP2 and PBP3, were recently shown to be folded and inserted into the CM by the concerted action of the membrane protein insertase/foldase YidC, and the Sec translocon [66].

The activity of PBP1A can be observed *in vitro* using radioactively-labelled lipid II [67]. By observing the resulting material by reversed-phase HPLC, PBP1A produces glycan chains that are, on average, 18.2 disaccharides in length with 26.4% of peptides participating in cross-links [67]. There is an initial delay in cross-link formation and PBP1A is unable to cross-link pre-formed glycan strands, implying that TPase reactions require ongoing GTase activity [67].

PBP1A/1B bind non-covalently to the peptide stem allowing the active site serine residue of the TPase domain to attack the carbonyl carbon atom of the D-Ala-D-Ala dipeptide [59,60]. This forms an acyl-enzyme intermediate that concomitantly cleaves the terminal D-Ala residue [59,60]. The energy released from this cleavage facilitates the formation of cross-links with an adjacent acceptor peptide stem [51].

Presently, there is no crystal structure for *E. coli* PBP1A, however, based on homology with PBP1A from *Acinetobacter baumanii* it possesses a small non-catalytic domain located close to the TPase domain. This region is termed the *O*uter-membrane *D*ocking *D*omain or ODD and is the predicted interaction site for the OM-anchored lipoprotein LpoA, an interaction essential for *in vivo* PBP1A function [31]. This interaction, and the role of PBP1A in cell elongation, will be discussed in section 1.3.4. PBP1A localises to the lateral cell wall and upon deletion causes the formation of cells with a narrower diameter [70]. This, and its interaction with PBP2, the Class B PBP essential for cell elongation, will be discussed in 1.3.3.3.

The crystal structure of *E. coli* PBP1B has been determined in complex with moenomycin which binds to the active site of the GTase domain [71]. The annotated GTase domain is similar to that found in the bifunctional PBP2 of *Staphylococcus aureus* and a GTase domain from a Class A PBP from *Aquifex aeolicus*, indicating a high degree of active site conservation [63,64]. Unlike the structure of the bifunctional PBP2 from the Gram-positive *S. aureus*, *E. coli* PBP1B possesses a non-catalytic domain, between the TPase and GTase domains, that is structurally homologous (24% sequence identity) to a domain found in the UvrB protein, termed the UvrB domain 2 homolog, or UB2H domain [65,62]. Recently this domain was characterised as the docking domain for the OM-anchored lipoprotein LpoB, an interaction essential for the *in vivo* function of PBP1B [75]. Like LpoB, the UB2H domain is only found in the γ-proteobacteria. PBP1B has been shown to dimerise with a K_D of 130 nM [76] and it is hypothesised that PBP1A also forms a homodimer.

As-of-yet there is no data purporting to the primary function of PBP1C (*pbpC*) which is anchored to the CM [77]. In affinity chromatography experiments it specifically retained PBP1B, PBP2, PBP3 and the lytic transglycosylase MltA, on sepharose beads, implying it exists as part of the multi-enzyme PG-synthesising complex, yet shows no phenotype upon deletion [77]. PBP1C polymerises PG and binds moenomycin, but a deletion in *pbpC* results in a loss of only 3% PG synthesis activity compared to 95% in a PBP1B deletion [77]. Dispensable for growth and expressed at ~20 copies per cell [62], it is thought unlikely that this protein has a major contribution to PG synthesis.

1.3.3.2 Monofunctional peptidoglycan synthases

The monofunctional PG synthases of *E. coli* are the Class B PBP TPases, PBP2 (*pbpA*) and PBP3 (*ftsI*) and the GTase, MtgA (*mtgA*). The Class B PBPs possess a non-catalytic N-terminal domain and a C-terminal catalytic TPase domain. The function of the N-terminal domain has been hypothesised to facilitate protein-protein interactions, and/or aid in substrate binding [43,49].

PBP2 is essential to bacterial viability and it has been shown, originally by Spratt (1975), if the activity of this monofunctional TPase is blocked by the β-lactam mecillinam, cells no longer grow as rods but adopt an ovoid morphology before lysis [78]. A GFP-PBP2 protein fusion was shown to predominantly localise in dynamic patches throughout the circumference of the lateral cell wall [79]. PBP2 is also capable of localising to the division site, albeit briefly, before the onset of constriction, but cannot in the presence of aztreonam which binds

with high specificity to PBP3 [70,53]. The localisation of PBP2 to the division site therefore relies on the activity of PBP3.

The monofunctional TPase PBP3 is essential for cell division [78]. If the activity of PBP3 is blocked by the specific binding of the β-lactam aztreonam, cells form filaments before lysing [81]. PBP3 forms a subcomplex with the lipid II flippase FtsW prior to localisation to the division site (see section 1.5.2) [82]. The crystal structure of PBP3 from *E. coli* shows a transmembrane helix followed by a bimodular periplasmic region consisting of a C-terminal catalytic TPase domain and the non-catalytic N-terminal domain [83]. The TPase domain shows structural homology to the corresponding catalytic domains of other published PBP3 crystal structures, including *Acinetobacter baumanii* and *Pseudomonas aeruginosa* [75,76].

MtgA is a CM-anchored, non-essential, monofunctional GTase that polymerises lipid II *in vitro* [77,78]. In cells absent of PBP1B, and expressing a temperature sensitive PBP1A, MtgA localises to sites of cell division. This localisation is thought to occur to compensate for the lack of GTase activity through direct or indirect interactions with PBP3, FtsW and FtsN [86]. However, at present, the primary role of MtgA is unknown.

1.3.3.3 Interactions between Class A and Class B peptidoglycan synthases

As described above, two monofunctional TPases have been characterised as essential for growth. PBP1A/1B are redundantly essential for growth, each being able to compensate for the lack of the other but a double deletion is synthetically lethal [55,79]. PBP1A is the primary Class A PBP during elongation (section 1.5.1) and PBP1B is the primary Class A PBP during cell division (section 1.5.2). As the cell is capable of propagating in the presence of only one of these PBPs, it suggests that there exist interactions between the components of their non-cognate complexes (section 1.5.3).

Bacterial two-hybrid analysis and affinity chromatography, using immobilised PBP2 incubated with a membrane fraction from *E. coli,* showed the specific interaction between PBP2 and PBP1A [70]. The continuous GTase activity of PBP1A can be measured *in vitro* using dansylated lipid II in which a fluorescent dansyl moiety is conjugated to the ε-amino group of the *m*-Dap residue. Polymerisation of dansylated lipid II and subsequent digestion with a muramidase (e.g. cellosyl) results in muropeptides with less fluorescence than the substrate [88]. Hence, GTase activity can be measured as fluorescence against time. Using this assay, PBP2, and not PBP3, was shown to stimulate lipid II consumption by PBP1A [70]. As PBP2 is essential for cell elongation, and both PBP1A and PBP2 localise to the lateral cell

wall, PBP1A and PBP2 are likely the primary PG-synthesising proteins during cell elongation and PBP2 is involved in the regulation of PBP1A GTase activity.

Affinity chromatography using immobilised PBP3, incubated with a membrane extract from *E. coli,* showed the specific retention of PBP1B [89]. The interaction was confirmed *in vivo* and *in vitro* using co-immunoprecipitation and surface plasmon resonance (SPR) and occurs with an estimated K_D of 435 nM. Like PBP3, PBP1B primarily localises to the cell division site, and this localisation is dependent on the presence, but not activity, of PBP3, implying that PBP3 and PBP1B are the primary PG synthases during cell septation [89].

1.3.4 Outer-membrane lipoprotein activators of PBPs

In *E. coli,* and presumably other Gram-negative bacteria, the cellular function of PBP1A and PBP1B relies on interactions with the OM-anchored lipoproteins, LpoA and LpoB, respectively [25,26]. The deletion of one Lpo and its non-cognate PBP is synthetically lethal, indicating that cells require either PBP1A and LpoA or PBP1B and LpoB for growth [25,26]. LpoA and LpoB are evolutionarily restricted to the γ-proteobacteria and the enterobacteria, respectively, while orthologs of PBP1A and PBP1B are expressed throughout walled bacteria [69]. LpoA and LpoB have coevolved with their respective PBP docking domains, hypothesised to be the ODD of PBP1A and confirmed to be the UB2H domain of PBP1B [25,67].

LpoB is comprised of a long OM-anchored N-terminal flexible region with a maximal length of ~145 Å and a small C-terminal globular domain (figure 1.4A) [75]. It is long enough to reach from the OM through pores in the PG layer to interact with the UB2H domain of PBP1B with an estimated K_D of 810 nM. Upon interaction, LpoB stimulates the GTase activity of PBP1B ~8 fold and stimulates cross-link formation from 53% to 73% of peptides [31]. LpoB stimulates the GTase domain of PBP1B causing a subsequent enhancement of TPase activity, indicating these domains are intrinsically connected, or that the TPase domain of PBP1B has specificity for polymerised substrate [90].

PBP1B/LpoB has another role in the coordination of OM constriction with PG synthesis, primarily through shared interactions with the Tol/Pal system [91]. The Tol-Pal system is a cell envelope-spanning complex of membrane-bound and periplasmic proteins required for coordination of membrane growth [92]. CpoB (*C*oordinator of *P*G synthesis and *O*M constriction, associated with PBP1*B*) is encoded by the last gene in the Tol/Pal operon, *ybgF*, and interacts directly with PBP1B and TolA [82,84]. Its localisation to the divisome is reliant

on ongoing PG synthesis but not PBP1B. PBP1B, LpoB, TolA and CpoB form a complex in which the activity of PBP1B is modulated based on the energy state of the Tol/Pal complex [82,85]. These functional interactions provide a mechanism for altering PG synthesis in response to OM invagination during daughter cell separation [91].

The structural model of LpoA was elucidated as part of this project (see section 3.1.2.2). LpoA exists as an elongated, bimodular monomer of ~70 kDa long enough to presumably reach through pores in the PG layer from the OM to interact with PBP1A (figure 1.4B) [95]. This interaction has not been characterised to the same degree as PBP1B/LpoB, in part due to the lack of a crystal structure for *E. coli* PBP1A [95]. The N-terminal domain ($LpoA^N$) consists primarily of tetratrico-peptide repeat (TPR) motifs which are frequently found in proteins with known interaction partners [96]. Between the helices of a number of these TPR motifs, are conserved amino acids [95]. LpoA stimulates the TPase activity of PBP1A, increasing the percentage of peptides in cross-links from 41% to 67% [31]. Conversely to LpoB/PBP1B, the stimulation of TPase activity by LpoA causes an increase in GTase activity, although this stimulation has not been observed using the same continuous fluorescence-based GTase activity assay used to show the stimulation of PBP1B by LpoB or PBP1A by PBP2 [81,88]. The catalytically active domains of PBP1A/B are clearly functionally linked and are activated in different ways by their cognate lipoprotein interaction partners.

The C-terminal domain of LpoA ($LpoA^C$) is capable of interacting with, and stimulating the activity of, PBP1A alone, inferring it is this domain with which LpoA interacts with PBP1A [25,62]. The structural model of *E. coli* $LpoA^C$ predicts two unstructured 'wing'-like domains, of presently unknown function, which are not present in the crystal structure of the Gram-negative organism *Haemophilus influenzae*, in which LpoA is essential [90,91]. These unstructured regions are thought to fold into rigid structures when engaged in protein-protein interactions [91,87]. Both $LpoA^N$ and CpoB possess TPR-like motifs and cells absent in both are synthetically sick inducing OM blebbing and lysis [83,87,85]. However, cells lacking PBP1A and CpoB do not have a phenotype, indicating a second role for LpoA, independent of PBP1A regulation. Specifically, *cpoB*$^-$*mrcA*$^-$*lpoA*(ΔTPR) cells re-establish the same defects as a *cpoB*$^-$*lpoA*$^-$ strain, implying it is $LpoA^N$ that possesses this additional role. Cells lacking CpoB and the TPR domain of LpoA are only sick in the absence of PBP1B, and grow normally in the presence of active PBP1A. $LpoA^N$ and CpoB are therefore thought to be redundantly essential for the coordination of PG and OM growth.

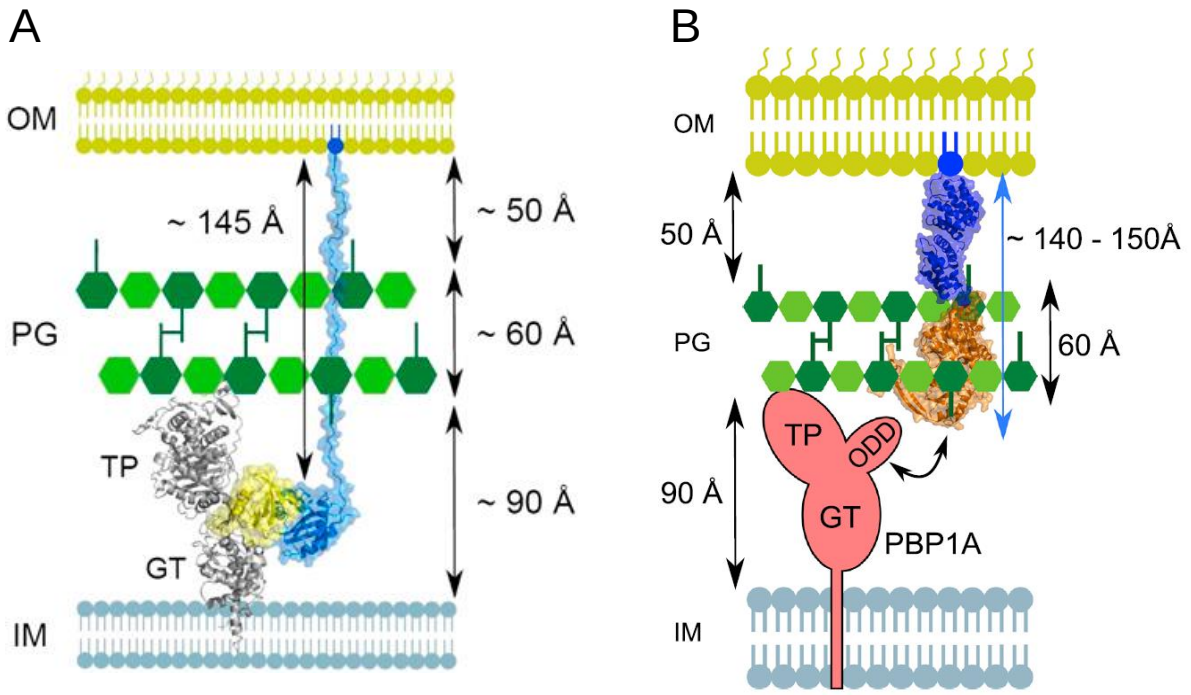

Figure 1.4 CM-anchored PG synthases are regulated by OM-anchored lipoproteins [67,87]

A. LpoB (blue) is anchored to the OM and uses its ~145 Å flexible N-terminal region to reach through pores in the PG layer to interact with the UB2H domain (yellow) of PBP1B (grey) to stimulate activity. **B.** LpoA is anchored to the OM and is predicted to reach through pores in the PG layer to interact with the ODD of PBP1A to stimulate activity. The C-terminal domain of LpoA (orange) is sufficient to stimulate PBP1A activity. The N-terminal domain of LpoA (dark blue) possesses TPR-like motifs and has an additional CpoB-related function. The crystal structure of *E. coli* PBP1A is not yet known.

1.4 Peptidoglycan hydrolysis in *E. coli*

1.4.1 The peptidoglycan hydrolases of *E. coli*

Current models of PG growth agree that simply synthesising and inserting nascent PG into the pre-existing PG layer would not facilitate successful growth of the sacculus. Instead, pre-existing PG must be cleaved or even removed prior to insertion of nascent PG. This process is accomplished by the PG hydrolases which turnover approximately 40-50% of the PG layer per generation [101]. In *E. coli* there are ~30 membrane-bound and soluble, periplasmic PG hydrolases, with hydrolytic activity identified for almost every glycosidic/amide bond of the sacculus (figure 1.5 and tables 1.2-1.6) [102]. They include the *N*-acetylmuramyl-L-alanine amidases, *N*-acetylglucosaminidases, lytic transglycosylases, endopeptidases and carboxypeptidases [94,95]. Those enzymes relevant to this project will be discussed in detail in the following sections.

The turnover products of PG hydrolysis are recycled for *de novo* PG synthesis, used for cell signalling, and are essential for the induction of β-lactamase production in response to antibiotic stress (section 1.6) [96,97]. PG hydrolases are also required for PG remodelling in response to extracellular challenges, influencing pathogenicity [102].

Single deletions of hydrolase genes show no effect on growth and many of the enzymes have multiple activities, therefore if PG hydrolysis is essential there must be a high degree of functional redundancy, which complicates the characterisation of specific hydrolases [103]. Some have specificities for intact sacculi or soluble muropeptides where others, termed autolysins, can be responsible for cell lysis. Relative to the number of PG hydrolases in *E. coli*, there are few known regulators, e.g. EnvC, NlpD and BolA (section 1.4.6). How these potentially autolytic enzymes are regulated is an important facet of PG growth and forms the basis for much of this project.

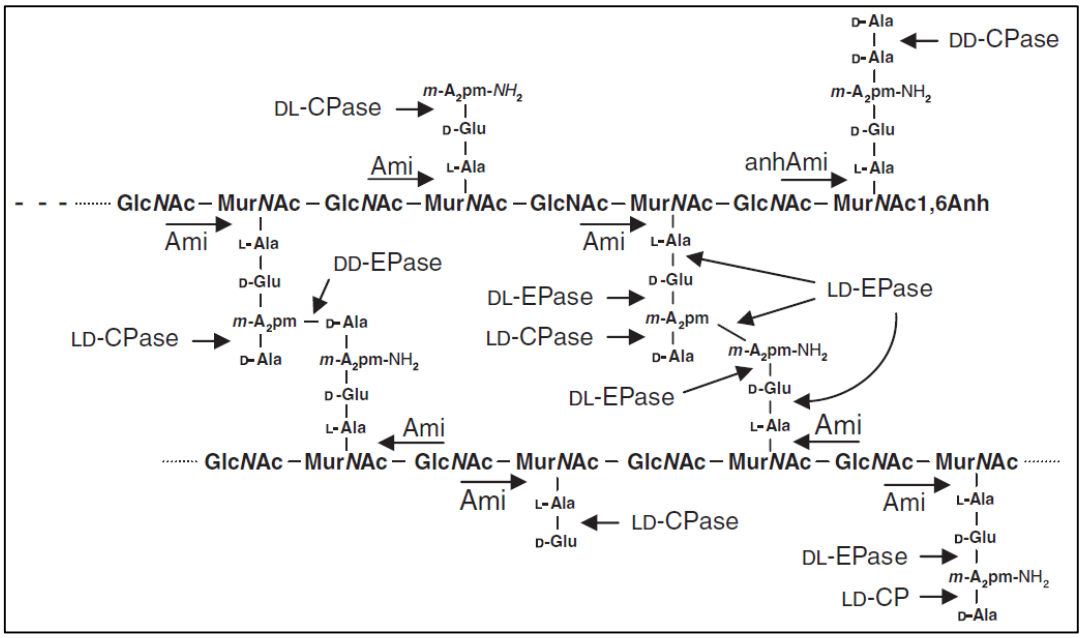

Figure 1.5 The peptidoglycan hydrolases of *E. coli* [103]

E. coli PG hydrolases cleave almost every amide and peptide bond in the PG network. The endopeptidases (EPase) cleave the amide bond between DD, LD, and DL-peptides. Carboxypeptidases (CPases) cleave the terminal D- or L-amino acids of peptide stems. Amidases (Ami) hydrolyse the bond between the D-lactoyl of Mur*N*Ac and the N-terminal L-Ala residue. The amidase AmiD is capable of cleaving this bond at an anhydro-Mur*N*Ac sugar.

1.4.2 Endopeptidases of *E. coli*

The endopeptidases (EPases) are the PG hydrolases responsible for the cleavage of amide cross-links. Those that cleave between D-Ala (position 4) and *m*-Dap (position 3) residues are termed DD-EPases [103]. These include the penicillin sensitive PBP4, PBP7, and AmpH, the penicillin-insensitive MepA (murein endopeptidase A), and three novel, redundantly essential, EPases Spr, YebA and YdhO, recently renamed to MepS, MepM and MepH, respectively [98-102]. MepA also possesses LD-EPase activity, however, monofunctional LD-EPases are less common in Gram-negative bacteria than Gram-positive. One such protein has been identified in *E. coli*, which remains uncharacterised, that releases the terminal D-Ala-D-Ala dipeptide upon cleavage of (L)-*m*-Dap-D-Ala cross-linked muropeptides, the opposite activity of the MurF ligase [109]. It is also hypothesised to catalyse the formation of (L)-*m*-Dap-(D)-*m*-Dap cross-linkages (LD-TPase activity), in correlation with an LD-TPase from *Enterococcus faecalis* which cleaves the D-Ala-D-Ala dipeptide to form the same bond [80,105,82]. See table 1.2 for a list of the EPases of *E. coli*.

Table 1.2 The endopeptidases of *E. coli*

Protein	Gene	MW (Da)	pI	Localisation/ Protein family	Activities /Primary role[1]	Interaction partners[1]	Copy number synthesised per generation[2]	
							MOPS	MOPS minimal
PBP4	*dacB*	51798	8.9	• SP/CM • Type 4 Class C PBP	• DD-EPase • DD-CPase • Deletion causes reduced β-lactamase induction	—	441	133
PBP7/8	*pbpG*	34271	9.9	• SP • Type 7 Class C PBP	• DD-EPase • Septum cleavage • Biofilm formation • PBP8 formed from action of OmpT • Stimulates Slt activity	• Slt	1005	242
AmpH	*ampH*	41849	9.5	• CM • Type AmpH Class C PBP	• DD-EPase • DD-CPase	—	460	116
MepA	*mepA*	30098	8.8	• SP • LAS Metallopeptidase	• DD-EPase • LD-EPase	—	625	273
MepS	*mepS/ spr*	21039	10	• OM • NlpC/P60 (CHAP superfamily)	• DD-EPase • Redundantly essential with MepM and MepH	—	3931	2535
MepM	*mepM/ yebA*	49057	9.5	• M23/LytM metallopeptidase	• DD-EPase • Metallopeptidase • Redundantly essential with MepS and MepH • Septum cleavage • LytM domain	—	341	379
MepH	*mepH/ ydhO*	30317	10.5	• NlpC/P60 (CHAP superfamily)	• DD-EPase • Redundantly essential with MepS and MepM	—	265	238

[1]See text for detailed discussions and references [2]Figures obtained from [62]

CM, cytoplasmic membrane; OM, outer membrane; SP, soluble periplasmic

MOPS, potassium morpholinopropane sulfonate

1.4.2.1 Penicillin-sensitive endopeptidases

Like all PG hydrolases, PBP4 (*dacB*) is non-essential in *E. coli*, however a single deletion in *dacB* results in the diminished induction of the β-lactamase AmpC [112]. PBP4 shows sequence similarity to the Class C family of β-lactamases and belongs to the type 4 family of PBPs [113]. It is soluble and periplasmic, although a loose association to the CM has been observed [107]. It possesses both DD-EPase and DD-CPase activity on sacculi and soluble muropeptides, and is potentially autolytic [99,106]. Like many of the hydrolases there is no known regulator of activity. The crystal structure of PBP4 shows a face-to-face-dimer with each monomer consisting of an interesting formation of three domains; the catalytic serine residue at position 62 is located within domain 1, into which domain 2 is inserted, into which domain 3 is inserted (figure 1.6) [115]. This Russian doll-like domain assembly is conserved between other type 4 PBPs with known crystal structures; *Actinomadura* R39 DD-peptidase and PBP4a of *B. subtilis* [108,109]. The active site of *E. coli* PBP4, and conserved among other type 4 PBPs, accommodates its substrate through the presence of a hydrophobic residue at the C-terminus of the β3 strand situated in the active site-containing domain 1. In addition, a number of residues of domain 2 are utilised to create a pocket to facilitate the binding of the terminal H_3N^+–CH–COO^- group of the *m*-Dap and its cross-linked amino acid [117]. Domain 3 is globular with a strong hydrophobic core, constitutes ~40% of the dimer surface, and has a hypothesised role in the regulation of substrate entry to the active site [118].

PBP7 (*pbpG*) is a soluble monofunctional EPase sharing 15% sequence identity with PBP4 [119]. It is the second most abundant PBP behind the CPase PBP5 (*dacA*) and while a deletion in *pbpG* causes no observable phenotype, a double deletion of both proteins causes considerable morphological defects [112-113]. It is reported that PBP7, and its proteolytic degradation product PBP8, are exclusively active against intact sacculi [122]. PBP8 is an artefact formed during purification as a result of C-terminal degradation of PBP7 by the OM protease OmpT [123]. Inactivation or overexpression of PBP7/8 has no effect on sacculi composition, but an interaction occurs with the soluble lytic transglycosylase, Slt70, causing stimulation of Slt activity, implying cooperativity of different hydrolytic activities [111,115]. Although individually non-essential, PBP4 and PBP7 have been implicated as determinants for controlling bacterial cell morphology in *E. coli* [121].

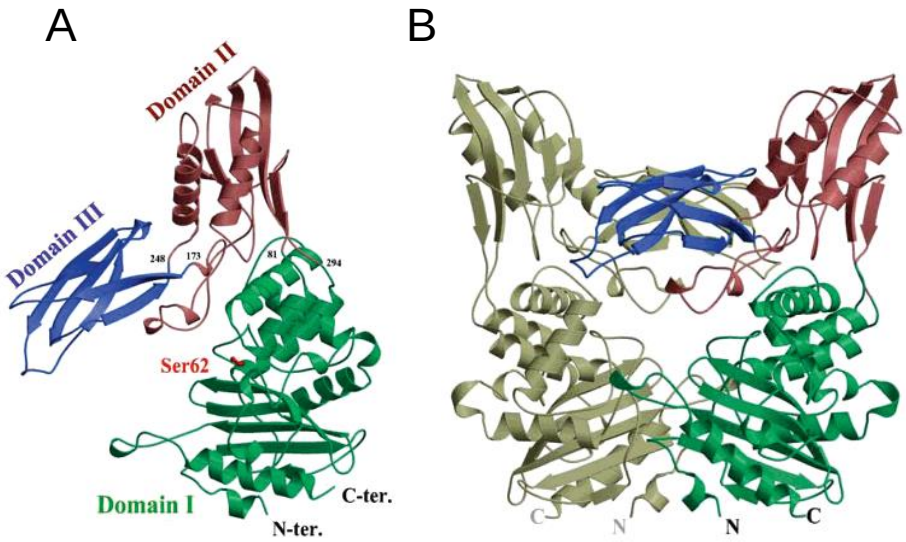

Figure 1.6 Monomeric and dimeric crystal structures of PBP4 [115]

The monomeric (**A**) and dimeric (**B**) crystal structures of PBP4 as determined by [115] reveals three distinct domains. The catalytic serine residue at position 62 is situated in domain 1, with domain 3 forming a distinct globular region. Domain 3 constitutes ~40% of the dimer surface

1.4.2.2 Penicillin-insensitive endopeptidases

MepA is a DD-EPase belonging to the LAS metallopeptidase family and contains a Zn^{2+}-binding catalytic triad (His-113, Asp-120, and His-211) at the active site, thus making it susceptible to metal chelators such as EDTA [116,117]. The crystal structure is an elongated dimer [127]. MepA is soluble and periplasmic and shows no morphological changes upon over-expression or deletion. It possesses both DD-EPase and LD-EPase activity, cleaving both D-Ala-*m*-Dap and *m*-Dap-*m*-Dap amide linkages [128].

MepS (Spr), MepM (YebA) and MepH (YdhO) DD-EPases of *E. coli*, and the DL-EPases CwlO and LytE of *B. subtilis*, were the first evidence of redundantly essential hydrolases for PG growth in their respective organisms [120,121]. In *E. coli*, MepS, MepM and MepH cleave the D-Ala-*m*-Dap peptide linkages and, like all other PG EPases, single deletions in each are viable. However, cells lacking all three lyse rapidly indicating redundant essentiality for PG growth and were shown to be the hydrolases responsible for creating the space required for nascent PG insertion in *E. coli* [129].

MepS belongs to the NlpC/P60 group of peptidases, and its structure has been determined by NMR spectroscopy [131]. It possesses a novel catalytic triad of Cys-His-His within a structurally-buried active site. MepH also belongs to this family of peptidases; however, only MepH has been shown to be active on intact sacculi [129]. The overexpression of active PBP7 is sufficient to phenotypically compensate for a deletion in *mepS* [132], implying that MepS is

active on sacculi *in vivo*. MepS is expressed at >2000 copies per cell during exponential phase but is rapidly subjected to proteolytic degradation facilitated by the OM-anchored New Lipoprotein I (NlpI) and the tail-specific protease, Prc (described in more detail in section 1.7) [108].

MepM belongs to the lysostaphin-like metalloprotease (LytM) M23 family of peptidases and has a Zn^{2+}-binding active site, and thus is inactivated by metal chelators [124,125]. It expresses a LytM domain, commonly found in PG-binding proteins, and proteins implicated in daughter cell separation such as the regulators of amidase activity, NlpD and EnvC (section 1.4.6) [135]. Deletion of *mepM* in an e*nvC*$^{-}$*nlpD*$^{-}$ background exacerbates cell division defects implying either an indirect role in amidase regulation or a direct role in cell separation [134]. However, despite this implicated role in cell separation, MepM has a disseminated peripheral localisation [134].

1.4.3 Carboxypeptidases of *E. coli*

Carboxypeptidase (CPase) activity results in the removal of the terminal D-Ala residue at position 5 of a pentapeptide [136]. Formation of the acyl-enzyme complex on the peptide stem, and the attack of the active site serine on the carbonyl moiety of the D-Ala-D-Ala dipeptide by the PBP, is the same as the TPase reaction [51]. The deacylation step of CPases utilises the proton of a H_2O molecule, rather than the amino group of an adjacent peptide stem, which is abstracted allowing nucleophilic attack and rupture of the scissile ester bond of the terminal dipeptide of the acyl-enzyme complex. The acyclic bond formed from this reaction is the same for CPase and TPase reaction and results in the release of the terminal D-Ala residue [60,128]. CPase activity acts to limit the amount of pentapeptides available for TPase reactions to around 1% [21]. Presumably, in the absence of CPase activity, excessive TPase reactions occur and the PG insertion process becomes unbalanced, or the percentage of inappropriate cross-links increases [21]. See table 1.3 for a list of the CPases of *E. coli*.

E. coli possesses six redundant DD-CPases; PBP4, PBP4b, PBP5, PBP6, PBP6b and AmpH [136]. As discussed, PBP4 is a bifunctional peptidase possessing both DD-EPase and DD-CPase activity, however, *in vivo*, it is thought to primarily act as an EPase [113,98]. PBP4b (*pbp4b*/*yfeW*) belongs to the AmpH type Class C PBP family and is a CM-bound DD-CPase. Cells grow normally upon a single gene deletion, and when combined with all other known DD-CPases [138]. It is also expressed at very low levels, indicating its activity is not essential for growth [62].

Table 1.3 The carboxypeptidases of *Escherichia coli*

Protein	Gene	MW (Da)	pI	Localisation	Activities /Primary role[1]	Interaction partners[1]	Copy number synthesised per generation[2]	
							MOPS	MOPS minimal
PBP4	*dacB*	51798	8.9	• SP/CM • Type 4 Class C PBP	• DD-CPase • DD-EPase	—	441	133
AmpH	*ampH*	41849	9.5	• CM • Type AmpH Class C PBP	• DD-CPase • DD-EPase	—	460	116
PBP4b	*yfeW*	47752	7.7	• CM • Type AmpH Class C PBP	• DD-CPase	—	26	15
PBP5	*dacA*	44444	8.3	• CM • Type 5 Class C PBP	• DD-CPase • Overproduction causes spherical cells and lysis • Transcriptionally regulated by BolA	—	4143	1180
PBP6	*dacC*	44461	7.7	• CM • Type 5 Class C PBP	• DD-CPase • Transcriptionally regulated by BolA	—	740	876
PBP6b	*dacD*	44346	6.2	• CM • Type 5 Class C PBP	• DD-CPase	—	29	6
LdcA	*ldcA*	33622	5.7	• C • S66 Peptidase	• LD-CPase	—	380	179
DdpX	*ddpX*	21281	4.9	• M15 Peptidase • VanY superfamily	• D-Ala-D-Ala recycling in stationary phase	—	—	19

[1]See text for detailed discussions and references [2]Figures obtained from [62]

CM, cytoplasmic membrane; OM, outer membrane; SP, soluble periplasmic; C, Cytoplasm

MOPS, potassium morpholinopropane sulfonate

The monofunctional CPase PBP5 (*dacA*) is the most abundant PBP in *E. coli* at ~800 copies per cell and is most highly expressed during exponential growth [120]. The crystal structure shows a bitopic homodimer anchored to the periplasmic face of the CM by a C-terminal amphipathic helix, that localises to both the septa and the lateral cell wall [139–141]. The N-terminal domain of PBP5 facilitates DD-CPase activity, while membrane binding via the C-terminal domain is essential for *in vivo* function [133,134]. PBP5 is thought to process newly synthesised pentapeptides not used in TPase reactions in order to maintain the overall percentage of pentapeptide-containing muropeptides to ~1%, inferring a close relationship with the bifunctional PG synthases, although no interactions have yet been observed [132,95]. Overexpression of PBP5 leads to the formation of stable spherical cells [144]. While the DD-CPases of *E. coli* are individually dispensable for growth, a *dacA* deletion in combination with other hydrolases have significant morphological abnormalities, highlighting the importance of this enzyme in the control of cell shape as well as septal hydrolysis, e.g. a *dacA*$^{-}$*dacC*$^{-}$ strain forms filaments and a *dacA*$^{-}$*amiA*$^{-}$*amiC*$^{-}$ triple mutant induces a twisted morphology [135,136]. Deletion of *dacB* in a *dacA*$^{-}$ background has severe morphological defects exacerbated by a deletion in *pbpG*. It is thought that the deletion of *dacA* causes an increase in the relative amount of pentapeptide substrate for TPase reactions resulting in aberrant cross-linking activity, thus causing morphological changes [143].

PBP6 (*dacC*) is a DD-CPase with 62% sequence homology to PBP5, and is also attached to the CM by a C-terminal amphipathic helix [146]. Cells absent of PBP6 possess an unchanged pentapeptide content, this is the converse for cells absent in PBP5, implying again that PBP5 is the major DD-CPase in *E. coli*. Transcription of both PBP5 and PBP6 is regulated by BolA (section 1.4.6) [144].

The amino acid sequence of PBP6b (*dacD*) is similar to that of PBP5 and PBP6 and as such the protein possesses DD-CPase activity and is anchored to the CM by an amphipathic C-terminal region [138,139]. However, it is expressed at low levels and is not essential for growth [54,138].

AmpH (*ampH*) is a PBP and, like PBP4, is a bifunctional peptidase possessing both DD-EPase and DD-CPase activity on intact sacculi and soluble muropeptides [140,141]. If *ampH* is deleted in a *mrcA*$^{-}$ or *dacA*$^{-}$ background, cells undergo significant morphological defects including an increased diameter and squared cell poles implying it contributes to regulation of normal cell shape [150].

E. coli possesses three LD-CPases which cleave the terminal D-Ala from L-Ala-D-iGlu-*m*-Dap-D-Ala rather than a pentapeptide [104]. Only the cytoplasmic LdcA has been characterised in appreciable detail, the other two, identified as active on UDP-Mur*N*Ac-tetrapeptide, being an 86 kDa periplasmic protein and a 12 kDa protein of unknown localisation [142,143]. LdcA is primarily involved in PG turnover, processing the internalised tetrapeptide products of PG hydrolysis (section 1.6) [153]. The tri-peptide formed from this catabolism is a crucial part of the PG recycling system of *E. coli*, producing substrate for MurF and Mpl to synthesise UDP-Mur*N*Ac-pentapeptide (figure 1.8) [154]. A deletion in *ldcA* results in increased frequency of lysis during stationary phase through the incorporation of UDP-Mur*N*Ac-tetrapeptide into the PG layer which can only act as acceptors for cross-linking [155].

DdpX is a Zn^{2+}-binding dipeptidase that cleaves the D-Ala-D-Ala dipeptide [110]. During stationary phase the primary role of DdpX is the recycling of D-Ala-D-Ala for *de novo* PG synthesis and for subsequent D-Ala oxidation as an energy source during nutrient starvation [156].

1.4.4 *N*-Acetylmuramyl-L-alanine amidases of *E. coli*

N-Acetylmuramyl-L-alanine amidases cleave the amide bond between the N-terminal L-Ala of the peptide and the D-lactoyl moiety of the Mur*N*Ac residue [157]. *E. coli* possesses five known amidases (table 1.4); three soluble, periplasmic amidases AmiA, AmiB and AmiC, the OM-tethered lipoprotein AmiD, and the cytoplasmic AmpD.

Table 1.4 The amidases of *E. coli*

Protein	Gene	MW (Da)	pI	Localisation	Activities /Primary role[1]	Interaction partners[1]	Copy number synthesised per generation[2]	
							MOPS	MOPS minimal
AmiA	*amiA*	31412	10	• SP • Division site (dependent upon EnvC) • Amidase 3 superfamily	• Septum cleavage • Activated by EnvC	• EnvC[3]	676	290
AmiB	*amiB*	47985	9.3	• SP • Division site (dependent upon EnvC) • Amidase 3 superfamily	• Septum cleavage • Activated by EnvC	• EnvC[3]	343	173
AmiC	*amiC*	45634	9.6	• SP • Division site (dependent upon NlpD) • Amidase 3 superfamily	• Septum cleavage • Activated by NlpD	• NlpD	410	68
AmiD	*amiD*	31072	7.1	• OM • Division site • Amidase 2 superfamily	• Cleaves MurNAc-L-Ala and 1,6-anhydro-Mur*N*Ac- L-Ala	—	141	82
AmpD	*ampD*	20536	5.3	• C • Amidase 2 superfamily	• Cleaves 1,6-anhydro-MurNAc-L-Ala • PG recycling	—	269	202

[1]See text for detailed discussions and references [2]Figures obtained from [62] [3]Genetic interaction

CM, cytoplasmic membrane; OM, outer membrane; SP, soluble periplasmic; C, cytoplasm

MOPS, potassium morpholinopropane sulfonate

The activity of AmiA, AmiB and AmiC is crucial for cell septation (section 1.5.2). AmiA and AmiB belong to the amidase 3 superfamily and AmiA is a Zn^{2+}-binding peptidase. A single deletion in *amiA* causes the formation of chains, 3-4 cells long, in 5-10% of a population [158]. The crystal structure of AmiC shows a novel N-terminal PG-binding AMIN domain required for divisome localisation [159].

A single deletion of AmiB causes no obvious phenotype whereas around 20-30% of cells lacking AmiC will grow as chains 3-6 cells long [151,152]. The amidases crucial for cell septation, AmiA, AmiB and AmiC, require activation by LytM domain-containing lipoproteins EnvC and NlpD, which is discussed in more detail in section 1.4.6 [162].

When deletions in these three amidases are combined with either, all of the lytic transglycosylases (Slt, MltA-F), or the EPases (PBP4, PBP7 and MepA) cells can form chains of up to 100 cells [152,154].

AmpD is a cytoplasmically localised amidase with exclusive activity for the amide bond in anhydro-Mur*N*Ac-L-Ala [164]. It has a crucial role in processing the internalised turnover products of PG hydrolysis to supply substrates for *de novo* PG synthesis and β-lactamase induction (see section 1.6 for more details).

1.4.5 Lytic transglycosylases of *E. coli*

E. coli encodes one soluble lytic transglycosylase (LT), Slt70, or simply Slt and seven membrane-bound LTs; MltA, MltB, MltC, MltD, MltE, MltF and MltG (table 1.5) [165]. The cleavage of the β1,4 glycosidic bond between the Mur*N*Ac and Glc*N*Ac residues forms an oxocarbonium ion intermediate, much like lysozyme, but instead of deprotonation by H_2O, it is the catalytic glutamate residue of the LT that deprotonates the hydroxyl group at C6 of the Mur*N*Ac sugar. This deprotonation facilitates the nucleophilic attack of C1 of the same Mur*N*Ac residue resulting in the formation of a 1,6-anhydro ring [166].

Table 1.5 The lytic transglycosylases of *E. coli*

Protein	Gene	MW (Da)	pI	Localisation	Activities/ Primary role[1]	Interaction partners[1]	Copy number synthesised per generation[2]	
							MOPS	MOPS minimal
Slt	*slt*	73353	8.8	• SP • LT family 1	• Septum cleavage • Inhibited by bulgecin A • Stimulated by PBP7	• PBP1B • PBP1C • PBP7 • PBP3	270	204
MltA	*mltA*	40410	9	• OM • LT family 2	• Septum cleavage • Overproduction causes spherical cells and lysis at 30°C	• PBP1B (through MipA) • PBP1C • PBP2 • PBP3	901	286
MltB	*mltB*	40255	9	• OM • LT family 3	• Septum cleavage • Overproduction causes spherical cells and lysis at 30°C • Soluble form termed Slt 35	• PBP1B • PBP1C • PBP2	926	274
MltC	*mltC*	40112	9.4	• OM • LT family 1	• Septum cleavage	—	392	148
MltD	*mltD*	49417	9.9	• OM • LT family 1	• Septum cleavage • LysM domain • Overproduction causes spherical cells and lysis	—	761	644
MltE/ EmtA	*mltE*	22212	9.2	• OM • LT family 1	• Septum cleavage	—	1942	609
MltF	*yfhD*	58302	5.3	• OM • LT family 1b	• Septum cleavage • Overproduction causes spherical cells and lysis	—	70	22
MltG	*yceG*	38247	9.4	• CM • YceG-like superfamily	• Endolytic • Glycan chain terminase	• PBP1B	312	70

[1]See text for detailed discussions and references [2]Figures obtained from [62]

CM, cytoplasmic membrane; OM, outer membrane; SP, soluble periplasmic

MOPS, potassium morpholinopropane sulfonate

The recycling of 1,6-anhydroMur*N*Ac-containing muropeptides is crucial for induction of the β-lactamase *ampC* in response to antibiotic stress (section 1.6) [167]. As previously mentioned, Slt interacts with and is stimulated by PBP7, but interactions with PBP3, PBP1B and PBP1C have also been observed [115,159]. Slt has been implicated as a quality control enzyme in PG synthesis, highlighted by the Slt-dependent degradation of nascent PG during β-lactam stress, in which TPase activity is abated preventing incorporation into the PG layer [169].

Recently a novel CM-bound endolytic transglycosylase, MltG, was characterised as a putative glycan chain terminase during PG synthesis by PBP1B [170]. The digestion of PG by MltG results in muropeptides possessing the anhydro-moiety, characteristic of LT activity, and like the other LTs, it is non-essential. MltG interacts with PBP1B, and does not interact with PBP1A. It is suggested therefore that the endolytic activity of MltG is linked to processing nascent PG synthesised by PBP1B, thereby controlling glycan chain length [170].

1.4.6 Regulators of peptidoglycan hydrolysis in *E. coli*

The regulation of PG synthesis has been well documented in recent years, both from the CM by cytoskeletal elements and associating proteins, and from the OM by membrane-anchored lipoproteins. Relative to the number of PG hydrolases in *E. coli*, regulators of PG hydrolysis are poorly understood and will be discussed here (see table 1.6).

Table 1.6 The regulators of peptidoglycan hydrolysis in *E. coli*

Protein	Gene	MW (Da)	pI	Localisation	Activities /Primary role[1]	Interaction partners[1]	Copy number synthesised per generation[2]	
							MOPS	MOPS minimal
EnvC	*yibP*	46594	9.9	• CM/SP • Division site	• Inactive • Activation of AmiA and AmiB • LytM domain	• AmiA[3] • AmiB[3]	258	106
NlpD	*nlpD*	40149	9.5	• OM • Division site • M23/LytM metallopeptidase	• Inactive • Activation of AmiC • LytM domain	• AmiC	1349	695
BolA	*bolA*	11922	6.2	—	• Control of *dacA* and *dacC* transcription	—	1945	2040

[1]See text for detailed discussions and references [2]Figures obtained from [62] [3]Genetic interaction

CM, cytoplasmic membrane; OM, outer membrane; SP, soluble periplasmic

MOPS, potassium morpholinopropane sulfonate

As alluded to in section 1.4.4 the amidases crucial for daughter cell separation during division, AmiA, AmiB and AmiC, are regulated by the LytM domain-containing lipoproteins EnvC and NlpD [134].

AmiA and AmiB are recruited to the site of septation and activated by the lipoprotein EnvC, itself recruited by the late division protein FtsN (section 1.5.2). The binding of EnvC to AmiB causes a conformational change releasing an α-helix from within the active site, normally occluding substrate binding, thus activating the enzyme [171]. EnvC (*yibP*) is a non-catalytic, CM-bound member of the LytM-like metallopeptidases [163,164]. EnvC was firstly shown to possess hydrolytic activity, however, this has now been disproven with its apparent activity

coming from its activation of AmiA and AmiB [164,125]. The crystal structure of the C-terminal LytM domain of EnvC purports a degenerate active site with the absence of a catalytic metal ion, highlighting its apparent lack of activity. EnvC also possesses a coiled-coil domain which is required for localisation to the division site through associations with FtsEX (see section 1.5.2) [153,165]. Site-directed mutagenesis identified the following amino acids as crucial for correct stimulation of amidase function; V353, R405, K321, V324. These amino acids are localised around the non-catalytic 'active site' of the LytM domain of EnvC, however, direct interactions with AmiA/B have not been identified thus far [162].

The activity of AmiC is regulated by the lipoprotein NlpD at the division site [162]. The N-terminal PG-binding AMIN domain of AmiC is required for divisome localisation. Like AmiB, AmiC possesses a helix which occludes the active site. NlpD interacts directly with AmiC, with an estimated K_D of ~12 μM, to remove the helix and activate the protein [159].

Like EnvC, NlpD is catalytically inactive and has no effect on its non-cognate amidases. Single deletions in EnvC and NlpD lead to morphological changes consistent with deletions in their cognate amidases [134]. *E. coli* encodes one OM-bound amidase, AmiD which does not participate in cell division, but also cleaves the amide bond in anhydro-Mur*N*Ac-L-Ala [175].

The gene *bolA* is responsible for transcriptionally regulating the DD-CPase genes *dacA* (PBP5) and *dacC* (PBP6) and is essential for correct cell morphology in exponential growth [144]. Overexpression of *bolA* results in osmotically stable spherical cells and has elevated expression during stationary phase and when cells are grown in nutrient-starved media [167,135].

1.5 Multi-enzyme complexes facilitating PG growth

Safe and coordinated enlargement of the sacculus is thought to be facilitated by multi-enzyme complexes of concomitantly active PG synthases and hydrolases [59]. As alluded to in section 1.3.2, insertion of new material is controlled from the cytoplasm by prokaryotic cytoskeletal elements and from the OM by membrane-anchored lipoproteins (section 1.3.4). These membrane-spanning complexes have evolved specificity for elongation and division and are termed the elongasome (figure 1.7) and the divisome (figure 1.8), respectively.

1.5.1 The elongasome

PG synthesis during elongation is controlled by the intracellular prokaryotic actin homologue, MreB. MreB is essential for the maintenance of cell shape in most rod-shaped bacteria and polymerises into helical filaments or discrete patches in an ATP-dependent manner [168,22]. The integral CM proteins, MreC and MreD are encoded by the same operon as MreB and are also essential for rod-shape in *E. coli* [178]. MreC interacts with both MreB and MreD to form a CM-bound complex [179]. MreC is a single transmembrane dimeric protein where MreD is a polytopic membrane protein, and deletion of either leads to spherical cells and lysis [171,172]. In the absence of MreC and MreD, MreB does not form helical filaments, this is also true of RodA [179].

RodA and FtsW are integral membrane proteins belonging to the SEDS (shape, elongation, division, and sporulation) family of proteins. FtsW is the lipid II flippase during cell division and RodA is predicted to be the flippase during elongation [48]. RodA interacts with MreB and is essential for rod-shape, forming spheroid cells upon deletion [173,174]. As discussed, PBP2 is the only PBP essential for cell elongation [78]. Active RodA is required for the proper function of PBP2, presumably for delivering nascent PG precursor to PBP1A [175,176].

The bitopic integral CM protein RodZ co-localises with MreB and interacts with both monomeric and filamentous forms as shown by co-crystallographic analyses [186]. RodZ assists in the association of MreB filaments to the CM to facilitate subsequent interactions with MreC and MreD [177,178].

MreB directly interacts with the penultimate and final enzymes of lipid II synthesis, MraY and MurG [188]. The localisation of MurG to the lateral cell wall is dependent on MreBCD and indicates that this subcomplex mediates the positioning or control of the PG synthesis machinery [169,19]. Supporting this, MreB moves helically and circumferentially throughout

the longitudinal axis of the cell and, using fluorescently-labelled vancomycin, the helical insertion of nascent PG into the lateral cell wall has been observed [189].

To date there is no definitive participation, or direct interactions, of PG hydrolases with components of the elongasome, perhaps owing to their high degree of functional redundancy (see section 1.4). Intuitively, hydrolases must be present to create space for the insertion of nascent PG. Three novel, redundantly essential *E. coli* DD-EPases have been identified and are discussed in section 1.4.2.2, although there are no direct interactions with the PG-synthesising complex [129].

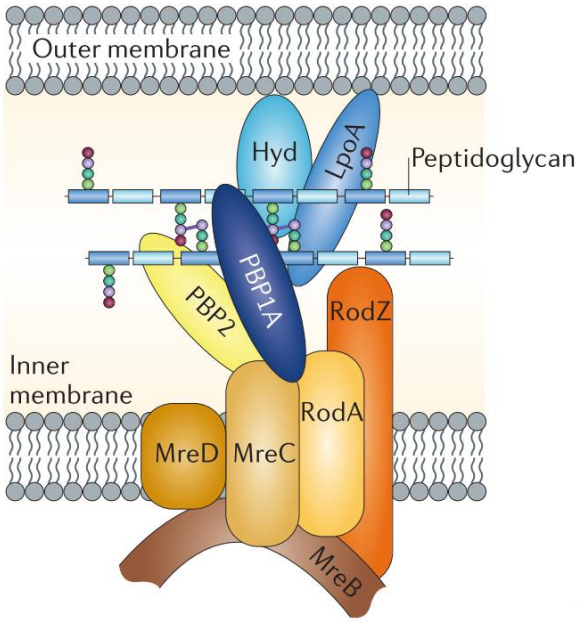

Figure 1.7 Schematic representation of the elongasome [24]

MreB, and the associated membrane proteins MreC, MreD, RodA and RodZ, act to position or control the PG synthases PBP1A and PBP2 during cell elongation. RodA is the predicted lipid II flippase during cell elongation and presumably delivers the PG precursor to PBP1A/2. RodZ facilitates the localisation of MreB to the CM. As-of-yet unidentified hydrolases (Hyd) are hypothesised to interact directly with components of the elongasome.

1.5.2 The divisome

Gram-negative bacteria employ a constrictive mode of cell division; invagination of the multi-layered cell envelope occurs simultaneously with septum formation, synthesis of daughter cell poles, and cell cleavage [4]. These processes are initiated by the reversible GTP-dependant polymerisation of the cytoplasmic prokaryotic tubulin homologue, FtsZ, into the cytokinetic Z ring, and its stabilisation at the mid-cell membrane [23,182,183]. ZipA and the actin-like FtsA simultaneously localise to the mid-cell through interactions with the conserved C-terminal tail of FtsZ [192–194]. ZipA and FtsA act to stabilise the Z ring and anchor it to the CM through the C-terminal amphipathic helix of membrane-bound FtsA protofilaments [187,188]. ZapA, ZapB, ZapC, and ZapD are also present at this stage but are not essential for division, as well as FtsEX whose association to the septum depends on FtsZ and ZipA [4].

FtsEX is an CM-bound subcomplex essential for the recruitment of EnvC which is required for the activation of the amidases AmiA/B (section 1.4.6) [154,166]. EnvC is recruited to the divisome through the periplasmic loop of FtsX, the transmembrane component of the complex [197]. The ATP hydrolysis facilitated by the cytoplasmically localised FtsE, allows EnvC to bind and activate AmiB (section 1.4.6) [171]. FtsE has been shown to interact with FtsZ and it is thought that FtsEX facilitates the coordination of amidase activity with the constriction of the Z ring [189,190]. During division, the septum formed by the PG-synthesising proteins of the divisome is initially shared between daughter cells. The activity of these periplasmic amidases and AmiC cleave the peptide stem from glycan strands at the newly formed septum and is a crucial step in daughter cell separation [149,167,191].

The hierarchical recruitment of the ‘late’ division proteins FtsK, FtsQ, FtsL, FtsB, FtsW, PBP3, PBP1B/LpoB and FtsN initiates formation of the septum [4]. PBP1B/LpoB are not essential as their function can substituted by PBP1A/LpoA [200]. FtsK is required for recruitment of the subcomplex FtsQLB which assembles prior to association to the divisome, of which, FtsQ is responsible for the recruitment of the predicted lipid II flippase during cell division, FtsW [193,194]. FtsW forms a complex with the monofunctional TPase PBP3 independent of the rest of the divisome [41,74,195]

PBP3 is the only PBP essential for cell division and interacts with and recruits the major PG synthase, PBP1B, and the last division protein recruited to the division site, FtsN [78]. FtsN interacts with a number of divisome proteins, yet its primary function is unknown [204]. However, FtsN has been shown to interact and stimulate the activity of PBP1B [205]. FtsN possesses a SPOR PG-binding domain which is not essential for function, and recruits the lipoprotein NlpD, which in turn activates the amidase AmiC (section 1.4.6) [198,199]. FtsN is

also responsible for recruiting, but not activating, AmiB [207]. Presumably, MraY and MurG are also present at the divisome to facilitate delivery of nascent lipid II precursor to the PG synthesis machinery, via FtsW. Indeed, although MurG is observed to form loci throughout the lateral cell wall, during division it localises at mid-cell [188].

The divisome has a secondary responsibility in coordinating OM invagination with septal PG growth and constriction, facilitated by the recruitment of the Tol/Pal system to the division site by FtsN [92]. The Tol/Pal complex traverses the CM and OM via various components; the CM-bound subcomplex, consisting of the integral membrane proteins TolQ, TolR and TolA; the periplasmic TolB, and the OM lipoprotein Pal, which is non-covalently bound to PG [208]. The last gene of the Tol/Pal operon encodes the protein CpoB. CpoB was discovered to be the functional link between the Tol/Pal system and the divisome and is discussed in section 1.3.4.

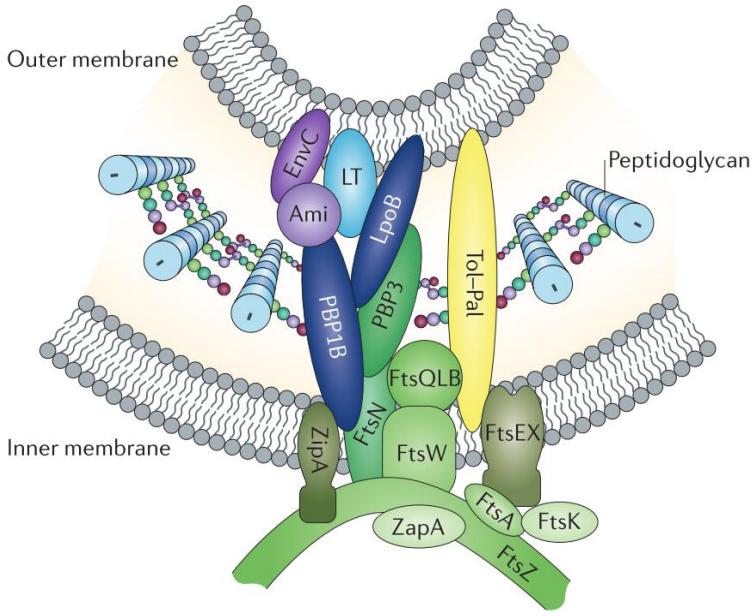

Figure 1.8 Schematic representation of the divisome [24]

The cytoplasmic prokaryotic tubulin homologue FtsZ polymerises in a GTP-dependant manner into the Z ring at the mid-cell membrane. ZipA and FtsA are essential for stabilisation and tethering the Z ring to the CM. Accessory proteins, ZapA-D are non-essential stabilisation proteins. FtsW is the lipid II flippase during cell division. FtsW interacts with PBP3 and presumably delivers nascent lipid II to the PG-synthesising core complex, PBP1B/3 and LpoB. FtsEX recruits EnvC which recruits and activates the amidases AmiA and AmiB. FtsN recruits NlpD to the division site for activation of AmiC. The Tol-Pal complex is recruited to the divisome by FtsN. The Tol/Pal system is functionally linked to the divisome via shared interactions with CpoB to coordinate OM constriction with PG synthesis.

1.5.3 Colocalisation of the elongasome and the divisome

The switch from PG growth during elongation, to the circumferential invagination at the mid-cell, remains elusive. However, there are number of interactions between the elongasome and the divisome, which suggest the complexes may co-localise and possess secondary functions [71,201,202].

A penicillin insensitive pre-septal PG synthesis phase between elongation and the onset of constriction was observed and termed PBP3 independent PG synthesis, or PIPS [211]. It has been suggested that it is PBP2 that is responsible for this pre-septal phase of PG growth facilitated by the Z ring which recruits the elongasome to the division site through a direct and essential interaction between FtsZ and MreB [30, 209, 212]. The identification of the transient localisation of MreBCD and PBP2 at the division site indicates that it is the elongasome that facilitates this pre-septal PG synthesis, coordinated by FtsZ [213]. It is thought that as the elongasome reaches the future site of septal synthesis, the PG-synthesising complex becomes uncoupled from MreB and is captured by the Z ring, and that it is this that redirects PG synthesis from lateral cell wall PG insertion to septal growth [204,205].

After this redirection, the rest of the divisome is formed and daughter cell separation can begin. FtsZ, independent of Z ring formation, has been shown to oscillate in a helical fashion throughout the lateral cell wall [215]. Divisome disassembly presumably releases FtsZ, and the associated PG-synthesising complex, to redistribute the PG synthesis machinery for lateral cell wall growth [215].

Localisation of PBP2 has been seen to overlap with that of PBP3 [79]. Direct interactions between the two, and of PBP2 with FtsQ, FtsN and FtsW have been observed at the division site [210]. MreB and PBP2 localise to the division site simultaneously with FtsZ, but disseminate by ~60% of division, implying they are not involved with the latter stages of divisome assembly or the synthesis of daughter cell poles [71,24].

1.6 Peptidoglycan recycling and β-lactamase induction

Around 50% of PG in *E. coli* is turned over per generation, with 6-8% lost to the culture supernatant, hence, a large percentage of the released material is reutilised [101]. PG recycling is a non-essential process, however, the turnover products of PG hydrolysis are internalised and reutilised for *de novo* PG synthesis and intracellular communication regarding the state of the PG layer, for example the induction of β-lactamase in response to antibiotic stress (figure 1.9) [207,208].

AmpG was the first link between PG turnover and β-lactamase induction in response to antibiotic stress [186]. A deletion in *ampG* prevents β-lactamase induction and results in the release of muropeptides into the medium [106]. AmpD is also essential for PG recycling and a deletion in *ampD* leads to the increased expression of AmpC, and the cytoplasmic accumulation of 1,6-anhydro-*N*-acetylmuramyl-L-Ala-D-iGlu-*m*-Dap (anhydro-MurNAc-tri-peptide) [218]. β-lactamase induction does not occur in *ampG*$^-$*ampD*$^-$ strains [219]. These data indicate that the major CM permease in Gram-negative organisms, for the internalisation of PG turnover products, is AmpG and that AmpD is a cytoplasmic amidase with specificity for anhydro-containing muropeptides.

AmpG has specificity for anhydro-containing muropeptides (Glc*N*Ac-β1,4-Mur*N*Ac-anhydro), formed by the action of LTs [106]. The internalisation of periplasmic anhydro-Mur*N*Ac-containing muropeptides by AmpG is thought to be dependent on PMF, as shown by susceptibility to the PMF inhibitor CCCP (carbonyl cyanide *m*-chlorophenyl hydrazine) [220].

Once internalised, anhydro-muropeptides are the substrate for the cytosolic *N*-acetyl-glucosamidase NagZ, which hydrolyses the β1,4-glycosidic bond removing the Glc*N*Ac residue [221]. The products of this reaction become the substrate for the anhydro-muropeptide specific amidase AmpD which removes the peptide stem from the D-lactoyl moiety of the Mur*N*Ac residue. This activity produces anhydro-Mur*N*Ac tetrapeptides which are processed by the LD-CPase LdcA, an activity which is essential during stationary phase (section 1.4.3).

AmpD can act directly on internalised anhydro-Mur*N*Ac-containing muropeptides to produce Glc*N*Ac-β1,4-Mur*N*Ac-anhydro. This is the substrate for a cascade of enzymes that produce the precursor for PG synthesis, UDP-Mur*N*Ac-pentapeptide (figure 1.9) [164].

Under normal conditions UDP-Mur*N*Ac-pentapeptide binds to the transcriptional regulator of the β-lactamase gene *ampC*, termed *ampR*, to repress its activity and thus prevent the

expression and export of AmpC [222]. Under antibiotic stress, the activity of PG hydrolases becomes unregulated resulting in a cytoplasmic accumulation of anhydro-containing muropeptides which act to displace UDP-Mur*N*Ac pentapeptide from *ampR*, leading to de-repression and induction of AmpC β-lactamase production [159,215]. *E. coli* does not possess an inducible *ampR*/*ampC* operon, therefore studies are generally carried out in cells transformed with a plasmid containing the operon from *Enterobacter cloacae* [224].

A minor percentage of PG turnover products are internalised by other CM integral membrane proteins including the oligopeptide permease (Opp) [225]. The Opp is composed of OppA, OppB, OppC, OppD and OppF, and its permease activity is modulated by the tripeptide binding capacity of MppA (murein peptide permease A) [218,219].

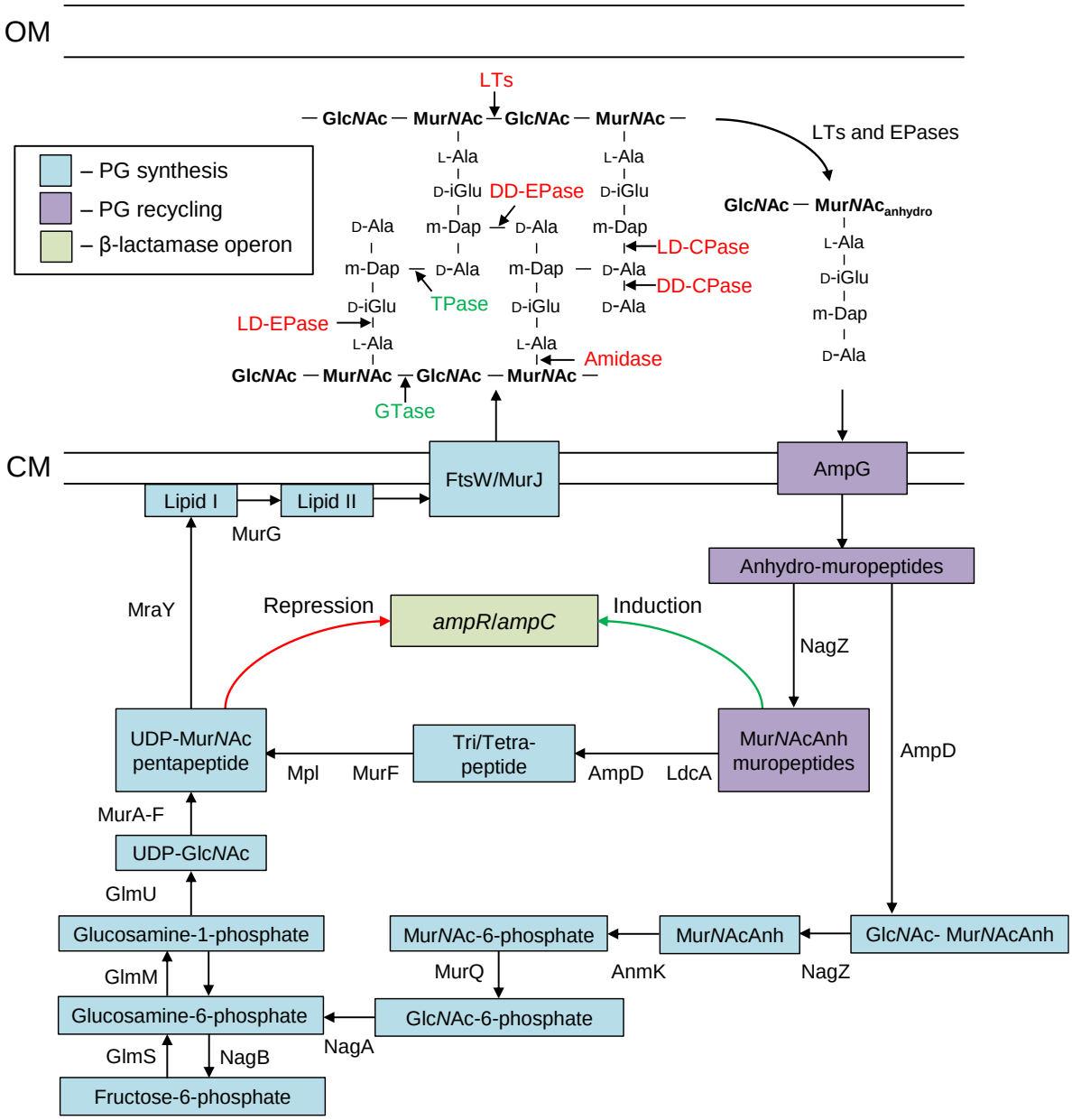

Figure 1.9 Peptidoglycan recycling and β-lactamase induction

The majority of the PG turnover products of EPase, CPase, amidase and LT digestion are internalised by the membrane permease AmpG. Anhydro-Mur*N*Ac-containing muropeptides, from LT digestion, are processed by NagZ, which removes the Glc*N*Ac residue. The products are catabolised by the cytoplasmic amidase AmpD, which removes the peptide chain to be reutilised for *de novo* PG synthesis. AmpD can also process the anhydro-containing muropeptides after internalisation to produce Glc*N*Ac-Mur*N*Ac$_{anhydro}$. The processive action of NagZ, the kinase AnmK, the etherase MurQ and NagA, which deacetylates Glc*N*Ac-6-phosphate, yields glucosamine-6-phosphate which can be utilised by the *de novo* PG synthesis pathway. Under normal circumstances, UDP-Mur*N*Ac-pentapeptide binds to the regulator of *ampC* expression, *ampR*, to repress expression. β-lactam stress results in the cytoplasmic accumulation of anhydro-containing muropeptides which displaces UDP-Mur*N*Ac-pentapeptide from *ampR*, leading to *ampC* expression, which is externalised to hydrolyse the antibiotic.

1.7 New lipoprotein I (NlpI)

NlpI is an OM-anchored lipoprotein with a currently unknown cellular function. Deletion of *nlpI* causes filamentation at elevated temperatures (42°C) and low osmolarity, whereas the overexpression of NlpI results in the formation of prolate spheroids [228]. NlpI has therefore been predicted to be involved in cell division. In concordance with this, NlpI interacts with two heat shock proteins, IpbA/B which are thought to be involved in nucleoid separation and correct localisation of the Z ring, with overexpression of NlpI leading to the disturbance of FtsZ [229].

Deletion of NlpI also leads to a hypervesiculation phenotype dependent on the activity of two EPases, PBP4 in stationary phase and MepS in exponential phase [230]. The *nlpI*$^-$ phenotype is suppressed by a deletion of *mepS* [230]. Complementation with a plasmid containing WT MepS, but not with that of an active site mutant, indicates it is the unregulated activity of MepS which causes the *nlpI*$^-$ phenotype. NlpI is therefore hypothesised to regulate EPase activity. In the absence of NlpI, it is thought that unregulated PG hydrolysis decouples Braun's lipoprotein (Lpp) from the PG layer which covalently connects the OM and the PG layer. Increased amounts of free Lpp (Lpp not bound to the PG layer) correlates with OM vesiculation [222,223]. Periplasm-containing OM vesicles are primarily utilised in host-pathogen interactions and biofilm formation [232].

Recently, NlpI has been shown to facilitate the proteolytic degradation of MepS, identifying a key role in the control of EPase activity and PG hydrolysis [108]. NlpI and MepS interact with the tail-specific protease Prc, but only MepS is subject to degradation, where 12 C-terminal amino acids of NlpI are removed [108]. In the absence of NlpI, the half-life of MepS increases from ~2 min to ~45 min.

The crystal structure of NlpI has been determined and shows the formation of a homodimer (see figure 1.10) [233]. Each monomer is 33 kDa with both OM-binding N-termini close together. Each monomer consists of 14 α-helices forming 4 canonical TPR-like domains; helices 2 and 4 (TPR1), 4 and 5 (TPR2), 6 and 7 (TPR3) and 12 and 13 (TPR4). However, unlike canonical TPR-containing proteins, the superhelical structure of NlpI folds back in on itself, with the C-terminus inserted into the N-terminus, forming a characteristic globularity. Within this fold, long-range contacts occur between the first helix of each helix-turn-helix ('A' helix) further strengthening this globularity. There is a putative binding cleft formed from the curvature of the helices on each monomer which would be available for protein-protein interactions [233].

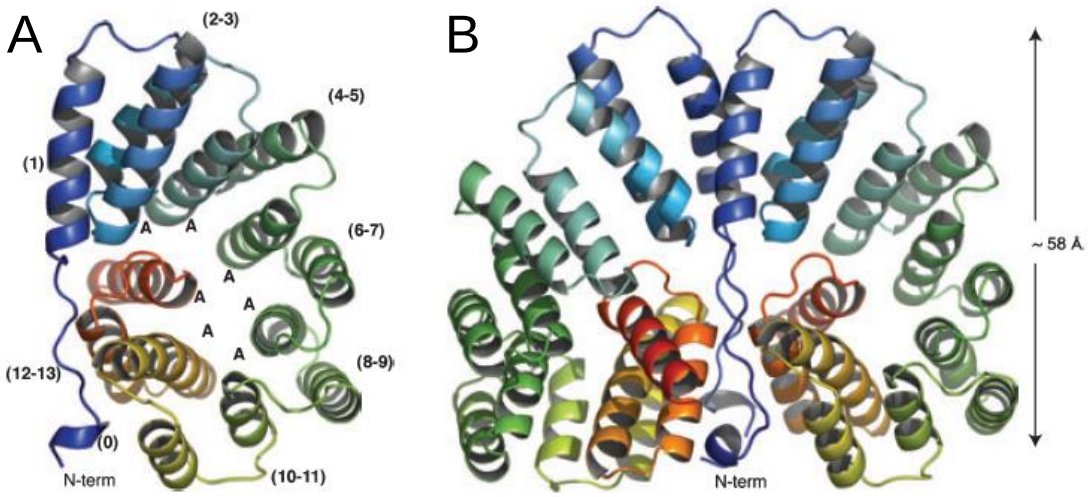

Figure 1.10 Crystal structure of NlpI [233]

A. Crystal structure of the monomer of NlpI. NlpI is composed of 14 α-helices forming 4 TPR-like motifs made of helices 2 and 4 (TPR1), 4 and 5 (TPR2), 6 and 7 (TPR3) and 12 and 13 (TPR4). The C-terminus is folded back inside the N-terminus forming an overall globular structure with 'A' helices forming long-range contacts with the C-terminal fold. **B.** Crystal structure of the dimer of NlpI. The dimer interface consists of the N-terminal regions, and helices 1, 2, 3, 11, 12, 13 and 14.

1.8 Aims

E. coli possesses around 30 PG hydrolases and many have potentially autolytic activity. While the understanding of how PG synthesis is regulated has developed in recent years, the processes by which PG hydrolysis is regulated remains poorly understood. Intuitively, these two processes are functionally linked in multi-enzyme complexes, however, few direct interactions have been observed, particularly during cell elongation. The aims of this project were to;

1. Determine the structural model of the OM-anchored lipoprotein regulator of PG synthesis during elongation, LpoA.
2. Characterise the interaction of LpoA and PBP1A.
3. Search for novel interactions partners of LpoA.
4. Identify direct connections between PG synthesis and PG hydrolysis.
5. Structurally and functionally characterise the PG hydrolases PBP4 and MepA.
6. Determine the primary function of the predicted PG hydrolase regulator, NlpI, *in vitro* and *in vivo.*

2 Methods

2.1 Microbial methods

2.1.1 Bacterial growth and storage

E. coli cells were cultivated as liquid culture in Luria Bertani (LB) media (10 g/L Tryptone, 10 g/L NaCl, 5 g/L yeast, pH 7.5), with growth monitored at regular intervals by spectrophotometry (578 nm), or on LB-agar plates (10 g/L Tryptone, 10 g/L NaCl, 5 g/L yeast, 1.5% agar, pH 7.5). When cultivating cells for the purification of proteins destined for nuclear magnetic resonance (NMR) spectroscopy analysis, M9 media was used, (5.29 g/L Na_2HPO_4, 3 g/L KH_2PO_4, 0.5 g/L NaCl, and 1 g/L [^{15}N]-NH_4Cl, 1 mM $MgSO_4$, 0.1 mM $CaCl_2$, 2 mM Thiamine, 0.3% [^{13}C]-glucose, pH 6.8-7.2) with more detail described in section 2.3.2. Orbital shaking and incubation at 25, 30 or 37°C was used to promote growth. For short term storage, bacteria were grown on LB-agar plates and stored at 4°C. For long term storage, cells were grown to an OD_{578} of 0.5-0.6 and stored at -80°C with 10% glycerol.

2.1.2 Production of competent *E. coli* cells

An o/n culture was used to inoculate 50 ml of LB and cells were grown to exponential phase at 37°C before harvesting by centrifugation (4500 × g, 4°C, 15 min). Pelleted cells were resuspended in 15 ml of ice cold TFB1 solution (100 mM RbCl, 50 mM $MnCl_2$, 10 mM $CaCl_2$, 15% glycerol, pH 5.8, adjusted with acetic acid) and were incubated for 90 min on ice. Cells were harvested again by centrifugation and resuspended in 2 ml of ice cold TFB2 solution (10 mM MOPS, 10 mM RbCl, 75 mM $CaCl_2$, 15% glycerol, pH 6.8, adjusted with KOH). Cells were resuspended and aliquoted on -70°C ethanol ice. Competent cells were frozen at -80°C, if not used immediately.

2.1.3 Isolation of plasmid DNA from *E. coli* cells

Plasmids were isolated from bacterial cells using either PeqGOLD Mini or Midi-prep plasmid extraction kits (PeqLAB), as per manufacturer's instructions. The concentration of isolated plasmids was estimated using Nanodrop ND1000 V3.7.1 software.

2.1.4 Transformation of plasmid DNA into competent *E. coli* cells

Aliquots containing 100 µl of competent *E. coli* cells were thawed on ice and 1-10 µl of purified plasmid were added. After a 10 min incubation on ice, cells were heat-shocked at 42°C for 1 min and placed back on ice for 15 min. Cells were incubated with 900 µl of LB for

1 h at 37°C before 100 µl and 900 µl of the cell suspension were plated on LB agar plates, containing any appropriate antibiotic, and incubated o/n at 37°C. For the overexpression and purification of proteins, BL21(DE3) competent cells, expressing the T7 promotor, were used. DH5α competent cells were used for long term storage and future plasmid isolation.

2.1.5 Excision of kanamycin resistance cassette using pCP20

The plasmid pCP20 was used to create antibiotic marker-less strains [226,227]. It encodes an Flp recombinase which acts to 'flip out' kanamycin resistance cassettes flanked by FRT (flippase recognition target) regions. It contains ampicillin and chloramphenicol resistance cassettes and is thermo-sensitive. This protocol was used prior to addition of other plasmids containing a kanamycin resistance cassette, or creating multiple deletions via P1 phage transduction.

The pCP20 plasmid was transformed as described in section 2.1.4 but, due to the thermosensitive nature of the plasmid, cells were incubated at 30°C instead of 37°C. Transformed cells were plated on either ampicillin or chloramphenicol plates o/n at 30°C to remove the kanamycin resistance cassette. A colony was picked and re-streaked on LB-agar without antibiotic, and incubated at 42°C to remove the pCP20 plasmid. A colony was picked and re-streaked on kanamycin, ampicillin/chloramphenicol and standard LB plates as a screen to check for the successful removal of kanamycin resistance, and of the pCP20 plasmid.

2.2 Protein methods

2.2.1 Sodium dodecyl sulphate polyacrylamide gel electrophoresis (SDS-PAGE)

For the observation of the yield and purity of proteins, as well as *in vitro*/*in vivo* interaction assays, proteins were separated according to their molecular weight using SDS-PAGE. Samples were mixed 2:1 with SDS-loading buffer (4 ml 1 M Tris/HCl, 5.1 ml 75% glycerol, 0.6 g SDS, 0.4 ml 0.1% bromphenol blue) and were boiled for 10 min with 10% β-mercaptoethanol to reduce disulphide linkages. Samples were briefly centrifuged to remove condensation and loaded onto polymerised acrylamide gels (12 or 15% acrylamide w/v) (see table 2.1). Electrophoresis was carried out at 100 V for 1-2 h in a BioRad gel tank system containing the appropriate volume of TGS running buffer (20 mM Tris, 192 mM glycine, 0.1% SDS). Gels were stained with Coomassie staining solution (1 g/L Coomassie brilliant blue R250, 50% methanol, 40% H_2O, 10% acetic acid) and destained in destaining solution (30% methanol, 60% H_2O, 10% acetic acid), until a clear background was obtained. In some cases a zinc staining kit (Biorad) or a silver staining kit (Sigma) were used as per manufacturer's instructions. Gels were scanned between two plastic sheets using an Epson perfection V350 scanner and cropped and annotated using Microsoft Paint/Picture manager and Microsoft PowerPoint.

Table 2.1 SDS-PAGE gel recipe for six gels

	Volume (ml)		
Components	**12% separation gel**	**15% separation gel**	**Stacking gel**
H_2O	7.2	4.2	4.9
Buffer	7.5 [1]	7.5 [1]	2.5 [2]
Acrylamide[3]	12	15	1.5
10% SDS	0.3	0.3	0.1
2% TEMED	1.5	1.5	0.5
1.4% APS	1.5	1.5	0.5

[1] 1.5 M Tris/HCl, pH 8.8

[2] 0.5 M Tris/HCl, pH 6.8

[3] Rotiphorese (Roth, Germany)

2.2.2 Western blotting procedure

For a list of the antibodies used in this project and their working dilutions see table 5.1.

Western blot

Proteins were separated by SDS-PAGE (section 2.2.1) before being transferred to a nitrocellulose membrane using a BioRad wet-blot system, as per manufacturer's instructions, for 1 h at a constant current of 350 mA in Western blot buffer (20 mM Tris, 192 mM glycine, 0.1% SDS, 10% methanol).

Immunodetection

Nitrocellulose membranes were removed and incubated o/n at 4°C, with gentle agitation, in 10 ml TBS (Tris-buffered saline) blocking buffer (10 mM Tris/HCl, 0.09% NaCl, 0.5% casein, pH 7.5). An optimised concentration of primary antibody was incubated with the nitrocellulose membrane in 10 ml TBS for 90 min at RT with gentle agitation. The membrane was washed with three cycles of 10 ml TBST (TBS + 0.1% Tween-20) for 5 min each. The membrane was incubated with a secondary antibody, usually goat α-rabbit-HRP, in 10 ml of TBS for 90 min at RT with gentle agitation.

Enhanced chemiluminescence visualisation

The membrane was washed as before in three cycles of TBST for 5 min each before visualisation using an enhanced chemiluminescence (ECL) kit (GE healthcare) as per manufacturer's instructions. An ImageQuant LAS4000mini biomolecular imager (GE Healthcare) was used to visualise blots and the accompanying software was used to process the images.

2.2.3 Estimation of protein concentration

The concentrations of purified proteins and cell lysates were estimated using bovine serum albumin (BSA) standards in a Pierce^{TM} BCA protein assay kit (Thermo scientific), as per manufacturer's instructions (see figure 2.1). Most often however, the concentration of purified protein samples, absent in Triton X-100, was estimated using a NanoDrop spectrophotometer and accompanying ND1000 V3.7.1 software which calculates the concentration of the sample based on the absorbance of the protein at 280 nm using the extinction coefficient and molecular weight of the sample.

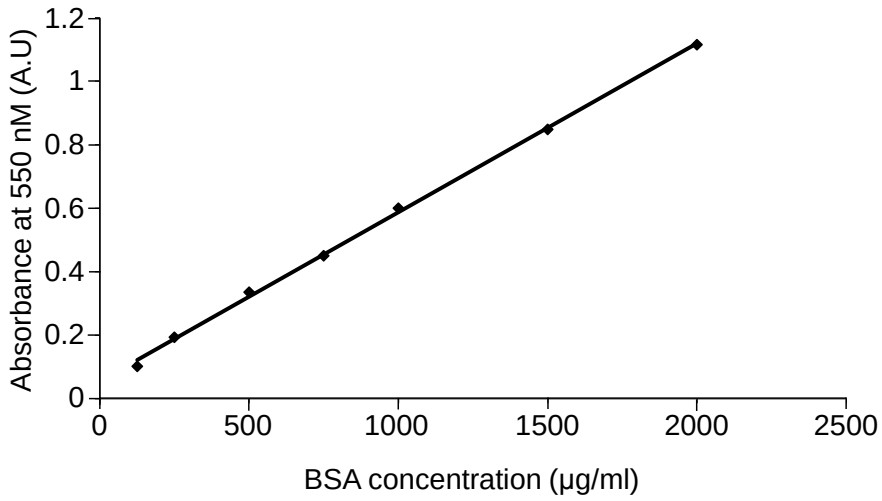

Figure 2.1 Example BSA standard curve

Bovine serum albumin (BSA) standards plotted as concentration against absorbance, read at 550 nM.

2.3 Protein purifications

A list of all plasmids for the overproduction of proteins is given in table 5.2.

2.3.1 Protein overproduction and cell fractionation

The procedure for soluble protein overproduction was the same for each protein purified, unless stated in the specific protein purification section. *E. coli* BL21(DE3) cells harbouring specific overexpression plasmids were grown o/n at 37°C with an appropriate antibiotic. O/n cultures were diluted 1:50 in 3 L of LB media and grown at 37°C with orbital shaking to an OD_{578} of 0.5-0.6. Protein overexpression was induced with the addition of 1 mM IPTG and incubation for a further three hours at 30°C. Cells were kept for 10 min on ice before harvesting by centrifugation (7500 × g, 4°C, 15 min) (Beckman Coulter – F500 rotor). Pelleted cells were resuspended in 40 ml of ice cold resuspension buffer (25 mM Tris/HCl, 10 mM $MgCl_2$, 300 mM NaCl, 10% glycerol, pH 7.5). A small amount of DNase, 1/1000 protease inhibitor cocktail (Sigma) and 100 μM phenylmethylsulfonylfluoride (PMSF) were added prior to sonication (3 × 20 s at 10, 20, 30, 40, 50, 60% power, 30 s rest between each setting) and ultracentrifugation (140000 × g, 4°C, 15 min) to remove the membrane fraction. For the purification of membrane proteins the supernatant was discarded, and the membrane-containing pellet solubilised by stirring o/n with extraction buffer (25 mM Tris/HCl, 10 mM $MgCl_2$, 1 M NaCl, 2% Triton X-100, 20% glycerol, pH 7.5). Purification steps continue as described in each specific protocol section.

2.3.2 Protein overproduction for NMR spectroscopy

In the case of protein purification for nuclear magnetic resonance (NMR) spectroscopy analysis, proteins were labelled with [^{13}C] and [^{15}N]. M9 minimal media was used (5.29 g/L Na_2HPO_4, 3 g/L KH_2PO_4, 0.5 g/L NaCl, and 1 g/L [^{15}N]-NH_4Cl, 1 mM $MgSO_4$, 0.1 mM $CaCl_2$, 2 mM Thiamine, 0.3% [^{13}C]-glucose, pH 6.8-7.2) in which [^{13}C] and [^{15}N] isotopes were the only carbon and nitrogen sources, respectively. Standard LB day cultures were made with the appropriate overexpression strain diluted 1/70 and grown at 37ºC for 8 h. Of this day culture, 1 ml was used to inoculate 100 ml of M9 media and grown o/n at 37ºC with orbital shaking. Cells were harvested by centrifugation (7500 × g, 4°C, 15 min), resuspended in 1 ml of fresh M9 media and used to inoculate the remaining 900 ml of M9 media in which cells were grown to an OD_{578} of 0.5-0.6. Subsequent purification steps are protein specific and the same for unlabelled protein purification.

2.3.3 Immobilised metal ion affinity chromatography (IMAC)

This is the first purification step for proteins with an oligo-histidine tag (His-tag) either from isolated cell lysate or a solubilised membrane fraction. All His-tags are N-terminal unless stated. Specific protein buffer conditions can be found under the relevant sections, however the most common buffer conditions are given here as an example. Isolated supernatant was applied to a 5 ml HisTrap HP column (GE healthcare) using an ÄKTA Prime^{+} (GE Healthcare) by 50 ml Superloop, pre-equilibrated with buffer 1 (25 mM Tris/HCl, 10 mM $MgCl_2$, 300 mM NaCl, 20 mM imidazole, 10% glycerol, pH 7.5) at 1 ml/min collecting 10 ml fractions. The column was washed with 5 column volumes of buffer 1 at 2 ml/min before the step-wise elution of bound proteins with buffer 2 (25 mM Tris/HCl, 300 mM NaCl, 400 mM imidazole, 10% glycerol, pH 7.5) at 2 ml/min collecting 4 ml fractions. Flow-through, wash, and elution fractions were analysed by SDS-PAGE and those containing the best yield and purity were either stored at -80°C with 10% glycerol, if purification was sufficient, or dialysed against the appropriate buffer for a second step of purification, usually IEX. If a native form of the protein was required, samples were incubated with 1 unit/ml of thrombin (Novagen) prior to dialysis and IEX to remove the cleaved His-Tag.

2.3.4 Ion exchange chromatography (IEX)

If IEX is the first step of purification, harvested cellular pellets were resuspended in a low/no NaCl buffer, if not, samples were dialysed against 2 × 2 L of IEX buffer 1 (50 mM Tris/HCl, pH 8.0), o/n and 1 hr in the morning. A 5 ml HiTrap SP HP or Q HP (depending on the charge of the protein) (GE healthcare) ion exchange column was prepared with 5 column volumes of dH_2O and 5 column volumes of IEX buffer 2 (50 mM Tris/HCl, 1 M NaCl, pH 8.0) before equilibration with IEX buffer 1. Protein was applied via 50 ml Superloop using an ÄKTA Prime^{+} at 1 ml/min collecting 10 ml fractions. The loaded column was washed with 15% IEX buffer 2 for 3 × 10 ml fractions at 2 ml/min. Proteins were eluted with a salt gradient of 15-100% IEX buffer 2 for 100 ml collecting 4 ml fractions. Fractions (flow-through, washes, and elutions) were analysed by SDS-PAGE and those containing the best yield and purity were either stored at -80°C with 10% glycerol, if purification was sufficient, or dialysed against the appropriate buffer for another method of purification.

2.3.5 Hydroxyapatite chromatography

Hydroxyapatite purification utilises positively charged calcium ions and negatively charged phosphate groups to separate proteins by metal affinity and cation exchange respectively [236]. Prior to purification, samples were dialysed o/n against buffer 1 (10 mM KPO_4, 300 mM NaCl, pH 6.8). A 5 ml hydroxyapatite column (BioRad Bioscale Mini CHT II 40 µm 5 ml cartridge) was washed with 5 column volumes of dH_2O and equilibrated with buffer 1 before application of the protein sample by 50 ml Superloop at 1 ml/min. The column was washed for 3 × 10 ml fractions with buffer 1 before elution of bound proteins using a gradient of 0-100% buffer 2 (500 mM KPO_4, 300 mM NaCl, pH 6.8) over 50 ml at 1 ml/min collecting 4 ml fractions. Fractions (flow-through, washes, and elutions) were analysed by SDS-PAGE and the fractions containing the best yield and purity were either stored at -80°C with 10% glycerol, if purification was sufficient, or dialysed against the appropriate buffer for another step of purification.

2.3.6 Size exclusion chromatography

Size exclusion chromatography (SEC) was usually the last step of protein purification. Samples were concentrated to 4-5 ml using a Vivaspin 6 column (Sartorius Stedim biotech) and applied to a HiLoad 16/60 Superdex 200 column prewashed with dH_2O and equilibrated with SEC running buffer (25 mM HEPES/NaOH, 300 mM NaCl, 10 mM $MgCl_2$, 10% glycerol, pH 7.5). Protein samples were loaded onto the column at 1 ml/min collecting 4 ml fractions. Peak UV fractions were analysed by SDS-PAGE and those of highest yield and purity were pooled, aliquoted and stored at -80°C.

2.4 Specific protein purification protocols

2.4.1 Purification of LpoA versions

The protocol is as described in [31]. His-LpoA from *E. coli* and *H. influenzae* ($LpoA_{H.i}$), as well as the truncated *E. coli* versions (N-terminal domain, $LpoA^N$ and C-terminal domain, $LpoA^C$), were grown and protein overexpression induced as described in section 2.3.1, with the exception of using 500 mM NaCl. Sonication and ultracentrifugation of the lysate was followed by IMAC (section 2.3.3) using buffer 1 (25 mM Tris/HCl, 10 mM $MgCl_2$, 500 mM NaCl, 20 mM imidazole, 10% glycerol, pH 7.5) and buffer 2 (25 mM Tris/HCl, 500 mM NaCl, 400 mM Imidazole, 10% glycerol, pH 7.5). LpoA, $LpoA_{H.i}$ and $LpoA^C$ required IEX using a HiTrap Q HP column as a second purification step (section 2.3.4), whereas $LpoA^N$ required only SEC (section 2.3.6), using 25 mM HEPES/NaOH, 500 mM NaCl, 10% glycerol, pH 7.5 as running buffer. After IEX, LpoA, $LpoA_{H.i}$ and $LpoA^C$ were also purified by SEC. Fractions with the highest yield and purity were pooled, concentrated and dialysed against storage buffer before being frozen at -80°C. See figure 2.2 for the SDS-PAGE gels of the purified LpoA versions.

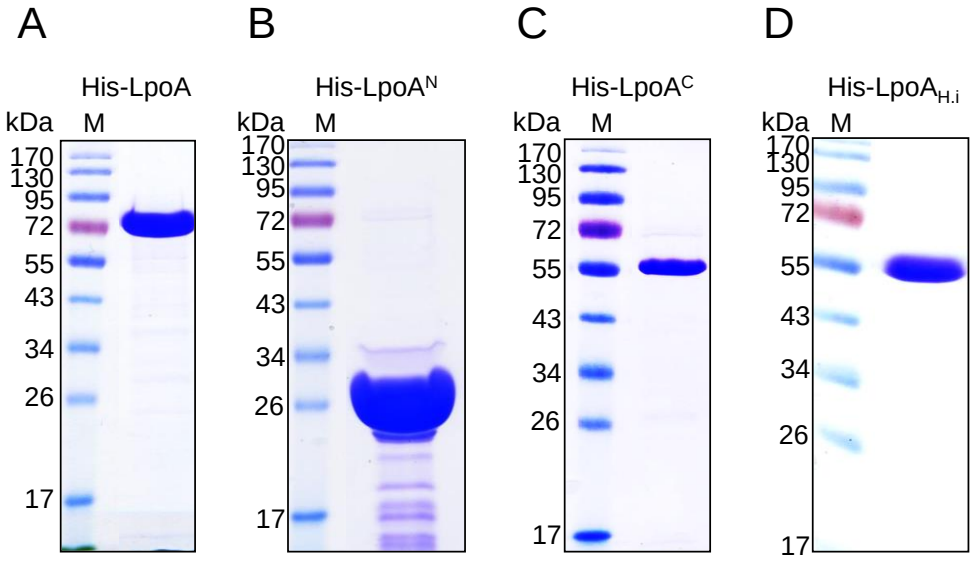

Figure 2.2 SDS-PAGE analysis of purified LpoA versions

Analysis of protein yield and purity of *E. coli* His-LpoA (72 kDa) (**A**), His-$LpoA^N$ (28 kDa) (**B**), His-$LpoA^C$ (55 kDa) (**C**) and full length His-LpoA from *H. influenzae* (55 kDa) (**D**). Proteins were separated by 12% SDS-PAGE and visualised by Coomassie staining.

2.4.2 Purification of PBP1A from *E. coli* and *H. influenzae*

This protocol is as described in [67]. *E. coli* BL21(DE3) cells carrying the plasmid pTK1A-His-PBP1A or pET28-His-PBP1A from *H. influenzae* were grown in 4 L of LB supplemented with 50 µg/ml kanamycin to an OD_{578} of 0.3 at 30°C. Overexpression was induced with 0.05 mM IPTG for a further 90 min at 30°C before harvesting the cells by centrifugation (7500 × g, 4°C, 15 min). Cells were resuspended in 30 ml of buffer 1 (25 mM Tris/HCl, 10 mM $MgCl_2$, 100 mM NaCl, pH 7.5) before sonication and ultracentrifugation (140000 × g, 4°C, 60 min). The resulting pellet was resuspended in 20 ml of salt buffer (25 mM Tris/HCl, 10 mM $MgCl_2$, 1 M NaCl, 20% glycerol, pH 7.5) and homogenised. The cells were ultracentrifuged again and the pellet resuspended in 20 ml of extraction buffer (25 mM Tris/HCl, 10 mM $MgCl_2$, 1 M NaCl, 2% Triton X-100, 20% glycerol, pH 7.5) before o/n incubation at 4°C with stirring.

The solubilised membrane-containing supernatant was obtained by ultracentrifugation (140000 × g, 4°C, 60 min) and applied to 2 ml of Ni^{2+}-Nitrilotriacetic acid (NTA) Superflow beads (Qiagen), prewashed with dH_2O and equilibrated with buffer A (25 mM Tris/HCl, 10 mM $MgCl_2$, 1 M NaCl, 5 mM imidazole, 20% glycerol, pH 7.5), for 2 h at 4°C with gentle mixing. Beads were obtained using a gravity column and were washed with 50 ml of buffer A. Elution of bound proteins was carried out with 10 × 1 ml of buffer B (25 mM Tris/HCl, 10 mM $MgCl_2$, 1 M NaCl, 400 mM imidazole, 20% glycerol, pH 7.5).

The protein buffer was gradually changed by o/n dialysis against dialysis buffer 1 (25 mM Tris/HCl, 10 mM $MgCl_2$, 1 M NaCl, 10% glycerol, pH 7.5), followed by 90 min against dialysis buffer 2 (10 mM NaAcetate, 10 mM $MgCl_2$, 500 mM NaCl, 10% glycerol, pH 4.8) and finally 90 min against dialysis buffer 3 (10 mM NaAcetate, 10 mM $MgCl_2$, 200 mM NaCl, 10% glycerol, pH 4.8). The protein sample was diluted 1:1 with dilution buffer (10 mM NaAcetate, 10 mM $MgCl_2$, pH 4.8) and applied to a prewashed and equilibrated 5 ml HiTrap SP HP column in IEX buffer 1 (10 mM NaAcetate, 10 mM $MgCl_2$, 100 mM NaCl, 0.1% Triton X-100, 10% glycerol, pH 4.8). The column was washed with 50 ml of IEX buffer 1 before eluting bound proteins using a 0-100% salt gradient with IEX buffer 2 (10 mM NaAcetate, 10 mM $MgCl_2$, 1 M NaCl, 0.1% Triton X-100, pH 4.8). After analysis by SDS-PAGE, fractions containing the highest yield and purity were dialysed o/n against storage buffer (25 mM HEPES/NaOH, 10 mM $MgCl_2$, 300 mM NaCl, 0.1% Triton X-100, pH 7.5) before being aliquoted and stored at -80ºC. See figure 2.3A/B for the SDS-PAGE gels of purified PBP1A versions.

2.4.3 Purification of the outer-membrane PBP1A docking domain (ODD)

This protocol was developed and optimised by Adeline Derouaux from the Vollmer lab. BL21(DE3) cells harbouring the plasmid pQE30-His-ODD were grown in 1 L of LB supplemented with 50 µg/ml of kanamycin to an OD_{578} of 0.6 at 37°C and left for a further 2 h (no IPTG induction required). Cells were pelleted by centrifugation (7500 × g, 15 min, 4°C) and resuspended in 12 ml of buffer 1 (25 mM Tris/HCl, 20 mM imidazole, 200 mM NaCl, 10% glycerol, pH 7.5) before sonication and ultracentrifugation (140000 × g, 1 h, 4°C). The resulting supernatant was applied to 2 ml of washed and equilibrated Ni^{2+}-NTA bead resin and incubated o/n at 4°C with mixing. The beads were washed with 40 ml of buffer 1 before elution of bound proteins with elution buffer (25 mM Tris/HCl, 400 mM imidazole, 200 mM NaCl, 10% glycerol, pH 7.5) collecting 10 × 1 ml fractions. Peak fractions were pooled and applied to a HiLoad 16/60 Superdex 200 column for SEC in 25 mM HEPES/NaOH, 100 mM NaCl, 10% glycerol, pH 7.5 (section 2.3.6). Peak fractions were collected and analysed by SDS-PAGE before being concentrated, aliquoted and stored at -80°C. See figure 2.3C for the SDS-PAGE gel of purified His-ODD.

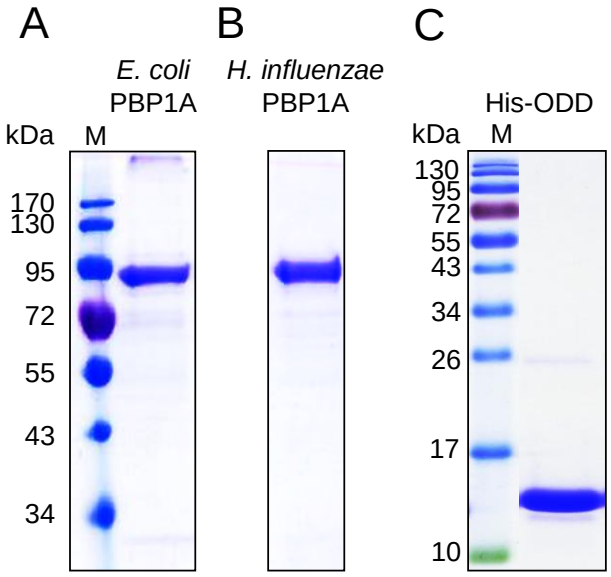

Figure 2.3 SDS-PAGE of PBP1A from *E. coli* and *H. influenzae* and the ODD from *E. coli*

Analysis of protein purity and yield of thrombin-cleaved His-PBP1A from *E. coli* (**A**) and *H. influenzae* (**B**) both at ~93 kDa and His-ODD from *E. coli* PBP1A (13 kDa) (**C**). Proteins were separated by 12% (A and B) or 15% (C) SDS-PAGE and visualised by Coomassie staining.

2.4.4 Purification of PBP4 versions

PBP4 and PBP4 S62A purification

This protocol is as described in [115]. Protocol for growth of cells is as stated in section 2.3.1. BL21(DE3) pET21-PBP4 or BL21(DE3) pET21-PBP4(S62A) were grown with 100 µg/ml ampicillin, and protein overexpression was induced with 1 mM IPTG for 8 hours at 20°C before harvesting cells by centrifugation. Cell pellets were resuspended in 40 ml of pre-cooled buffer 1 (50 mM Tris/HCl, 30 mM NaCl, pH 6.8). After sonication and ultracentrifugation, native PBP4 versions were purified using a 5 ml HiTrap SP HP IEX column (section 2.3.4) before hydroxyapatite purification (section 2.3.5) and SEC using 25 mM HEPES/NaOH, 300 mM NaCl, 10% Glycerol, pH 6.8 as a running buffer (section 2.3.6). Fractions of the highest yield and purity were concentrated, aliquoted and stored at -80°C. See figure 2.4A/B for the SDS-PAGE gel of purified PBP4 and PBP4(S62A).

His-PBP4 delta domain 3 (PBP4ΔD3)

BL21(DE3) pET28a-His-PBP4 Δ173-247 (domain 3) cells were cultivated and protein overexpression induced as described in section 2.3.1 in LB supplemented with 50 µg/ml kanamycin. After harvesting, sonication and ultracentrifugation, the protein was purified via IMAC, IEX and SEC by the standard protocols described in sections 2.3.3, 2.3.4 and 2.3.6, with a final storage buffer consisting of 25 mM HEPES/NaOH, 300 mM NaCl, 10% glycerol, pH 7.5. Purified protein samples were pooled, concentrated and stored at -80°C. This construct encodes a non-cleavable His-Tag. See figure 2.4C for the SDS-PAGE gel of purified His-PBP4ΔD3.

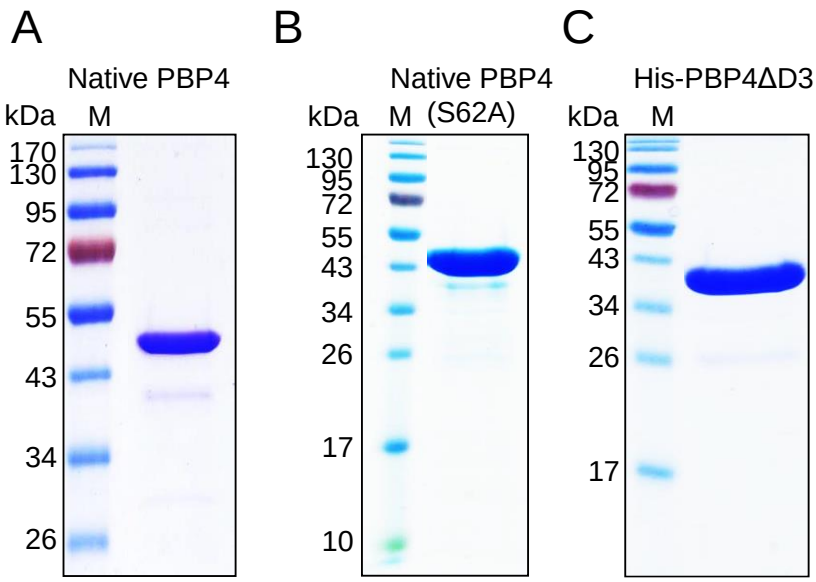

Figure 2.4 SDS-PAGE analysis of purified PBP4 versions

Analysis of final protein purity and yield of PBP4 (51 kDa) (**A**), PBP4(S62A) (51 kDa) (**B**) and His-PBP4ΔD3 (42 kDa) (**C**). Proteins were separated by 12% SDS-PAGE and visualised by Coomassie staining.

2.4.5 Purification of PBP7 versions

PBP7 and PBP7 S67A purification

BL21(DE3) pET28a-His-PBP7 or BL21(DE3) pET28a-His-PBP7(S67A) cells were grown and protein overexpression induced as described in section 2.3.1 in LB supplemented with 50 µg/ml kanamycin. Purification was carried out by IMAC using buffer 1 (25 mM HEPES/NaOH, 500 mM NaCl, 20 mM imidazole, 10% glycerol, pH 7.5) and buffer 2 (25 mM HEPES/NaOH, 300 mM NaCl, 400 mM imidazole, 10% glycerol, pH 7.5) (section 2.3.3) and SEC using (25 mM HEPES/NaOH, 500 mM NaCl, 10% glycerol, pH 7.5) (section 2.3.6). Purified protein was analysed by SDS-PAGE, concentrated, aliquoted and stored at -80°C. See figure 2.5A/B for the SDS-PAGE gels of purified PBP7 and PBP7(S67A).

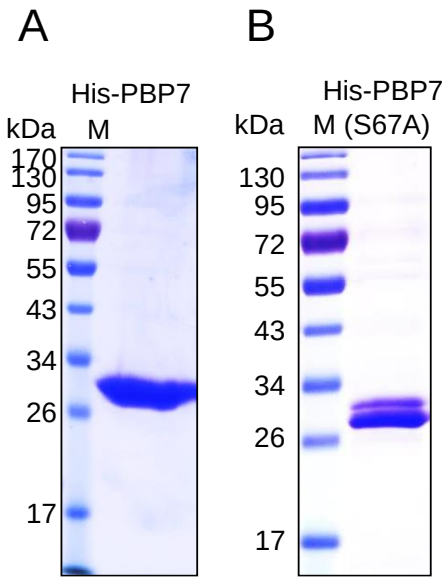

Figure 2.5 SDS-PAGE analysis of purified PBP7 versions

Analysis of final protein purity and yield of His-PBP7 (33 kDa) (**A**) and His-PBP7(S67A) (32 kDa) (**B**). Proteins were separated by 12% SDS-PAGE and visualised by Coomassie staining.

2.4.6 Purification of MepS versions

MepS and MepS C68A purification

This protocol was optimised as part of this project. BL21(DE3) pET21b-His-MepS or BL21(DE3) pET21b-MepS(C68A) cells were grown in 4 L of LB supplemented with 50 µg/ml kanamycin at 37°C to an OD_{578} of 0.5-0.6 before the induction of protein overexpression with 1 mM IPTG for 90 min at 37°C. Purification was carried out by IMAC and SEC as described in 2.3.3 and 2.3.6 using 25 mM HEPES/NaOH, 300 mM NaCl, 10% glycerol, pH 7.5 as SEC running buffer. Purified protein was analysed by SDS-PAGE concentrated, aliquoted, and stored at -80°C. See figure 2.6A/B for the SDS-PAGE gels of purified MepS and MepS(C68A).

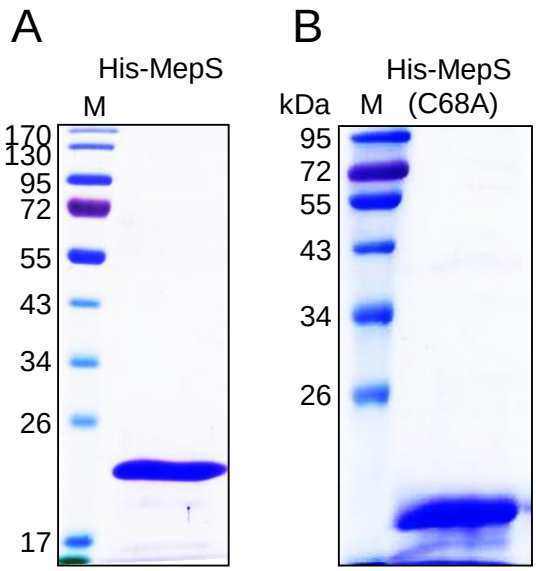

Figure 2.6 SDS-PAGE analysis of purified MepS versions

Analysis of final protein purity and yield of His-MepS (21 kDa) (**A**) and His-MepS(C68A) (21 kDa) (**B**). Proteins were separated by 12% SDS-PAGE and visualised by Coomassie staining.

2.4.7 Purification of MepM

This protocol was optimised as part of this project. BL21(DE3) pET21b-His-MepM cells were grown in 3 L of LB at 37°C in LB supplemented with 50 µg/ml kanamycin to an OD_{578} of 0.5-0.6 before the induction of protein overexpression with 50 µM IPTG for 2 h at 25°C. Purification was carried out by IMAC and SEC as described in 2.3.3 and 2.3.6 using 25 mM HEPES/NaOH, 300 mM NaCl, 10% glycerol, pH 7.5 as SEC running buffer. After analysis by SDS-PAGE, fractions with the highest purity and yield were concentrated, aliquoted and stored at -80°C. See figure 2.7 for the SDS-PAGE gel of purified MepM.

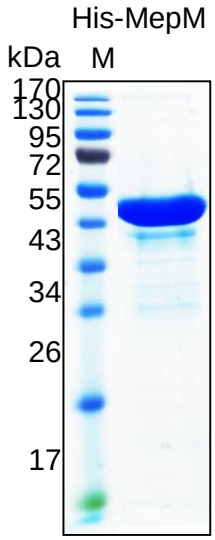

Figure 2.7 SDS-PAGE analysis of purified MepM

Analysis of final protein purity and yield of His-MepM (49 kDa). Protein was separated by 12% SDS-PAGE and visualised by Coomassie staining.

2.4.8 Purification of MepA

This protocol belongs to the Vollmer group. MC1061 pJFK-MepA cells lacking the soluble lytic transglycosylase, Slt, were grown o/n with 0.8% glucose and 50 µg/ml kanamycin and inoculated 1:200 into 5 L of LB supplemented with 12% sucrose and 50 µg/ml kanamycin to an OD_{578} of 0.6 at 37°C. Overproduction of native MepA was induced with 1 mM IPTG for a further 1 h at 37°C. After 10 min on ice and harvesting by centrifugation, cells were resuspended in 50 ml buffer 1 (10 mM Tris/Maleate, 10 mM $MgCl_2$, pH 6.5) and lysed by sonication. The soluble fraction was obtained by ultracentrifugation and IEX was carried out using a 5 ml HiTrap SP HP column in buffer A (10 mM Tris/Maleate, 10 mM $MgCl_2$, pH 5.2) and washed for 50 ml before the elution of bound proteins using a 100 ml salt gradient of 0-100% buffer B (10 mM Tris/Maleate, 10 mM $MgCl_2$, 1 M NaCl, pH 5.2) at 2 ml/min collecting 4 ml fractions. Appropriate fractions were pooled and concentrated for SEC in 25 mM HEPES/NaOH, 300 mM NaCl, 10% glycerol, pH 7.5. Fractions with the highest yield and purity were pooled, concentrated and stored at -80°C. See figure 2.8 for the SDS-PAGE gel of purified native MepA.

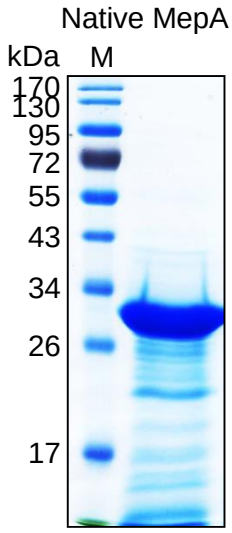

Figure 2.8 SDS-PAGE analysis of purified MepA

Analysis of protein purity and yield of native MepA (31 kDa). Protein was separated by 12% SDS-PAGE and visualised by Coomassie staining.

2.4.9 Purification of NlpI(sol)/NlpIΔC11(sol)

This protocol is as described in [233]. BL21(DE3) pET28-His-NlpI or BL21(DE3) pET28-His-NlpIΔC11 were grown in LB supplemented with 50 µg/ml kanamycin, and overproduction induced, as described in section 2.3.1. Cells were pelleted by centrifugation (7500 × g, 15 min, 4°C) and resuspended in 40 ml of buffer 1 (25 mM Tris/HCl, 200 mM NaCl, pH 7.5) before sonication and ultracentrifugation. His-NlpI or His-NlpIΔC11 were purified using IMAC using buffer 1 as running buffer and buffer 1 with 400 mM imidazole for the step-wise elution of bound proteins. The resulting purification was excellent, and only SEC was necessary as a second purification method, in 25 mM HEPES/NaOH, 200 mM NaCl, 10% glycerol, pH 7.5. IEX was carried out if a thrombin cleavage step was required after IMAC. Purified proteins were pooled, concentrated and stored at -80°C. See figure 2.9 for the SDS-PAGE gel of purified His-NlpI and His-NlpIΔC11.

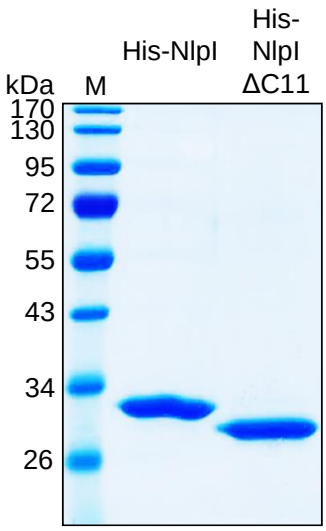

Figure 2.9 SDS-PAGE analysis of purified His-NlpI and His-NlpIΔC11

Analysis of protein purity and yield of His-NlpI(sol) (33 kDa) and His-NlpIΔC11 (32 kDa). Proteins were separated by 12% SDS-PAGE and visualised by Coomassie staining.

2.4.10 Purification of EnvC

E. coli BL21(DE3) cells harbouring the plasmid pET28-His-EnvC, were cultivated in LB supplemented with 50 µg/ml kanamycin, and protein overexpression induced as described in section 2.3.1. Cells were harvested by centrifugation, resuspended in buffer 1 (25 mM HEPES/NaOH, 300 mM NaCl, pH 7.5), sonicated and ultracentrifuged to obtain the soluble fraction. His-EnvC was purified by IMAC and SEC as described in section 2.3.3 and 2.3.6 using buffer 1 as SEC running buffer. Fractions with the highest yield and purity were pooled, concentrated and stored at -80°C in 10% glycerol. See figure 2.10 for the SDS-PAGE gel of purified His-EnvC.

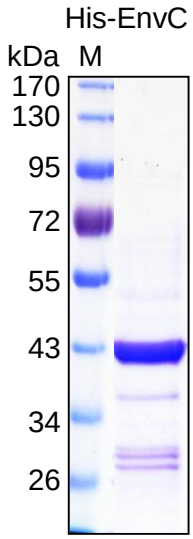

Figure 2.10 SDS-PAGE analysis of purified His-EnvC

Analysis of protein purity and yield of His-EnvC (43 kDa). Protein was separated by 12% SDS-PAGE and visualised by Coomassie staining.

2.5 Advanced protein methods

2.5.1 Interaction assays

2.5.1.1 Preparation of *E. coli* periplasmic extract for affinity chromatography

This protocol was adapted from [237]. O/n cultures of MC1061 cells were used to inoculate 2 L of LB which were grown, with orbital shaking at 37°C, until an OD_{578} of 0.5-0.6 was reached. Cells were harvested by centrifugation (7500 × g, 4°C, 15 min) and resuspended in 16 ml of 100 mM Tris/HCl, pH 8.0. Cells were centrifuged again and resuspended in 8 ml of 200 mM Tris/HCl, pH 8.0. Another 8 ml of 200 mM Tris/HCl, pH 8.0 was added, this time containing 1 M sucrose, 1 mM EDTA and 1 ml of 1 mg/ ml lysozyme. Cells were incubated with 17.6 ml of H_2O and DNase for 30-60 min at RT until cells became 90% spheroplasts as observed by light microscopy (see figure 2.11). Cells were centrifuged (12000 × g, 4°C, 30 min) and the periplasm-containing supernatant dialysed in equal volumes against high salt buffer (10 mM Tris/Maleate, 10 mM $MgCl_2$, 400 mM NaCl, 10% glycerol, pH 7.2) and low salt buffer (10 mM Tris/Maleate, 10 mM $MgCl_2$, 150 mM NaCl, 10% glycerol, pH 7.2).

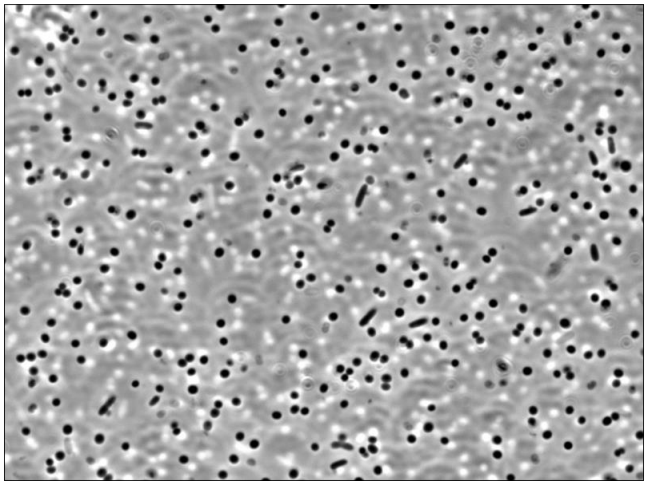

Figure 2.11 Light microscopy image of spheroplasts during periplasmic extraction

Cells after an osmotic shock became spheroplasts.

2.5.1.2 Preparation of *E. coli* membrane extract for affinity chromatography

This protocol was adapted from [237]. O/n cultures of MC1061 cells were grown in 2 L of LB at 37ºC with orbital shaking to an OD_{578} of 0.5-0.6 before harvesting by centrifugation (7500 × g, 4°C, 15 min). Cells were resuspended in 20 ml of 10 mM Tris/maleate, pH 7.2 with the addition of 1/1000 PIC, 100 µM PMSF and DNase. Cells were disrupted by sonication and were ultracentrifuged (140000 × g, 4°C, 1 h). The supernatant was discarded and the membrane-containing pellet was resuspended in 20 ml of 10 mM Tris/maleate, 1 mM EDTA, 1 M NaCl, 2% Triton X-100, pH 6.8 and incubated at 4°C o/n with agitation. Solubilised membrane extract was isolated by ultracentrifugation (140000 × g, 4°C, 1 h) and the supernatant dialysed in equal volumes against high salt buffer (10 mM Tris/Maleate, 10 mM $MgCl_2$, 400 mM NaCl, 10% glycerol, pH 7.2) and low salt buffer (10 mM Tris/Maleate, 10 mM $MgCl_2$, 150 mM NaCl, 10% glycerol, pH 7.2).

2.5.1.3 Affinity chromatography

This protocol was adapted from [237]. For the immobilisation of purified protein, 0.8 g of desiccated CNBr-activated sepharose beads (GE Healthcare) were re-hydrated with 200 ml of 1 mM HCl before the addition of 8-10 mg of purified protein in 10 ml of coupling buffer (100 mM $NaHCO_3$, 10 mM $MgCl_2$, 500 mM NaCl, 0.1% Triton X-100, pH 8.3) o/n with agitation. A control column was used in parallel, absent of protein. The beads were washed with 25 ml of coupling buffer and any remaining active groups were blocked with high Tris blocking buffer (200 mM Tris/HCl, 10 mM $MgCl_2$, 500 mM NaCl, 0.1% Triton X-100, pH 8.0) o/n with agitation at 4°C. The beads were washed with three cyclic alterations of blocking buffer and acetate buffer (100 mM NaAcetate, 10 mM $MgCl_2$, 500 mM NaCl, 0.1% Triton X-100, pH 4.8) before washing with 10 ml of binding buffer (10 mM Tris/HCl, 10 mM $MgCl_2$, 50 mM NaCl, 0.1% Triton X-100, pH 7.2). Depending on the desired experiment, 10 ml of the low salt isolated membrane or periplasmic extracts from section 2.5.1.1 and 2.5.1.2 respectively, were applied to the beads o/n with agitation at 4°C. Alternatively, a 1:1 mixture of the extracts was also used.

After incubation, the whole sample was applied to a gravity column and the flow-through was collected. The isolated beads were washed with 50 ml of binding buffer before the elution of weakly bound proteins using 20 ml of low salt elution buffer 1 (10 mM Tris/HCl, 10 mM $MgCl_2$, 150 mM NaCl, 0.1% Triton X-100, pH 7.2) plus a final elution step with low salt elution buffer 2 (10 mM Tris/HCl, 10 mM $MgCl_2$, 1 M NaCl, 0.1% Triton X-100, pH 7.2).

The columns were washed with 10 ml of high salt binding buffer (10 mM Tris/HCl, 10 mM $MgCl_2$, 400 mM NaCl, 0.1% Triton X-100, pH 7.2) before 10 ml of high salt membrane/periplasmic/mixture extract was applied and incubated o/n with agitation at 4°C. As before, the flow-through was collected and the beads washed with binding buffer and bound proteins eluted with high salt elution buffer 3 (10 mM Tris/HCl, 10 mM $MgCl_2$, 2 M NaCl, 0.1% Triton X-100, pH 7.2).

Samples from each fraction (flow-through, washes, elution 1, elution 2 and elution 3) were resolved by SDS-PAGE and proteins transferred to a nitrocellulose membrane by Western blotting, using purified antibodies for primary immunodetection.

2.5.1.4 Proteomics-based identification of interacting proteins

Equal volumes of membrane and periplasmic fractions (low salt or high salt) were combined 1:1 with dialysis buffer (10 mM Tris/Maleate, 10 mM $MgCl_2$, 100 mM NaCl, pH 7.2) and dialysed o/n against 3 L of the same dialysis buffer. The protein of choice was diluted to 2 mg/ml in coupling buffer (50 mM NaH_2PO_4, 500 mM NaCl, pH 8.0) and was dialysed o/n against the same buffer.

To a 2 ml reaction tube, 300 µl of Affigel (BioRad) bead suspension was added and washed with ice cold H_2O, and equilibrated with coupling buffer before the addition of 500 µl of dialysed protein. The samples were incubated o/n at 4°C with gentle agitation. In parallel, coupling buffer was applied to washed Affigel beads absent of protein, as a negative control. After incubation, the beads were obtained by centrifugation (4000 × g, 4 min, 4ºC) and were firstly washed with blocking buffer (200 mM Tris/maleate, 500 mM NaCl, pH 8.0) before incubation with blocking buffer for 3 h at 4°C with agitation.

Beads were isolated by centrifugation as before and washed with elution buffer (10 mM Tris/maleate, 500 mM NaCl, 0.2% N-lauroylsarcosine), to remove any non-specifically bound contaminants, and equilibrated with binding buffer (10 mM Tris/maleate, 10 mM $MgCl_2$, 100 mM NaCl, 1% Triton X-100, pH 7.2). To the protein-loaded beads, 1.5 ml of the dialysed membrane/periplasmic fraction was added and incubated o/n at 4°C with agitation. Samples were centrifuged and the supernatant collected before transferring the beads to clean tubes and washing with binding buffer and low triton wash buffer (10 mM Tris/Maleate, 10 mM $MgCl_2$, 100 mM NaCl, pH 7.2). The beads were again transferred to spin-dry columns (Generon Proteus Clarification Mini Spin Column) and any retained proteins were eluted with 250 µl of elution buffer. Eluted proteins were precipitated with 750 µl of ethanol and stored at -20°C

o/n. For the identification of novel interaction partners, samples were centrifuged (14000 × g, 20 min, 4°C) and the supernatant removed and left to air-dry. Once complete, the samples were sent for mass spectroscopy analysis by Dr. Joe Gray at the Pinnacle Institute, Newcastle University.

2.5.1.5 *In vitro* cross-linking and pull-down experiments

The hexahistidine tag, used for the purification of many of the proteins in this project, binds to Ni^{2+}-NTA bead resin (Qiagen) and proteins lacking this tag are not retained. We utilise these properties for the rapid identification of *in vitro* interactions. The retention of one native protein of interest in the presence of another possessing a hexahistidine tag by Ni^{2+} beads, whilst not being retained alone, is indicative of an interaction.

Equimolar concentrations (2 µM unless stated) of purified proteins of interest were incubated in 200 µl of binding buffer (10 mM HEPES/NaOH, 10 mM $MgCl_2$, 150 mM NaCl, 0.05% Triton X-100, pH 7.5) for 10 min on ice. Proteins of interest (one tagged, one native) were cross-linked with 1.08 µl of 30% formaldehyde (final concentration 0.2% by volume). After incubating the samples at 37ºC for 15 min, any excessive cross-linking was blocked with 100 mM Tris/HCl, pH 7.5. In each experiment, the individual His-tagged and native proteins were treated the same as the mixture. An aliquot was taken prior to incubation with Ni^{2+}-NTA beads as an applied sample for subsequent SDS-PAGE analysis.

Ni^{2+}-NTA beads were prepared by washing 100 µl bead suspension, per sample, with 2 × 1.5 ml of H_2O and equilibration with 2 × 1.5 ml of binding buffer. Protein samples were applied to equilibrated beads with 1.3 ml of binding buffer and incubated o/n with agitation at 4°C. Samples were centrifuged (4000 × g, 4 min, 4°C) and the beads washed 6 × 1 ml with wash buffer (10 mM HEPES/NaOH, 10 mM $MgCl_2$, 150 mM NaCl, 50 mM imidazole, 0.05% Triton X-100, pH 7.5). Beads were resuspended in 250 µl of wash buffer and transferred to spin-dry columns and centrifuged (4000 × g, 5 min, RT). The isolated beads were transferred to clean reaction tubes and bound proteins eluted, and cross-linking reversed, by the addition of 50 µl of SDS-PAGE loading buffer and boiling for 10 min. Samples were centrifuged (10000 × g, 5 min, RT) and resolved by SDS-PAGE alongside the respective applied samples (table 2.2).

His-protein + Native protein		His-protein		Native protein	
Applied	Elution	Applied	Elution	Applied	Elution

Table 2.2 Example SDS-PAGE scheme of an *in vitro* Ni^{2+}-bead pull-down experiment

An aliquot was taken prior to incubation with Ni^{2+}-NTA beads (Applied). A sample was taken after thorough washing, reversing of cross-linkage and elution. A mixture of a His-tagged protein and a native protein are compared to the individual proteins.

2.5.1.6 Surface plasmon resonance (SPR)

The protocol is as described in, and adapted from [237] and carried out using a ProteOn XPR36 system (Biorad). Running buffer consisted of 10 mM Tris/maleate, 150 mM NaCl, 0.05% Triton X-100, pH 7.5.

All immobilised proteins, excluding PBP1A, were immobilised directly to a GLC general amine coupling SPR sensorchip, after activation of the chip using N-Hydroxysuccinimide (NHS) and 1-ethyl-3-(3-dimethylaminopropyl)-carbodiimide hydrochloride (EDC) coupling, as per manufacturer's instructions. An empty control lane was activated and applied with running buffer absent of protein. After activation and immobilisation, the chip surface was washed with high salt regeneration buffer (10 mM Tris/maleate, 1 M NaCl, 0.05% Triton X-100, pH 7.5) and any remaining unsaturated amino groups blocked with the application of ethanolamine. The surface was washed again with regeneration buffer and equilibrated with running buffer. Up to 6 analytes could be applied to the surface at 75-100 µl/min for 3-5 min at 25°C.

For the creation of a PBP1A surface, 10 mg/ml of ampicillin in 0.1 mM sodium acetate, pH 4.6 was firstly immobilised by general amine coupling as per manufacturer's instructions, before the application of 75 µg/ml PBP1A at 30 µl/min for 5 min, at 35ºC. As before, a control lane was activated in parallel in which ampicillin was immobilised but no protein was applied. After the immobilisation of PBP1A, the surface was washed with regeneration buffer, before any free ampicillin was hydrolysed with the application of 1 µM of the β-lactamase Vim4 (*Pseudomonas aeruginosa*, Adeline Derouaux, Vollmer group). Prior to application of the analyte, the surface was washed with regeneration buffer and equilibrated with running buffer.

The associated ProteOn software was used to calculate the equilibration response (R_{eq}) values which were plotted against analyte concentration. Scratchard analysis by non-linear regression was used to estimate the dissociation constant (K_D) of an interaction.

2.5.1.7 Microscale thermophoresis (MST)

Microscale thermophoresis (MST) is a technique by which biomolecular interactions can be observed in solution and without the need for immobilisation, thereby providing a 'close-to native' environment. MST refers to the movement of molecules along a microscopic temperature gradient; a movement which is sensitive to minute changes in the solvation state of a protein, as well as its charge and size, changes that occur upon an interaction with another protein. By titrating a serially-diluted unlabelled ligand with a fluorescently-tagged protein of constant concentration, these changes can be tracked and dissociation constants estimated from any resulting equilibration/cooperative binding events [238]. Movement of the fluorescently-tagged protein can occur along the temperature gradient, or against the temperature gradient. It is not yet known which protein properties are attributable to this effect, but binding events may occur from a low FNorm to a high FNorm or vice versa. In both instances K_D estimation can be undertaken.

The protocol was carried out as per manufacturer's instructions and as described in [238] using a Monolith NT.115^{TM} series MST machine (Nanotemper).

One protein of interest was fluorescently-labelled, as per manufacturer's instructions, using either amine reactive dye (NT-647 N-hydroxysuccinimide [NHS]) or cysteine reactive dye (NT-647 malaimide). The choice of dye can depend upon, for example, the participation of cysteines in structurally integral disulphide bonds or perhaps the lack of surface exposed lysines for amine-based labelling. Both methods are suitable for use and neither gives better or worse results, however, cysteine labelling can be better for estimating interaction sites due the amino acid specificity of labelling. Optimisation of an appropriate concentration of fluorescently-labelled protein (200-1500 fluorescence units) was carried out by adjusting the LED power and capillary coating (standard, hydrophobic, hydrophilic, or premium) before starting the experiment. The unlabelled ligand was two-fold serially diluted 16 times in MST running buffer (25 mM HEPES/NaOH, 150 mM NaCl, 0.05% Triton X-100, pH 7.5) before the addition of an optimised constant concentration of fluorescently-labelled protein, taking into account the resulting dilution effect of combining labelled and unlabelled proteins. Prior to every experiment a 'cap scan' was completed to measure the fluorescence of each sample and determine the exact position of each capillary. The resulting temperature jump and subsequent thermophoresis data were used to trace unlabelled ligand concentration against normalised fluorescence trace (FNorm). The dissociation constant (K_D) can be estimated using the accompanying Nanotemper Analysis software. Figure 2.12 depicts how the machine works and a typical MST timetrace.

SDS-Denaturation (SD) test

Occasionally, during the pre-experiment cap-scan, it was clear that the binding of the unlabelled ligand caused a concentration-dependent fluorescence change, either fluorescence quenching or enhancement. If this change resulted in a binding curve it was possible to use the raw fluorescence data to estimate the apparent K_D. In these cases, an SDS-Denaturation (SD) test was completed to rule out fluorescence changes due to protein aggregation. Once the initial samples have been run and the cap-scan completed, the samples containing the three highest and three lowest concentrations of unlabelled ligand were centrifuged (10000 × g, 5 min). The supernatant was collected and 10 µl was mixed 1:1 with 4% SDS and 40 mM DTT before boiling for 10 min. Samples were briefly centrifuged before analysing the fluorescence again by cap-scan. If the fluorescence across all six samples was now uniform, the initial change in fluorescence was due to a ligand binding event close to where the fluorophore was situated and the apparent K_D could be calculated using the raw fluorescence values (see figure 2.13). In these instances the y-axis will be labelled 'fluorescence' instead of the usual 'FNorm' and the capillary scan of the SD-test will be shown in the corresponding raw data figure in the appendix. If the change in fluorescence was still evident, the fluorescently-labelled protein may be aggregating. To solve this problem the samples were centrifuged again to remove large aggregates, the capillary coating changed, or 0.05% BSA or Tween 20 was added.

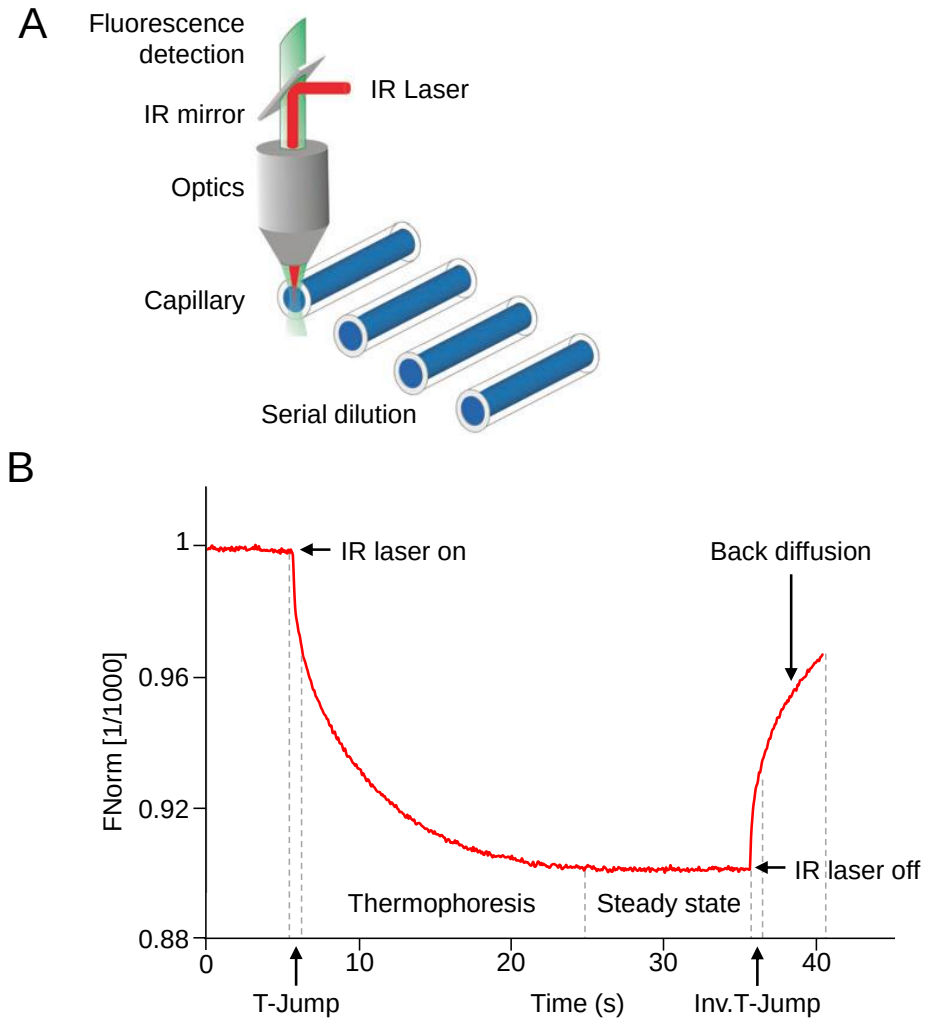

Figure 2.12 Principles of Microscale Thermophoresis (MST)

A. Adapted from [238]. An infrared (IR) laser (wavelength 1470 nm) is used to create a localised temperature gradient. The laser is coupled into the path of fluorescent excitation and emission using an IR dichroic mirror. Each capillary contains a fluorescently-labelled protein of constant concentration and a serially diluted unlabelled ligand. The thermophoretic movement of the fluorescently-labelled protein is measured. Interactions between proteins of interest lead to changes in solvation state, size and charge of the fluorescent protein which change its thermophoretic movement. **B.** A typical MST timetrace. The IR laser causes an initial temperature jump (T-Jump) before thermophoretic movement is observed away, or towards the site of excitation. Turning off of the IR laser leads to a rapid inverse temperature jump (Inv.T-jump) before the back diffusion of molecules. Serial dilution of an unlabelled ligand allows observation of concentration dependent changes on the thermophoretic movement of the fluorescently-labelled proteins. The accompanying software is used to estimate the dissociation constant of an interaction.

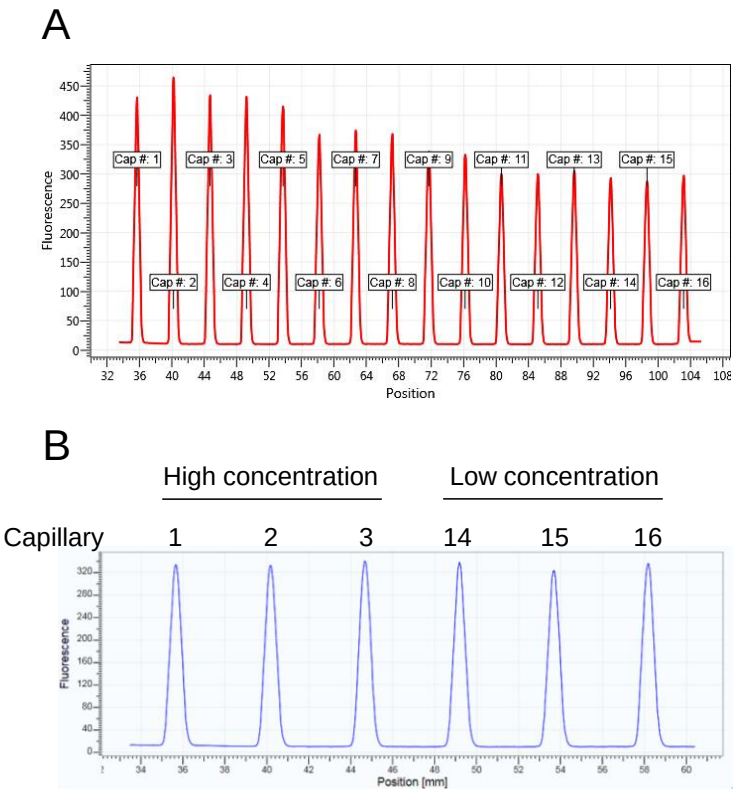

Figure 2.13 Ligand dependent fluorescence quenching/enhancement

A. Example of a pre-experiment cap-scan showing ligand concentration-dependent fluorescence enhancement (cap 1 – cap 16 = High concentration – low concentration). **B.** Cap-scan of the three highest and lowest ligand concentration samples after performing an SDS-denaturation (SD) test. Fluorescence is the same for each sample indicating the fluorescence enhancement was due to a ligand binding event and an apparent K_D can be calculated from the raw fluorescence data.

2.5.1.8 *In vivo* co-immunoprecipitation assay

Method is described in, and adapted from [205]. An o/n culture of *E. coli* BW25113 cells and an appropriate mutant strain was used to inoculate 150 ml of Lennox LB (Fisher Scientific) and was cultivated to an OD_{578} of 0.5-0.6 at 37°C before harvesting by centrifugation (4500 × g, 4°C, 25 min). Cells were resuspended in 6 ml of CL buffer 1 (50 mM NaH_2PO_4, 20% sucrose, pH 7.4). The amine reactive cross-linker, DTSSP (3,3'-dithiobis (sulfosuccinimidylpropionate) (ThermoFisher), was freshly dissolved (20 mg/ml in dH_2O) and added to the isolated cell suspension and incubated at 4°C with agitation for 1 h. Cross-linked cells were then harvested by centrifugation (4500 × g, 4°C, 25 min) and resuspended in 6 ml CL buffer 2 (100 mM Tris/HCl, 10 mM $MgCl_2$, 1 M NaCl, pH 7.5). DNase, PIC and PMSF were added prior to sonication at low levels before ultracentrifugation of the lysate (140000 × g, 4°C, 1 h). The membrane pellet was resuspended in 2.5 ml of CL buffer 3 (25 mM Tris/HCl, 10 mM $MgCl_2$, 1 M NaCl, 1% Triton X-100, 20% glycerol, pH 7.5) and the solubilised membrane extracted o/n with stirring at 4°C.

Samples were ultracentrifuged (140000 × g, 4°C, 1 h) to remove debris, before removing 2 × 1.2 ml of each supernatant to be subsequently diluted with 0.6 ml of CL buffer 4 (75 mM Tris/HCl, 10 mM $MgCl_2$, 1 M, NaCl, pH 7.5). One sample was incubated with an optimised concentration of specific antibody with the other used as a negative control. Both samples were incubated at 4°C with agitation for 5 h. For the isolation of antibodies, and thus cross-linked interaction partners, 100 µl of protein G-coupled agarose bead resin (Roche) were washed (2 × CL buffer 4, 2 × CL wash buffer [2:1 CL buffer 3 and CL buffer 4]) and added to each sample, and incubated o/n at 4°C with agitation.

Samples were centrifuged and the supernatant retained before washing the beads 10 × 1 ml with CL wash buffer. After the final wash, beads were resuspended in 250 µl CL wash buffer and transferred to 2 ml spin dry columns and centrifuged to isolate the beads. These were then resuspended in 50 µl of fresh SDS-loading buffer and boiled to elute bound proteins, and reverse cross-linkage, and were collected by centrifugation (10000 × g, RT, 5 min). Supernatant and elution samples were resolved by SDS-PAGE and transferred to a nitrocellulose membrane by Western blotting to detect for specific interaction partners using purified antibodies (see section 2.2.2). The secondary antibody used here is Trueblot Anti-Rabbit IgG-HRP specific for native antibodies. See table 2.3 for an example SDS-PAGE scheme for a typical *in vivo* co-immunoprecipitation experiment.

WT strain				**Mutant strain**			
Supernatant		**Elution**		**Supernatant**		**Elution**	
IP	C	IP	C	IP	C	IP	C

Table 2.3 Example SDS-PAGE scheme for an *in vivo* co-immunoprecipitation experiment

Supernatant samples after incubation with protein G-coupled agarose beads were compared to samples of washed and eluted beads. IP; immunoprecipitated. C; control (no-antibodies).

2.5.2 Activity assays

2.5.2.1 Fluorescent-bocillin binding assay

This assay utilises a fluorescent form of a β-lactam, bocillin (Molecular Probes, Inc., Eugene), which binds to the serine residue at the active site of PBPs for detection after resolving by SDS-PAGE. A typical sample consists of 10 μg/ml of purified PBP, 20 ng of FL-bocillin, in a final volume of 50 μl with 10 mM HEPES/NaOH, 10 mM $MgCl_2$, pH 7.5. A negative control sample was pre-incubated for 10 min with 10 ng of penicillin G to block the active site of the PBP. Samples were incubated for 10 min at 37°C before all samples were boiled for 30 min with 30 μl of SDS-PAGE loading buffer and resolved by SDS-PAGE. Fluorescence was observed using a Typhoon Fluoroimager (Excitation laser; 488 nm, emission filter; 520 BP20, PMT voltage; 400-800). Figure 2.14 depicts PBP1A from *E. coli* as an example.

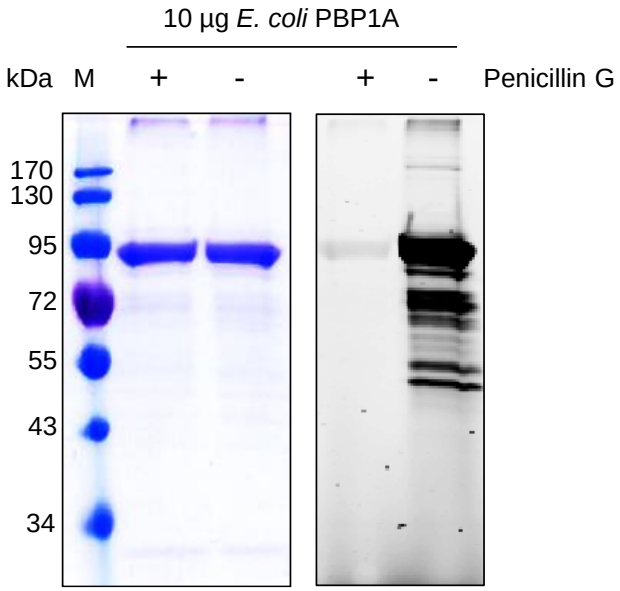

Figure 2.14 Fluorescent-bocillin binding assay using PBP1A

Fluorescent-bocillin binding assay to demonstrate the correct folding of the active site of PBP1A after purification. Coomassie-stained 12% SDS-PAGE gel (Left) and protein after visualising bocillin fluorescence using a Typhoon Fluoroimager (Excitation laser; 488 nm, emission filter; 520 BP20, PMT voltage; 400-800) (Right). Pre-incubation with penicillin G prevents the binding of bocillin to the protein as a negative control.

2.5.2.2 Muropeptide/sacculi-based endopeptidase activity assays

Muropeptides of the appropriate strain were isolated by o/n cellosyl digestion of 100 µl of intact sacculi at 37°C with 10 µg of cellosyl and 20 mM $NaPO_4$, pH 4.8, before boiling for 10 min, centrifugation (10000 × g, 10 min, RT) and retention of the supernatant [21]. Alternatively, isolated high molecular weight sacculi, of the appropriate strain, obtained as described in section 2.7.1, were used. Hydrolases were incubated at optimised concentrations in 100 µl of EPase buffer (10 mM HEPES/NaOH, 10 mM $MgCl_2$, 150 mM NaCl, and 0.05% Triton X-100, pH 7.5). To begin the reaction, 10 µl of isolated muropeptides/sacculi were added. Muropeptide-containing samples were incubated for 30 min-18 h at 37°C with shaking and those containing intact sacculi were incubated for 2-18 h. In some muropeptide-based assays, a 50 µl sample was taken at 5 min and the remaining sample left for a further 25 min. To stop the reaction, samples were boiled for 10 min prior to centrifugation (10000 × g, RT, 10 min). In some cases 20 mM EDTA was required to fully abate the reaction. After stopping the reaction, samples incubated with intact sacculi were subjected to an o/n cellosyl digestion at 37°C with shaking in 10 µg of cellosyl and 20 mM $NaPO_4$, pH 4.8, before boiling for 10 min, centrifugation (10000 × g, 10 min, RT) and retention of the supernatant. The released muropeptide-containing supernatants were reduced and analysed by reversed-phase HPLC as described in section 2.5.2.5. EPase activity was expressed as the relative amounts of Tetra monomers and TetraTetra dimers. An example of EPase digestion chromatograms are shown in figure 2.15. The chemical structure of detected muropeptides can be found in figure 2.17.

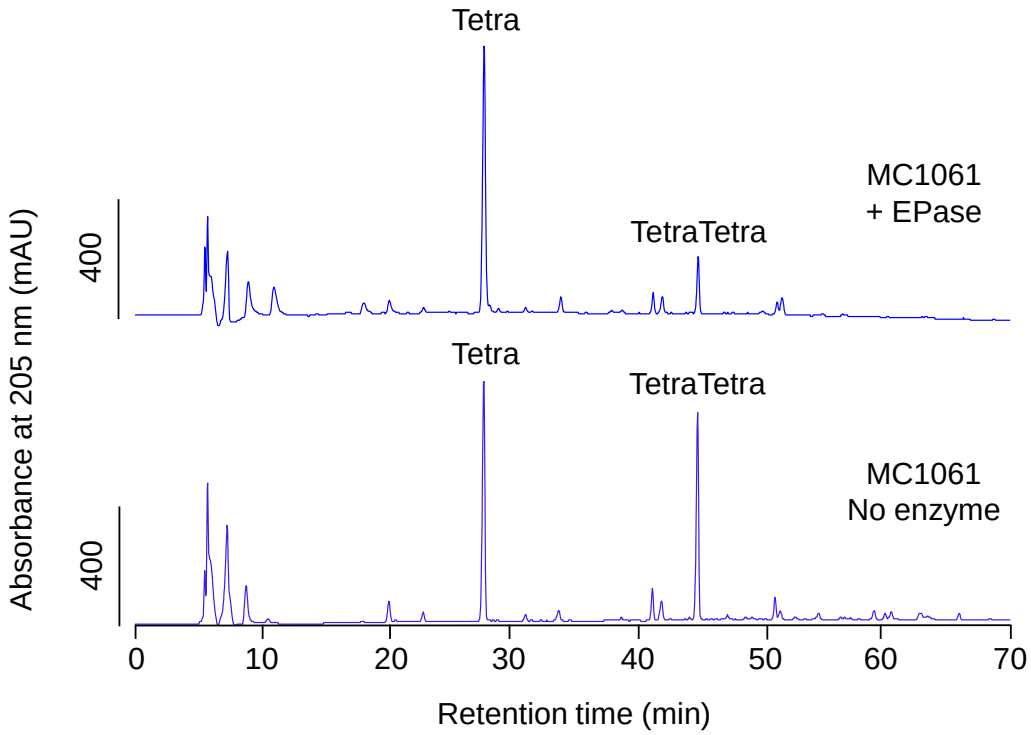

Figure 2.15 Chromatograms of a sacculi-based endopeptidase activity assay

Example of an intact WT sacculi (MC1061) EPase assay, incubated with and without EPase. The released muropeptides were reduced with sodium borohydride and separated by reversed-phase HPLC using an Agilent Technologies series 1200 HPLC system with a Prontosil 120-3-C18-AQ 3 µm (Bischoff) reversed-phase column and detected by UV. The chemical structure of detected muropeptides can be found in figure 2.17.

2.5.2.3 Spectrophotometric D-Alanine release assay

This protocol is adapted from [118] and was carried out in collaboration with Dr. David Roper, Warwick University before optimisation at Newcastle University by Katharina Peters. The carboxypeptidase (CPase) activity of PG hydrolases results in the release of the terminal D-Ala residue from the pentapeptide stem of PG precursors. Using UDP-Mur*N*Ac pentapeptide as a substrate, and in this case PBP4, it was possible to spectrophotometrically measure the release of D-Ala.

Each reaction sample consisted of 200 µl of CPase buffer (50 mM HEPES/NaOH, 10 mM $MgCl_2$, pH 7.6), 3 units of D-amino acid oxidase (Sigma), 6 units of horseradish peroxidase (HRP) (Sigma), Amplex Red (Sigma), and an optimised concentration of protein.

All constituents of the reaction were added and mixed directly in a quartz cuvette (Hellma, 10 mM light path, 15 mM centre), before the addition, and brief mixing by pipette, of purified UDP-Mur*N*Ac pentapeptide (BACWAN, Warwick University) to begin the reaction. The released D-Ala residues from the CPase activity of PBP4 are oxidatively deaminated by the action of D-amino acid oxidase to produce pyruvate and hydrogen peroxide (H_2O_2). The released H_2O_2 is reduced to H_2O by HRP using Amplex Red as an electron donor. Oxidised Amplex Red produces resorufin which has an intense pink colour and the production of which was measured spectrophotometrically using a Cary 100 Bio UV-visible spectrophotometer (wavelength 555 nM) (See figure 2.16 for a schematic of the reaction). The change in absorption over 10 min was measured and analysed using the complementing software.

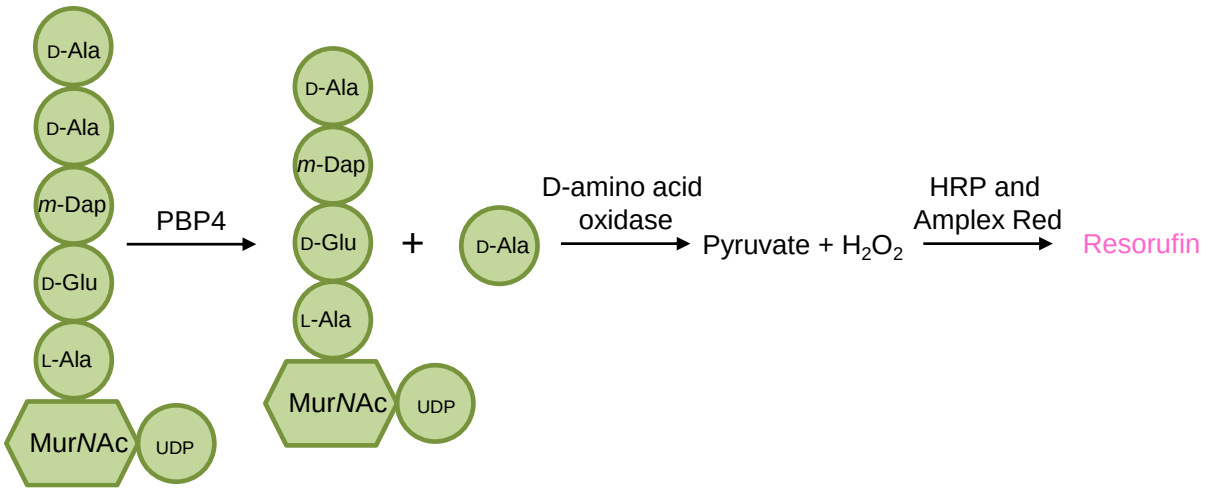

Figure 2.16 Schematic diagram of the spectrophotometric carboxypeptidase activity assay

The CPase activity of PBP4 cleaves the terminal D-Ala residue from UDP-Mur*N*Ac pentapeptide substrate, which is deaminated by D-amino acid oxidase. The released H_2O_2 is reduced by HRP using Amplex red as an electron donor. Oxidation of Amplex red generates the pink compound resorufin which can be measured at 555 nM using a spectrophotometer.

2.5.2.4 *In vitro* transpeptidase activity assay

This protocol is adapted from [67]. Radioactively-labelled lipid II ([^{14}C]-Dap) was dried in glass reaction tubes using a speed-vac (ScanVac) whilst preparing reaction solutions. Standard reactions consisted of 100 µl total volume containing 10 mM HEPES/NaOH, 10 mM $MgCl_2$, 150 mM NaCl, 0.025-0.1% Triton X-100 (NaCl and Triton concentrations are inclusive of that brought with the addition of proteins and resuspended [^{14}C]-Dap Lipid II). For a single reaction, 15 µM [^{14}C]-Dap Lipid II (resuspended in 5 µl of 0.2% Triton X-100) was added to the reaction solution for 1 h at 37°C. Samples were boiled for 10 min before the addition of cellosyl buffer (20 mM $NaPO_4$, pH 4.8) and 10 µg of purified cellosyl and were incubated at 37°C for 90 min. Samples were again boiled for 15 min, centrifuged (14000 × g, RT, 10 min) and supernatants transferred to clean tubes with holes pierced in the lids for standard borohydride reduction for reversed-phase HPLC analysis (see section 2.5.2.5). Using the associated Laura software, muropeptides corresponding to monomeric and cross-linked muropeptides were integrated and TPase activity calculated as a percentage of muropeptides in cross-links.

2.5.2.5 HPLC analysis

Reduction of released muropeptides

Released muropeptide-containing supernatants, obtained as described in section 2.5.2.2 and section 2.5.2.4, were transferred to new tubes with holes pierced in the lids and were reduced using an equal volume of sodium borohydride buffer (boric acid adjusted to pH 9.0 with phosphoric acid) and a small spatula of solid sodium borohydride prior to centrifugation (3000 × g, RT, 30 min) as described in [21]. The pH of the samples was reduced to 4.5-5 using 85% phosphoric acid and were analysed by reversed-phase HPLC (see below).

Reversed-phase HPLC analysis of muropeptides

Protocol is as described in [21]. HPLC analysis of reduced muropeptides (see above) was performed using an Agilent Technologies series 1200 HPLC system with a Prontosil 120-3-C18-AQ 3 μm (Bischoff) reversed-phase column. A 180 min linear gradient of 100% solvent A (50 mM sodium phosphate, pH 4.31 + 0.0002% NaN_3) to 100% solvent B (75 mM sodium phosphate, pH 4.95 + 15% methanol) was used to separate muropeptides at 55°C. Often a shorter run of 90 min was used. Unlabelled muropeptides were detected using a UV-detector at 205 nm, where [^{14}C]-labelled muropeptides were detected with an online scintillation counter (LabLogic). Specific values (mAU or counts per min) of each muropeptide peak were recorded and analysed using the accompanying Laura software v4.1.7.70 (LabLogic Systems Ltd). The structures of detected muropeptides are depicted in figure 2.17.

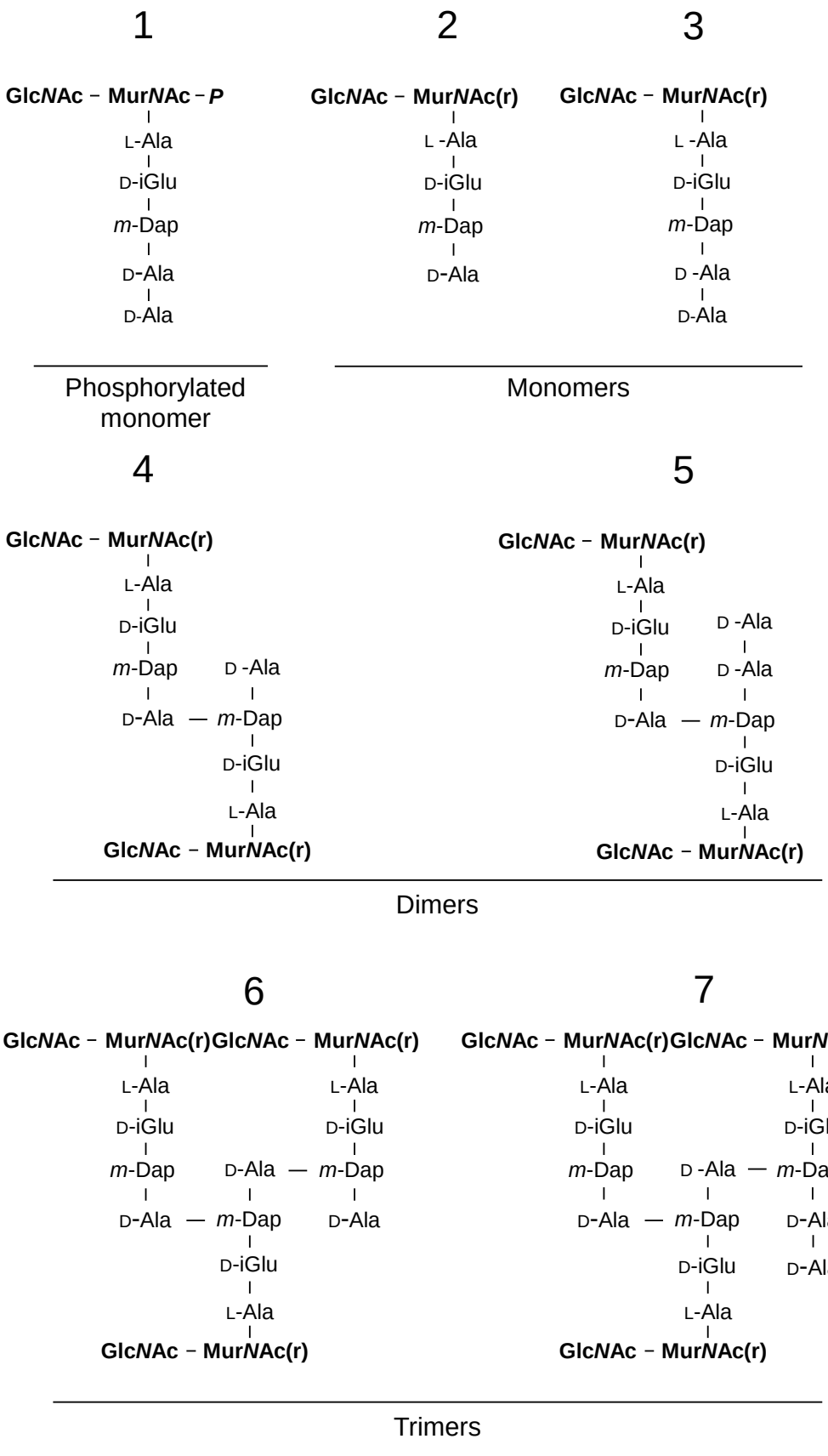

Figure 2.17 Chemical structure of muropeptides detected by HPLC

Chemical structure of muropeptides detected by HPLC analysis from *in vitro* TPase reactions and EPase reactions. 1; Penta phosphate, the unreacted substrate of a TPase reaction. 2; Tetra. 3; Penta. 4; TetraTetra. 5; TetraPenta. 6; TetraTetraTetra. 7; TetraTetraPenta. Mur*N*Ac$_{(r)}$; reduced *N*-acetylmuramic acid residue. P; Phosphate.

2.6 Cellular methods

2.6.1 β-lactamase induction assay

E. coli does not have an inducible operon for the production of the β-lactamase AmpC, therefore for the observation of AmpC induction in *E. coli*, this protocol requires that all strains carry the pJP1 plasmid harbouring the *ampR*/*ampC* operon from *Enterobacter cloacae* [224]. This plasmid carries a kanamycin resistant marker, therefore any prior kanamycin resistance cassette must be excised using the pCP20 plasmid (see section 2.1.5) before transformation of pJP1.

Preparation of the induced and uninduced lysates

Protocol is adapted from [224] and [239]. O/n cultures of appropriate strains were used to inoculate 20 ml of pre-warmed LB and cells were grown to an OD_{578} of 0.5-0.6. Two universal tubes containing 5 ml LB each, per strain, were pre-warmed to 37ºC. To one tube 2 µg/ml imipenem (N-formimidoyl thienamycin) was added. A negative control was used in which no antibiotic was added. To each sample, 5 ml of exponentially growing cells was added for 30 min at 37°C, diluting the concentration of imipenem to 1 µg/ml. Samples were placed on ice for 5 mins before harvesting by centrifugation (4500 × g, 20 min, 4°C). Cell pellets were resuspended in 10 ml of 50 mM sodium phosphate buffer, pH 7.0 and centrifuged again. The pellets were resuspended in 1 ml of the same sodium phosphate buffer. To lyse cells, 50 µl of lysis buffer (400 mM Tris/HCl, 8 mM EDTA, 200 µg/ml lysozyme, pH 8.0) was added to 50 µl of resuspended cells. The remaining 950 µl of resuspended cells were frozen at -20°C. Lysis was induced by the addition of 100 µl of H_2O and a 5 min incubation at RT. Cellular debris was removed by centrifugation (14000 × g, 15 min, RT) and the supernatant was collected and placed on ice. The protein concentration of the lysate was determined using a Pierce™ BCA Protein Assay Kit (Thermo Scientific) (See section 2.2.3).

Measuring β-lactamase activity using Nitrocefin

The chromogenic β-lactam nitrocefin was used to measure β-lactamase activity [240]. The hydrolysis of nitrocefin causes a colour change of yellow to pink which can be measured using a spectrophotometer. Each sample consisted of;

- 50 µl sample lysate
- 50 µl 1 mM nitrocefin
- 900 µl 50 mM sodium phosphate buffer, pH 7.0

Sample lysate was added directly to a standard cuvette and the reaction was started at the last second with the addition of nitrocefin and sample buffer. Absorbance was read at 492 nm for 10 min, with a reading taken every 30 s. The purified form of the β-lactamase Vim4 was used as a positive control at a concentration of 10 μM. The rate of nitrocefin hydrolysed per min per mg of protein was calculated and β-lactamase induction was expressed as the fold difference over the control, containing no imipenem.

2.6.2 Antibody purification from immunised rabbit serum

Antibodies were purified from isolated antisera from rabbits immunised with the specific antigen of interest (Eurogentec, Belgium) using affinity chromatography with immobilised purified antigen to purify the antibody.

The coupling of antigen to CNBr-activated sepharose beads was carried out as described in section 2.5.1.3 with the purified protein of choice.

The antigen-immobilised beads were washed with one column volume of elution buffer 1 (100 mM glycine/HCl, 0.1% Triton X-100, pH 2) to avoid contamination by loosely-bound protein during the antibody elution step, followed by equilibration with 30 ml buffer 1 (10 mM Tris/HCl, 10 mM $MgCl_2$, 1 M NaCl, 0.1% Triton X-100, pH 7.2). Rabbit serum (10 ml) was diluted with 35 ml of diluent (10 mM Tris/HCl, 0.1% Triton X-100, pH 7.4) and centrifuged to remove unwanted debris (4500 × g, 4°C, 10 min). The supernatant was applied to the antigen-bound sepharose beads and incubated o/n at 4°C with gentle agitation. Beads were collected with a gravity column allowing the rest of the solution to flow through. The beads were washed with 20 ml of buffer 1 and 20 ml of buffer 2 (10 mM Tris/HCl, 10 mM $MgCl_2$, 150 mM NaCl, 0.1% Triton X-100, pH 7.2). The antibodies were eluted using 10 × 1 ml elution buffer 1 and collected in 2 ml reaction tubes containing 200 μl of elution buffer 2 (2 M Tris/HCl, pH 8.0), to neutralise the pH, and 300 μl of 100% glycerol for storage at -80°C. Samples were mixed by inversion and 20 μl of each was resolved by SDS-PAGE analysis. Coomassie-staining was carried out to observe heavy and light chains of the purified antibodies. Fractions possessing the highest concentrations of antibody were combined, aliquoted and stored at -80 °C.

Antibody test

BW25113 WT cells, and a mutant strain lacking the specific antigen, were grown to an OD_{578} of 0.5-0.6 at 37°C with shaking. A 1 ml sample of exponentially growing cells was harvested by centrifugation (4500 × g, RT, 10 min) and resuspended in 100 µl TBS and 100 µl of SDS-loading buffer before boiling for 10 mins. Samples were analysed by SDS-PAGE and transferred to a nitrocellulose membrane by Western blotting, using the newly purified antibody for primary immunodetection (section 2.2.2).

2.7 Cell wall methods

2.7.1 Isolation of peptidoglycan from *E. coli*

This protocol was adapted from [21]. O/n cultures of the appropriate strain were used to inoculate 2 L of LB and cells were grown with orbital shaking at 37ºC until an OD_{578} of 0.5-0.6 was reached. Cells were harvested by centrifugation (4500 × g, 4°C, 20 min) and resuspended in 25 ml of ice cold dH_2O. The cell suspension was added drop-wise by Pasteur pipette to an equal volume of boiling 8% SDS solution and the sample was boiled for a further 30 min. The sample was left to cool to RT before collecting the sacculi by centrifugation (140000 × g, 1 h, RT). The pellet was resuspended in 25 ml of dH_2O and centrifuged as before to remove the SDS. This takes 6-8 repetitions, testing for presence of SDS using the Hayashi test (section 2.7.2). After the successful removal of SDS, the sacculi pellet was resuspended in 2.2 ml of 10 mM Tris/HCl, 10 mM NaCl, pH 7.0, 250 µl of 3.2 M imidazole pH 7.0 and 37.5 µl of 10 mg/ml amylase (for the removal of any residual high molecular weight glycogen). After incubation for 2 hours at 37°C, 50 µl of 10 mg/ml Pronase E (pre-activated at 60°C for 2 h) was added to remove covently-bound lipoproteins and was incubated for 1 h at 60°C. The addition of 2.5 ml of 4% SDS solution and boiling for 15 min was used to stop the reaction. Samples were left to cool to RT and the SDS washing step, as described before, was repeated using a benchtop ultracentrifuge (Optima^{TM} TLX, Beckman Coulter) (420000 × g , RT, 60 min). Once free of SDS, the isolated sacculi were resuspended in 1.2 ml of dH_2O containing 0.02% NaN_3 and stored at 4°C.

2.7.2 Hayashi Test for the detection of Sodium dodecyl sulphate

The Hayashi test was performed to check for the absence of SDS during pellet washing steps and is as described in [241]. After centrifugation, 335 µl of the supernatant was added to 170 µl of 0.7 M sodium phosphate, pH 7.2, 7 µl of 0.5% methylene blue and 1 ml of chloroform. After vigorous vortexing, two phases were observed. If SDS was present it formed a water-insoluble blue complex in the lower phase. When the sample was free of SDS, the lower phase was clear/pink.

2.7.3 Peptidoglycan binding assay

The protocol was modified from [206] and [31]. A 100 µl sample of ~1 mg/ml purified PG suspension was pelleted by centrifugation (10000 × g, 10 min, RT) and resuspended in 100 µl of PG binding buffer (10 mM Tris/Maleate, 10 mM $MgCl_2$, 50 mM NaCl, pH 7.5). To the resuspended PG solution, 10 µg of the protein of interest was added and incubated on ice for 30 min. A negative control was used in parallel containing no PG. Samples were centrifuged (10000 × g, 10 min, RT) and the supernatant collected (sample S). The pelleted material was washed with 200 µl of PG binding buffer, centrifuged and the supernatant collected as before (sample W). The pelleted PG was resuspended in 100 µl of 2% SDS solution and stirred for 1 h. Samples were centrifuged again and the supernatant collected (sample P). Each sample (S, W and P) was analysed by SDS-PAGE in comparison to samples absent of PG. Protein retention in the P sample, in the presence of PG, is indicative of PG binding. See table 2.4 for an example SDS-PAGE scheme for a typical experiment.

+ Peptidoglycan				**No Peptidoglycan**		
S	W	P	**M**	S	W	P

Table 2.4 Example SDS-PAGE scheme for a typical peptidoglycan binding assay

Example layout of samples from a PG binding assay. S; Supernatant. W; Wash. P; Pellet. Samples containing PG were directly compared to those absent of PG. M; Marker.

3 Results

3.1 Structural characterisation of LpoA and its interaction with PBP1A

3.1.1 Introduction

PBP1A is the major PG synthase during cell elongation and relies on an interaction with the OM-anchored lipoprotein LpoA for *in vivo* function [25,26]. Typas *et al.*, (2010) used a proteomics-based search for novel PBP1A interaction partners, using immobilised PBP1A incubated with membrane/periplasmic fractions from *E. coli*, to identify LpoA. This was confirmed *in vivo* by co-immunoprecipitation and, independently, by Paradis-Bleau *et al.*, (2010), who used a synthetic lethal screen to identify the same cognate relationship.

In this section we develop on the *in vitro* characterisation of the interaction between PBP1A and LpoA to estimate a K_D value and attempt to identify putative interaction sites. We also present here the structural model of LpoA using NMR spectroscopy of $LpoA^N$ in collaboration with the group of Jean-Pierre Simorre at the Institute de Biologie Structurale (IBS) Grenoble, France. Combined with other techniques, we published the structural model of full length LpoA in 2014 [95]. The structural model identified 'wing'-like domains, not present in LpoA from *H. influenzae,* in which LpoA in essential [98]. We go on to directly compare and contrast *E. coli* LpoA/B and PBP1A/B with LpoA and PBP1A/B from *H. influenzae*.

3.1.2 Characterisation of the interaction between LpoA and PBP1A

3.1.2.1 LpoA interacts with PBP1A *in vitro*

In order to further characterise the known interaction between LpoA and PBP1A, and to estimate the dissociation constant (K_D), we employed two *in vitro* techniques not previously performed for this interaction, surface plasmon resonance (SPR) and microscale thermophoresis (MST).

PBP1A (75 µg) was immobilised to an SPR sensorchip surface using immobilised ampicillin (section 2.5.1.6). LpoA was applied at various concentrations (0, 0.25, 0.5, 1, 2 and 4 µM) in standard running buffer (10 mM Tris/Maleate, 150 mM NaCl, 0.05% Triton X-100, pH 7.5) at 75 µl/min for 4 min. A control surface was activated without immobilisation of PBP1A. The concentration-dependent increase in response units (RU) observed upon application of LpoA to the PBP1A-immobilised lane, in comparison to the control lane, was indicative of an interaction (figure 3.1A). Unfortunately, the curves generated were not applicable for K_D value estimation as no equilibrium steady state was reached. We therefore applied MST.

PBP1A was fluorescently-labelled at amine residues and used at a concentration of 41.5 nM (section 2.5.1.7) (fluorescently-labelled proteins will be herein referred to with the prefix, FL, e.g. FL-PBP1A). Unlabelled LpoA was two-fold serially diluted from 30 µM to 0.916 nM and titrated with the constant concentration of FL-PBP1A. The MST binding curve is shown in figure 3.1B and generated an estimated K_D of 852 ± 146 nM, using the accompanying Nanotemper MST software.

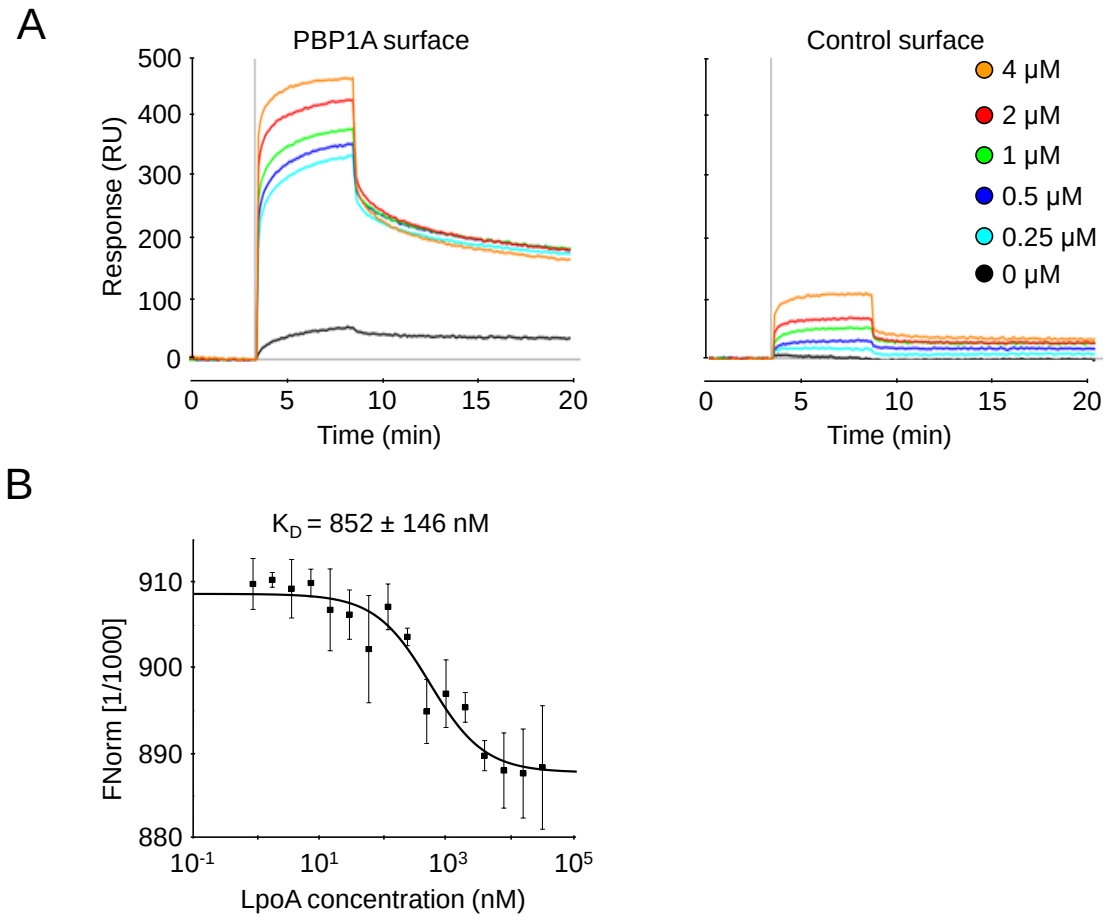

Figure 3.1 LpoA and PBP1A interact directly *in vitro*

A. SPR sensorgrams (response units against time) of LpoA injected at 75 µl/min for 4 min over a sensorchip surface containing PBP1A, immobilised by amine-coupled ampicillin, or an activated control lane containing no protein. **B.** MST of FL-PBP1A (at amine residues) titrated with unlabelled, serially diluted LpoA from a concentration of 30 µM – 0.916 nM. The estimated K_D generated was 852 ± 146 nM. MST conditions were 80% LED power and 20% MST power. The values are the mean ± standard deviations of three independent experiments. The raw MST data are shown in figure 5.1.

3.1.2.2 LpoA is elongated with a TPR-rich N-terminal domain

We sought to determine the structure of LpoA in order to identify regions crucial for the interaction with PBP1A and use the optimised *in vitro* methods from 3.1.2.1 to further characterise the interaction between LpoA and PBP1A. Multiple attempts have been made to obtain the crystal structure of PBP1A, work which is currently ongoing, and, during the course of this project, we also attempted to determine the crystal structure of LpoA, but have been unsuccessful thus far. We therefore focussed efforts on structure determination by nuclear magnetic resonance (NMR) spectroscopy. Full length LpoA is too large for NMR analysis, therefore $LpoA^N$ (residues 28-256), was purified to homogeneity with [^{15}N] and [^{13}C] labelling as described in section 2.3.2. The double labelled protein was purified at Newcastle University and was sent for NMR spectroscopy by Nicholas Jean in the lab of Jean-Pierre Simorre, IBS, Grenoble who carried out the structural determination experiments presented in this section.

To determine if the protein was suitable for structural determination at the conditions required for NMR spectroscopy, the double labelled $LpoA^N$ was subjected to ^{1}H-^{15}N heteronuclear single quantum coherence (^{1}H-^{15}N-HSQC) at a range of temperatures (5°C–50°C) and pH (4.5–7.5), to test if unfolding would occur. Structural determination by NMR spectroscopy was then carried out at 50°C and pH 4.5, and chemical shifts assigned to reveal the structure shown in figure 3.2A.

$LpoA^N$ contains 12 α-helices forming a number of tetratrico-peptide repeat (TPR) motifs, organised individually into super-helical structures, as observed with canonical TPR-containing proteins. These domains are commonly found in proteins with known interaction partners. The elongated spherical shape of $LpoA^N$ is ~30 Å in width and ~70 Å in length, with a number of highly conserved residues within the grooves formed between helices H7-H8 and H3 and H5 [95].

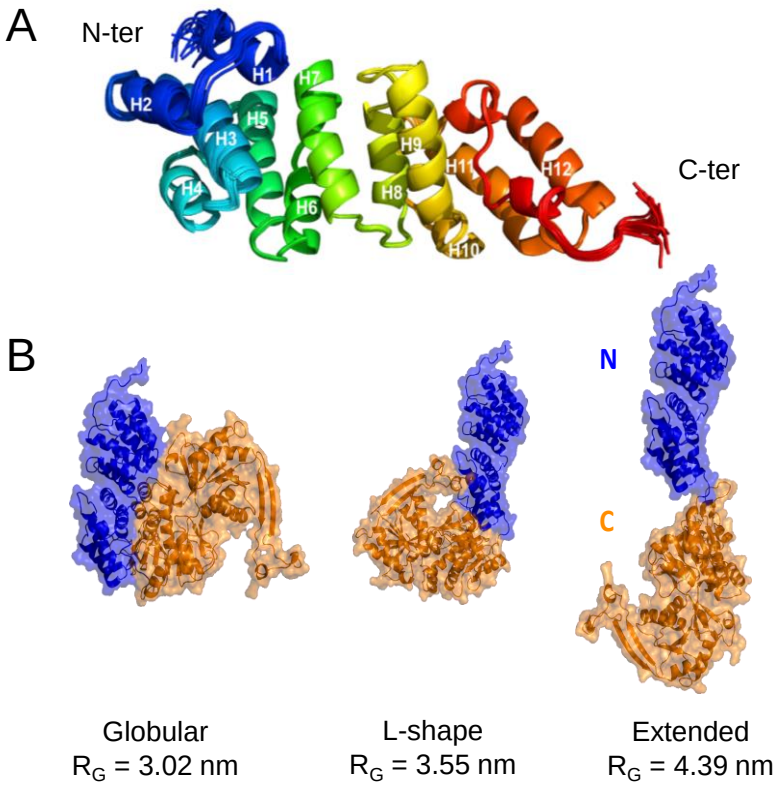

Figure 3.2 LpoA^N consists of TPR-like motifs and full length LpoA has an elongated shape

Figures adapted from [95]. **A.** Structural model of LpoA^N based on the NMR spectra of [^{13}C][^{15}N]-LpoA^N which consists of 12 α-helices adopting TPR-like folding. **B.** Structural model of full length LpoA, based on the NMR structure of LpoA^N, the crystal structural model of LpoA^C from *H. influenzae* [100], and AUC and SAXS of the full length *E. coli* protein. The radius of gyration (R_G) measured by SAXS was 4.22 nm which best fitted an elongated shape.

The large size of full length LpoA (~72 kDa) means it is not possible to carry out structure determination by NMR spectroscopy. However, ^{1}H-^{15}N band-selective excitation short-transient transverse optimised spectroscopy (^{1}H-^{15}N-BEST-TROSY) NMR spectra of the full length protein was compared to that of LpoA^N, in which none of the signals from the LpoA^N spectra were found. As LpoA^N was concluded to be well ordered, these data imply tumbling of the protein due to unstructured regions within LpoA^C. As such, the detected ^{1}H, ^{13}C, and ^{15}N resonances from the full length double-labelled LpoA spectra were analysed by HNCACB and BEST-TROSY-(H)N(COCA)NH experiments. We identified two regions forming unstructured 'wing'-like domains absent from the crystal structure of *H. influenzae* LpoA^C [100]. These two regions corresponded to 30 assigned residues between N285 and P351 and 16 assigned residues between S493 and N531 (figure 3.3A) generated using IUPRED for the prediction of intrinsically unstructured proteins (figure 3.3B). Sequence alignment of LpoA^C from *E. coli* and *H. influenzae* showed that these unstructured regions are only present in *E. coli* LpoA (figure 3.3C).

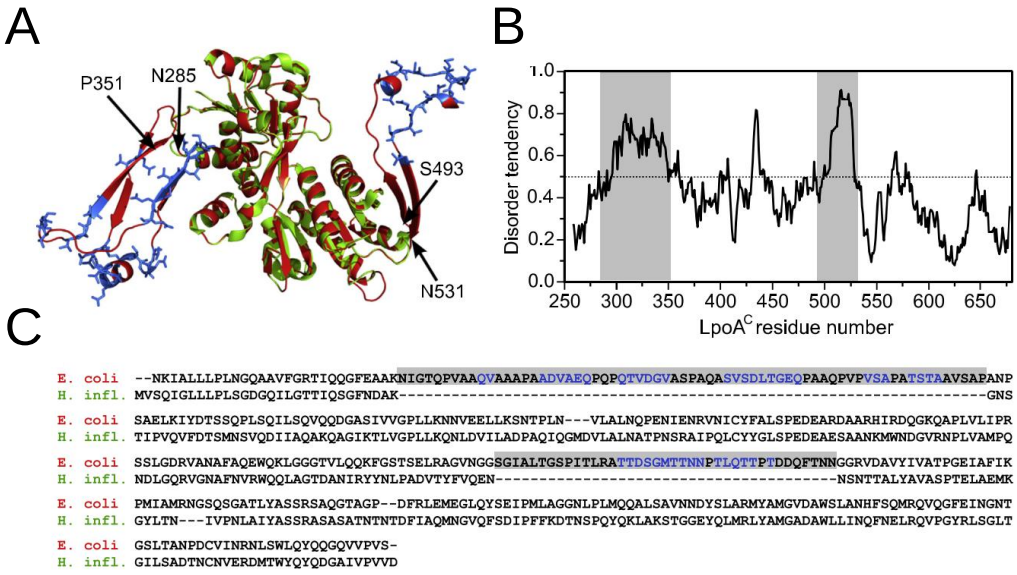

Figure 3.3 ***E. coli*** **LpoA^C possesses unstructured regions not present in** ***H. influenzae*** **LpoA^C**

Figure adapted from [95]. **A.** Crystal structure of *H. influenzae* LpoA^C superimposed with unstructured regions (N285-P351 and S493-N531) from *E. coli* in blue. **B.** IUPRED analysis of LpoA^C from *E. coli* predicts which residues comprise the two unstructured regions. **C.** Sequence alignment of *H. influenzae* and *E. coli* LpoA showing unstructured regions in LpoA^C from *E. coli* are absent in *H. influenzae*.

The structural model of full length *E. coli* LpoA was created using Phyre [242]. The crystal structure of *H. influenzae* LpoA^C was used as a template, superimposed with the identified unstructured regions from *E. coli* LpoA NMR analysis. This was combined with analytical ultracentrifugation (AUC) and small angle X-ray scattering (SAXS) of full length *E. coli* LpoA. AUC of full length LpoA predicted an elongated monomer with low flexibility between the two domains [95]. SAXS was applied to generate the experimental radius of gyration (R_G) of full length LpoA compared to three theoretical structural models; globular, L-shaped and extended (figure 3.2B). Experimental distance distribution function curves obtained from the SAXS data of the three models, and of the experimental run, were calculated. The experimental R_G determined by SAXS was 4.33 nm, which best matched that of the extended model (figure 3.2B).

Finally, using the calculated length of LpoA, and the estimated measurements of the bacterial cell envelope, we were able to model the structure of LpoA in the cell. We show an extended structure, long enough to reach through pores in the PG network to interact with the non-catalytic ODD domain of PBP1A (figure 3.4).

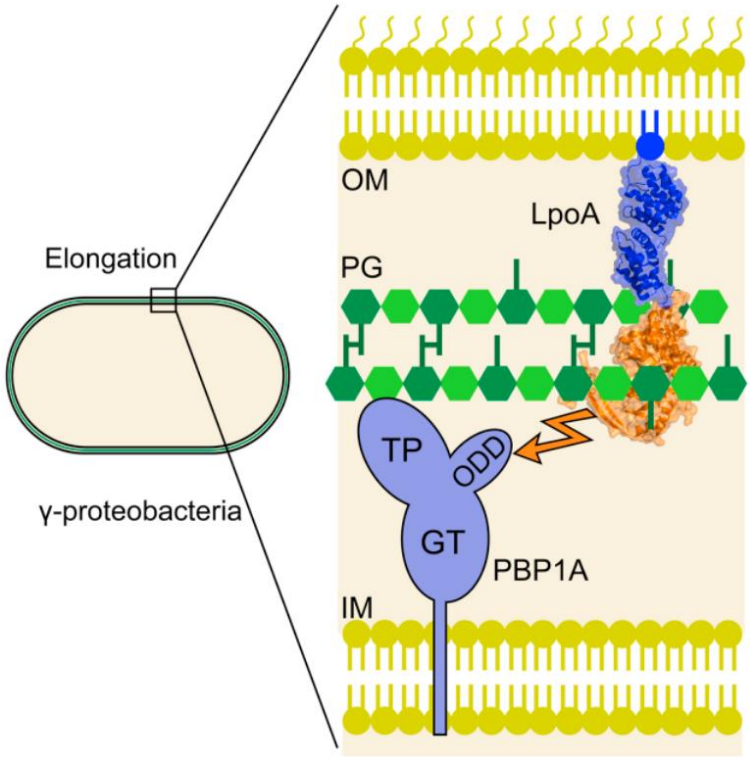

Figure 3.4 Predicted mechanism of interaction of LpoA and PBP1A

Based on the elongated structural model, we propose that LpoA, anchored to the OM via $LpoA^{N}$, reaches through pores in the PG layer to interact with PBP1A via the non-catalytic ODD domain, to stimulate activity.

3.1.2.3 *E. coli* LpoA^{C} possesses 'wing'-like domains not required for interaction with PBP1A

Two unstructured regions in LpoA^{C} were identified which prevented structural determination of this domain, and which were not present in the *H. influenzae* equivalent. As LpoA^{C} is responsible for the interaction with PBP1A and is sufficient to stimulate TPase activity in *E. coli* [70], it is possible that these unstructured regions are PBP1A interaction sites. Having identified the amino acids comprising these 'wing'-like domains (wing 1; N285–P351 and wing 2; S493–N531) Andrew Gray from the group of Carol Gross at the University of California, San Francisco, constructed chromosomal mutations in these proteins. These strains only express LpoA lacking wing 1, wing 2, both wings, or lacking the C-terminal domain or the TPR domain, and for the WT protein. Purification plasmids for these proteins proved unsuccessful, which we hypothesise was due to increased instability upon overexpression.

Using the chromosomal mutants we were able to carry out multiple *in vivo* co-immunoprecipitation assays, in which 10 µl of anti-LpoA antibodies were used to immunoprecipitate DTSSP cross-linked membrane extracts from cells expressing the various truncated LpoA versions (section 2.5.1.8). Protein G-coupled agarose beads were used to obtain anti-LpoA antibodies and conjugated LpoA with any cross-linked interaction partners. After thorough washing of the beads, elution of bound proteins, and separation by 12% SDS-PAGE, proteins were transferred to a nitrocellulose membrane by Western blot. Immunodetection with anti-PBP1A antibodies was used to test for interaction in the absence of these domains (table 5.1 for working dilutions of antibodies).

The interaction between LpoA and PBP1A does not rely on the 'wing'-like domains of LpoA, with single and double wing deletions still allowing for interaction (figure 3.5A). However, the fainter bands in the truncated LpoA strains in comparison to WT indicate a weaker interaction or reduced protein amounts. Western blot analysis revealed there was no change in the cellular amounts of LpoA versions in comparison to WT LpoA (Alex Egan, Vollmer group, unpublished). The deletion of both the C-terminal domain and TPR domain of LpoA prevents the interaction with PBP1A. If the wing-like domains of LpoA are not present to facilitate the interaction with PBP1A, we hypothesised that they could be responsible for preventing inappropriate interactions with other proteins, for example PBP1B. The experiment was repeated with the same immunoprecipitation with α-LpoA antibodies, but using anti-PBP1B antibodies for immunodetection. We observe no interaction upon single and double deletions of the 'wing' domains (figure 3.5B).

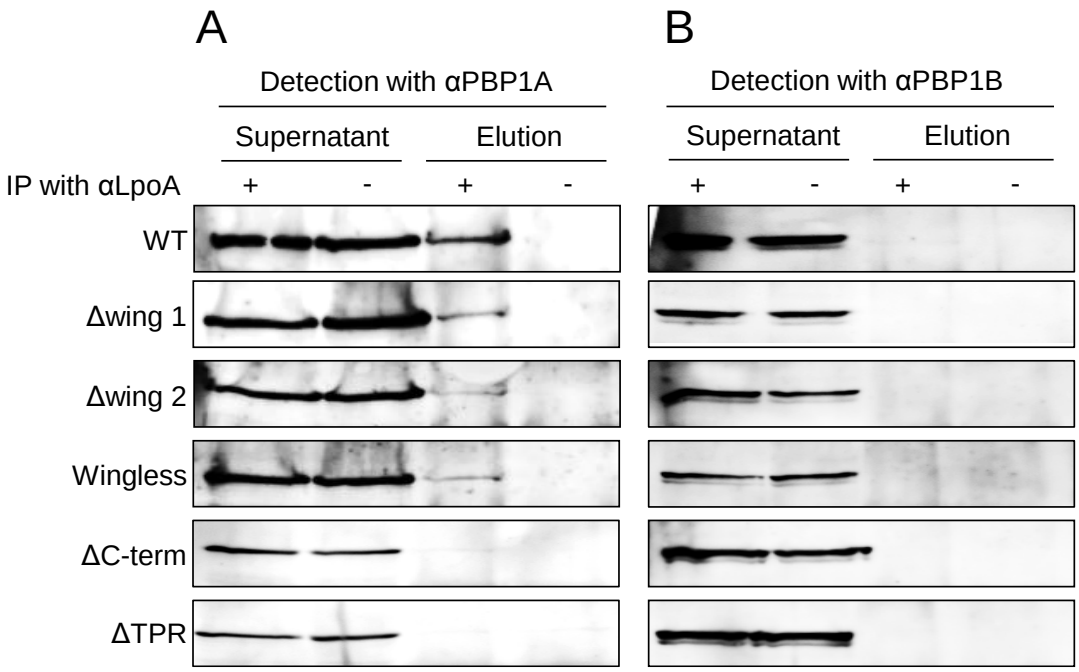

Figure 3.5 ***In vivo*** **co-immunoprecipitation of LpoA variants with PBP1A and PBP1B**

A. WT cells, and cells expressing the truncated forms of LpoA, were cross-linked with DTSSP and the membrane fraction immunoprecipitated with anti-LpoA antibodies. After incubation with protein G-coupled agarose beads and centrifugation, the supernatant was collected. The beads were washed and bound proteins eluted. The cross-linkage was reversed prior to SDS-PAGE, Western blotting and immunodetection with anti-PBP1A antibodies. **B.** Same as above but immunodetection was carried out using anti-PBP1B antibodies. +, with antibody; - without antibody.

3.1.3 Comparison of *E. coli* and *H. influenzae* LpoA

In an attempt to characterise these unstructured domains, which are not present in LpoA from *H. influenzae*, we directly compared the PBPs and Lpos from *H. influenzae* and *E. coli*. Intriguingly, *H. influenzae* possesses both PBP1A and PBP1B, but does not express LpoB, and LpoA is essential. PBP1A, PBP1B, and LpoA from both organisms and LpoB from *E. coli* were purified to homogeneity (sections 2.4.1 and 2.4.2) and compared using the established *in vitro* PBP activity assays.

Both purified PBP1A versions were analysed by 12% SDS-PAGE analysis after undergoing identical purification protocols (figure 2.3A/B). In the interest of keeping the proteins as similar as possible, the proteins were purified simultaneously and were not incubated with thrombin to remove the His-tag.

Figure 3.6 shows the complementing FL-bocillin binding assay gel visualised using a Typhoon Fluoroimager (section 2.5.2.1). In each case, 10 µg of protein was either directly subjected to FL-bocillin or after pre-incubation with penicillin G, to block the active site. We show that both versions of PBP1A were purified successfully and have folded active sites. *H. influenzae* LpoA was purified in tandem with that of *E. coli* LpoA, as show in figure 2.2. PBP1B from both organisms, and LpoB from *E. coli*, were purified to homogeneity by Alex Egan from the Vollmer group (not shown). Both PBP1B versions were similarly successful upon examination by FL-bocillin binding assay.

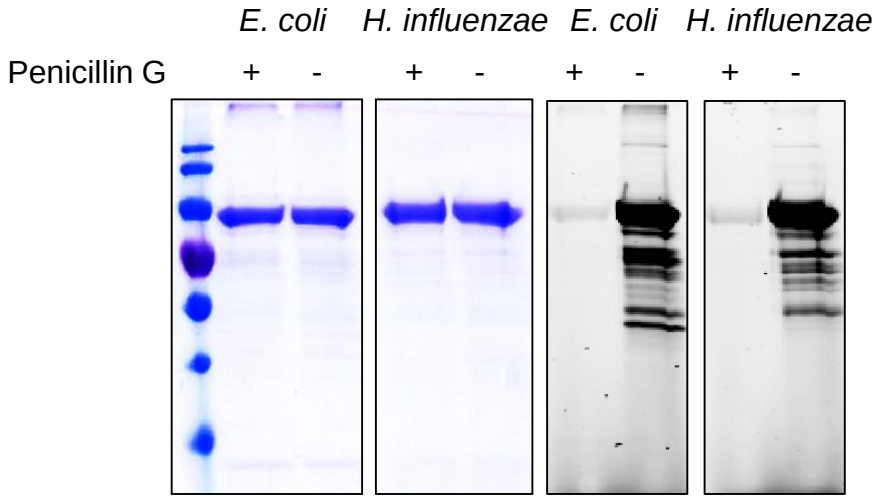

Figure 3.6 Purified PBP1A from *E. coli* and *H. influenzae* have correctly folded active sites

PBP1A from *E. coli* and *H. influenzae* were purified to homogeneity and subjected to a FL-bocillin binding assay in which 10 µg of each protein were incubated either directly with 20 ng of FL-bocillin (-), or after pre-incubation with 10 ng of penicillin G (+). Fluorescence was observed using a Typhoon Fluoroimager (Excitation laser; 488 nm, emission filter; 520 BP20, PMT voltage; 400-800).

In vitro TPase activity assays were performed to test the effect of the three Lpo proteins on PBP activity (section 2.5.2.4). Each PBP was incubated with 15 µM [^{14}C]-Dap Lipid II at a concentration of 0.4 mg/ml in the presence or absence of each Lpo, cognate or otherwise, at a concentration of 1.2 mg/ml. After a 1 h incubation at 37°C, samples were subjected to cellosyl digestion, reduction with sodium borohydride and analysis by reversed-phase HPLC using the associating Scintillation counter (section 2.5.2.5). Integration of peaks corresponding to monomeric peptides and those in cross-links was completed and plotted, and is shown in figure 3.7.

E. coli PBP1A and PBP1B alone produced PG with ~30% and ~50% of peptides in cross-links, respectively, as published [31]. Similarly, the stimulation of cross-linking in the presence of their cognate Lpo was also as published; in the presence of LpoA, the percentage of peptides in cross-links produced by PBP1A was stimulated by 15.9% and PBP1B in the presence of LpoB was stimulated by 13.1% [31]. We also confirmed that there was no effect on activity of non-cognate *E. coli* Lpo proteins on *E. coli* PBPs. Likewise, there was no effect of *H. influenzae* LpoA on PBP1A or PBP1B activity from *E. coli.*

The *in vitro* PG-synthesising activity of *H. influenzae* PBP1A has been shown previously [243]. However, it has not been quantified to the same degree or by the same method described in this work. Here we showed that the degree of cross-linkage of PBP1A alone was already as high as that of *E. coli* PBP1A in the presence of its cognate Lpo. The presence of either LpoA version had no effect on the amount of peptides in cross-links produced by *H. influenzae* PBP1A, nor did LpoB, with the percentage of peptides in cross-links remaining around 50%.

Despite confirmation of a correctly folded active site using a FL-bocillin binding assay, PBP1B from *H. influenzae* was extremely poor at forming cross-links, either alone or in the presence of any Lpo protein.

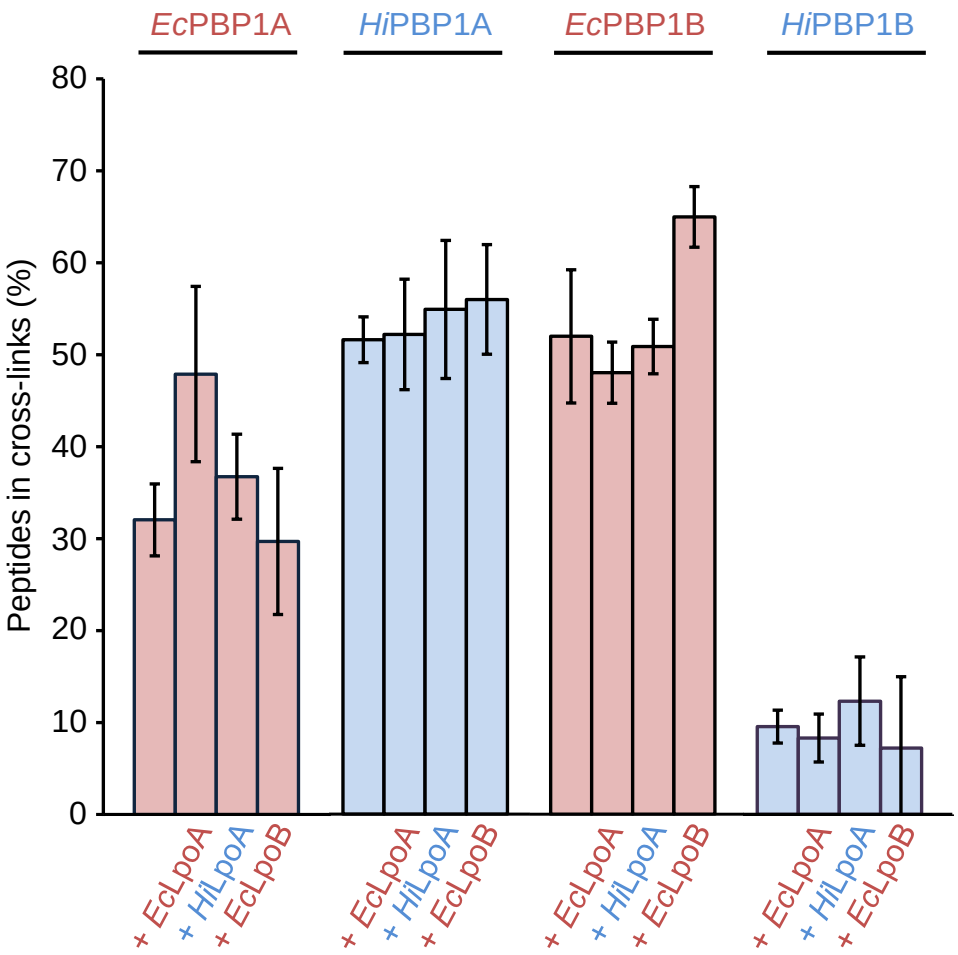

Figure 3.7 ***In vitro*** **transpeptidase assay comparing Class A PBPs from *E. coli* and *H. influenzae***

PBP1A and PBP1B from *E. coli* and *H. influenzae* were incubated with radioactively-labelled lipid II at 0.4 mg/ml with 1.2 mg/ml of LpoA from *E. coli* and *H. influenzae* and LpoB from *E. coli* for 1 h before boiling and cellosyl digestion. Samples were reduced with sodium borohydride and analysed by reversed-phase HPLC. After integration, the percentage of muropeptides in cross-links was calculated and plotted. The values are the mean ± standard deviations of three independent experiments. See figure 5.2 for the corresponding HPLC chromatograms.

3.1.4 Conclusions and discussion

Interaction between LpoA and PBP1A

In this section we have further characterised LpoA and PBP1A by confirming the interaction identified by [31] and [32] using alternative *in vitro* methods. Using SPR we showed the interaction between immobilised PBP1A and LpoA applied as an analyte. K_D determination was not possible from the curves generated by SPR, we therefore performed MST. PBP1A was fluorescently-labelled at amine residues and used at a constant concentration of 41.5 nM. Two-fold serially diluted unlabelled LpoA was titrated from a concentration of 30 µM to 0.916 nM. MST measurements were taken and a K_D of 842 ± 146 nM was estimated using the accompanying software. This K_D closely correlates with that of PBP1B and LpoB which has a K_D of 810 ± 80 nM [75]. It is likely that within the cell the affinity for this interaction may change with the environmental conditions and with phases of bacterial growth. Changes in the PG layer during growth may allow LpoA to interact with different affinity, or perhaps more frequency, and exert different stimulation to coordinate the growth of the PG layer with that of the rest of the cell.

Structural model of LpoA

NMR spectroscopy of $LpoA^N$ determined a monomeric domain of ~30 Å in width and ~70 Å in length consisting of TPR-like motifs, formed by 12 α-helices. Between helices H7 and H8 and H3 and H5 are conserved amino acid residues. The presence of TPR-like motifs and conserved residues within $LpoA^N$ suggest as-of-yet unidentified LpoA interaction partners, the search for which will be presented in the next section.

NMR spectra of the full length version showed unstructured regions not present in that of $LpoA^N$. Using IUPRED we identified these unstructured regions within $LpoA^C$ and, using sequence alignment, found that these unstructured regions were not present in *H. influenzae* LpoA. To obtain a model of *E. coli* $LpoA^C$ the amino acids corresponding to these unstructured regions were superimposed onto the published crystal structure of $LpoA^C$ from *H. influenzae*. This was combined with SAXS and AUC data for the full length *E. coli* protein and the NMR structure of $LpoA^N$. In doing so we present a structural model for full length *E. coli* LpoA which was published in 2014 [95]. The model predicts an elongated, bimodular, monomeric protein, anchored to the OM via $LpoA^N$, long enough to presumably reach through pores in the PG layer to interact with the ODD of PBP1A, via $LpoA^C$.

Identification of 'wing'-like domains in LpoA^C

We initially hypothesised that the 'wing'-like domains identified within LpoA^C were putative PBP1A interaction sites. However, using *in vivo* co-immunoprecipitation assays, we show that this is not the case, nor are they present to prevent the interaction between LpoA and PBP1B. Due to the inability to purify the truncated versions of LpoA, lacking each wing individually or both, we cannot exclude the possibility that these domains have a role in modulating the interaction with PBP1A, for example the strengthening of interaction. It is also possible that these domains are crucial for interactions with novel LpoA binding partners. In future, we plan to continue the optimisation of purification of these truncated versions, and will further investigate this interaction using the *in vitro* methods described here.

Deletion of the C-terminal region of LpoA prevents the interaction with PBP1A, consistent with work from our lab showing that LpoA^C is the domain required for interaction and stimulation of PBP1A activity [70]. The deletion of the TPR domain (LpoA^N) also prevents an interaction and we hypothesise that without this region the protein may be too short to reach through the PG layer to interact with the ODD of PBP1A.

We have yet to show the direct interaction of the ODD domain and LpoA. However, a recent paper showed, by NMR spectroscopy, the interaction between LpoB and the UB2H domain of PBP1B [75]. Unfortunately, due to the size of LpoA it would not be possible to use full length LpoA to show this interaction by NMR spectroscopy. Instead, we plan to use LpoA^C to show the direct interaction with the ODD domain. We hypothesise that upon binding of LpoA^C with the ODD domain, the unstructured 'wing'-like regions may become rigid to facilitate interaction. If this were true we would be able to analyse this interaction by NMR spectroscopy. This could identify the amino acids responsible for the interaction, which we would subsequently mutate and analyse the effects *in vitro* and *in vivo*.

Comparison of **E. coli** *and* **H. influenzae** *PBPs and Lpos*

LpoA^C from *H. influenzae* does not possess the 'wing'-like domains observed in the *E. coli* protein [95]. We therefore sought to compare the interactions and activities of both sets of PBPs and Lpos to elucidate the function of the 'wing'-like domains of *E. coli* LpoA, and investigate why LpoA is essential in *H. influenzae*. All four PBPs were purified in parallel for a direct comparison, as were the two LpoA versions and LpoB from *E. coli.*

We showed that both PBP1A versions have correctly folded active sites, using an FL-bocillin binding assay. The same was performed for the PBP1B versions by Alex Egan from the Vollmer group (not shown).

We showed that *H. influenzae* LpoA does not stimulate its cognate PBP1A and that there is no effect of activity of either LpoA on non-cognate PBP1A proteins. PBP1A from *H. influenzae* synthesises PG with the same percentage of muropeptides in cross-links as *E. coli* PBP1A in the presence of its cognate LpoA. It is therefore probable that PBP1A from *H. influenzae* does not require stimulation by LpoA.

H. influenzae, in comparison to *E. coli,* is small and slow growing with an average cell length of 0.3 µm compared to 2 µm for *E. coli*. It is therefore possible that the stimulation observed in *E. coli* by LpoA is not required in *H. influenzae* and cells exist with basal levels of PBP activity. This may also explain the lack of activity observed for PBP1B from *H. influenzae* which had almost no TPase activity. The unstimulated activity of one PBP may be all that is required for successful growth.

Why then is LpoA essential in *H. influenzae*? It is possible, that although there is no effect on PBP activity, LpoA is still able to interact with PBP1A, or with PBP1B, and exert an effect different to that of *E. coli* LpoA. In *H. influenzae,* rather than regulating PBP activity, which might not be required due the small size and growth rate of the organism, the primary role may be to coordinate membrane growth during proliferation. Without LpoA, and with no LpoB to compensate, growth may be uncoordinated leading to cell death. In *E. coli*, a secondary CpoB-related function of LpoA has been identified for the coupling of the Tol-Pal system to PG synthesis for the coordination of OM growth [91]. We speculate that this secondary function of *E. coli* LpoA may be the primary function of *H. influenzae* LpoA, however, more work is required to test these hypotheses.

Final word

The data in this section characterised the interaction between LpoA and PBP1A *in vitro* and *in vivo.* The structural model of full length LpoA was presented which we used to identify unstructured regions in $LpoA^{C}$ that are not interaction sites for PBP1A, and are not present in the equivalent from *H. influenzae,* which we use as a direct comparison of Lpo and PBP activities from different organisms, and hypothesise different primary functions for LpoA in each. We also identified TPR-like domains and conserved residues within $LpoA^{N}$ which we hypothesise may facilitate novel interactions, the search for which is described in section 3.2.

3.2 Coordination of peptidoglycan synthases and hydrolases in cell elongation

3.2.1 Introduction

The structural model of $LpoA^N$ showed a number of TPR-like motifs, between the helices of which are a number of conserved amino acids (figure 3.2A) [95]. As $LpoA^C$ is sufficient for the interaction and the stimulation of PBP1A [70], we hypothesised that the TPR motifs and conserved residues of $LpoA^N$ could facilitate novel LpoA interactions (figure 3.8).

This section describes the search for these putative interactions and the identification of the PG hydrolase PBP4 as an interaction partner of LpoA. We showed that LpoA interacts with a PG synthase and a PG hydrolase and continued by identifying and characterising interactions between proteins involved in PG synthesis and hydrolysis, providing significant evidence to the hypothesised multi-enzyme complexes for PG growth.

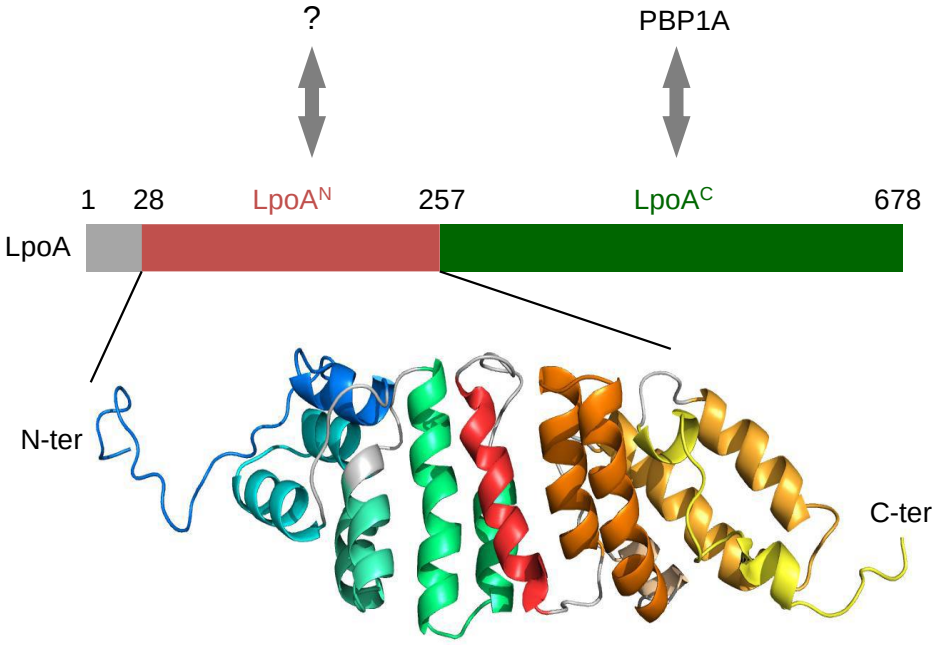

Figure 3.8 The TPR motifs of $LpoA^N$ may facilitate novel interactions

The C-terminal domain of LpoA interacts with PBP1A, yet the NMR structure of the N-terminal domain shows a number of TPR motifs which could facilitate interactions with unknown partners.

3.2.2 Identification of PBP4 as an interaction partner of LpoA

3.2.2.1 Proteomics-based search for novel LpoA^N interactions partners

Purified LpoA^N (10 mg) was immobilised to sepharose beads with a sample taken before and after bead incubation to ensure the successful coupling of an appropriate quantity of protein (figure 3.9A) (section 2.5.1.4). After washing and equilibration, the protein-loaded column was incubated with a combined membrane and periplasmic fraction from a Δ*lpoA E. coli* strain (obtained as described in sections 2.5.1.1 and 2.5.1.2). After incubation and thorough washing, bound proteins were eluted and samples were air-dried before analysis by mass spectrometry (MS) performed by Joe Gray at the Pinnacle Institute, Newcastle University. A control column was used in which no protein coupling took place. The resulting liquid chromatography-mass spectrometry (LC/MS) data yielded a large number of peptide fragments that were not present in the control MS report (table 3.1). After analysis using the online pBLAST software (National Centre for Biotechnology Information), one 27 amino acid peptide fragment was found to match the PG hydrolase PBP4, more specifically, an amino acid sequence found within the active site-containing domain 1 (figure 3.9B).

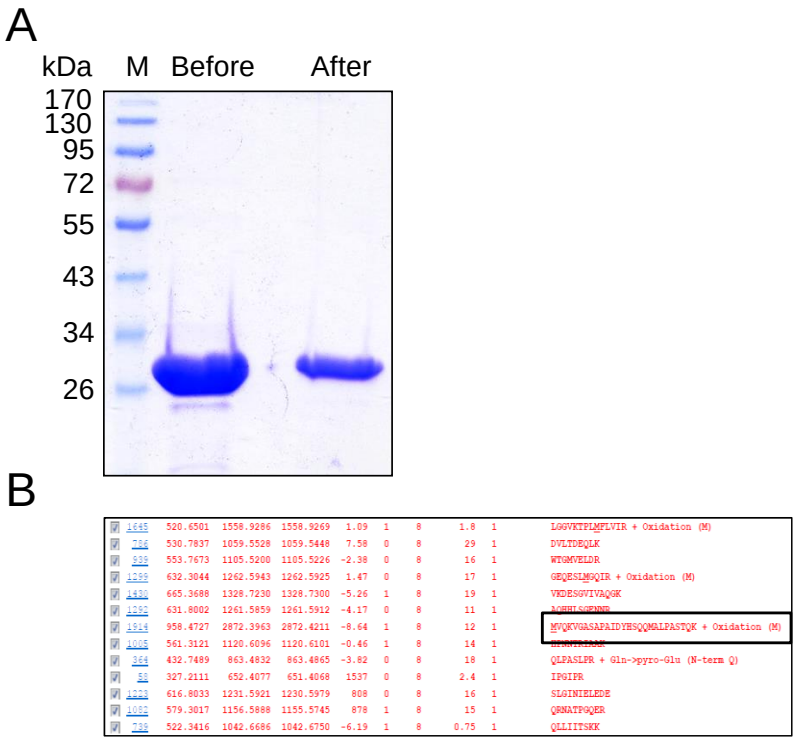

Figure 3.9 Proteomics-based search for LpoA^N binding partners finds PBP4

A. Before and after samples of coupling LpoA^N (10 mg) to sepharose beads. Proteins were separated by 12% SDS-PAGE and visualised by Coomassie staining. After incubation with a combined *E. coli* membrane/periplasmic fraction, any bound proteins were eluted, dried and sent for MS analysis. **B.** Section of resulting MS report showing a large number of peptide fragments. A 27 amino acid fragment is highlighted which, after analysis using the online pBLAST software, corresponded to the PG hydrolase PBP4, and was not present in the control column report.

Table 3.1 List of proteins retained by $LpoA^N$

Protein corresponding to peptide fragment[1]	Function/Predicted function
PBP4	DD-Epase/DD-CPase
FtsK	Cell division protein
YdeV	Sugar Kinase
PheS	Phenylalanine tRNA synthase
YhfA	GTP-binding protein
MglB	Methyl-Galactose substrate binding protein
YbjY	Macrolide transporter subunit
SapB	Peptide transport permease
IntZ	Prophage integrase
AppA	Periplasmic phosphatase
RpoB	RNA polymerase B subunit
HrpA	RNA helicase
YfhC	Deaminase
PldB	Lysophospholipase
YaeS	Undecaprenol pyrophosphatase synthase
AdhE	Alcohol dehydrogenase
YgiM	Predicted signal transduction protein
YebS	Inner membrane protein
DsdX	D-serine transport
NfrB	ATP-binding inner membrane transport protein
YegH	Inner membrane protein
YgeK	DNA-binding transcriptional regulator
YheS	ABC transporter ATP-binding protein
YhjG	Predicted outer membrane biogenesis
AcpD	NAD-azoreductase
GyrB	DNA gyrase subunit B
WcaJ	UDP-glucose lipid carrier transferase
FabF	3-oxoacyl-ACP synthase
UraA	Uracil permease
Ssb	ss-DNA binding protein
RluA	rRNA/tRNA pseudouridine synthase
YhaK	Pirin-related protein
MenF	Isochorismate synthase
YebS	Inner membrane protein
FadH	2,4-dienoyl CoA reductase
PhnN	Carbon-phosphorous lyase complex
YlcF	Prophage tail fiber assemly
YciW	Oxidoreductase
EvgS	Sensor kinase
YcdU	Predicted inner membrane protein
YcgF	FAD-binding phosphodiesterase
YhfT	Predicted inner membrane protein
YfbQ	Aminotransferase
YjiR	DNA-binding transcriptional regulator

[1]Proteins corresponding to peptide fragments retained by $LpoA^N$ not present in the control in no particular order.

3.2.2.2 LpoA interacts directly with PBP4 *in vivo* and *in vitro*

The MS report contained a large list of peptide fragments, mostly from ubiquitous proteins unrelated to PG. We therefore sought to test for a specific interaction between LpoA and PBP4 *in vitro* and *in vivo*. Native PBP4 was purified to homogeneity (section 2.4.5) and SPR was carried out in which full length LpoA (4 µg/ml) was immobilised to the SPR sensorchip surface by general amine coupling (section 2.5.1.6). PBP4 was injected at varying concentrations (0, 0.25, 0.5, 1, 2 and 4 µM) at 75 µl/min over the LpoA surface and a control surface to which no LpoA had been immobilised. The concentration-dependent increase in response units (RU) against time over the LpoA surface was indicative of an interaction in comparison to the control surface (figure 3.10A). Unfortunately, the SPR binding curves did not yield an equilibrium binding phase suitable for accurate K_D determination. Instead, a 'biphasic' interaction was observed (see discussion for more details). We therefore applied MST to confirm the interaction by a second *in vitro* method and estimate the dissociation constant.

LpoA was fluorescently-labelled at cysteine residues as per manufacturer's instructions (section 2.5.1.7). A concentration of 166 nM was optimised and unlabelled PBP4 was two-fold serially diluted from a concentration of 30 µM to 0.916 nM and titrated with the constant concentration of FL-LpoA. During the pre-experiment capillary scan, there was a clear concentration-dependent fluorescence enhancement (figure 3.10B). An SDS-denaturation (SD) test was performed as described in section 2.5.1.7 (figure 5.3). Samples were re-analysed and all samples contained a uniform fluorescence value, indicating that the fluorescence change observed was induced by the binding of unlabelled protein. The raw fluorescence data were plotted against PBP4 concentration and an apparent K_D of 315 ± 37.7 nM was estimated using the accompanying software.

We sought to test the interaction *in vivo* using co-immunoprecipitation (section 2.5.1.8). WT cells (BW25113) and cells lacking PBP4 (BW25113Δ*dacB*) were cross-linked with DTSSP and their membrane fractions obtained as described in 2.5.1.8. The cross-linked membrane fractions were immunoprecipitated with 15 µl of anti-PBP4 antibodies, with subsequent immunodetection using anti-LpoA antibodies (table 5.1 for working dilutions of antibodies). The visualised nitrocellulose membranes are shown in figure 3.10C. LpoA can be observed in anti-PBP4 immunoprecipitated samples, indicative of an interaction. The interaction was not observed in samples with no immunoprecipitation, or in cells lacking PBP4.

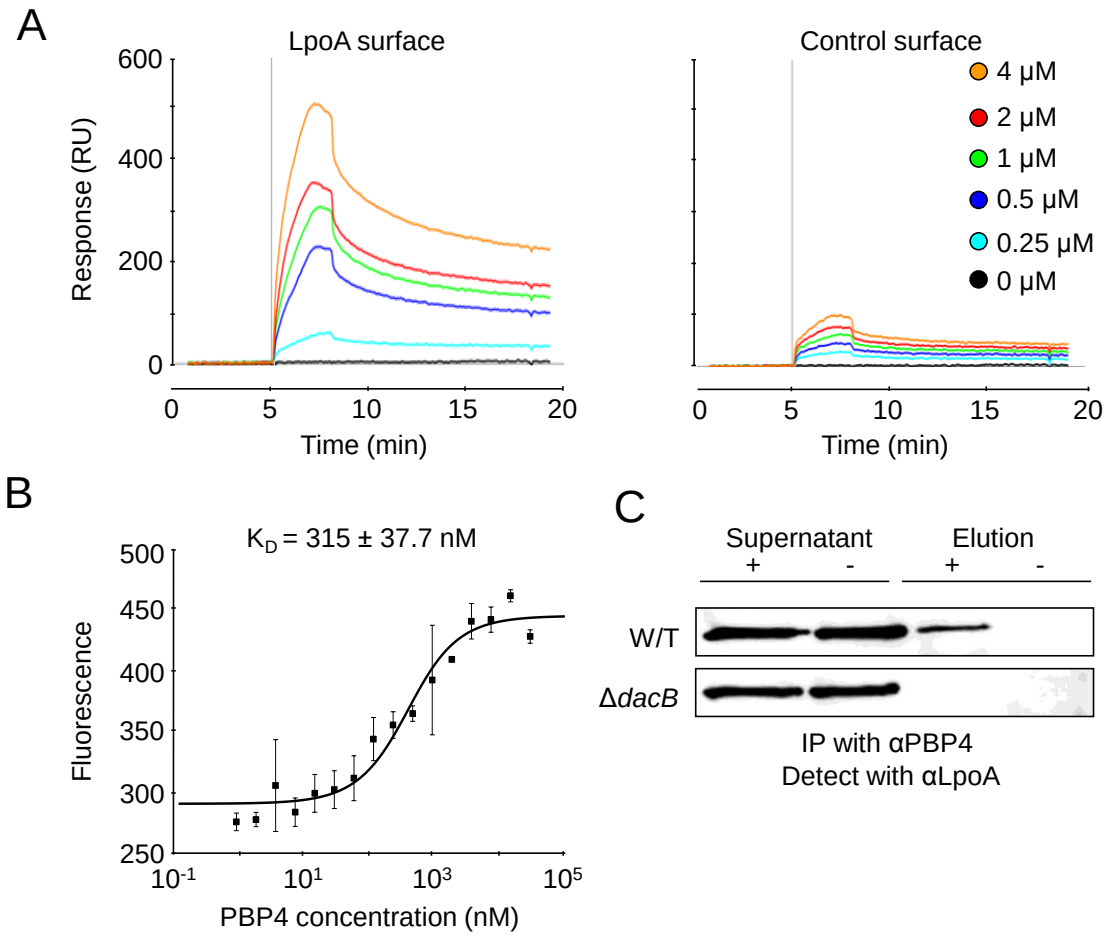

Figure 3.10 LpoA interacts directly with PBP4 *in vitro* and *in vivo*

A. SPR sensorgrams (response units against time) of PBP4 injected (5 min, 75 µl/min) over a sensorchip surface containing LpoA (4 µg/ml) immobilised by general amine coupling, or an activated control surface containing no protein. Contrary to manufacturer's instructions, the pH for the immobilisation of LpoA was not altered and kept at pH 7.5. **B.** MST of FL-LpoA (at cysteine residues) at a concentration of 166 nM and serially diluted PBP4 from 30 µM to 0.916 nM (20% MST power, 100% LED power). An apparent K_D of 315 ± 37.7 nM was estimated using the raw fluorescence values. The values are the mean ± standard deviations of three independent experiments. Raw MST data and SD test are shown in figure 5.3. **C.** *In vivo* co-immunoprecipitation of PBP4 and LpoA. Anti-PBP4 antibodies were used to immunoprecipitate DTSSP-cross-linked membrane fractions from WT and Δ*dacB* cells. Samples were incubated with protein G-coupled beads to obtain PBP4 antibodies and any cross-linked interaction partners. Detection with anti-LpoA antibodies shows the presence of LpoA after elution from protein G-coupled beads in WT immunoprecipitated samples.

3.2.2.3 Dissecting the LpoA-PBP4 interaction

The crystal structure of PBP4 (figure 1.4) shows a structure with three domains [115]. The active site-containing domain 1 has domain 2 inserted into it, and domain 2 itself has domain 3 inserted. It is suggested, that due to the globular nature and hydrophobic core of domain 3, that it may be removed without losing structural integrity to the rest of the protein. With this in mind, our collaborators at EMBL, Heidelberg constructed a purification plasmid for PBP4 lacking domain 3, herein referred to as PBP4ΔD3. PBP4ΔD3 was used here to dissect the interaction with LpoA in order to infer interaction sites. PBP4ΔD3 was purified to homogeneity (section 2.4.4), and used in MST (section 2.5.1.7).

PBP4ΔD3 was two-fold serially diluted from 10 µM to 0.31 nM and titrated with 166 nM of the same FL-LpoA as full length PBP4. The interaction observed did not cause a concentration-dependent fluorescence change and yielded an equilibrium MST binding curve (figure 3.11B). Using the accompanying software, a K_D of 153 ± 31 nM was estimated, an affinity within the same range as the interaction with full length PBP4 (shown again in figure 3.11A).

We sought to dissect this interaction further by purifying $LpoA^N$ and $LpoA^C$ (section 2.4.1) and testing for interaction with full length PBP4 and PBP4ΔD3 by MST.

Purified $LpoA^C$ was fluorescently-labelled at cysteine residues and used at a concentration of 125 nM. MST was performed with two-fold serially diluted unlabelled PBP4 from 30 µM to 0.916 nM. The resulting MST binding curve is shown in figure 3.11C. The apparent K_D was estimated to be 226 ± 15 nM. Purified PBP4ΔD3 was serially diluted from 10 µM to 0.31 nM and used to observe the interaction with FL-$LpoA^C$. The interaction between these truncated versions occurred with an estimated K_D of 315 ± 21 nM (figure 3.11D).

$LpoA^N$ was fluorescently-labelled at amine residues, used at a standard concentration of 62.5 nM, and was tested for interaction with full length unlabelled PBP4. The resulting binding curve generated an apparent K_D of 954 ± 52 nM, significantly weaker than observed for the other LpoA versions (figure 3.11E). Interestingly, when testing the interaction between $LpoA^N$ and PBP4ΔD3 the apparent K_D generated was 17 ± 4 nM, one the strongest interactions observed by MST in this work (figure 3.11F).

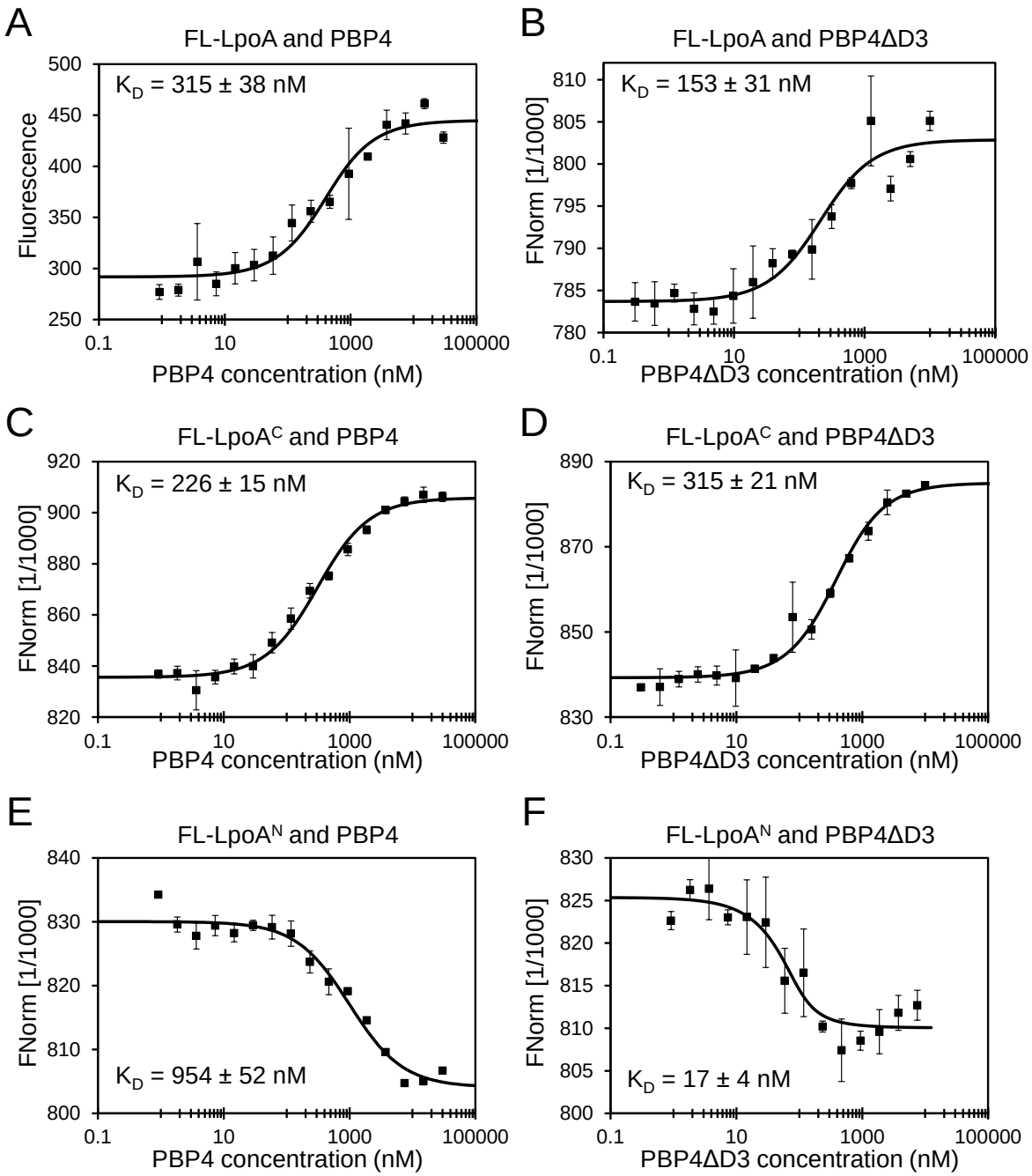

Figure 3.11 Microscale thermophoresis of LpoA and PBP4 versions

MST was carried out using serially diluted PBP4 from a concentration of 30 µM – 0.916 nM or PBP4ΔD3 from 10 µM – 0.31 nM with cysteine-labelled full length LpoA at 166 nM (**A** and **B**) (40% MST power, 100% LED power), cysteine-labelled LpoA^C at 125 nM (**C** and **D**) (20% MST power, 80% LED power) and amine-labelled LpoA^N at 62.5 nM (**E** and **F**) (40% MST power, 20% LED power). The annotated K_D of each interaction was estimated using the accompanying software. The values are the mean ± standard deviations of at least two independent experiments. Raw MST data are shown in figures 5.3-5.8.

3.2.2.4 LpoA moderately inhibits PBP4 activity

LpoA is a regulator of PG synthesis during cell elongation [25,26]. We hypothesised that LpoA may also regulate PG hydrolysis, thus providing a direct link between the two processes.

PBP4 possesses both DD-endopeptidase (DD-EPase) and DD-carboxypeptidase (DD-CPase) activity. We therefore performed assays to measure both activities of PBP4, alone and in the presence of LpoA, to investigate any potential regulatory function of the interaction.

To investigate the CPase activity of PBP4, I visited the laboratory of Dr. David Roper at the University of Warwick who developed a spectrophotometric D-alanine (D-Ala) release assay for measuring DD-CPase activity [118]. The assay measures the release of the terminal D-Ala residue from the PG precursor UDP-Mur*N*Ac-pentapeptide using a coupled enzymatic reaction (section 2.5.2.3).

The concentration of PBP4 was optimised to 17.3 nM in CPase assay buffer (50 mM HEPES/NaOH, 10 mM $MgCl_2$, pH 7.6) where it would be possible to observe any stimulation or inhibition of activity. Figure 3.12A shows absorbance over time of PBP4 alone (light grey) and in the presence of 5 μM LpoA (dark grey). LpoA moderately inhibited the CPase activity of PBP4.

A HPLC-based muropeptide digestion assay was performed to measure PBP4 EPase activity in the presence of LpoA (section 2.5.2.2). Isolated muropeptides from WT (MC1061) sacculi were incubated with PBP4 (1 μM) in the presence or absence of LpoA (2 μM). After a 30 min incubation at 37°C with shaking, the samples were boiled, centrifuged and the digested muropeptides reduced for analysis by reversed-phase HPLC (section 2.5.2.5). The chromatograms were integrated and the percentage of TetraTetra-containing muropeptides consumed was calculated (structure of muropeptides found in figure 2.17). Figure 3.12B shows that LpoA moderately inhibited the EPase activity of PBP4 after a 30 min incubation.

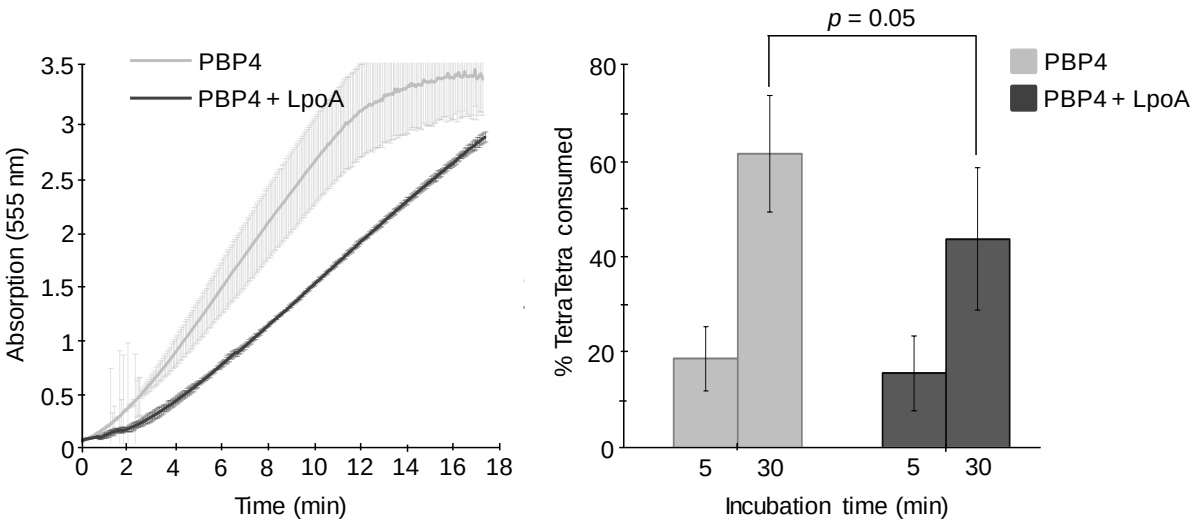

Figure 3.12 LpoA moderately inhibits the activity of PBP4

A. Spectrophotometric-based D-alanine release assay showing PBP4 with and without LpoA. The release of the terminal D-Ala residue from UDP-Mur*N*Ac-pentapeptide by the action of PBP4, and subsequent deamination of the residue by D-amino acid oxidase, results in the formation of H_2O_2. H_2O_2 is reduced to H_2O by HRP using Amplex Red (Molecular Probes) as an electron donor. Oxidised Amplex Red produces an intense pink colour which is measured using a spectrophotometer (555 nm). The values are the mean ± SD of three independent experiments. **B.** HPLC-based muropeptide digestion assay. PBP4 was incubated with isolated MC1061 muropeptides at a concentration of 1 μM for 30 min at 37°C with shaking, alone or in the presence of 2 μM LpoA. The reaction was stopped with boiling and, after centrifugation to remove any debris, the samples were reduced with sodium borohydride for HPLC analysis. The percentage of TetraTetra dimer-containing muropeptides digested was calculated. The values are the mean ± standard deviations of three independent experiments. A *p* value of 0.05 for the 30 min samples was calculated using Microsoft Excel showing this data to be statistically significant.

3.2.3 PBP1A interacts with PBP4

3.2.3.1 PBP1A interacts directly with PBP4 *in vitro* and *in vivo*

Having shown that LpoA interacts with PBP4 and PBP1A, we hypothesised that there may also be a direct interaction between the two PBPs. Using SPR, 75 µg of PBP1A was immobilised via amine-coupled ampicillin, and PBP4 was applied at varying concentrations (0, 0.25, 0.5, 1, 2 and 4 µM) (section 2.5.1.6). A control lane containing no immobilised protein was used in parallel. The positive binding curve generated is shown in figure 3.13A, which showed no dissociation phase, preventing the estimation of a K_D value. As there is no binding event observed for the control lane, we hypothesise that the unusual binding curve is due to a strong interaction which prevented dissociation of the analyte after washing.

To estimate a K_D, MST was performed using FL-PBP1A (at amine residues) at a constant concentration of 41.5 nM (section 2.5.1.7). FL-PBP1A was mixed with two-fold serially diluted unlabelled PBP4 from 30 µM to 0.916 nM. MST measurements yielded a binding curve suitable for the estimation of an apparent K_D of 66.8 ± 9.1 nM (figure 3.13B).

A co-immunoprecipitation assay was performed to test for an *in vivo* interaction (section 2.5.1.8). Anti-PBP4 antibodies (15 µl) were used to immunoprecipitate DTSSP-cross-linked membrane fractions from WT (BW25113) cells and cells lacking PBP4 (BW25113Δ*dacB*). Anti-PBP1A antibodies were used for immunodetection after extraction of PBP4 and any cross-linked interaction partners using protein G-coupled beads. Figure 3.13C shows that in the presence of anti-PBP4 antibody, and only in WT, PBP1A interacts with PBP4 *in vivo*.

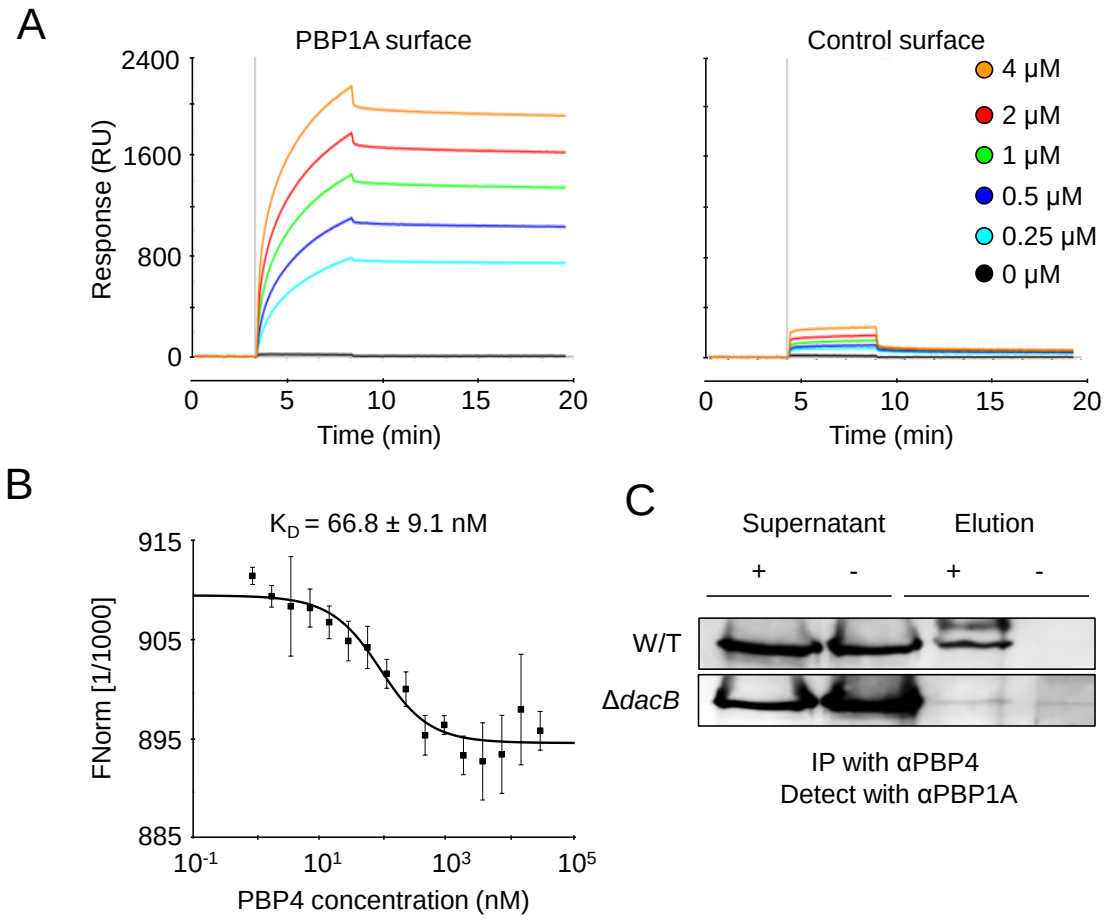

Figure 3.13 PBP1A interacts with PBP4 *in vitro* and *in vivo*

A. SPR sensorgrams (response units against time) of PBP4 injected (5 min, 75 µl/min) over a sensorchip surface containing PBP1A immobilised by ampicillin coupling, or an activated control surface containing no protein. **B.** MST of FL-PBP1A (at amine residues) at a concentration of 41.5 nM and serially diluted PBP4 from 30 µM to 0.916 nM (20% MST power, 80% LED power). An apparent K_D of 66.8 ± 9.1 nM was estimated using accompanying software. The values are the mean ± standard deviations of three independent experiments. Raw MST data are shown in figure 5.9. **C.** *In vivo* co-immunoprecipitation of PBP4 and PBP1A. Anti-PBP4 antibodies were used to immunoprecipitate DTSSP-cross-linked membrane fractions from WT and Δ*dacB* cells prior to incubation with protein G-coupled beads to obtain PBP4 antibodies and any cross-linked interaction partners. Detection with anti-PBP1A antibodies shows the presence of PBP1A after elution from protein G-coupled beads in immunoprecipitated WT cells.

3.2.4 PBP7 interacts with PBP1A, LpoA and PBP4

3.2.4.1 PBP7 interacts directly with PBP1A, LpoA and PBP4 *in vitro*

We have now confirmed the *in vitro* and *in vivo* interactions of PBP4 with two components of the elongation machinery; LpoA and PBP1A. We hypothesised that there may be a larger synthase/hydrolase complex in which these proteins belong. PBP7 is also a member of the Class C family of PBPs, and is a monofunctional EPase. PBP7 was purified to homogeneity by Hamish Yau from the Vollmer group (section 2.4.5) and was tested for interactions with PBP1A, LpoA and PBP4.

MST was performed with FL-PBP7 (at amine residues) which was used at an optimised constant concentration of 62.5 nM (section 2.5.1.7). Two-fold serially diluted LpoA was titrated with FL-PBP7 from a concentration of 10 μM to 0.31 nM (figure 3.14A). The pre-experiment capillary scan yielded a concentration-dependent fluorescence enhancement, and was confirmed as due to ligand binding by an SD test (figure 5.10). The raw fluorescence values were plotted against unlabelled ligand concentration and used to generate a binding curve. The accompanying software was used to estimate a K_D of 217 ± 92.5 nM.

FL-PBP1A (at amine residues) was used at a concentration of 41.5 nM. Two-fold serially diluted PBP7 was titrated with FL-PBP1A from a concentration of 30 μM to 0.916 nM. The MST binding curve generated was used to estimate a K_D of 78.5 ± 8.24 nM using the accompanying software, similar to that of PBP4 and PBP1A (figure 3.14B).

We show here that PBP7 interacts with both LpoA and PBP1A with similar affinity as PBP4. We therefore hypothesised that there may be a direct interaction between the two hydrolases. Using FL-PBP7, at the same concentration of 62.5 nM, titrated with two-fold serially diluted PBP4 from a concentration of 30 μM to 0.916 nM, we observed an interaction (figure 3.14C). The pre-experiment capillary scan showed a concentration-dependent fluorescence enhancement, and was confirmed as due to ligand binding by an SD test (figure 5.12). The raw fluorescence values were used to generate an estimated K_D of 332 ± 85.8 nM.

An *in vitro* Ni^{2+} bead pull-down assay was used to confirm the interaction between PBP7 and PBP4 using His-PBP7 and native PBP4 (section 2.5.1.5). We could show that PBP4 is only retained in the presence of His-PBP7 (figure 3.14D).

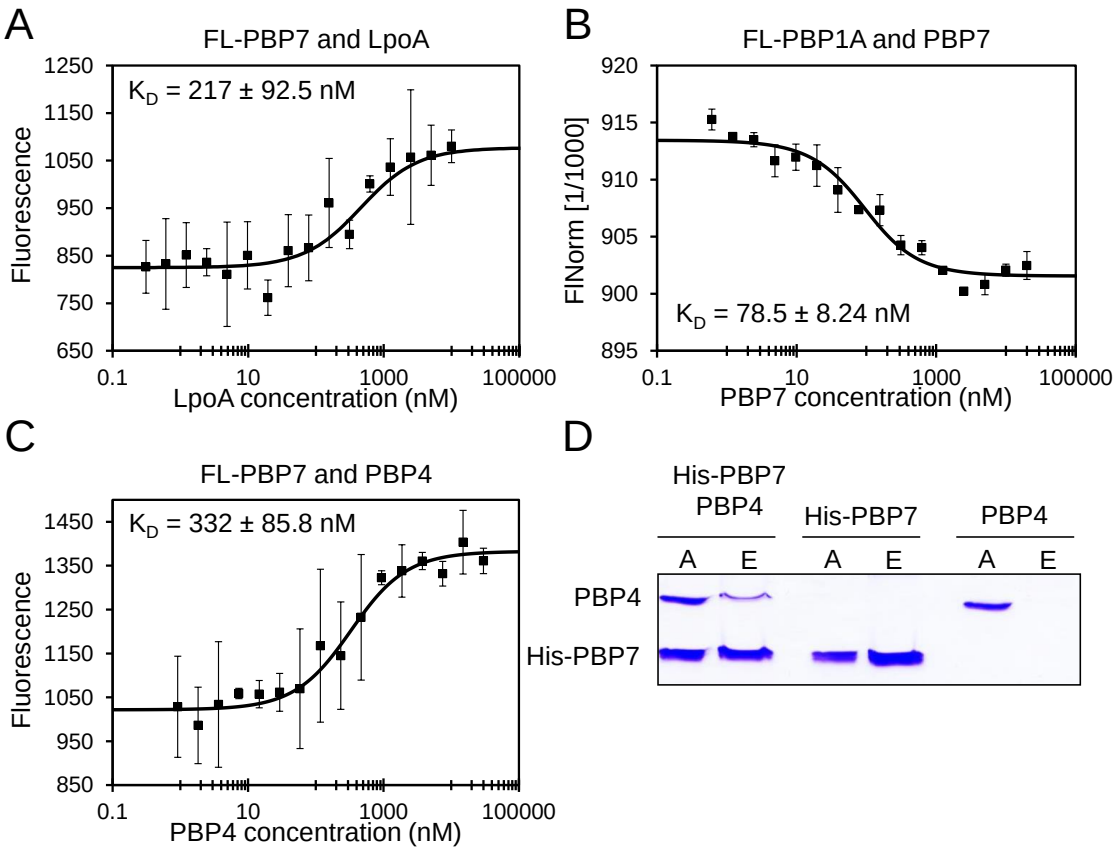

Figure 3.14 PBP7 interacts with PBP1A, LpoA and PBP4 *in vitro*

A. Purified PBP7 was labelled for MST at amine residues and used at a concentration of 62.5 nM. LpoA was serially diluted from 10 μM – 0.31 nM and MST measured at 20% LED power and 40% MST power. A concentration-dependent fluorescence change was observed and analysed by SD test. An estimated K_D of 217 ± 92.5 nM was determined using accompanying software. The values are the mean ± standard deviations of three independent experiments. Raw MST data are shown in figure 5.10. **B.** PBP1A was labelled at amine residues and used at a concentration of 41.5 nM. PBP7 was serially diluted from 30 μM and MST measured at 80% LED power and 20% MST power. An estimated K_D of 78.5 ± 8.24 nM was determined using accompanying software. Raw MST data are shown in figure 5.11. The values are the mean ± standard deviations of two independent experiments **C.** FL-PBP7 was titrated with serially diluted PBP4 from a concentration of 30μM – 0.916 nM. MST measurements were taken at 40% LED power and 40% MST power. A K_D of 332 ± 85.8 nM was estimated using accompanying software. The values are the mean ± standard deviations of three independent experiments. Raw MST data are shown in figure 5.12. **D.** *In vitro* Ni^{2+} bead pull-down assay using 2 μM His-PBP7 and native PBP4. Proteins were cross-linked with formaldehyde and an applied (A) sample taken prior to incubation with Ni^{2+} beads. After thorough washing, proteins were eluted (E), and cross-linking reversed, by boiling with SDS-loading buffer. Proteins were separated by 12% SDS-PAGE and visualised by Coomassie staining.

3.2.4.2 PBP7 - Non-interacting proteins or contradictory interactions

In addition to the positive PBP7 interactions observed so far, we present a number of proteins which do not interact with PBP7. Figure 3.15A/B shows the MST measurements of the negative interactions of PBP7 with MepS and MepM, respectively. In each case PBP7 was used as a serially diluted and titrated unlabelled ligand. FL-MepS (at amine residues) was used at a concentration of 62.5 nM to show no interaction when titrated with PBP7 serially diluted from 20 µM to 1.22 nM (figure 3.15A). Likewise, when unlabelled PBP7 was serially diluted from 50 µM to 1.526 nM and titrated with FL-MepM (at amine residues), at a concentration of 125 nM, there was no interaction (figure 3.15B). We tested the interaction between PBP7 and MepS by a second *in vitro* method using a Ni^{2+} bead pull-down assay using 2 µM of His-MepS and native PBP7. No retention of PBP7 was observed (figure 3.15C). However, when attempting to confirm the interaction between PBP1A and PBP7 by a Ni^{2+} bead pull-down assay, using His-PBP7 and thrombin-cleaved PBP1A, we observed no retention of PBP1A, contradicting the MST data (figure 3.15D).

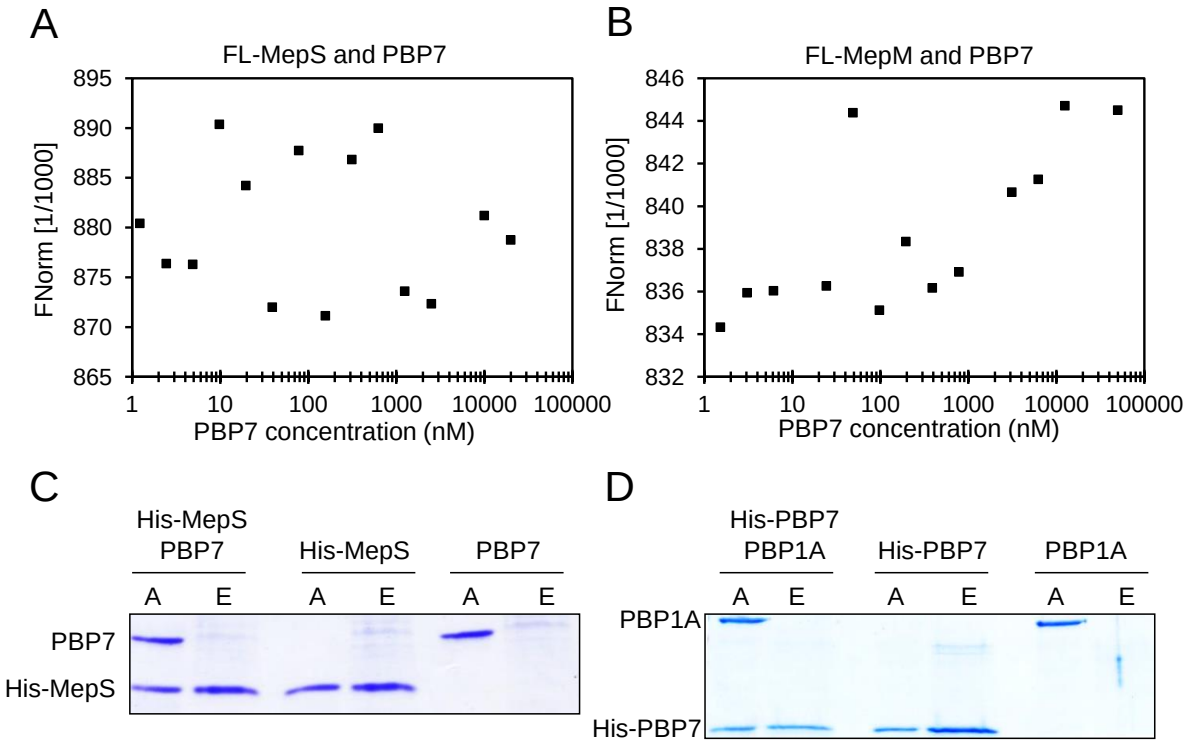

Figure 3.15 PBP7 does not interact with MepS and MepM, or PBP1A by Ni^{2+} bead pull-down assay

A. FL-MepS (at amine residues) was used at a concentration of 62.5 nM, and was titrated with two-fold serially diluted PBP7 from 20 µM – 1.22 nM for MST. Conditions were 40% MST power and 20% LED power. Raw MST data are shown in figure 5.13. **B.** FL-MepM (at amine residues) at a concentration of 125 nM was titrated with two-fold serially diluted PBP7 from 50 µM – 1.526 nM and tested for interaction by MST. Conditions were 40% MST power and 20% LED power. Raw MST data are shown in figure 5.14. **C.** *In vitro* Ni^{2+} bead pull-down assay using His-MepS and thrombin-cleaved PBP7. Proteins were cross-linked with formaldehyde and an applied (A) sample taken prior to incubation with Ni^{2+} beads. After thorough washing proteins were eluted (E) and cross-linking reversed by boiling with SDS buffer. Proteins were separated by 12% SDS-PAGE and visualised by Coomassie staining. **D.** Same as above using His-PBP7 and thrombin-cleaved PBP1A.

3.2.5 Interactions of MepS and MepM

3.2.5.1 Novel MepS interaction partners

Continuing the investigation of the interactions between the PG hydrolases, we tested the interaction of MepS and MepM using MST (section 2.5.1.7). MepM was fluorescently-labelled (at amine residues) and optimised to a working concentration of 125 nM. Unlabelled MepS was two-fold serially diluted from 30 µM to 0.916 nM and titrated with FL-MepM. We observed a repeatable binding curve that yielded an estimated K_D of 1175 ± 390 nM using the accompanying software (figure 3.16A).

We have identified direct associations between the PG hydrolases and the PG synthases, and it is known that MepS is redundantly essential for cell growth (section 1.4.2.2). We therefore tested for an interaction between MepS and PBP1A by MST. FL-PBP1A (at amine residues) was used at a concentration of 41.5 nM and was titrated with two-fold serially diluted unlabelled MepS from 30 µM to 0.916 nM. The experiment yielded a concentration-dependent fluorescence enhancement which was confirmed as due to ligand binding using an SD test (figure 5.16). The raw fluorescence values were used to generate an estimated K_D of 940 ± 127 nM (figure 3.16B).

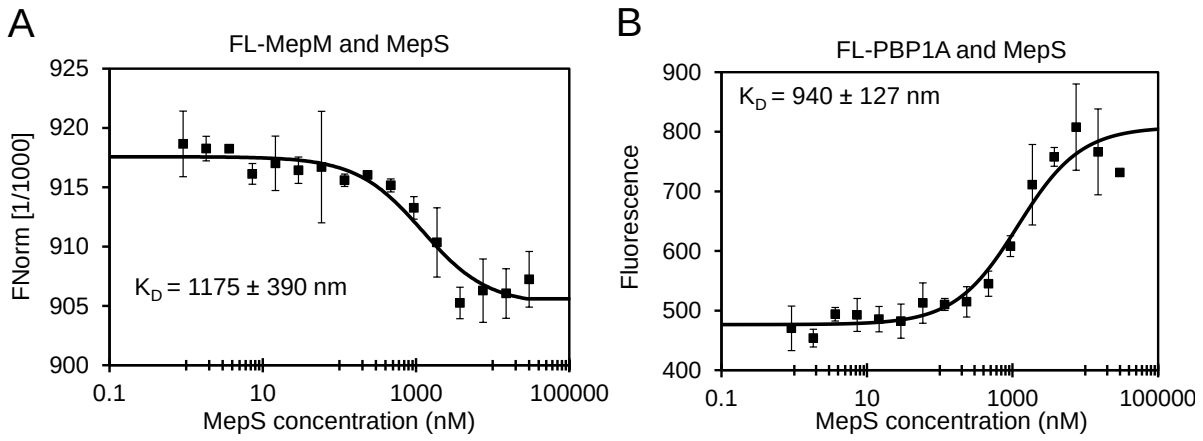

Figure 3.16 MepS interacts with MepM and PBP1A *in vitro*

A. FL-MepM (at amine residues) at 125 nM was titrated with two-fold serially diluted MepS from 30 µM – 0.916 nM. A K_D of 1175 ± 390 nM was estimated using accompanying software. MST power 20%, LED power 40%. The values are the mean ± standard deviations of two independent experiments. **B.** FL-PBP1A (at amine residues) at 41.5 nM was titrated with two-fold serially diluted MepS from 30 µM – 0.916 nM. A K_D of 940 ± 127 nM was estimated using accompanying software. MST power 40%, LED power 20%. The values are the mean ± standard deviations of two independent experiments. Raw MST data are shown in figures 5.15 and 5.16.

3.2.5.2 MepS - Non-interacting proteins or contradictory interactions

There appears to be a weak, yet direct interaction between MepS and PBP1A. We therefore tested for an interaction between MepS and LpoA, using MST (section 2.5.1.7). FL-MepS (at amine residues) was used at a concentration of 62.5 nM and was titrated with two-fold serially diluted unlabelled LpoA from 30 µM to 0.916 nM. No interaction was observed (figure 3.17A).

Using the same FL-MepS concentrations, we saw no interaction upon titration of unlabelled PBP4 from 50 µM to 1.526 nM (figure 3.17B). Unfortunately, this is in contradiction to a Ni^{2+} bead pull-down assay that was performed in which His-MepS was able to retain native PBP4 on Ni^{2+} beads (figure 3.17C) (section 2.5.2.2).

The final potential MepS interaction partner tested was EnvC. Again, FL-MepS was titrated with serially diluted unlabelled EnvC from 15 µM to 0.458 nM, and no interaction was observed (figure 3.17D).

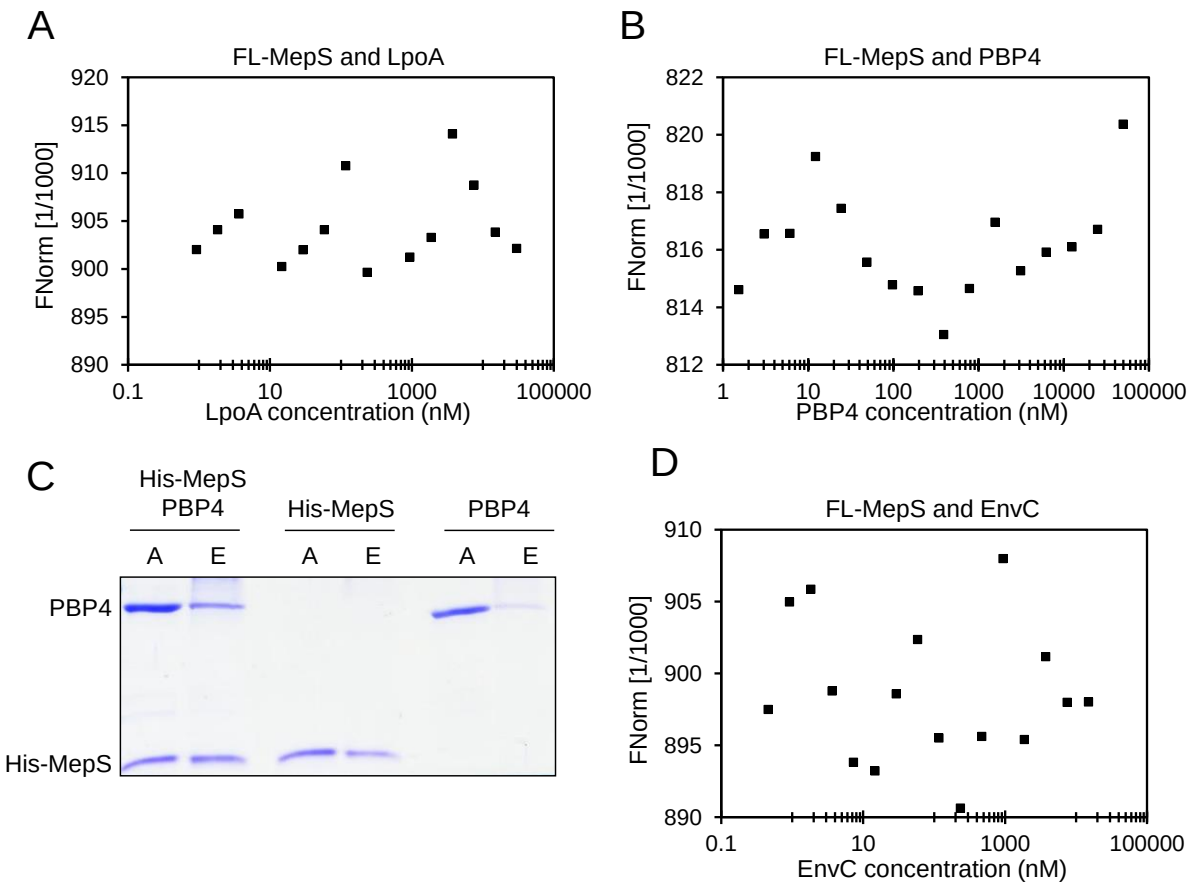

Figure 3.17 MepS – Non-interacting proteins or contradictory interactions

A. MST of FL-MepS (at amine residues) at 62.5 nM titrated with two-fold serially diluted unlabelled LpoA from 30 µM – 0.916 nM. MST power 40%, LED power 20%. Raw MST data are shown in figure 5.17. **B.** MST as above using unlabelled PBP4 from 50 µM – 1.526 nM. MST power, LED power 40%. Raw MST data are shown in figure 5.18. **C.** *In vitro* Ni^{2+} bead pull-down assay using His-MepS and native PBP4. Proteins were cross-linked with formaldehyde and an applied (A) sample taken prior to incubation with Ni^{2+} beads. After thorough washing, proteins were eluted (E), and cross-linking reversed, by boiling with SDS buffer. Proteins were separated by 12% SDS-PAGE and visualised by Coomassie staining. **D.** MST as above using unlabelled EnvC from 15 µM – 0.458 nM. MST power 20%, 20% LED power. Raw MST data are shown in figure 5.19.

3.2.5.3 MepM - Non-interacting proteins

In this section we have shown that MepM interacts with MepS (figure 3.16A) and does not interact with PBP7 (figure 3.15B). We present here two other negative MepM interaction partners; PBP4 and LpoA.

We performed MST to test for an interaction between PBP4 and MepM and showed that there is no interaction. FL-MepM (at amine residues) at a constant concentration of 125 nM was titrated with two-fold serially diluted unlabelled PBP4 from 30 µM to 0.916 nM. The negative MST measurement is shown in figure 3.18A.

We have shown that each of the hydrolases so far has an association to the elongasome through a direct interaction with PBP1A, LpoA or both. We therefore tested for an interaction between MepM and LpoA. Using the His-tagged form of MepM and an untagged version of LpoA we performed an *in vitro* Ni^{2+} bead pull-down assay and observed no retention of tag-less LpoA (figure 3.18B).

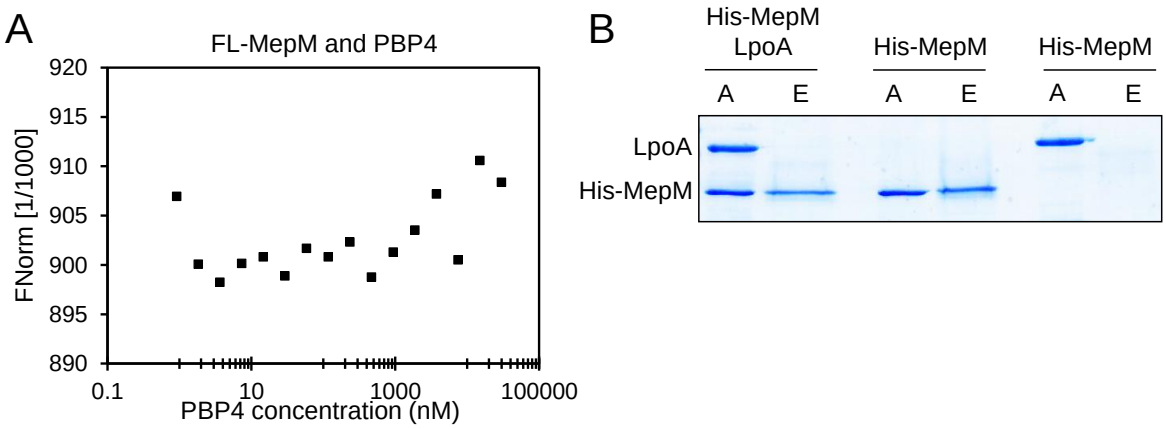

Figure 3.18 Non-interacting protein of MepM

A. FL-MepM (at amine residues) at a concentration of 125 nM was titrated with two-fold serially diluted PBP4 from 30 µM – 0.916 nM and tested for interaction by MST. Conditions were 20% MST power and 20% LED power. Raw MST data are shown in figure 5.20. **B.** *In vitro* Ni^{2+} bead pull-down assay using His-MepM and native LpoA. Proteins were cross-linked with formaldehyde and an applied (A) sample taken prior to incubation with Ni^{2+} beads. After thorough washing, proteins were eluted (E) and cross-linking was reversed by boiling with SDS buffer. Proteins were separated by 12% SDS-PAGE and visualised by Coomassie staining.

3.2.6 Conclusions and discussions

The data presented in this section followed from the results in section 3.1, primarily the characterisation of the structure of the OM-anchored lipoprotein LpoA, and the identification of multiple TPR-like motifs within $LpoA^N$. None of the interactions/activity effects in this section had been reported or published previously.

Interactions between LpoA, PBP1A and PBP4

A proteomics-based search for LpoA interaction partners identified PBP4. We confirmed this as a direct interaction *in vitro* using SPR. Unfortunately the sensorgrams generated were not suitable for K_D determination due to a 'biphasic' binding pattern. After consultation with an SPR analyst we hypothesised that a dimer of PBP4 was binding to the LpoA surface to cause the first increase in response units before disassociation of a PBP4 monomer. We speculate that the released monomer re-associated to the LpoA surface, causing the unique binding curve observed. To confirm the interaction by a second *in vitro* method, and to estimate a K_D value for the interaction, we performed MST.

The interaction between unlabelled PBP4 and FL-LpoA generated a concentration-dependent fluorescence enhancement. After confirmation that the change occurred as result of ligand binding by SD test, the raw fluorescence data was used to estimate a K_D of 315 ± 38 nM. The concentration-dependant fluorescence enhancement implies the interaction occurs close to sites of LpoA labelling. The two cysteine residues of LpoA are located in $LpoA^C$, implying it is this domain that is the primary interaction site of PBP4. We were also able to confirm the *in vivo* interaction using co-immunoprecipitation.

We tested the relevance of this interaction *in vitro* by showing that LpoA had a moderate inhibitory effect on both the EPase and CPase activities of PBP4. However, we hypothesise that the primary role of this interaction is spatio-temporal. LpoA may interact with PBP4 in order to coordinate hydrolase activity with ongoing PG synthesis, to create the space required for nascent PG insertion by the core PG synthesis complex during elongation. Due to the lack of a strong effect on activity we hypothesise that LpoA acts to target PBP4 activity, rather than regulate activity, however, localisation studies will have to be undertaken to test this hypothesis.

We continued to investigate this interaction using truncated versions of both proteins ($LpoA^C$, $LpoA^N$, and PBP4ΔD3) in MST experiments. We show that full length LpoA interacts with both PBP4 and PBP4ΔD3, the resulting binding curves generating estimated dissociation

constants of 315 ± 38 nM and 153 ± 31 nM, respectively. As the interaction takes place with similar affinity, the LpoA interaction sites of PBP4 likely lie in domains 1 and/or 2. As discussed earlier the interaction between full length LpoA and full length PBP4 inferred that the PBP4 interaction sites of LpoA lie in $LpoA^C$. We continued to search for information regarding interaction sites using the truncated versions of LpoA.

We show that $LpoA^C$ interacts with full length PBP4 with an estimated K_D of 226 ± 15 nM, and with PBP4ΔD3 with an apparent K_D of 315 ± 21 nM. These dissociation constants are within the same range as that of full length LpoA and indicate firstly, that the interaction may indeed take place primarily through $LpoA^C$, and secondly, that domain 3 of PBP4 is likely not important for the interaction with LpoA. It is interesting to note that binding of PBP4 to full length fluorescently-labelled LpoA at cysteine residues caused a concentration-dependent fluorescence enhancement, but the binding of PBP4 to cysteine-labelled $LpoA^C$ did not. $LpoA^N$ does not contain any cysteines, and implies multiple PBP4 binding sites within $LpoA^C$, involving the cysteines when the protein is in its full length form, and not requiring the cysteine residues in the truncated form. The cysteines of $LpoA^C$ are not present in the 'wing'-like domains of LpoA indicating these may not be important interaction sites when the full length versions of both proteins interact. However, we speculate that these 'wing'-like domains become more important when the need to stabilise an interaction arises, in this case with roughly 30% of its structure missing. This means the interaction would not take place through the labelled cysteine residues, as with full length LpoA, leading to the standard MST binding curve observed, rather than the concentration-dependent fluorescence enhancement observed for full length LpoA and full length PBP4.

We also used $LpoA^N$ in MST to test for the interaction with full length PBP4 and PBP4ΔD3. While the interaction of $LpoA^N$ took place with both PBP4 versions, the interaction between $LpoA^N$ and full length PBP4 occurred with three times less affinity than full length LpoA, at 954 ± 52 nM. This indicated again that $LpoA^C$ is primarily responsible for the interaction with PBP4.

However, the interaction between $LpoA^N$ and PBP4ΔD3 occurred with the highest affinity observed in this work with an estimated K_D of 17 ± 4 nM. We hypothesise that the interaction between $LpoA^N$ and PBP4 is dependent on the conformational state of domain 3. A conformational change in this domain, or in this case a deletion, may reveal a larger interaction site promoting an interaction with $LpoA^N$ with ~50 times higher affinity. This conformational change may occur upon binding of another PBP4 interaction partner, which may reveal more of the active site and thus increase activity, the affinity for $LpoA^N$ may then

increase in order to exert the inhibitory effect observed in this work, thus moderating the activity of PBP4. This also implies that the two domains of LpoA may have different primary functions; perhaps $LpoA^N$ acts to control PBP4 activity where $LpoA^C$ acts to recruit PBP4 to sites of ongoing PG synthesis. More work is required to test these hypotheses.

In addition to LpoA, we show that PBP4 interacts directly *in vitro* and *in vivo* with PBP1A. We applied the same interaction assays as used to confirm the LpoA-PBP4 interaction including SPR, which again yielded a binding curve not suitable for K_D determination. The lack of dissociation of PBP4 over the PBP1A surface, and absence of a concentration-dependent response over the control surface, indicates that the specific interaction of PBP4 with PBP1A takes place with high affinity. MST was performed using unlabelled PBP4 and FL-PBP1A to estimate a K_D value for the interaction of 66.8 ± 9.1 nM. This high affinity interaction correlates with the lack of PBP4 dissociation observed in the SPR experiment.

Like the interaction between LpoA and PBP4, we hypothesise that the role of this interaction is to recruit PBP4 to sites of ongoing PG synthesis during cell growth, however, localisation studies will be required to confirm these hypotheses.

Interactions of PBP7 with LpoA, PBP1A and PBP4

Using purified PBP7 as both the labelled protein (at amine residues) and unlabelled serially diluted ligand in MST, we identified interactions between PBP7 and both PBP1A and LpoA. The estimated K_D values generated were 78.5 ± 8.24 nM and 217 ± 92.5 nM, respectively, strikingly similar affinities to those observed for PBP4 with PBP1A and LpoA. The interaction between PBP1A and PBP7 was observed by MST only, showing no interaction by Ni^{2+} bead pull-down. It is speculated that the lack of interaction by pull-down assay may be due the hexahistidine tag that may either occlude interaction sites with PBP1A or cause PBP7 to be immobilised to the Ni^{2+} resin in such a way that prevents PBP1A binding, a situation that would not occur in solution, as with MST. We aim to optimise another *in vitro* technique, such as SPR with which to confirm this interaction.

These data infer that PBP7 may also be recruited to the elongasome through direct interactions with the core synthesis complex. In addition, we observed a direct interaction with PBP4 using a Ni^{2+} bead pull-down assay and MST experiments, by which we estimated a K_D value of 332 ± 85.8 nM. We have yet to show any effect of PBP7 on the activity of PBP1A or the stimulation of PBP1A by LpoA, and thus hypothesise, that like PBP4, the

primary role of these interactions could be spatio/temporal. If both PBP4 and PBP7 are recruited to sites of ongoing PG synthesis by PBP1A/LpoA, this could allow a greater degree of hydrolase activity during elongation. PBP4 and PBP7 have implicated auxiliary roles in the maintenance of cell morphology [121]. We speculate that upon deletion of both of these proteins, there is an imbalance in PG synthesis and hydrolysis during elongation leading to the morphological changes observed.

Interactions of MepM and MepS

We have observed the interaction between PBP4 and PBP7 and thus hypothesised the existence of interactions between the other hydrolases. We showed the negative interactions of both PBP4 and PBP7 with MepS and MepM, however, we showed that MepS and MepM interact directly by MST, with an estimated K_D of 1175 ± 390 nM.

We hypothesise that these four EPases are all associated to the PG synthesis complex, yet exist as two separate hydrolase complexes. Both PBP4 and PBP7 interact with each other and with LpoA and PBP1A, and thus may associate through these interactions. We observe the interaction between MepS and PBP1A, with an estimated K_D of 940 ± 127 nM, and thus hypothesise that a complex of MepS and MepM could associate this way. The PG hydrolase complexes may be recruited to the elongasome at different conditions or possess different substrate specificities to allow for a robust system of hydrolysing activity at sites of ongoing PG synthesis. More experiments will be required to test this hypothesis.

We continued by showing that MepS does not interact with LpoA or EnvC. However, using a Ni^{2+} pull-down assay, we obtain inconsistent results for the interaction between PBP4 and MepS. We observed no interaction between MepS and PBP4 by MST, yet showed that His-MepS was able to retain native PBP4. It is possible that a weak interaction takes place and was strengthened by the addition of the formaldehyde cross-linker, or that the fluorophore of the labelled MepS prevented binding of PBP4. We aim to test this interaction using another method, for example ITC, SPR or AUC.

We also show the negative interaction of MepM and LpoA; however we have yet to test the interaction of MepM and PBP1A. We therefore propose that any association of MepM to the PG synthesis complex would be indirect, facilitated by the interaction of MepS and PBP1A.

Final word

In this section we have employed *in vitro* and *in vivo* approaches to characterise a number of novel interactions. We significantly enhance the knowledge of how the PG synthases and hydrolases could be coordinated as members of a multi-enzyme complex. The interactions and activities identified in this section, and subsequent sections, are summarised in figure 3.28 at the end of the section 3.4.

3.3 Biochemical characterisation of PBP4

3.3.1 Introduction

Before this work there were no known PBP4 interaction partners, or regulators of activity. As described in the previous section, we have now identified at least three novel interaction partners; two members of the PG synthesis complex during cell elongation, PBP1A and LpoA, and another Class C PBP with EPase activity, PBP7. The crystal structure of PBP4 has been elucidated, alone and with covalently bound β-lactam antibiotics [115]. It is comprised of three domains each embedded in the other; the active site serine-containing domain 1 is embedded with the non-catalytic domain 2, which in turn is embedded with the globular, non-catalytic domain 3. This Russian doll-like architecture is thought to prevent flexibility between the three domains. PBP4 crystallises as a tight face-to-face dimer [115].

In section 3.2 we showed that domain 3 is not required for the interaction with LpoA. To further characterise PBP4, biochemically and structurally, we investigated the substrate binding capabilities and activities of the full length protein in comparison to the truncated form of PBP4, PBP4ΔD3.

3.3.2 PBP4 is a dimer in solution

As mentioned above, the published data predicts that PBP4 exists as a dimer, however, we sought to determine the oligomeric state of PBP4 in solution at the conditions used for interaction and activity assays. We therefore performed analytical ultracentrifugation (AUC) in collaboration with Dr. Alexandra Solovyova, Newcastle University. Purified PBP4 was dialysed o/n against 25 mM HEPES/NaOH, 150 mM NaCl, pH 7.5 and was analysed using the fringe displacement (interference) technique at 20°C to determine the sedimentation velocity of PBP4 at varying concentrations (5.6, 11.68, 17.27, 19.38 and 20.82 mg/ml) (figure 3.19). Results were corrected for the viscosity/density of H_2O at 20°C. The amino acid sequence and the known crystal structure data were used to predict the sedimentation velocity of a PBP4 dimer as 5.54 S with a molecular weight of 98.6 kDa. The experimental data collected had a sedimentation velocity of 5.35 S which corresponded to a dimer with a different monomer orientation than the published crystal structure. These data, and the absence of a PBP4 monomer peak, suggests that PBP4 is a dimer in solution with a different structure than that determined by X-ray crystallography.

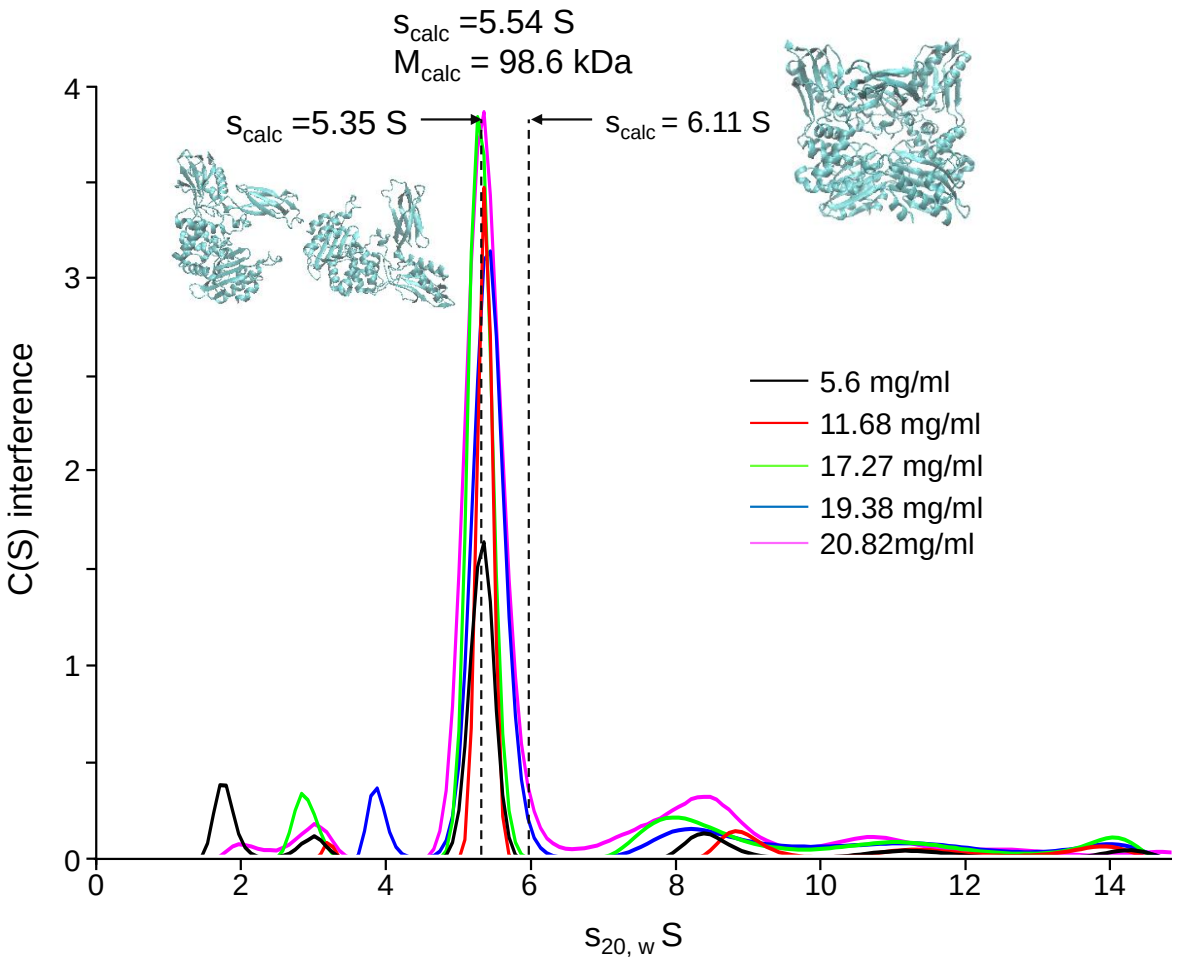

Figure 3.19 Analytical ultracentrifugation shows that PBP4 exists as a dimer in solution

Size distribution plots showing the sedimentation velocity of PBP4. The calculated sedimentation velocity by fringe displacement interference and subsequent estimation of molecular weight suggests PBP4 forms a dimer in solution with a different monomeric orientation to that of the published crystal structure. $s_{20,w}$S (Sedimentation coefficient corrected for the viscosity and density of the solvent, relative to that of water at 20°C) plotted against absorbance (280 nM).

3.3.3 Domain 3 of PBP4 is crucial for activity

Substrate binding of PBP4 versions

Domain 3 of PBP4 is predicted to be globular with a strong hydrophobic core suggesting that the domain can be removed without loss of structural integrity to the rest of the protein [115]. The purification and subsequent use in interaction assays of PBP4ΔD3 was addressed in section 3.2.

The successful purification of PBP4ΔD3 indicated that the protein was correctly folded. However, we performed Circular Dichroism (CD), in comparison to full length PBP4, to further study the structural integrity of the truncated version, in collaboration with Prof. Jeremy Lakey, Newcastle University. Proteins were dialysed o/n against 10 mM $NaPO_4$, pH 7.5 and concentrated/diluted to 0.4 mg/ml. CD measurements were taken using a Jasco J-810 spectropolarimeter using a wavelength range of 180-250 nm. The average of 10 runs was taken for each protein with a buffer control subtraction. For a direct comparison, correcting for the differing amino acid sequences, the collected data was converted to molecular CD and plotted against wavelength (nm). The resulting CD spectra are compared in figure 3.20A and show that PBP4 lacking domain 3 is folded, consisting of both α-helices (~190 nm) and β-sheets (~210 nm).

To investigate the folding of the active site, an FL-bocillin binding assay was performed (section 2.5.2.1). The catalytically inactive version of PBP4, containing a single base substitution of serine 52 to alanine (S52A), was also purified as a negative control (section 2.4.4). All PBP4 versions (10 µg) were incubated in 50 µl with 20 ng/µl of a fluorescently-labelled version of the β-lactam bocillin (FL-bocillin) (Sigma). As a negative control, penicillin G was pre-incubated with protein samples at 1 ng/µl for 10 min to block the active site. Samples were resolved by 12% SDS-PAGE and fluorescence visualised using a Typhoon Fluoroimager (Excitation laser; 488 nm, emission filter; 520 BP20, PMT voltage; 400-800). As expected, full length PBP4 was capable of binding FL-bocillin, and the catalytically inactive version of PBP4 was not (figure 3.20B). However, we show that PBP4ΔD3 was also capable of binding FL-bocillin, which suggests that PBP4ΔD3 has a correctly folded active site.

We also investigated whether domain 3 of PBP4 was crucial for PG binding. A PG-binding assay was performed (section 2.7.3) in which 100 µl of WT MC1061 PG was pelleted by centrifugation and resuspended in 100 µl binding buffer (10 mM Tris/maleate, 10 mM $MgCl_2$,

50 mM NaCl, pH 7.5) and incubated with 10 µg of either PBP4 or PBP4ΔD3. Control samples were used for each PBP4 version which contained no PG. After a 30 min incubation, samples were centrifuged and washed with 200 µl of PG-binding buffer. A final SDS incubation was performed to release bound proteins before resolving the samples by SDS-PAGE (figure 3.20C). We showed that both PBP4 and PBP4ΔD3 were retained by PG. In addition to the CD spectra and the FL-bocillin binding assays, these data indicate that the truncated version of PBP4 has a correctly folded secondary structure and active site, and is capable of substrate binding.

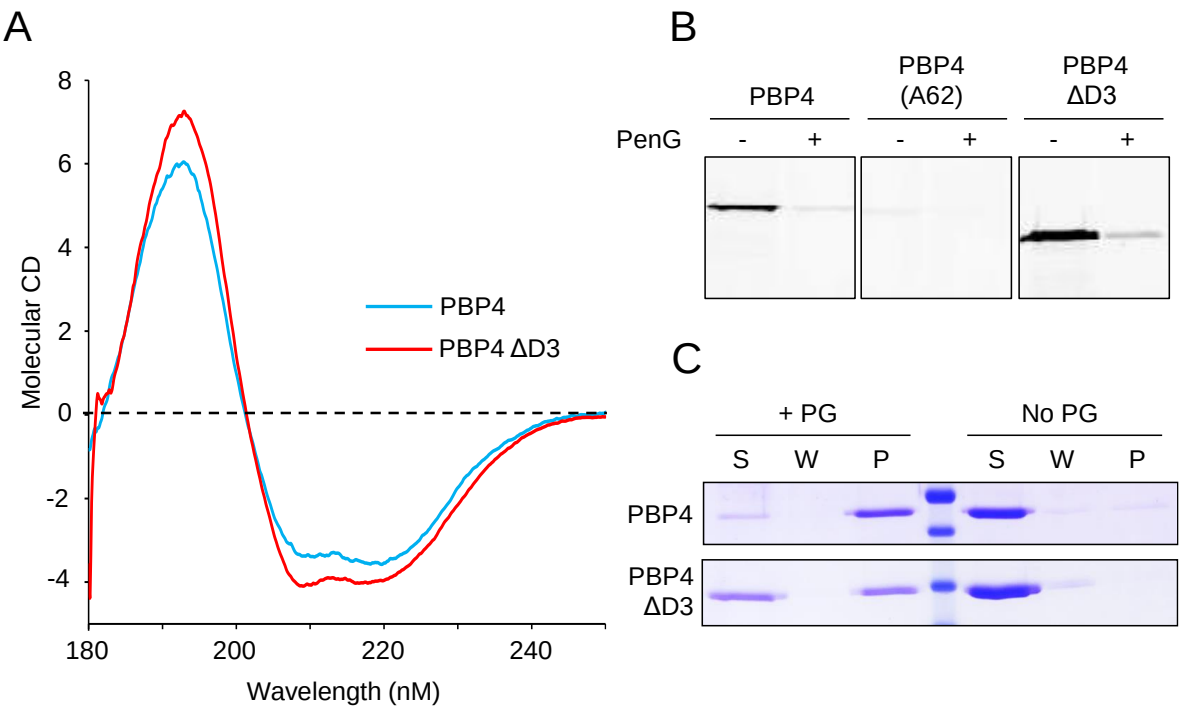

Figure 3.20 PBP4ΔD3 is folded and capable of binding substrates

A. Circular Dichroism spectra of PBP4 and PBP4ΔD3 showing molecular CD against wavelength. Full length PBP4 and PBP4ΔD3 are folded, consisting of α-helices and β-sheets. **B.** PBP4 (full length), inactive PBP4 (S62A) and PBP4ΔD3 were incubated 10 µg in 50 µl with FL-bocillin. Proteins were either pre-incubated with penicillin G (+) or not (-) before boiling with SDS-loading buffer. Proteins were separated by 12% SDS-PAGE and visualised using a Typhoon Fluoroimager (Excitation laser; 488 nm, emission filter; 520 BP20, PMT voltage; 400-800). **C.** The resuspended pellet of a 100 µl PG suspension was incubated with 10 µg of PBP4 (full length), inactive PBP4 (S62A) and PBP4ΔD3 for 30 min. Samples were centrifuged and the supernatant was retained (S) before being washed with binding buffer and centrifuged. The supernatant was retained (W) and the PG pellets were resuspended in 2% SDS solution and incubated for 1 h with stirring. Samples were centrifuged and the supernatant retained (P). Proteins were separated by 12% SDS-PAGE and visualised by Coomassie staining in comparison to samples lacking PG.

Hydrolytic activity of PBP4 versions

In order to study the EPase and CPase activity of PBP4ΔD3, assays were performed with all three versions of PBP4. A HPLC-based muropeptide digestion assay was performed as described in section 2.5.2.2. Muropeptides from the MC1061 strain were incubated with each PBP4 version at 1 µM for 30 min at 37°C in standard EPase reaction buffer (10 mM HEPES/NaOH, 10 mM $MgCl_2$, 150 mM NaCl, 0.05% Triton X-100, pH 7.5). The reaction was stopped by boiling, and the samples were reduced for analysis by reversed-phase HPLC (2.5.2.5). The relative percentages of Tetra-containing muropeptides (monomers and dimers) were calculated and plotted. The results show that despite its correctly folded active site, PBP4ΔD3 was inactive (figure 3.21A). This lack of inactivity was also demonstrated with intact sacculi from the MC1061 strain using 1 µM of each protein incubated for 4 h in EPase reaction buffer at 37°C (figure 3.21B). Using isolated muropeptides from the penta-peptide rich sacculi, CS703-1 at the same conditions as the MC1061 muropeptide digestion assay, we also observed the inactivity of PBP4ΔD3, while the full length protein was active on all substrates (figure 3.21C).

To address the CPase activity of PBP4, a spectrophotometric D-Ala release assay was performed using all three PBP4 versions (section 2.5.2.3). Figure 3.21D shows the absorbance against time for each protein at 10 µM. The only activity observed is that of full length PBP4. Both the catalytically inactive version and PBP4ΔD3 have no activity.

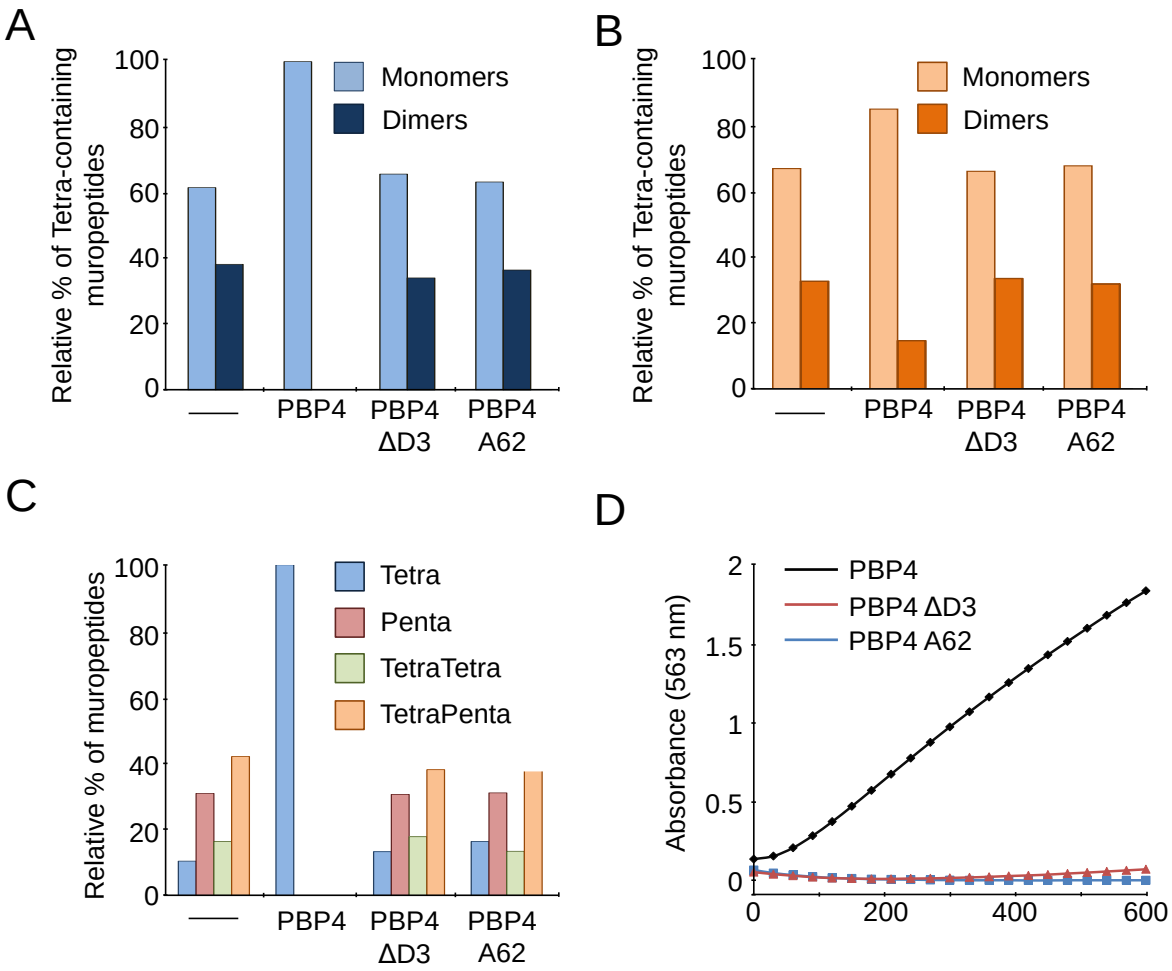

Figure 3.21 Domain 3 of PBP4 is required for activity

PBP4 versions were incubated at 1 µM with isolated muropeptides from MC1061 PG (**A**) for 30 min, or intact MC1061 sacculi (**B**) for 4 hours. Isolated muropeptides from the pentapeptide rich sacculi CS703-1 (**C**) were also used for 30 min at 37°C before boiling and reducing with sodium borohydride and analysis by HPLC. All assays were undertaken at 37°C with shaking. **D.** Spectrophotometric D-Ala release assay with PBP4 versions (10 µM) using UDP-Mur*N*Ac-pentapeptide as substrate. Absorbance read at 563 nm.

3.3.4 PBP4ΔD3 is a dimer in solution

The data gathered thus far suggest that domain 3 has a crucial role in the hydrolytic activity of PBP4, yet the removal of this domain does not affect the binding of PG substrate or β-lactams. Domain 3 constitutes ~40% of the dimer surface [115]. We therefore hypothesised that without this domain, PBP4 would remain in an inactive, yet substrate-binding, monomeric state.

We performed AUC in collaboration with Alexandra Solovyova. Samples were dialysed o/n against 25 mM HEPES/NaOH, 150 mM NaCl, pH 7.5 and the fringe displacement (interference) technique was used at 20°C to determine the sedimentation velocity of varying concentrations of PBP4ΔD3 (5.9, 9.4, 17.3, 27.3 and 34.7 mg/ml). Results were corrected for the viscosity/density of H_2O at 20°C. Using the amino acid sequence and the known crystal structure data, the predicted sedimentation velocity of PBP4ΔD3 in the dimeric state was predicted to be 5.3 S (figure 3.22). Like the full length version, there was no monomeric peak, predicted to have a molecular weight of ~45 kDa. At the higher concentrations, trimer and tetramer peaks could be observed. However, the dimer peak was the most prominent at all concentrations tested. These data support that PBP4ΔD3 is a dimer in solution, but that the monomers may arrange in a different orientation to those of full length PBP4.

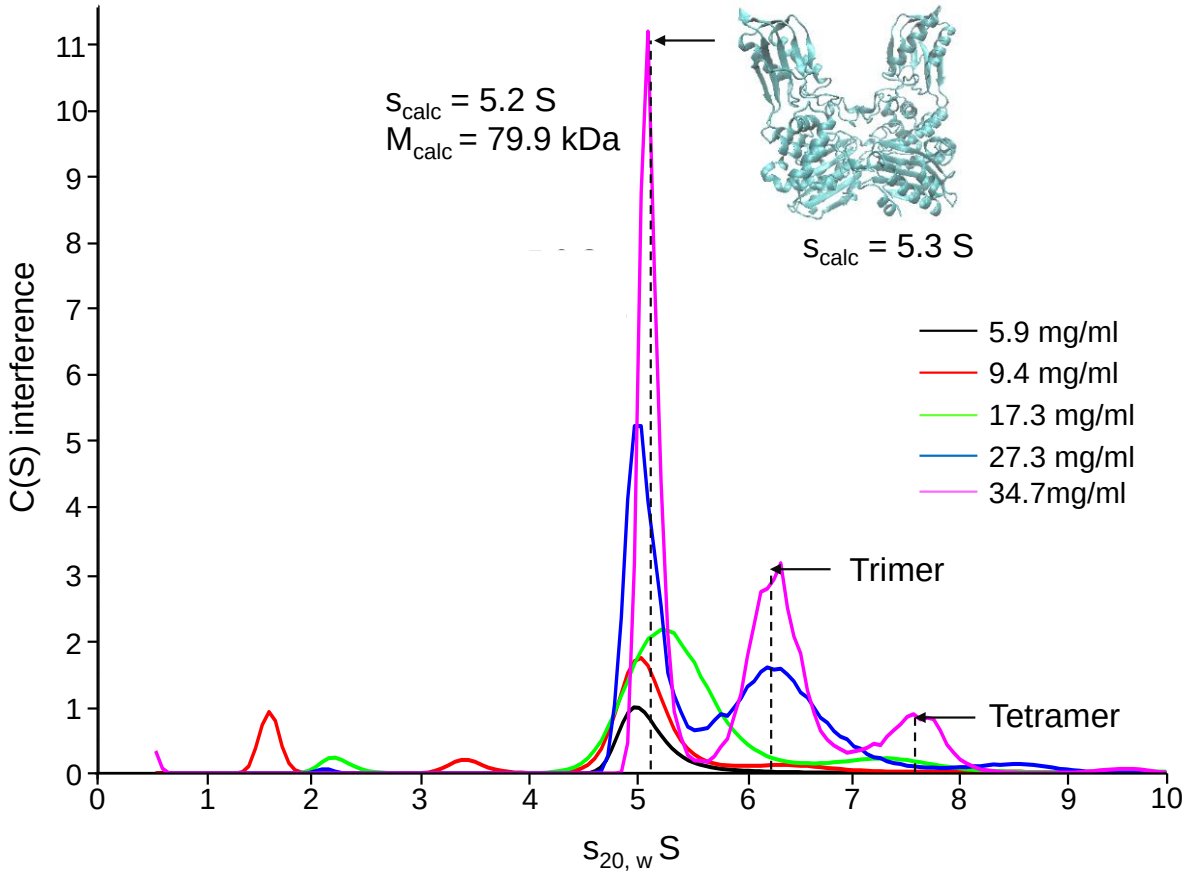

Figure 3.22 Analytical ultracentrifugation shows that PBP4ΔD3 exists as a dimer in solution

Size distribution plots showing the sedimentation velocity of PBP4ΔD3. The calculated sedimentation velocity by fringe displacement interference and subsequent estimation of molecular weight suggests PBP4ΔD3 forms a dimer in solution. $s_{20,w}$S (Sedimentation coefficient corrected for the viscosity and density of the solvent, relative to that of water at 20°C) plotted against absorbance (280 nM).

3.3.5 Domain 3 of PBP4 is not required for interaction with PBP1A

Domain 3 of PBP4 constitutes 15.3% of the amino acid sequence of the PBP4 monomer. We hypothesised that it could also be an interaction site for the PBP4 interaction partners identified in the section 3.2.

In section 3.2.2.3 we show that PBP4ΔD3 was capable of binding full length LpoA. Here we performed MST in which PBP4ΔD3 was two-fold serially diluted and titrated as the unlabelled ligand from a starting concentration of 10 μM (section 2.5.1.7) and tested for interaction with FL-PBP1A (at amine residues), which was used at 41.5 nM.

LpoA interacts with PBP4ΔD3 with similar affinity to that of the full length, with an apparent K_D of 153 ± 31 nM compared to 315 ± 37.7 nM. PBP1A was also capable of interacting with PBP4ΔD3, with an apparent K_D of 246 ± 49.7 nM compared to 66.8 ± 9.11 nM for full length PBP4 (figure 3.23). These data show that domain 3 is not a crucial interaction site for at least two of its known interaction partners implying it is domain 1 and/or 2 that possess the LpoA/PBP1A interaction sites.

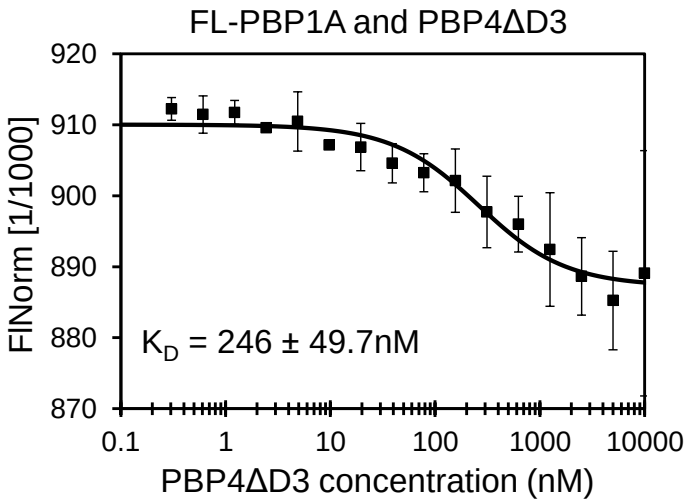

Figure 3.23 PBP1A interacts with PBP4 independently of domain 3

MST of two-fold serially diluted PBP4ΔD3 (10 μM – 0.305 nM) with FL-PBP1A (at amine residues) at 41.5 nM (20% MST power, 80% LED power). The K_D value was estimated to be 246 ± 49.7 nM and was calculated using the accompanying software. The values are the mean ± standard deviation of three independent experiments. Raw MST data are shown in 5.21.

3.3.6 Conclusions and discussion

In this section we present further efforts to structurally and biochemically characterise full length PBP4 and a truncated form of the protein, PBP4ΔD3, in which the globular domain 3 of the protein is removed. The structural model of the PBP4 dimer, presented in [115], suggests a tight face-to-face monomeric orientation which, using AUC, we predicted would sediment at 6.11 S. In concordance with the published data we show that PBP4 exists exclusively as a dimer in solution at the concentrations tested. However, our AUC data suggest a different orientation of the monomers. Instead of a face-to-face orientation the experimental data predicted an end-to-end monomer arrangement. This may highlight a hitherto uncharacterised oligomeric flexibility that we may see at the milder conditions of AUC rather than those required for X-ray crystallography. Nevertheless, our data showed that PBP4 is a dimer in solution.

Using circular dichroism (CD) we show that domain 3 can be removed from PBP4, and the truncated version purified, without loss of secondary structure. Of note firstly is that the PBP4ΔD3 CD spectra corresponds to a folded protein consisting of both α-helices and β-sheets. The crystal structure of PBP4 (figure 1.4) predicts that domain 3 consists mainly of β-sheets, with the rest of the structure comprised of a mixture of β-sheets and α-helices. These data suggest that PBP4ΔD3 is folded but cannot predict whether the rest of the unaltered domains of the protein are the same as native PBP4.

We showed that the active site of PBP4ΔD3 is folded using two substrate-binding assays. In comparison to full length PBP4 and the active site mutant PBP4S62A we show that PBP4ΔD3 binds a fluorescent form of the β-lactam bocillin, indicating that PBP4ΔD3 has a folded active site. Using a PG-binding assay we show that PBP4ΔD3 is able to bind high molecular weight sacculi, albeit with less efficiency, although this is not quantitative.

Domain 3 has thus far been shown to be non-essential for structural integrity and substrate binding. We therefore directly assayed the *in vitro* activity of this truncated form in comparison to full length PBP4 and PBP4S62A. We showed in EPase activity assays using both isolated muropeptides and intact sacculi from the MC1061 WT strain, and muropeptides from a penta-peptide rich strain (CS703-1), that PBP4ΔD3 is inactive. Similarly, using a spectrophotometric D-Ala release assay, we show that PBP4ΔD3 has no CPase activity.

Our initial hypothesis to explain this lack of activity, having studied the crystal structure which depicts domain 3 as a major dimer interface, was that domain 3 facilitates the correct dimerisation of PBP4, and that PBP4 is only active in a dimeric state. At the same conditions

as full length PBP4 we showed that PBP4ΔD3 also exists as a dimer by AUC, however with a slightly different monomeric orientation. Whether this is significant is yet to be determined, however, we speculate that the orientation of the dimers, whilst not preventing the binding of the substrate to the active site of PBP4ΔD3, could in some way abate activity. It is possible that PBP4ΔD3 monomers are capable of dimerising in a face-to-face orientation but, without domain 3, encloses the active sites of both monomers. While this may not prevent substrate binding we hypothesise that it could prevent degradation of bound material. Alternatively, if the PBP4ΔD3 monomers dimerise in a back-to-back fashion, with their active sites facing away from each other, this could allow substrate binding to the active site of each monomer, but for activity to occur, coordination of both monomers may be required. A third possibility is that, while not required for general substrate binding, domain 3 is required to correctly position substrate for degradation.

In section 3.2.2.3 we showed that domain 3 is not required for an interaction with LpoA. LpoA interacts with full length PBP4 with an estimated K_D of 315 ± 37.7 nM and with PBP4ΔD3 with an estimated K_D of 153 ± 31 nM. We showed in this section that the interaction between PBP4 and PBP1A is also not reliant on domain 3, however, PBP1A interacts with PBP4ΔD3 with less affinity than full length PBP4, decreasing from 66.8 ± 9.11 nM to 246 ± 49.7 nM when domain 3 is absent. We hypothesise that domain 3 may play an auxiliary role in the interaction with PBP1A, but its presence is not essential. These data suggest the interaction of LpoA and PBP1A with PBP4 occurs primarily through domain 1 and/or 2 of PBP4. More detail regarding the LpoA/PBP4 interaction was shown in section 3.2.2.3 using truncated forms of both proteins. Neither LpoA nor PBP1A have major enzymatic effects on the activity of PBP4 and neither require domain 3 as an interaction site, a domain which seems critical for activity. We therefore hypothesise that any regulator of PBP4 activity would interact with domain 3.

Final word

The data presented in this section are the first to examine and dissect the domains of PBP4, with respect to investigating the mechanisms of the interactions and activities of this protein. We also present domain 3 of PBP4 as crucial for activity through an as-yet-unknown mechanism, but one that could represent a way of regulating hydrolase activity in *E. coli*.

3.4 The biochemical characterisation of MepA

3.4.1 Introduction

The LAS metallopeptidase MepA has no known interaction partners and *in vitro* activity has only been analysed using the sacculi and isolated muropeptides of *P. putida* [116,117], isolated [^{14}C]-disaccharide tetrapeptide from *E. coli* [244] and DL-*meso*-[^{3}H]-diaminopimelic acid labelled sacculi [245]. It was also not identified as a potential interaction partner of any protein in the proteomics screens carried out by the Typas group (Manuel Banzhaf, unpublished).

In section 3.2, we presented a large number of interactions, regulatory or otherwise, between the PG hydrolases and the PG synthases. We identified the direct interaction between PBP7 and PBP4 and between MepS and MepM. These data could imply an uncharacterised level of cooperative activity between the PG hydrolases. It was possible that there could be more interactions between the PG hydrolases.

This section describes the characterisation of MepA, the last EPase successfully purified in this work, through novel interactions with other EPases, and the discovery of pH-dependent activity using unlabelled sacculi from *E. coli*. This work continues to investigate novel ways by which PG hydrolase activity is regulated in *E. coli*.

3.4.2 MepA interacts with PBP4, PBP7 and MepS

Native MepA was purified to homogeneity as described in section 2.4.8 and tested for interactions with many of the proteins in this project by MST.

Figure 3.24 shows the interaction of MepA with PBP7, PBP4 and MepS using MST (section 2.5.1.7). MepA was fluorescently-labelled at cysteine residues and used at a constant concentration of 125 nM. Two-fold serially diluted PBP7, from 50 µM to 1.53 nM, was titrated with FL-MepA to yield a binding curve that generated an estimated K_D of 160 ± 23.7 nM (figure 3.24A). PBP4 was titrated from a concentration of 30 µM to 0.916 nM to yield an estimated K_D of 84 ± 14 nM (figure 3.24B). Finally, MepS was titrated from a concentration of 30 µM to 0.916 nM to yield an estimated EC_{50} of 101 ± 41.3 nM (figure 3.24C).

The interaction between MepA and MepS yielded a binding curve that did not fit an equilibrium binding model. As such, the Hill model was applied to estimate the EC_{50} shown and a Hill coefficient of 2.57, indicating positive cooperativity upon binding.

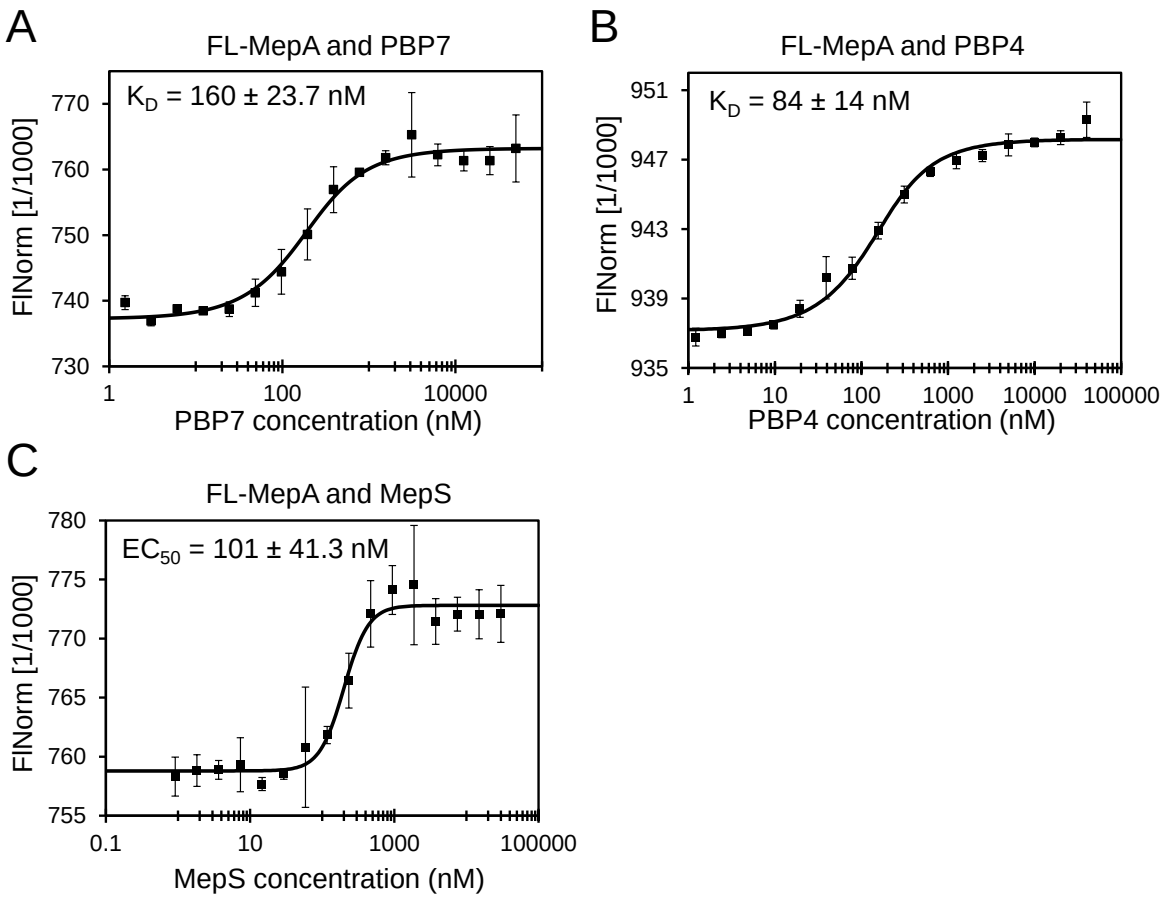

Figure 3.24 MepA interacts with PBP7, PBP4 and MepS *in vitro*

A. Purified MepA was labelled for MST at cysteine residues and used at a concentration of 125 nM. PBP7 was two-fold serially diluted from 50 μM – 1.526 nM and MST measured at 40% LED power and 60% MST power. An estimated K_D of 160 ± 23.7 nM was determined using accompanying software. **B.** Using the same FL-MepA conditions, PBP4 was two-fold serially diluted from 30 μM – 0.916 nM and MST measured at 40% LED power and 60% MST power. An estimated K_D of 84 ± 14 nM was determined using accompanying software. **C.** Again, using the same FL-MepA conditions, MepS was two-fold serially diluted from a concentration of 30 μM – 0.916 nM and MST measured at 40% LED power and 60% MST power. The Hill model was applied and an EC_{50} of 101 ± 41.3 nM was estimated using accompanying software. The interaction was calculated to have a Hill coefficient of 2.57. The values for each graph are the mean ± standard deviations of three independent experiments. Raw MST data are shown in figures 5.23-5.25.

3.4.3 MepA – Non-interacting proteins or contradictory interactions

We performed Ni^{2+} bead pull-down assays as a second method of testing the *in vitro* interactions of MepA (section 2.5.1.5). Ni^{2+} bead pull-down assays were performed using His-PBP4 and His-MepS to test for retention of native MepA. Figure 3.25A shows that His-PBP4, in the presence of formaldehyde, did not retain native MepA after washing. The same was true for the interaction between His-MepS and native MepA (figure 3.25B). Unfortunately, due to the similar sizes of MepA and PBP7, it was difficult to obtain a clear result after separation by SDS-PAGE.

FL-MepA was used at the same conditions as previously and tested for interaction with serially diluted MepM from 20 µM to 0.61 nM using MST, by which we observed no interaction (figure 3.25C). A Ni^{2+} bead pull-down assay was performed using His-MepM and native MepA by which we also observed no interaction (figure 3.25D).

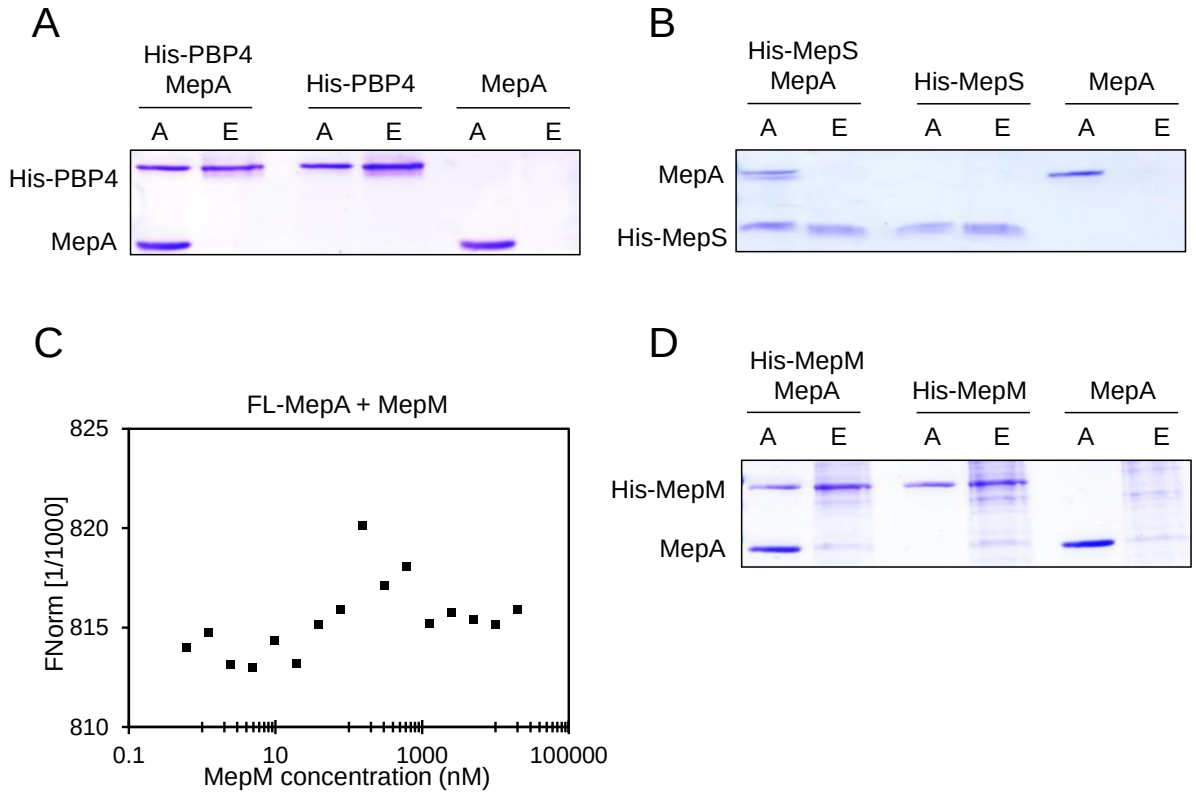

Figure 3.25 MepA does not interact with PBP4 and MepS by Ni^{2+} bead pull-down or MepM

A. *In vitro* Ni^{2+} bead pull-down assay using His-PBP4 and native MepA. Proteins were cross-linked with formaldehyde and an applied (A) sample taken prior to incubation with Ni^{2+} beads. After thorough washing, proteins were eluted (E) and cross-linking reversed by boiling with SDS buffer. Proteins were separated by 12% SDS-PAGE and visualised by Coomassie staining. **B.** Identical to above using His-MepS. **C.** MST of FL-MepA at 125 nM titrated with two-fold serially diluted unlabelled MepM from 20 µM – 0.61 nM. MST power 40%, LED power 40%. Raw MST data are shown in figure 5.26. **D.** Identical to A and B using His-MepM and native MepA.

3.4.4 MepA activity against intact sacculi is pH dependent

To date, *in vitro* MepA activity assays have either used substrate from *P. putida* or radioactively-labelled *E. coli* substrate. We therefore sought to characterise MepA activity against purified high molecular weight unlabelled sacculi from *E. coli* (section 2.5.2.2).

MepA was incubated with sacculi from the D456 *E. coli* strain at a concentration of 2 µM, o/n or for 2 h, at 37°C, alone or pre-incubated with 20 mM EDTA. Standard EPase reaction buffer was used (10 mM HEPES/NaOH, 150 mM NaCl, 0.05% Triton X-100, pH 7.5) and compared to that of a pH 5.0 reaction buffer (10 mM NaAcetate/acetic acid, 150 mM NaCl, 0.05% Triton X-100, pH 5.0). Samples were inactivated by boiling in the presence of 20 mM EDTA, before an o/n cellosyl digestion. Released muropeptides were obtained by centrifugation, reduced with sodium borohydride and analysed by reversed-phase HPLC (section 2.5.2.5). The percentage of dimeric muropeptides was calculated and is shown in figure 3.26.

MepA was almost inactive against sacculi at pH 7.5 and significantly more active at pH 5.0 at both incubation times tested. These data highlight a pH dependent activity not observed for the other EPases (see figure 5.27 and 5.28 for raw chromatograms of MepA activity assays) (see section 3.4 and figures 5.29-5.31 for PBP7, MepS and MepH activity at different conditions).

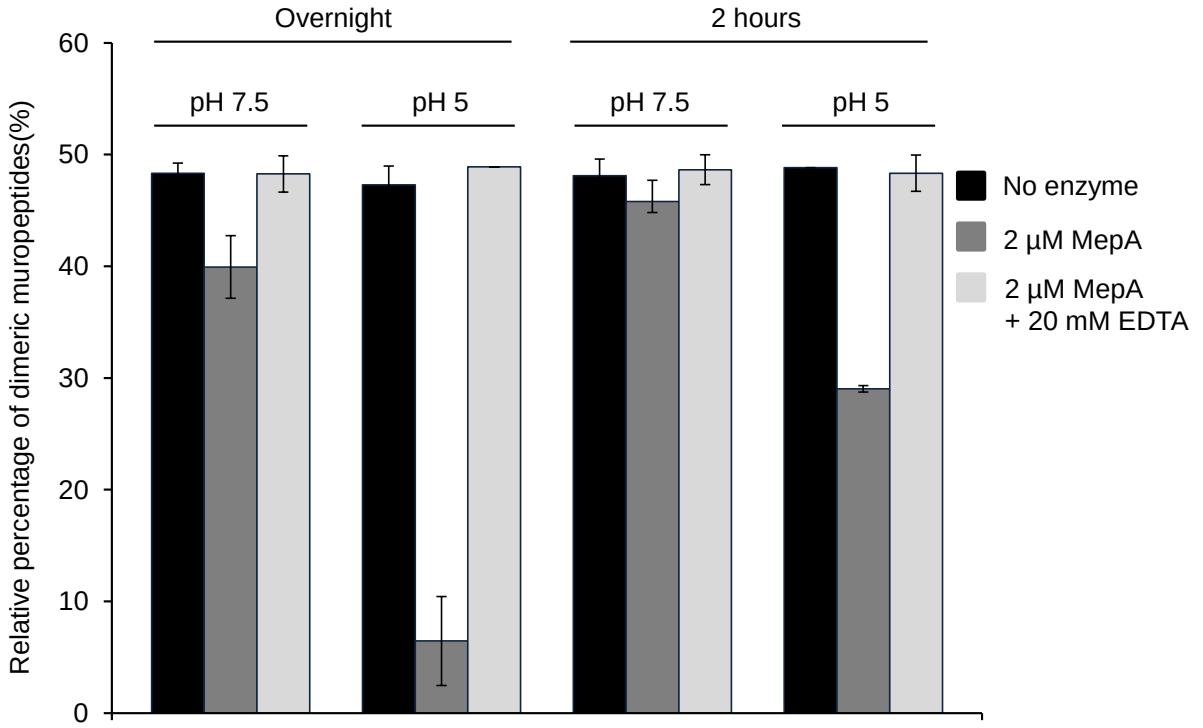

Figure 3.26 MepA has higher activity at lower pH

MepA was tested for EPase activity at a concentration of 2 µM with intact D456 sacculi at pH 7.5 and pH 5.0, o/n or for 2 h, alone or in the presence of 20 mM EDTA. Samples were inactivated by boiling and the addition of 20 mM EDTA before centrifugation and o/n cellosyl digestion of the supernatant. Samples were boiled and centrifuged. Released muropeptides were reduced for analysis by reversed-phase HPLC. The relative percentage of muropeptides in cross-links was calculated and plotted. The values are the mean ± standard deviation of three independent experiments. Raw chromatograms are shown in figures 5.27 and 5.28.

To investigate the lack of activity on sacculi by MepA at pH 7.5, a PG-binding assay was performed (section 2.7.3) in comparison to the other EPases investigated in this work (figure 3.27). Sacculi from the MC1061 strain (100 µl) were pelleted and resuspended in PG-binding buffer (10 mM Tris/Maleate, 10 mM $MgCl_2$, 50 mM NaCl, pH 7.5) and mixed with 10 µg of each protein for 30 min on ice before centrifugation and retention of the supernatant (S sample). Pelleted PG was washed with 200 µl of PG-binding buffer before centrifugation and collection of the supernatant (W sample). SDS (2% solution) was used to resuspend the pellet with stirring for 1 h to release any bound protein before a final centrifugation (P sample). In parallel, control samples were used in which no PG was included. After resolving the samples by 12% SDS-PAGE, we found that all EPases studied in this work were retained by PG at pH 7.5, except MepA.

The assay was repeated using a pH 5.0 PG-binding buffer (10 mM NaAcetate/acetic acid, 10 mM $MgCl_2$, 50 mM NaCl, pH 5.0) to test if the binding of MepA to PG is pH dependent, which we show to be the case. It should be noted that NlpI and the other EPases have not yet been tested for PG binding at pH 5.0.

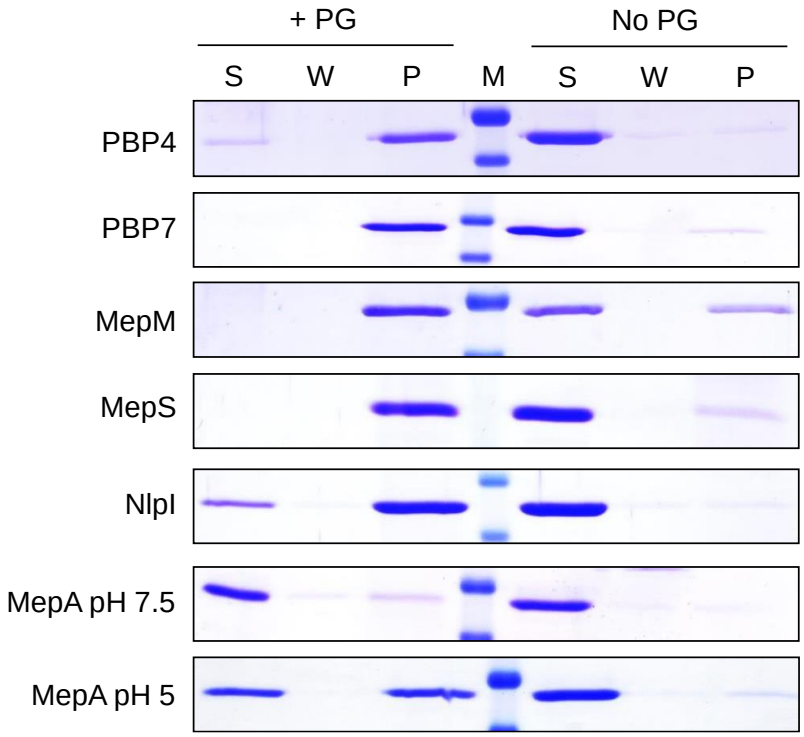

Figure 3.27 Peptidoglycan binding of EPases and NlpI at pH 7.5 and pH 5.0

Pelleted and resuspended sacculi from the MC1061 strain were incubated with 10 µg of PBP4, PBP7, MepM, MepS and NlpI at pH 7.5 and MepA at pH 7.5 and pH 5.0. After a 30 min incubation, samples were centrifuged and the supernatant collected (S). Samples were washed and centrifuged with the supernatant retained (W). Pelleted sacculi were incubated with 2% SDS solution for 1 h to release any bound protein. Samples were centrifuged and the supernatant was retained (P). Control samples were carried out in parallel without PG. Proteins were separated by 12% SDS-PAGE and visualised by Coomassie staining.

3.4.5 Conclusions and discussion

This section described the characterisation of three novel interaction partners of MepA; PBP4, PBP7 and MepS by MST, and the investigation into the activity of MepA against *E. coli* sacculi.

MST was performed using FL-MepA and unlabelled PBP7, PBP4 and MepS. We showed the interaction with PBP7 has an apparent K_D of 160 ± 23.7 nM, with PBP4, which has an apparent K_D of 194 ± 39.5 nM and with MepS, which has an apparent EC_{50} of 101 ± 41.3 nM. However, we were unable to confirm these interactions by Ni^{2+} pull-down assays. We speculate that the presence of the His-tag may be preventing the interaction from being observed in this assay, either occluding an interaction site or immobilised to the nickel resin in such a way that prevents interaction. Unfortunately, we have no His-tagged version of MepA with which to test these interactions in the opposite way. We therefore aim to optimise a second *in vitro* method, for example SPR, and to test all interactions *in vivo* by co-immunoprecipitation.

Interestingly, the binding curve generated for the interaction between MepA and MepS was not an equilibrium binding event, therefore the Hill model was applied to estimate an EC_{50} of 101 ± 41.3 nM and a Hill coefficient of 2.57. This value implies positive cooperativity; the binding of MepS to MepA may cause a conformational change to allow MepA to bind more protein. This also implies multiple MepS binding sites on MepA. As MepA exists as a dimer, it is possible that the binding of MepS to one of the monomers induces a conformational change that causes the other monomer to bind MepS, perhaps necessitated by the rapid turnover rate of MepS [108]. This observed positive cooperativity may not only be to promote subsequent interactions with MepS, but to prevent the binding of other MepA interaction partners. We speculate that under certain conditions the interaction between MepA and MepS, and presumably the coordination of their activity, could be more favourable than that of MepA with PBP4 or PBP7. We aim to test whether the interaction between MepA and MepS prevents the interaction of MepA with PBP4 and PBP7.

MepM is the only EPase investigated here to not interact with MepA, but it is possible that in the cellular environment MepM is a member of this EPase subcomplex through its interaction with MepS.

We have also characterised the pH dependent EPase activity of MepA. We sought to optimise a MepA activity assay similar to that of the other EPases studied in this work. Using the standard EPase conditions, i.e. pH 7.5, we observed high activity of MepA on isolated

muropeptides, with little to no activity on intact sacculi at high concentrations (20 µM) and long incubations (o/n) (figure 5.22). We investigated this using a MepA PG-binding assay in comparison to the other hydrolases used in this work. We showed that while the other hydrolases bound to PG at pH 7.5, MepA did not. If MepA activity was specific for muropeptides rather than high molecular weight material, this could be beneficial for the complete degradation of PG in the cell, and contribute to the robustness of the hydrolase network. However, we repeated the MepA PG-binding assay at different conditions and observed the retention of MepA by PG at pH 5.0. We hypothesised therefore that the binding and cleavage of PG by MepA could be pH dependent. Indeed, using the same HPLC-based sacculi digestion assay, but at pH 5.0, we observed almost complete digestion of dimeric muropeptides in an o/n incubation at 2 µM, and an intermediary digestion after 2 h. The 2 h incubation will be used to test the effect of the inactive interaction partners of MepA.

Final word

The data presented in this section describes three more interactions between the PG hydrolases of *E. coli*, deepening our understanding of how hydrolase activity could be coordinated in the cell. We also present the pH dependent activity of MepA, highlighting another method of how hydrolase activity could be controlled in *E. coli*. We speculate that the hydrolase redundancy observed in *E. coli* arises from conditional specificity, with enzymes having more or less activity at different intracellular and extracellular conditions. As the pH of the periplasm changes in relation to the external conditions [14], having an enzyme with an optimal activity at pH 5.0 could ensure correct PG breakdown in situations when other enzymes lose their activity. This could become important for example, when colonising the gastrointestinal tract, the pH of which varies between 5.5 and 7.5 [246]. A summary of all the interactions presented in this work so far is shown in figure 3.28.

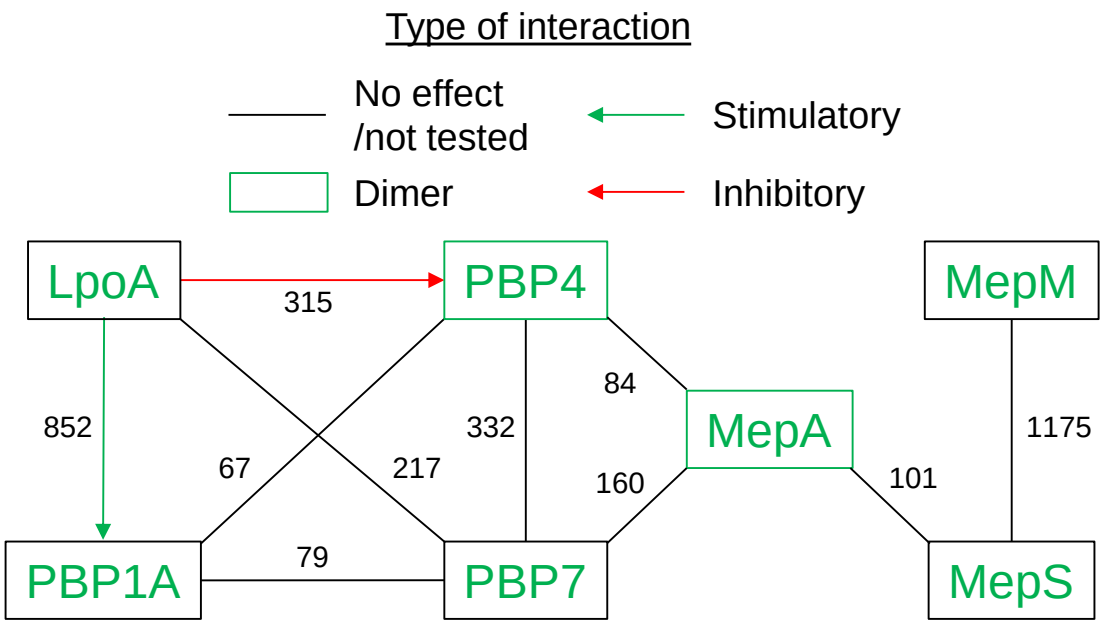

Figure 3.28 Interactions within a PG synthesis/hydrolysis subcomplex

Schematic to show the summary of interactions, and effects on activity, described in this work to this point. There exists a large number of interactions between the PG hydrolases, PBP4, PBP7, MepA, MepS and MepM which are directly or indirectly associated to two components of the PG synthesis complex during elongation, LpoA and PBP1A. The numbers are K_D values given in nanomolar. Dissociation constant for the interaction between MepA and MepS was calculated using the Hill model (EC_{50}).

3.5 New Lipoprotein I (NlpI) is a novel regulator of endopeptidases

3.5.1 Introduction

A number of papers have published data with respect to the possible functions of New Lipoprotein I (NlpI). It has been implicated in the regulation of cell division and the control of amidases because of a temperature sensitive filamentation upon deletion [228]; the regulation of hypervesiculation through control of PG turnover [230]; and may have a role in the mediation of complement-based cell death [247]. Most recently NlpI has been shown to regulate the proteolytic degradation of MepS [108]. *E. coli* possesses ~27 hydrolases that have no known regulators of activity. Intuitively therefore, there may be as-of-yet unidentified regulators for some of these proteins. In addition to the phenotypes described above, cells lacking *nlpI* are synthetically sick when combined with that of deletions in *mrcB* and *lpoB* indicating a role in the regulation of cell elongation (Manjula Reddy, unpublished). These data, and the recently published material regarding its regulation of the proteolytic degradation of MepS, led to our interest in the protein.

NlpI was comprehensively investigated in this section using *in vitro* interaction assays to identify numerous direct, novel interactions with PG hydrolases. This work also explored the *in vitro* effects of these interactions and highlights the primary role of NlpI as a novel regulator of EPases.

3.5.2 NlpI exists as a dimer in solution

The crystal structure of NlpI predicts the formation of a strong dimer (see figure 1.10) [233]. However, we sought to determine the oligomeric state in solution at the conditions used for *in vitro* interaction assays. This would also allow us to infer stoichiometry should we find any novel interaction partners. AUC was performed in collaboration with Alexandra Solovyova using purified NlpI (section 2.4.9). NlpI was dialysed o/n against 25 mM HEPES/NaOH, 150 mM NaCl, pH 7.5 and analysed using the absorbance optical system at 20°C to determine the sedimentation velocity of NlpI at varying concentrations (0.31, 0.46, 0.6, 0.75, 0.9, 1.05, and 1.2 mg/ml). Results were corrected for the viscosity/density of H_2O at 20°C. Using the amino acid sequence and the known crystal structure data, the sedimentation velocity of monomeric NlpI was predicted to be 2.83 S with a molecular weight of 30.35 kDa, and the dimer was predicted to sediment at 4.16 S with a molecular weight of 60.7 kDa. The size distribution plots obtained showed that NlpI exists exclusively as a dimer at these concentrations, with a sedimentation velocity of 4.52 S (figure 3.29).

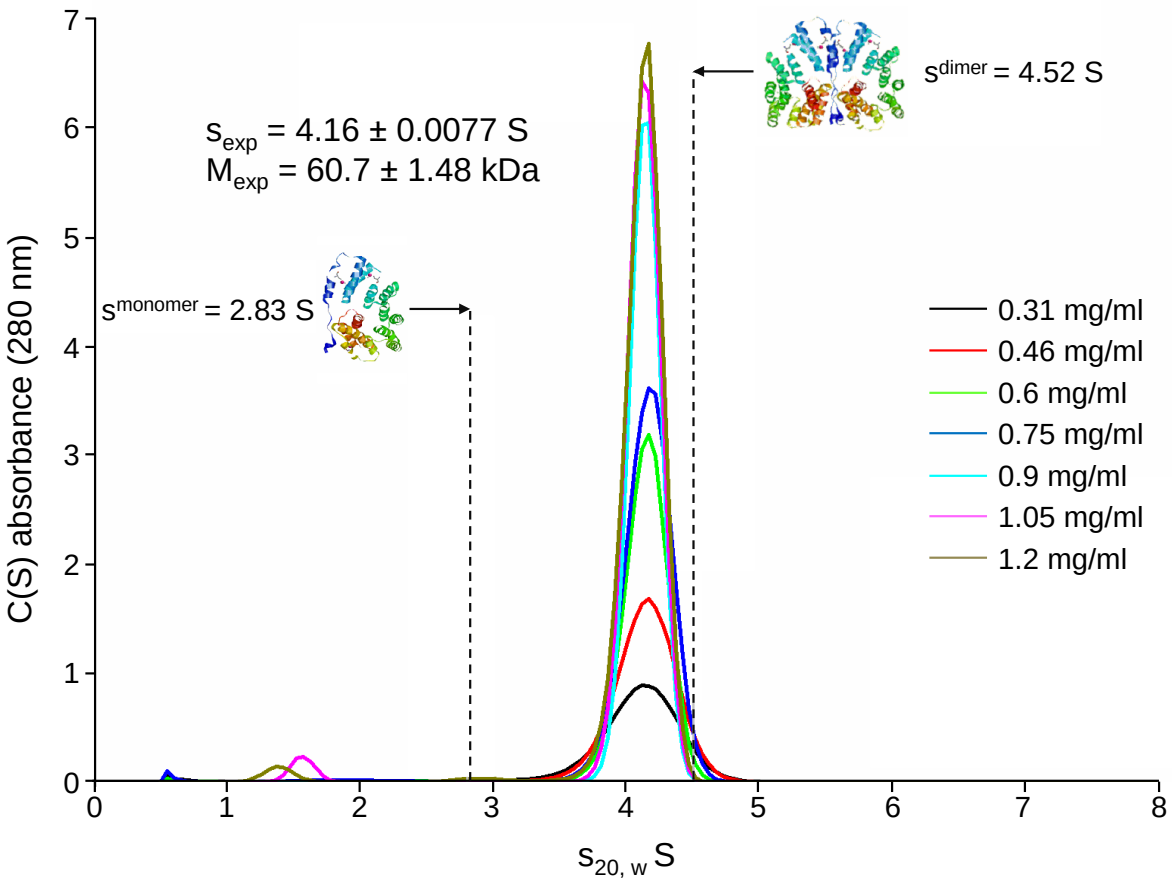

Figure 3.29 Analytical ultracentrifugation reveals that NlpI exists as a dimer in solution

Size distribution plots showing the sedimentation velocity of NlpI. Both the calculated molecular weight and the measured molecular weight for NlpI as a monomer or dimer are shown. $s_{20,w}S$ (Sedimentation coefficient corrected for the viscosity and density of the solvent, relative to that of water at 20°C) plotted against absorbance (280 nM) reveals NlpI exists exclusively as a strong dimer at these conditions.

For use in interaction assays, such as MST, the experimental concentrations for proteins of interest are in the nanomolar range. We therefore sought to use NlpI in MST to determine the dissociation constant of dimer formation (section 2.5.1.7). A concentration of 62.5 nM of FL-NlpI (at amine residues) was low enough to yield a good fluorescence signal and was estimated to be below the K_D of dimerisation. Unlabelled NlpI was two-fold serially diluted from 30 µM to 0.916 nM, and titrated against the constant concentration of FL-NlpI. Normalised fluorescence readings were measured at 40% MST power and 50% LED power and the resulting MST binding curve is shown in figure 3.30. The K_D of NlpI dimerisation was estimated to be 126 ± 9.14 nM using the accompanying software.

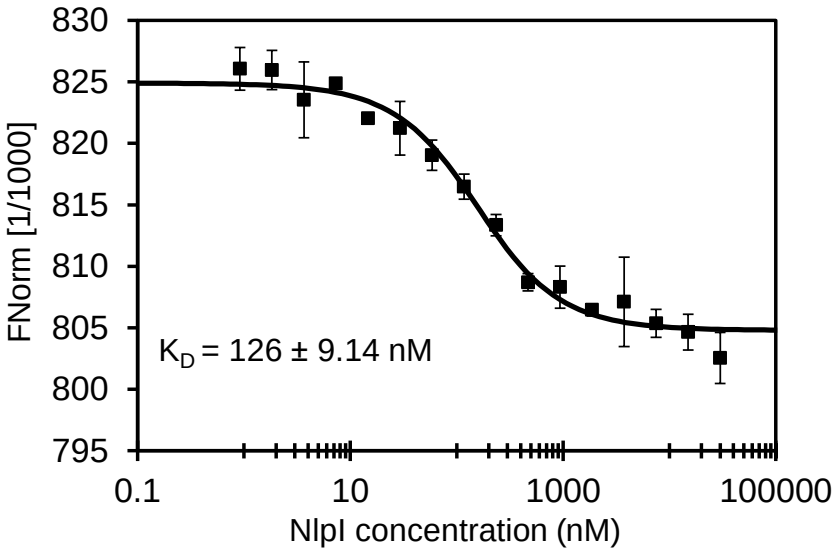

Figure 3.30 NlpI dimerisation by MST

MST of FL-NlpI (at amine residues) at a concentration of 62.5 nM titrated with two-fold serially diluted unlabelled NlpI from 30 μM - 0.916 nM (40% MST power, 50% LED power). An apparent K_D of 126 ± 9.14 nM was estimated using accompanying software. The values are the mean ± standard deviation of three independent experiments. Raw MST data are shown in figure 5.32.

3.5.3 NlpI interacts with PBP4 and stimulates its activity

3.5.3.1 NlpI interacts with PBP4 *in vitro*

NlpI was identified as potentially involved in PG synthesis/hydrolysis regulation through genetic studies performed by our collaborators at EMBL, Heidelberg (unpublished). These patterns identified NlpI as being associated with PBP1A/LpoA and/or PBP1B/LpoB. These findings were further substantiated by our collaborator Manjula Reddy in Hyderabad, India, who identified a synthetic sick phenotype when an NlpI deletion was combined with that of deletions in PBP1B/LpoB (unpublished). The Typas lab performed affinity chromatography using immobilised purified NlpI(sol), incubated with a combined membrane/periplasmic fraction from *E. coli* and identified a number of proteins enriched in comparison to a control column. PBP4 was identified as a potential interaction partner of NlpI. Like MepS, PBP4 had been implicated as being regulated by NlpI [230]. We therefore sought to test the specificity of this interaction with the purified proteins.

SPR was performed in which NlpI (4 µg/ml) was immobilised to an SPR sensorchip surface by general amine coupling (2.5.1.6). PBP4 was applied at varying concentrations (0, 0.25, 0.5, 1, 2, and 4 µM) as an analyte. The experiment yielded a concentration dependent increase in response units (RU) which was plotted against time (figure 3.31A). The equilibrium binding state was optimal for K_D determination by Scatchard analysis (non-linear regression), in which the equilibrium response values (R_{eq}) were calculated using the accompanying software and plotted against analyte concentration. We estimated a K_D of 310 ± 46 nM (figure 3.31B). A negative control lane was activated without immobilisation of NlpI.

To test the interaction by another method, we performed MST (section 2.5.1.7). NlpI was fluorescently-labelled at amine residues and optimised to a concentration of 62.5 nM. Unlabelled PBP4 was two-fold serially diluted from 50 µM to 1.53 nM and titrated with FL-NlpI. The binding curve generated an estimated K_D of 177 ± 48.8 nM using the accompanying software (figure 3.31C).

An *in vitro* Ni^{2+} bead cross-linking pull-down assay was performed in which His-NlpI and native PBP4 were incubated with Ni^{2+} beads before washing and elution (section 2.5.1.5). An applied sample was taken prior to bead incubation and compared to a sample taken after elution of retained proteins. Native PBP4 was only retained in the presence of His-NlpI (figure 3.31D).

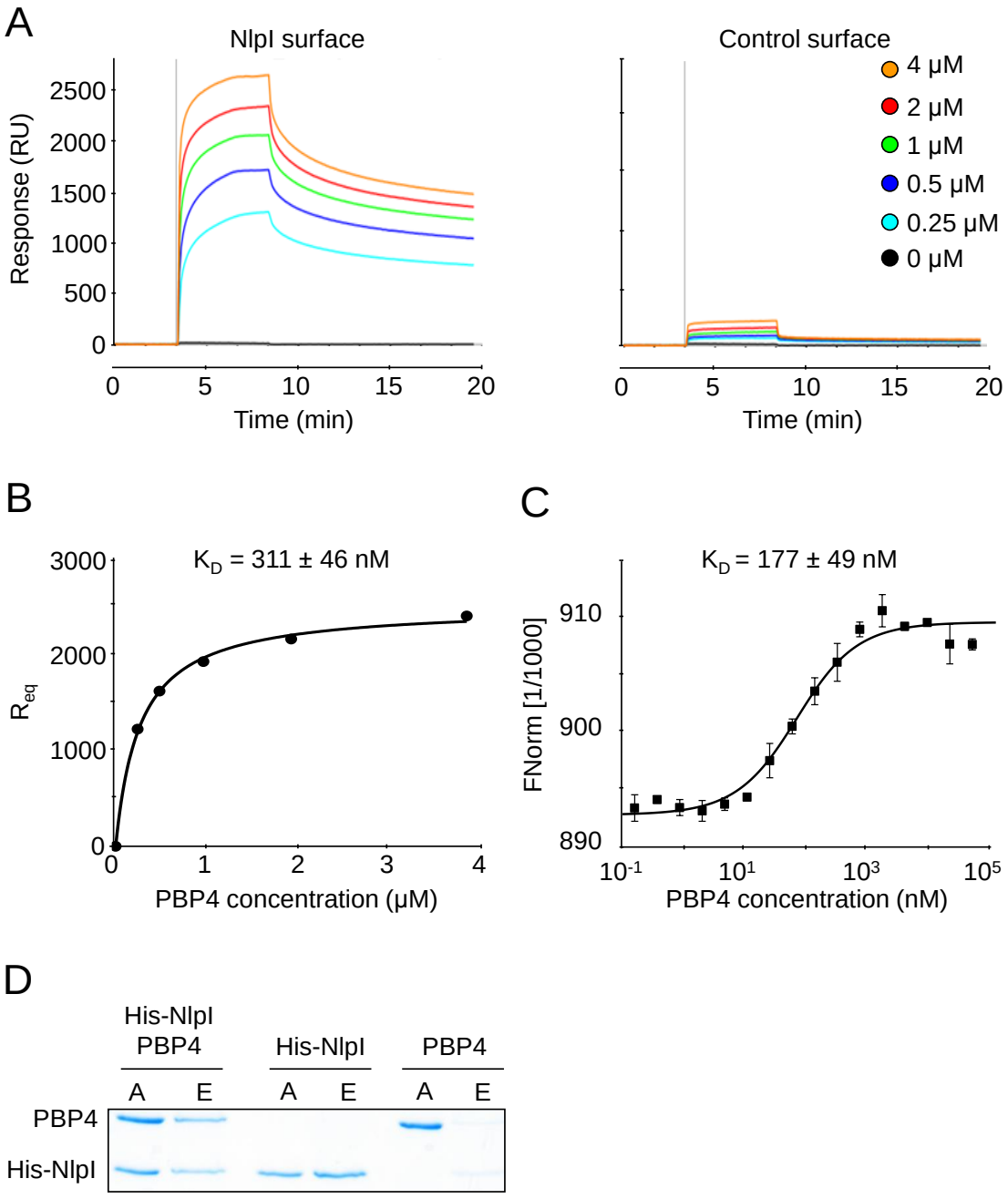

Figure 3.31 **NlpI interacts with PBP4 *in vitro***

A. SPR sensorgrams of NlpI immobilised by general amine coupling, applied with varying concentrations of PBP4 in comparison to a surface activated without immobilisation of protein. **B.** Equilibration response (R_{eq}) values were obtained and plotted against analyte concentration for Scratchard analysis by non-linear regression. A K_D of 310 ± 46 nM was estimated. **C.** MST of FL-NlpI (at amine residues) at a concentration of 62.5 nM was titrated with two-fold serially diluted PBP4 from 50 µM – 1.53 nM (20% MST power, 40% LED power). An apparent K_D of 177 ± 49 nM was estimated using the accompanying software. The values are the mean ± standard deviation of three independent experiments. Raw MST data are shown in figure 5.33. **D.** *In vitro* Ni^{2+} bead pull-down assay using His-NlpI and native PBP4. An applied sample (A) was taken prior to incubation of cross-linked proteins with Ni^{2+} beads. After thorough washing and elution of bound proteins by boiling with SDS-loading buffer (E) proteins were separated by 12% SDS-PAGE and visualised by Coomassie staining.

3.5.3.2 NlpI stimulates the endopeptidase activity of PBP4

The interaction characterised here could highlight NlpI as a novel regulator of hydrolase activity. Further, through this interaction with PBP4, NlpI could be linked to the multi-enzyme PG-synthesising complex during cell elongation.

To address our hypothesis of hydrolase regulation we investigated the effect of NlpI on PBP4 activity using the EPase assay already established in this work. Intact MC1061 sacculi were incubated with 1 µM PBP4 in the presence and absence of 2 µM NlpI for 2 hours at 37°C with shaking (section 2.5.2.2). The reaction was stopped by boiling and centrifuged to obtain the released muropeptide-containing supernatant. Released muropeptides were reduced and analysed by reversed-phase HPLC (section 2.5.2.5). We show that in the presence of NlpI, the hydrolytic EPase activity of PBP4 is stimulated, cleaving virtually all TetraTetra dimers to Tetra monomers (figure 3.32). PBP4 alone reduced the percentage of dimeric muropeptides from 44.4% to 16.3%, but in the presence of NlpI, PBP4 cleaves virtually all dimeric muropeptides to yield a relative percentage of 0.52%.

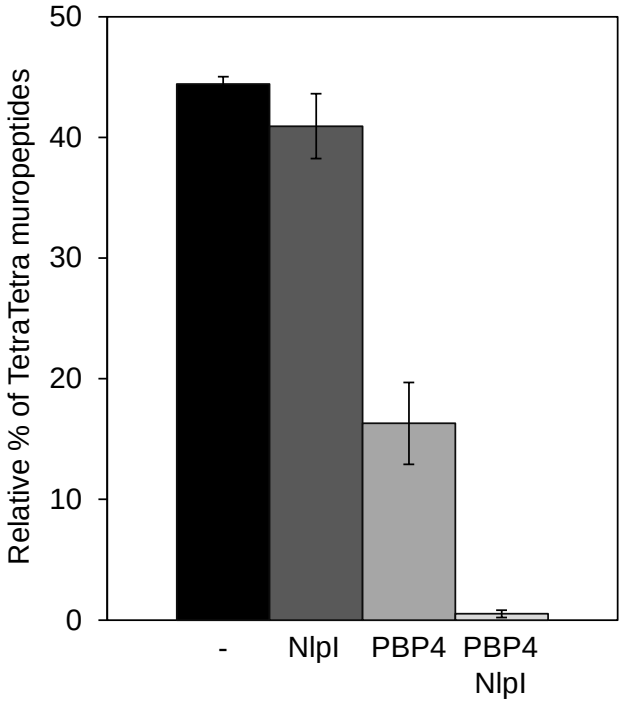

Figure 3.32 NlpI stimulates the endopeptidase activity of PBP4 on sacculi

HPLC-based PBP4 sacculi digestion assay. Isolated sacculi from the *E. coli* WT strain, MC1061, were incubated with 1 µM PBP4 for 2 hours with shaking at 37°C either alone or in the presence of 2 µM NlpI. The reaction was stopped by boiling and the released muropeptides were obtained by centrifugation, reduced with sodium borohydride and analysed by reversed-phase HPLC. HPLC chromatograms are shown in figure 5.34. The values are the mean ± standard deviation of three independent experiments.

3.5.3.3 Domain 3 of PBP4 is likely the NlpI interaction site

We sought to use the truncated version of PBP4, PBP4ΔD3, to elucidate potential binding sites. Our previous hypothesis was that a potential regulator of PBP4 activity would interact with domain 3, the domain seemingly crucial for both EPase and CPase activity. We therefore carried out a Ni^{2+} bead cross-linking pull-down assay using His-PBP4ΔD3 and an untagged version of NlpI (section 2.5.1.5). After thorough washing and elution of retained proteins, and comparison of the applied and elution samples, we showed that His-PBP4ΔD3 did not retain native NlpI, indicating that the proteins do not interact (figure 3.33A).

We continued by showing that domain 3 of PBP4 is a major interaction site for NlpI using MST (section 2.5.1.7). FL-NlpI was used at a concentration of 62.5 nM and was titrated with two-fold serially diluted PBP4ΔD3 from a concentration of 10 µM to 0.31 nM (figure 3.33B). The absence of a concentration-dependent change in normalised fluorescence (FNorm) was indicative of the absence of an interaction. In section 3.3.5 we showed that domain 3 was not required for the interaction between PBP1A and LpoA, however, domain 3 seems to be crucial for the interaction with NlpI.

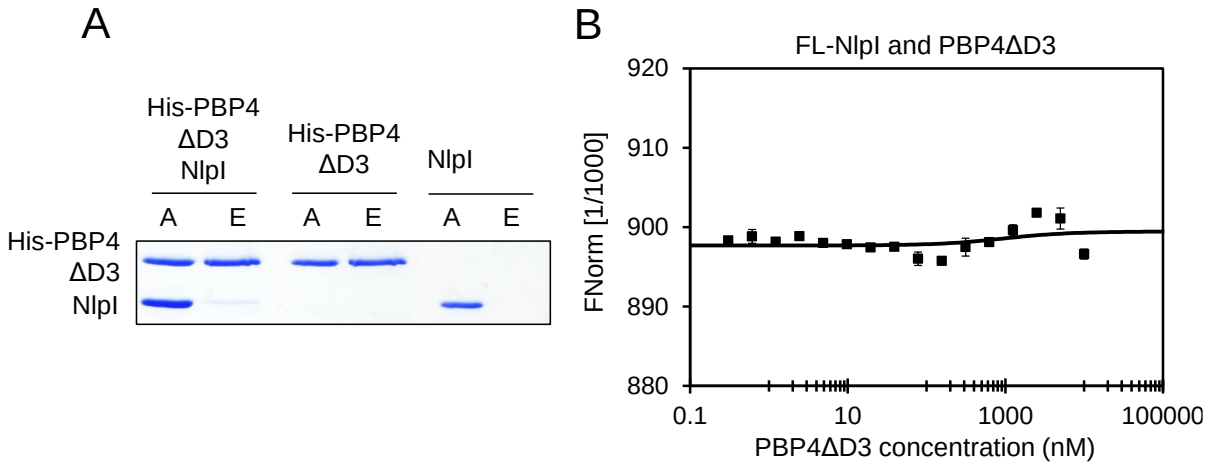

Figure 3.33 Domain 3 of PBP4 is required for interaction with NlpI

A. *In vitro* Ni^{2+} bead pull-down assay using His-PBP4ΔD3 and native NlpI. After an o/n incubation with Ni^{2+} beads, His-PBP4ΔD3 was unable to retain untagged NlpI. **B.** MST measurement of FL-NlpI (at amine residues) at a concentration of 62.5 nM titrated with serially diluted unlabelled PBP4ΔD3 from a concentration of 10 µM – 0.31 nM (20% LED power and 40% MST power). Raw MST data are shown in figure 5.35.

3.5.3.4 NlpI can interact with PBP4 in the presence of PBP1A/LpoA

In this work, we have identified five novel PBP4 interaction partners; LpoA, PBP1A, PBP7, MepA and NlpI. Here we tested the possibility that PBP4 may possess multiple binding sites for its interaction partners with particular interest in NlpI, the regulator of its hydrolytic activity, and PBP1A and LpoA which we hypothesise act to recruit PBP4 to sites of ongoing PG synthesis. As shown in previous sections we predicted that domain 3 of PBP4 is the main interaction site of NlpI, and domain 1 and/or 2 the likely interaction site for PBP1A and LpoA. We therefore hypothesised that the presence of NlpI should not prevent the binding of PBP4 to PBP1A. The standard MST protocol was modified such that an unlabelled ligand was not titrated with the fluorescently-labelled protein, but an appropriate concentration chosen that would reach the 'bound state' upon application, as determined using the standard MST protocol. A third protein that interacted with the unlabelled protein, but not the fluorescently-labelled protein, was pre-incubated in excess with the unlabelled ligand, prior to addition to the fluorescently-labelled protein. We predicted this pre-incubation would saturate all potential binding sites and would allow us to measure the formation of multi-protein complexes and provide insight into interaction sites, shared or otherwise. Using this protocol, PBP4 (0.5 µM) was applied to FL-PBP1A (at amine residues) at a concentration of 20.8 nM, and we observed an increase in FNorm, indicative of an interaction (figure 3.34A). We show in figure 3.48 that NlpI was capable of interacting with PBP1A (discussed in more detail in section 3.5.9), we therefore used a concentration of NlpI lower than that of the K_D of interaction with PBP1A, but in excess of PBP4. As such, we observed no interaction upon application of 1 µM NlpI. NlpI was incubated with PBP4 at the same concentrations as used individually to block the NlpI binding sites of PBP4. Upon application of this mixture, the increase in FNorm was the same as that of PBP4 alone, indicating the presence of NlpI did not disrupt the interaction of PBP1A with PBP4.

The experiment was repeated in the same way using FL-LpoA. Using the regular MST protocol we observed no interaction between FL-LpoA and NlpI (figure 3.45A discussed in more detail in section 3.5.9) and we reproduced this using FL-LpoA (166 nM) (at cysteine residues) and 30 µM NlpI (figure 3.35A). The interaction observed previously between FL-LpoA and PBP4 yielded a concentration-dependent fluorescence enhancement (figure 3.10B). In the presence of 5 µM PBP4, the fluorescence signal is enhanced, indicative of an interaction (figure 3.35A). PBP4, in the presence of excess NlpI, caused the same fluorescence enhancement observed for that of PBP4 alone. These data indicate that the presence of NlpI does not prevent the interaction of PBP4 with LpoA.

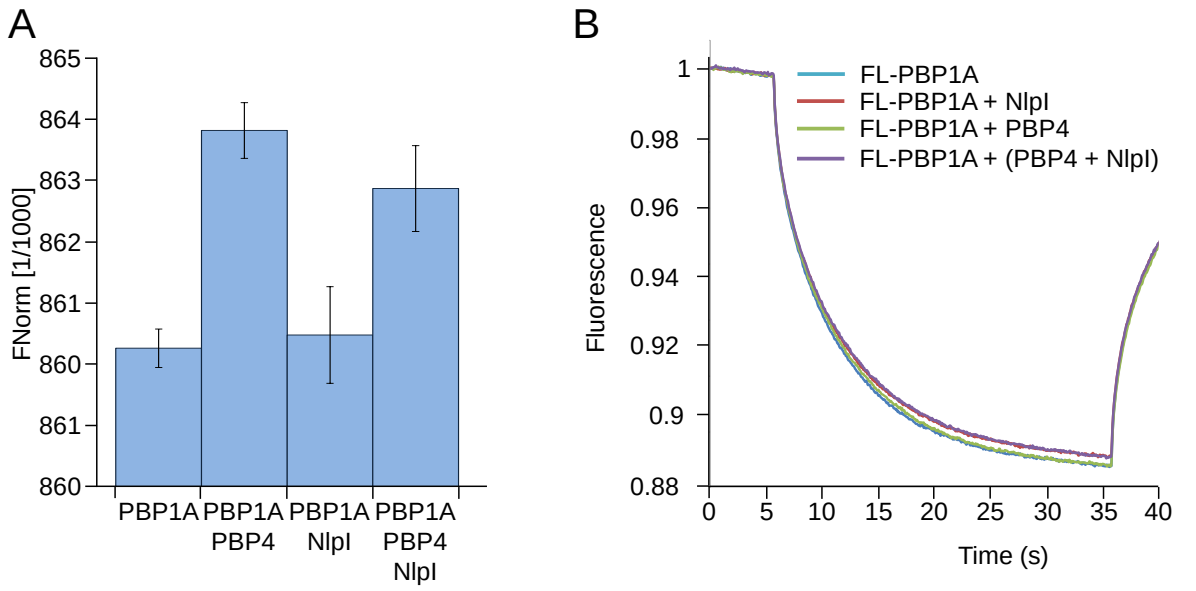

Figure 3.34 PBP4 possesses different interaction sites for PBP1A and NlpI

A. End-point normalised fluorescence (FNorm) showing the presence of NlpI does not prevent binding of PBP4 to PBP1A. The MST of FL-PBP1A (20.8 nM) was measured either alone, or in the presence of PBP4 (0.5 µM) or NlpI (1 µM). The same concentrations were used to pre-incubate NlpI with PBP4, before addition to FL-MepS. MST measurements were carried out with 80% LED power, 40% MST power. The values are the mean ± the standard deviation of three independent experiments. **B.** MST time traces of the experiments shown in A. The values are the mean of three independent experiments.

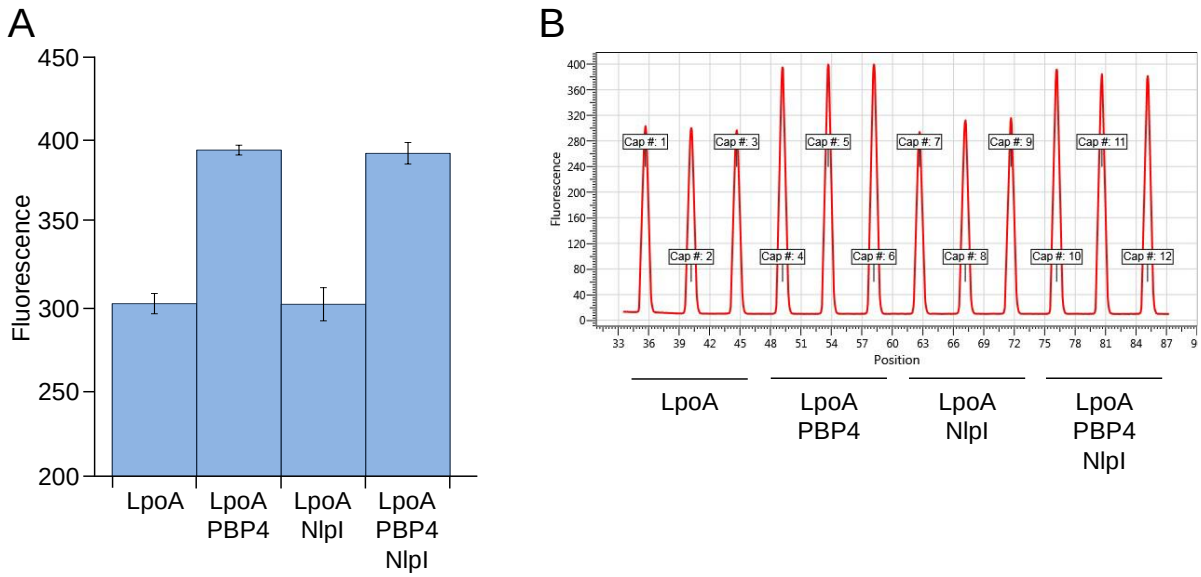

Figure 3.35 PBP4 possesses different interaction sites for LpoA and NlpI

A. Raw fluorescence values showing the presence of NlpI does not prevent binding of PBP4 to LpoA. MST measurements were taken of FL-LpoA (166 nM) alone, or in the presence of PBP4 (5 µM) or NlpI (30 µM). The same concentrations were used to pre-incubate NlpI with PBP4, before addition to FL-LpoA. MST measurements were carried out with 100% LED power, 20% MST power. The values are the mean ± the standard deviation of three independent experiments **B.** Pre-experiment capillary scans of A.

3.5.4 Interaction of NlpI with PBP7

3.5.4.1 NlpI interacts with PBP7 *in vitro*

Having confirmed the *in vitro* interaction of NlpI with PBP4, we hypothesised that NlpI may interact with other EPases. PBP7, one of the other Class C PBP hydrolases, was tested for interaction. Our initial hypothesis was that NlpI could be a global regulator of EPases. PBP7 was also identified as a potential interaction partner by affinity chromatography by Manuel Banzhaf, Heidelberg (unpublished).

His-PBP7 was purified by Hamish Yau from the Vollmer group and a Ni^{2+} bead cross-linking pull-down assay was performed using a tagless form of NlpI (section 2.5.1.5). We show that NlpI is only retained by Ni^{2+} beads in the presence of His-PBP7 (figure 3.36A).

We continued by testing this interaction using MST. NlpI was fluorescently-labelled at amine residues and used at a concentration of 62.5 nM. Unlabelled PBP7 was two-fold serially diluted from 30 µM to 0.916 nM and titrated with FL-NlpI. The binding curve generated did not correspond to an equilibrium binding event. Instead, the Hill model was applied to determine an EC_{50} of 422 ± 25 nM (figure 3.36B). The Hill model also generated an estimated Hill coefficient of 3.06, implying positive cooperativity.

Interestingly, when we analysed the same interaction using unlabelled NlpI and FL-PBP7, the MST measurements generated a standard equilibrium binding curve which yielded an estimated K_D of 90 ± 8.9 nM (figure 3.36C). In this instance, FL-PBP7 was used at a concentration of 62.5 nM and was titrated with two-fold serially diluted NlpI from a concentration of 10 µM to 0.31 nM.

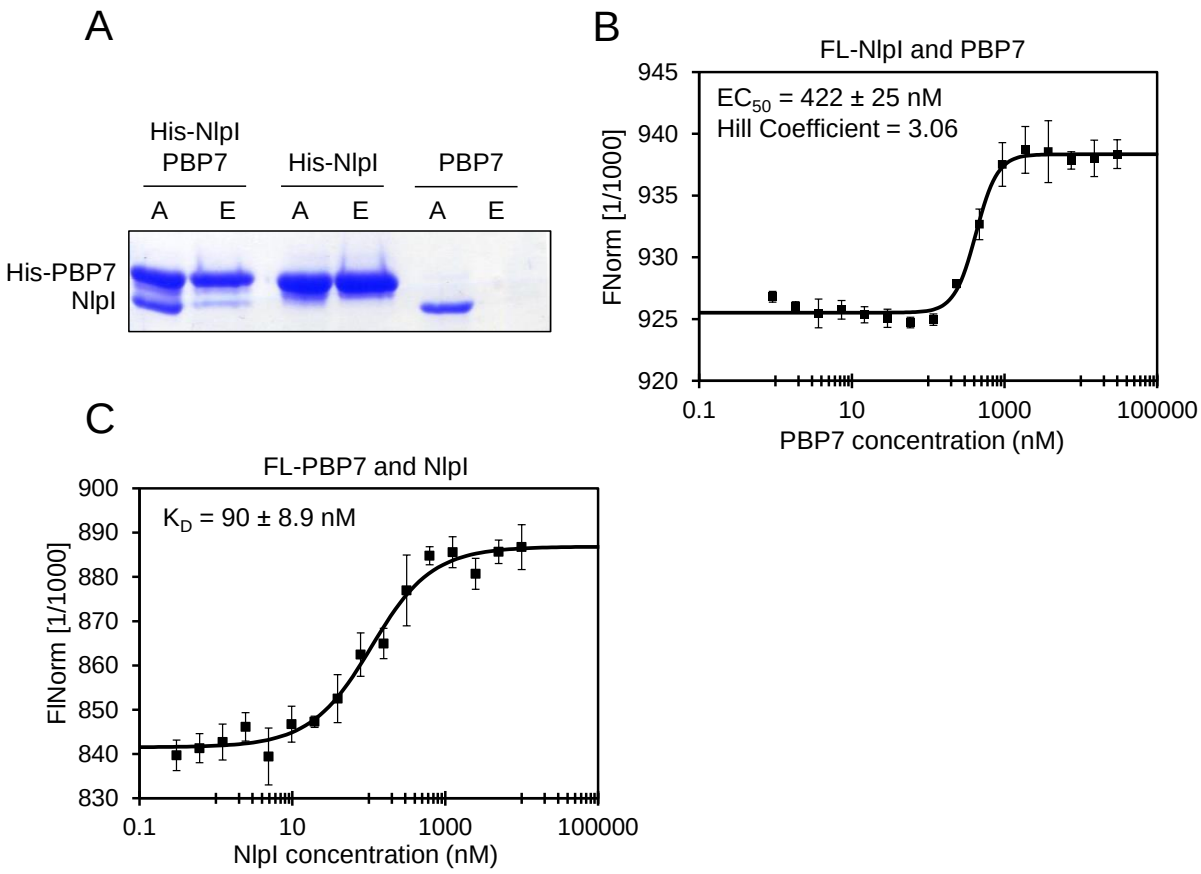

Figure 3.36 NlpI interacts with PBP7 *in vitro*

A. *In vitro* Ni^{2+} bead pull-down assay using His-PBP7 and native NlpI. After an o/n incubation with Ni^{2+} beads, His-PBP7 was able to retain native NlpI. **B.** MST measurement of FL-NlpI (at amine residues) at a concentration of 62.5 nM and serially diluted unlabelled PBP7 from a concentration of 30 µM – 0.916 nM (50% LED power and 10% MST power). The Hill model was applied and an apparent EC_{50} of 422 ± 25 nM was estimated using accompanying software. A Hill coefficient of 3.06 was determined, implying positive cooperativity. Raw MST data are shown in figure 5.36. **C.** MST measurement of FL-PBP7 (at amine residues) at a concentration of 62.5 nM titrated with serially diluted unlabelled NlpI from a concentration of 10 µM – 0.31 nM (40% LED power and 20% MST power). An apparent K_D of 90 ± 8.9 nM was estimated using accompanying software. Raw MST data are shown in figure 5.37. The values for each MST graph are the mean ± standard deviation of three independent experiments.

3.5.4.2 NlpI has no effect on PBP7 activity

In section 3.5.3.2 we show a stimulatory effect of NlpI on PBP4. We therefore tested the effect of NlpI on the EPase activity of PBP7, to determine whether there is a broader role of NlpI in hydrolase regulation.

An EPase assay was performed using muropeptides from the MC1061 strain (section 2.5.2.2). Muropeptides were incubated with 2 µM PBP7 and/or 4 µM NlpI for 4 h at 37°C with shaking, before stopping the reaction by boiling. Reactions were carried out in standard EPase reaction buffer (10 mM HEPES/NaOH, 10 mM $MgCl_2$, 150 mM NaCl, 0.05% Triton X-100, pH 7.5). Muropeptides were reduced with sodium borohydride and analysed by HPLC (section 2.5.2.5). The Tetra-containing muropeptides were integrated and the relative amount of TetraTetra dimers was calculated as a percentage of the total amount of Tetra-containing muropeptides. There was no effect of NlpI on the EPase activity of PBP7 (figure 3.37). We also performed the reaction at four different conditions, including low/high salt and pH, and observed no effect of NlpI (figure 5.29). PBP7 activity was highest at 150 mM NaCl at pH 7.5 with activity affected at lower pH and higher NaCl concentration, but in all cases the presence of NlpI had no effect on the percentage of TetraTetra dimers.

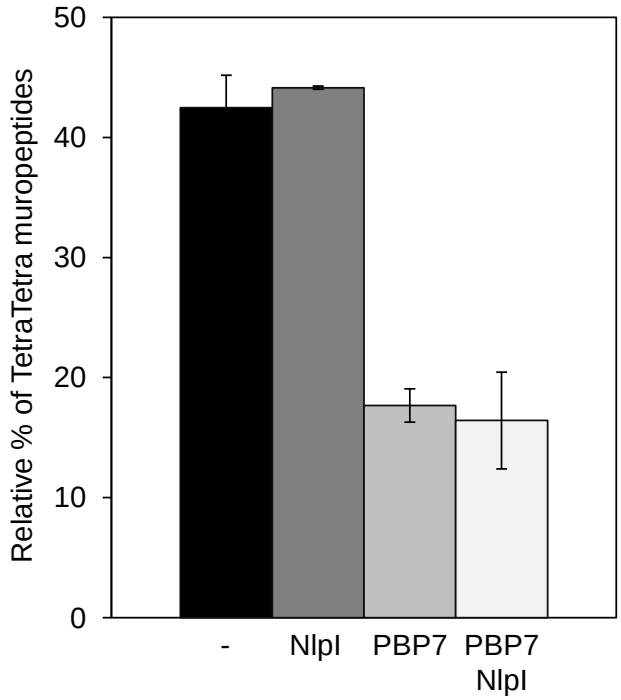

Figure 3.37 NlpI has no effect on the endopeptidase activity of PBP7

Isolated muropeptides from the WT *E. coli* strain MC1061 were incubated with PBP7 (2 µM) and/or NlpI (4 µM) for 4 hours at 37°C with shaking prior to stopping the reaction by boiling, reduction of muropeptides with sodium borohydride and analysis by HPLC. Peaks corresponding to the Tetra monomer and TetraTetra dimer muropeptides were integrated using the accompanying Laura software. The relative percentage of TetraTetra-containing muropeptides was plotted as a representation of EPase activity. The values are the mean ± standard deviation of three independent experiments.

3.5.5 Interaction of NlpI and MepS

3.5.5.1 NlpI interacts with MepS *in vitro*

The deletion of *nlpI* causes a hypervesiculation phenotype, which is suppressed when combined with a deletion in *mepS* [230]. A recent paper from the group of our collaborator Manjula Reddy, Hyderabad, shows that NlpI facilitates the proteolytic degradation of MepS [108]. However, these proteins may be functionally linked. As-of-yet there have been no data characterising the direct interaction between the two proteins, and we therefore sought to test the interaction *in vitro*. We hypothesised that NlpI may interact or regulate the activity of more than the just the Class C PBP hydrolases PBP4 and PBP7.

Using the established *in vitro* Ni^{2+} bead cross-link pull-down assay (section 2.5.1.5), we showed that His-MepS retained native NlpI after incubation with Ni^{2+} beads and thorough washing (figure 3.38A). Native NlpI alone was not retained.

MST was performed to confirm this *in vitro* interaction and to estimate a dissociation constant (section 2.5.1.7). MepS was fluorescently-labelled (at amine residues) and used at a concentration of 62.5 nM. Unlabelled NlpI was two-fold serially diluted from 50 µM to 1.53 nM and titrated with FL-MepS. The binding curve yielded an apparent K_D of 145 ± 51.6 nM using the accompanying software (figure 3.38B).

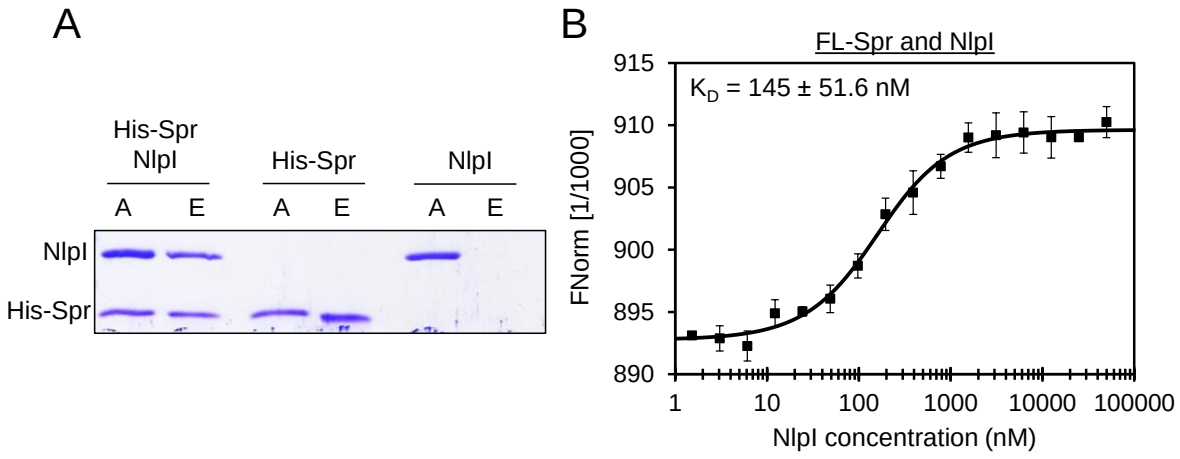

Figure 3.38 NlpI interacts with MepS *in vitro*

A. *In vitro* Ni^{2+} bead pull-down assay using His-MepS and native NlpI. After o/n incubation with Ni^{2+} beads and thorough washing, His-MepS retained native NlpI. **B.** MST measurement of FL-MepS (at amine residues) at a concentration of 62.5 nM titrated with serially diluted unlabelled NlpI from a concentration of 50 µM – 1.53 nM (20% LED power and 40% MST power). An apparent K_D of 145 ± 51.6 nM was estimated using accompanying software. The values are the mean ± standard deviation of three independent experiments. Raw MST data are shown in figure 5.38.

3.5.5.2 MST saturation test of MepS and NlpI

We attempted to determine the stoichiometry of this interaction using a modified version of the MST protocol. MepS exists as a monomer [131] and we show in this work that NlpI has a dissociation constant for dimerisation of 126 nM (figure 3.31). We used a higher concentration of FL-MepS than the standard MST protocol and a narrow, linear range of unlabelled NlpI, to observe saturation of FL-MepS and thus infer stoichiometry. FL-MepS was used at a constant concentration of 125 nM and was titrated with a linear concentration gradient of unlabelled NlpI from 0 – 300 nM. This concentration range allowed for saturation in 1:1 and 1:2 ratios.

The saturation curve is shown in figure 3.39 in which the TJump data was chosen for analysis as this gave the clearest saturation point. The increase in TJump value correlates with the increasing concentrations of NlpI until saturation of FL-MepS was achieved. Using Microsoft Excel, the gradient of the exponential TJump phase and the saturation plateau was calculated. Using the values generated we calculated the NlpI concentration which saturates 125 nM FL-MepS as 197.3 nM, which corresponds to a ratio of 1:1.6.

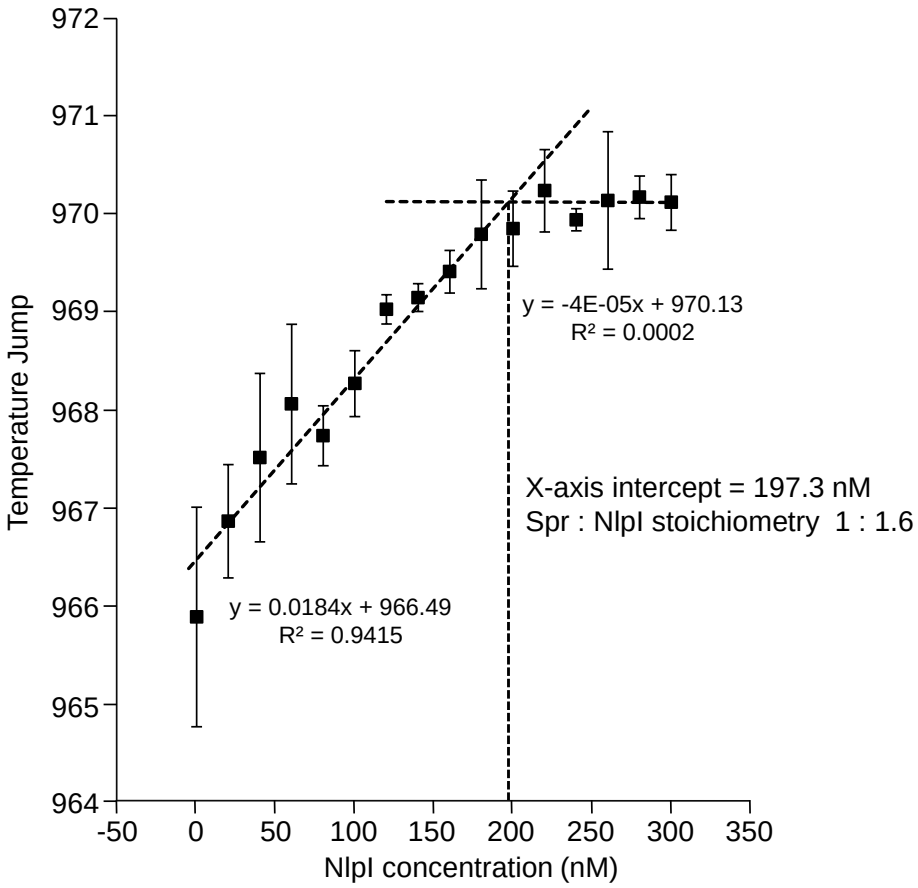

Figure 3.39 Saturation of MepS with NlpI by MST

A constant concentration of 125 nM FL-MepS (at amine residues) was mixed with a narrow, linear range of unlabelled NlpI (0 – 300 nM). The initial TJump from the MST analysis and Microsoft Excel were used to determine the concentration at which NlpI saturates 125 nM of FL-MepS. MST measurements taken at 40% LED power and 20% MST power. The values are the mean ± standard deviation of three independent experiments.

3.5.5.3 NlpI activates MepS on muropeptides

Having obtained the first evidence of a direct interaction between NlpI and MepS, we sought to test the effect of NlpI on MepS activity using intact sacculi. MepS is only weakly active against isolated muropeptides, even at high concentrations (5 μM) and long incubations (o/n) [129]. The NMR structure of MepS shows a structurally closed active site, which may occlude ready access of substrate [131]. We hypothesised that NlpI may activate MepS by causing a conformational change and cause the active site to open.

To study the effect of NlpI on MepS activity, we performed a sacculi-based EPase assay. MepS was incubated at a concentration of 5 μM in the presence or absence of 10 μM NlpI, o/n at 37°C with shaking, in standard EPase reaction buffer (section 2.5.2.2). The reaction was stopped by boiling and the sample was subjected to cellosyl digestion. Samples were centrifuged and the muropeptide-containing supernatant was retained and reduced with sodium borohydride for HPLC analysis (2.5.2.5). The relative percentage of TetraTetra-containing muropeptides was calculated from the total amount of Tetra-containing muropeptides and plotted. Even at these high concentrations and long incubation time, no activity was observed of MepS alone or in the presence of NlpI (figure 5.39). This assay was completed at four different conditions including high and low NaCl (300 mM and 150 mM) and pH (pH 7.5 and pH 5.0) with no activity observed (figure 5.39).

We performed the same assay using isolated muropeptides from the MC1061 WT strain in which MepS, with and without NlpI, was incubated at the same concentrations and conditions as above. The relative percentage of TetraTetra-containing muropeptides was calculated as before. Figure 3.40 shows the results of this assay using the standard EPase buffer (25 mM HEPES/NaOH, 150 mM NaCl, 0.05% Triton X-100, pH 7.5). Figure 5.30 shows the assay performed at four different conditions. We again did not detect any activity of MepS alone at any of the four conditions tested, which is contrary to the published data which show MepS to be active after an o/n incubation with muropeptides [129]. However, in the presence of NlpI, MepS was activated. MepS alone did not significantly reduce the percentage of muropeptides in cross-links, remaining at 42.6%. However, in the presence of NlpI, the percentage of TetraTetra dimers was 16.8%. We show that NlpI activated MepS EPase activity at three of the conditions tested (figure 5.30). MepS remained inactive at low pH and high salt. At 150 mM NaCl and pH 7.5 the stimulation of activity was most drastic and is shown in figure 3.40. These data provide evidence for a functional interaction between NlpI and MepS, and is further evidence of NlpI being a regulator of EPases.

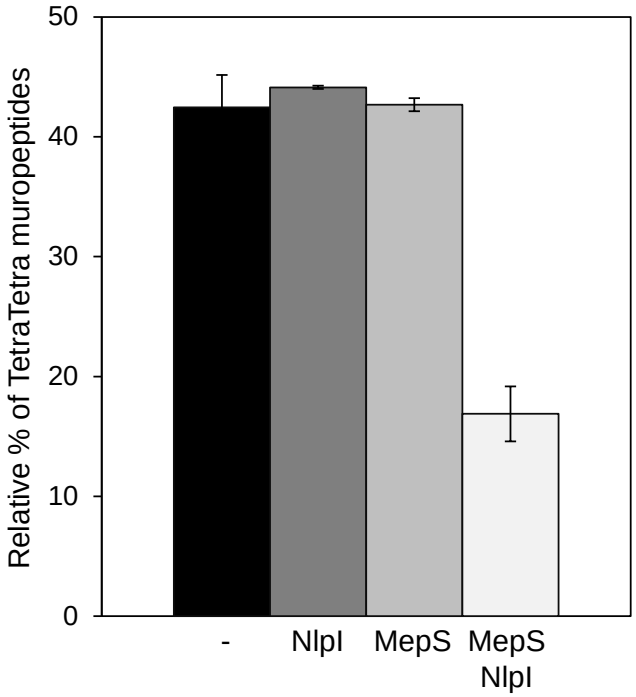

Figure 3.40 NlpI activates MepS on muropeptides

Isolated muropeptides from the cellosyl digestion of the WT *E. coli* strain, MC1061, were incubated o/n at 37°C with 5 μM MepS alone or in the presence of 10 μM NlpI (standard EPase reaction buffer was used here; 25 mM HEPES/NaOH, 150 mM NaCl, 0.05% Triton X-100, pH 7.5). Samples were inactivated by boiling and centrifuged. The digested muropeptides were reduced with sodium borohydride and analysed by HPLC. The relative amounts of TetraTetra dimer were calculated as a percentage of the total number of Tetra-containing muropeptides. The values are the mean ± standard deviation of three independent experiments. Raw HPLC chromatograms are shown in figure 5.40.

3.5.5.4 Deletion of *mepS* suppresses a Δ*nlpI* phenotype

To investigate the relationship between NlpI and MepS *in vivo*, we analysed the growth curves of single or double deletions in both genes, in the presence of various concentrations of the β-lactam, imipenem. Briefly, as it will be discussed in section 3.6, we showed that NlpI is crucial for induction of β-lactamase in response to imipenem. This could be consistent with a role of NlpI in regulating the EPases and/or lytic transglycosylases, whose hydrolytic products are crucial for the induction of the AmpC β-lactamase (section 1.6).

BW27783 cells lacking NlpI, MepS or both, provided by the Reddy lab, were grown to an OD_{578} of 0.2 in LB media before inoculation with varying concentrations of imipenem (0, 0.5, 1, 3 and 5 µg/ml). Growth was monitored using a spectrophotometer (578 nm) every 30 min for 4 h and plotted against time (min). A deletion in MepS had little effect on cell growth (figure 3.41A) in comparison to WT (figure 5.41). However, growth of cells lacking NlpI was impaired, most drastically with 1 µg/ml imipenem (figure 3.41B). In an *nlpI*$^-$*mepS*$^-$ strain, the *nlpI*$^-$ phenotype was supressed and the cells were no longer susceptible to the antibiotic (figure 3.41C).

We performed a β-lactamase induction assay using the same deletion strains in comparison to WT (section 2.6.1). The same strains used for the aforementioned growth curves were cultivated to an OD_{578} of 0.5-0.6. Equal volumes of these strains were added to tubes containing the same volume of fresh, pre-warmed LB containing 1 µg/ml of imipenem. In parallel, cells were also added to fresh LB containing no antibiotic. Samples were incubated for a further 30 min before being placed on ice. Cells were harvested by centrifugation and washed with sodium phosphate buffer, before being centrifuged again. Cell pellets were resuspended in 1 ml of sodium phosphate buffer and 50 µl of the cell suspension was lysed by osmotic shock. After centrifugation and retention of the supernatant, the protein concentration of the lysate was estimated using a BCA kit (section 2.2.3). The lysate was then tested for its ability to hydrolyse the chromogenic β-lactam nitrocefin, using a spectrophotometer. Pure β-lactamase from *P. aeruginosa*, Vim4, was used to determine maximal hydrolytic activity. The rate of nitrocefin hydrolysed per min per mg of protein was calculated and β-lactamase induction was expressed as the fold difference over the control, containing no imipenem. The deletion of *mepS* had no effect on the induction of β-lactamase in response to imipenem and cells lacking NlpI were incapable of inducing a response (figure 3.41D). However, cells with deletions in both *nlpI* and *mepS* showed no impaired β-lactamase induction, correlating with the growth curve experiments.

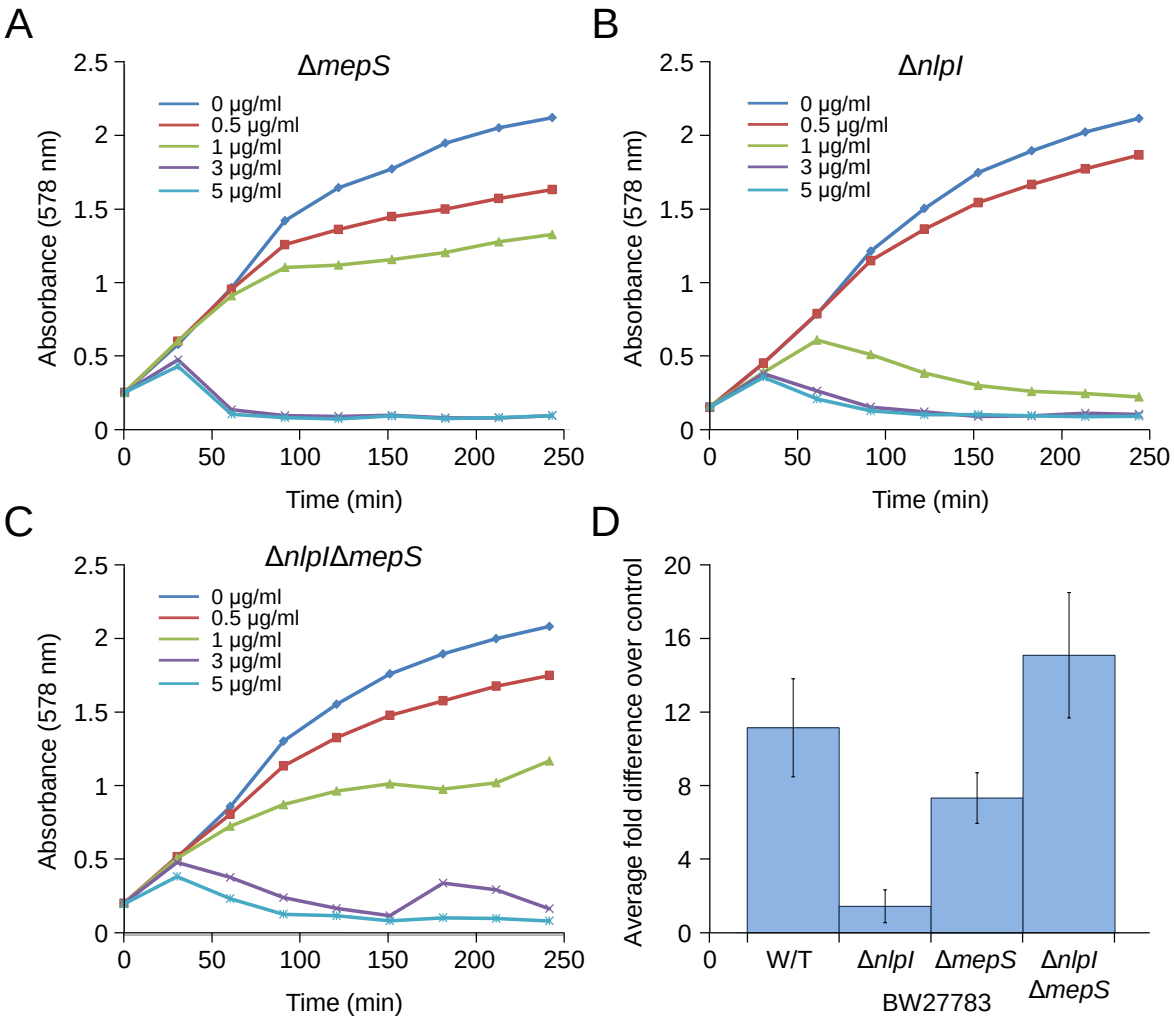

Figure 3.41 Deletion of *mepS* rescues Δ*nlpI* phenotypes

BW27783 strains lacking *mepS* **(A)**, *nlpI* **(B)** or both **(C)** were grown to an OD_{578} of 0.2 before inoculation with varying concentrations of imipenem (0, 0.5, 1, 3, 5 µg/ml). Growth was measured using a spectrophotometer every 30 min for 4 hours. BW27783 WT growth curves shown in figure 5.41. **D.** β-lactamase induction assay of the same strains transformed with the *ampR/ampC* operon-containing plasmid, pJP1. Fold difference calculated against a control not subjected to imipenem stress. The values are the mean ± standard deviation of three independent experiments.

3.5.6 Interaction of NlpI and MepM

3.5.6.1 NlpI interacts with MepM *in vitro*

We have identified interactions between NlpI and three EPases. Two EPases belong to the Class C group of PBPs, PBP4 and PBP7, and the other belonging to the NlpC/P60 family of peptidases, MepS. The latter also belongs to a group of recently identified redundantly essential EPases for cell elongation, together with MepM and MepH. Unfortunately, we have been unable to purify MepH. However, we were able to purify MepM, belonging to the M23 LytM family of metallopeptidases, to homogeneity and test for an interaction with NlpI.

His-MepM was purified by a past member of the Vollmer group, Astrid Schwaiger (section 2.4.7). An *in vitro* cross-linking pull-down assay was performed using His-MepM and native NlpI (section 2.5.1.5). NlpI was only retained in the presence of His-MepM, indicative of an interaction (figure 3.42A).

We confirmed this *in vitro* interaction using MST in which 125 nM of FL-NlpI (at amine residues) was titrated with two-fold serially diluted MepM from 30 µM to 0.915 nM (figure 3.42B). The binding of MepM caused a concentration-dependent fluorescence enhancement which was confirmed as due to ligand binding using an SD test (figure 5.42). The raw fluorescence data was used to generate a binding curve which yielded an apparent K_D of 152 ± 42.1 nM.

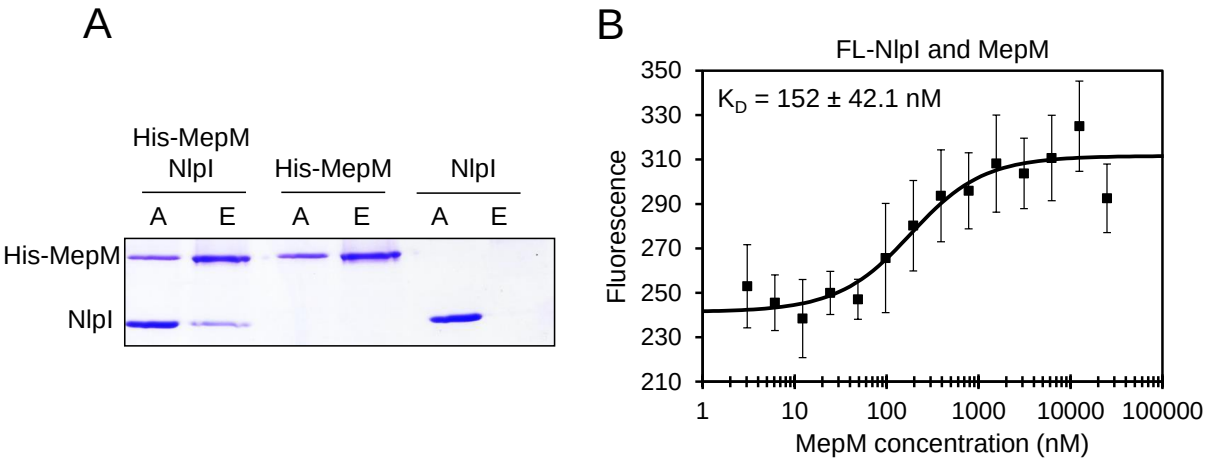

Figure 3.42 NlpI interacts with MepM *in vitro*

A. *In vitro* Ni^{2+} bead pull-down assay using His-MepM and native NlpI. After o/n incubation with Ni^{2+} beads, His-MepM is able to retain native NlpI. Proteins were separated by 12% SDS-PAGE and visualised by coomassie staining. **B.** Raw fluorescence measurement of FL-NlpI (at amine residues) at a concentration of 125 nM and serially diluted unlabelled MepM from a concentration of 30 µM – 0.915 nM (100% LED power and 20% MST power). An apparent K_D of 152 ± 42.1 nM was estimated using accompanying software. The values are the mean ± standard deviation of three independent experiments. Raw MST data are shown in figure 5.42.

3.5.6.2 NlpI inhibits the endopeptidase activity of MepM

To determine whether NlpI was a regulator of MepM EPase activity, a HPLC-based sacculi digestion assay was performed (2.5.2.2). Purified sacculi from the WT *E. coli* strain MC1061 were incubated with 2 μM MepM in the presence and absence of 4 μM NlpI for 4 hours with shaking at 37°C. Standard EPase reaction buffer was used (25 mM HEPES/NaOH, 150 mM NaCl, 0.05% Triton X-100, pH 7.5). The reaction was stopped by boiling and samples were centrifuged to collect the released muropeptide-containing supernatant. Muropeptides were reduced with sodium borohydride and analysed by HPLC (section 2.5.2.5). The relative percentage of TetraTetra-containing muropeptides was calculated from the total amount of Tetra-containing peptides and plotted (figure 3.43).

NlpI had an inhibitory effect on the EPase activity of MepM (figure 3.43). MepM alone reduced the relative percentage of dimeric muropeptides from 43.6% to 22.2%. In the presence of NlpI, MepM only reduced the percentage of dimeric muropeptides to 36.4%. We show that like PBP7 and MepS, the degree of activity was dependent on which conditions were applied (figure 5.31). However, MepM was active at each condition, and its activity was inhibited in the presence of excess NlpI.

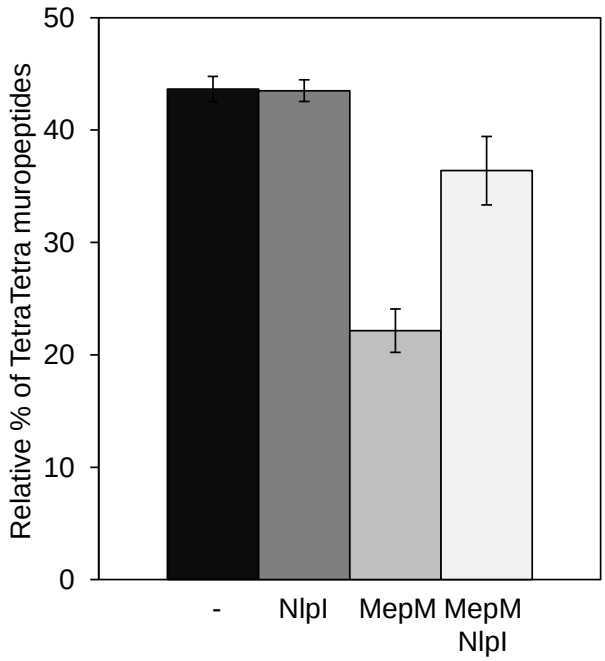

Figure 3.43 MepM endopeptidase activity is inhibited in the presence of NlpI

MepM was incubated with isolated intact sacculi from the WT strain, MC1061, at a concentration of 2 μM alone or in the presence of 4 μM NlpI for 4 hours at 37°C. Samples were inactivated by boiling and centrifuged to obtain released muropeptides. Muropeptides were reduced with sodium borohydride and analysed by HPLC. The relative amount of TetraTetra dimers were plotted as a percentage of the total number of Tetra-containing muropeptides. The values are the mean ± standard deviation of three independent experiments. See figure 5.43 for raw HPLC chromatograms.

3.5.7 Interaction of NlpI and MepA

3.5.7.1 The interaction of NlpI and MepA is pH dependent

In section 3.4 we showed that MepA has a pH dependent EPase activity and substrate binding. At pH 7.5 MepA does not bind intact PG and exerts no EPase activity, whereas at pH 5.0, it is capable of both. The interaction between NlpI and MepA was firstly tested at pH 7.5. FL-MepA (at cysteine residues) was used at a concentration of 125 nM and was titrated with two-fold serially diluted unlabelled NlpI from 30 µM to 0.916 nM. The MST experiment showed no interaction (figure 3.44B).

We therefore reasoned that some interactions of MepA may also be pH dependent. The MST experiment was repeated, however, both the unlabelled NlpI and FL-MepA were diluted against pH 5.0 buffer (10 mM NaAcetate/Acetic acid, 150 mM NaCl, 0.05% Triton X-100, pH 5.0). Measurements were taken at the same conditions as previously and an interaction was observed, generating a binding curve that was used to generate an estimated K_D of 140 ± 21.9 nM (figure 3.44). The experiment was repeated using the same stock of unlabelled NlpI and FL-MepA, diluted in pH 7.5 buffer, and again no interaction was observed.

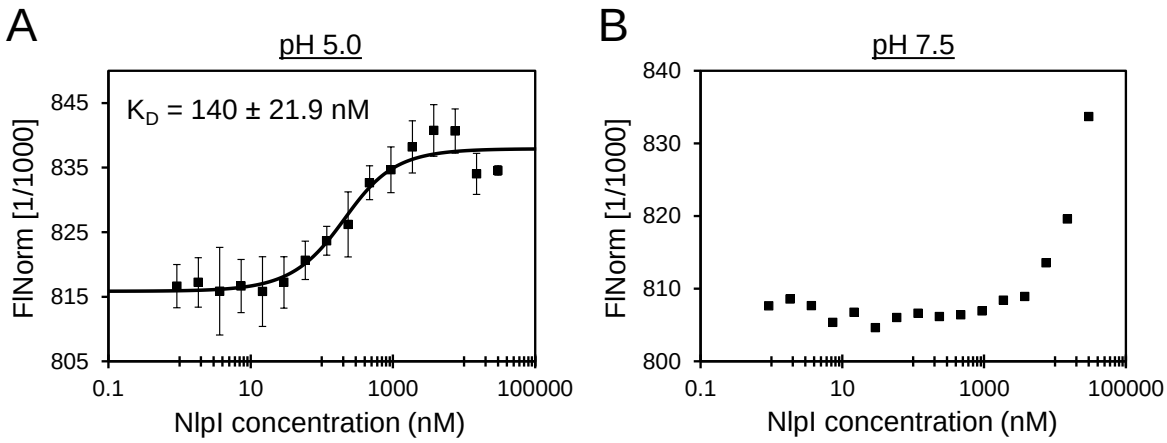

Figure 3.44 Interaction between NlpI and MepA is pH dependent

A. MST measurement of FL-MepA (at cysteine residues) at a concentration of 125 nM titrated with serially diluted unlabelled NlpI from a concentration of 30 µM – 0.916 nM (60% LED power and 40% MST power). Unlabelled NlpI and FL-MepA were diluted into pH 5.0 MST buffer. An apparent K_D of 140 ± 21.9 nM was estimated using accompanying software. The values are the mean ± standard deviation of three independent experiments. **B.** MST measurement of FL-MepA (at cysteine residues) at a concentration of 125 nM titrated with serially diluted unlabelled NlpI from a concentration of 30 µM – 0.916 nM (60% LED power and 40% MST power). Unlabelled NlpI and FL-MepA were diluted into pH 7.5 MST buffer. Raw MST data are shown in figures 5.44 and 5.45.

3.5.7.2 NlpI has no effect on MepA activity at pH 5.0

As the activity of MepA and the interaction between MepA and NlpI are both pH dependent, we performed an activity assay, as described in section 2.5.2.2, using pH 5.0 EPase reaction buffer. Section 3.4.4 shows the optimisation of the MepA EPase assay on intact sacculi. MepA was incubated with D456 sacculi at 2 µM, with and without 4 µM NlpI, for 2 h at 37°C. The reaction was stopped by boiling with 20 mM EDTA and digested with cellosyl o/n. The sample was boiled again and centrifuged. The released muropeptide-containing supernatant was retained and analysed by reversed-phase HPLC and the total number of muropeptides in dimers were calculated (section 2.5.2.5). We show in figure 3.45 that NlpI had no effect on the activity of MepA at pH 5.0.

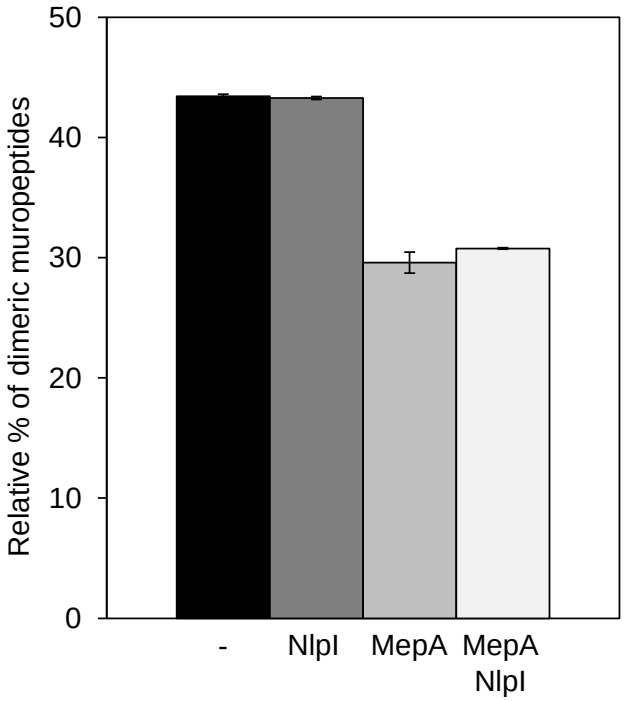

Figure 3.45 NlpI has no effect on the activity of MepA at pH 5.0

MepA was incubated with D456 sacculi at a concentration of 2µM in the presence or absence of 4 µM NlpI. Samples were incubated for 2 h at 37°C before stopping the reaction by boiling with 20 mM EDTA. Samples were digested o/n with cellosyl and boiled again. Released muropeptides were obtained by centrifugation, reduced with sodium borohydride and analysed by reversed-phase HPLC. D456 sacculi contain Tetra and Penta monomers as well as TetraTetra and TetraPenta dimers. The relative percentage of dimeric muropeptides was calculated and plotted. The values are the mean ± standard deviation of three independent experiments. Raw HPLC chromatograms are shown in figure 5.46.

3.5.8 NlpI has multiple EPase interaction sites

NlpI has been shown to interact with five enzymes with EPase activity; PBP4, PBP7, MepA, MepM, and MepS, which themselves are connected by multiple direct and indirect interactions. We questioned whether NlpI would preferentially interact with a particular EPase in the presence of another, or if NlpI had different interaction sites for each EPase. We sought to test these hypotheses by challenging interactions with the presence of other interaction partners using modified MST (described in section 3.5.3.4) and Ni^{2+} bead pull-down assays. We used these methods to test if NlpI could interact with more than one EPase simultaneously.

NlpI, MepS and PBP4

FL-MepS (at amine residues) was used at a concentration of 62.5 nM and was tested for interaction using 3 µM NlpI, a concentration within the bound state for the interaction (figure 3.38B). An increase in the FNorm was indicative of an interaction with MepS (figure 3.46A). PBP4 has been shown not to interact with MepS by MST but interacts with NlpI with an apparent K_D of 177 ± 49 nM (figure 3.31C). Here, the addition of PBP4 (30 µM) to FL-MepS did not produce a change in FNorm significant enough to indicate an interaction. NlpI was mixed with 30 µM PBP4, which we predicted would saturate all PBP4 binding sites of NlpI. The mixture was then added to FL-MepS and the FNorm recorded. An increase in FNorm was observed indicative of an interaction, and was significantly larger than that of NlpI alone. These data indicate that the presence of excess PBP4 did not prevent the binding of NlpI to FL-MepS and that a larger complex formed that slowed the thermophoretic movement of FL-MepS (figure 3.46B). As a control, we showed that 12 µM of BSA did not incur the same thermophoretic effect as excess PBP4 indicating that the ternary complex formed between MepS, NlpI and PBP4 was specific.

These MST data were verified using an *in vitro* Ni^{2+} bead pull-down assay with His-MepS and untagged forms of NlpI and PBP4. Figure 3.46C shows that His-MepS retained both NlpI and PBP4 individually, but also retained both proteins simultaneously.

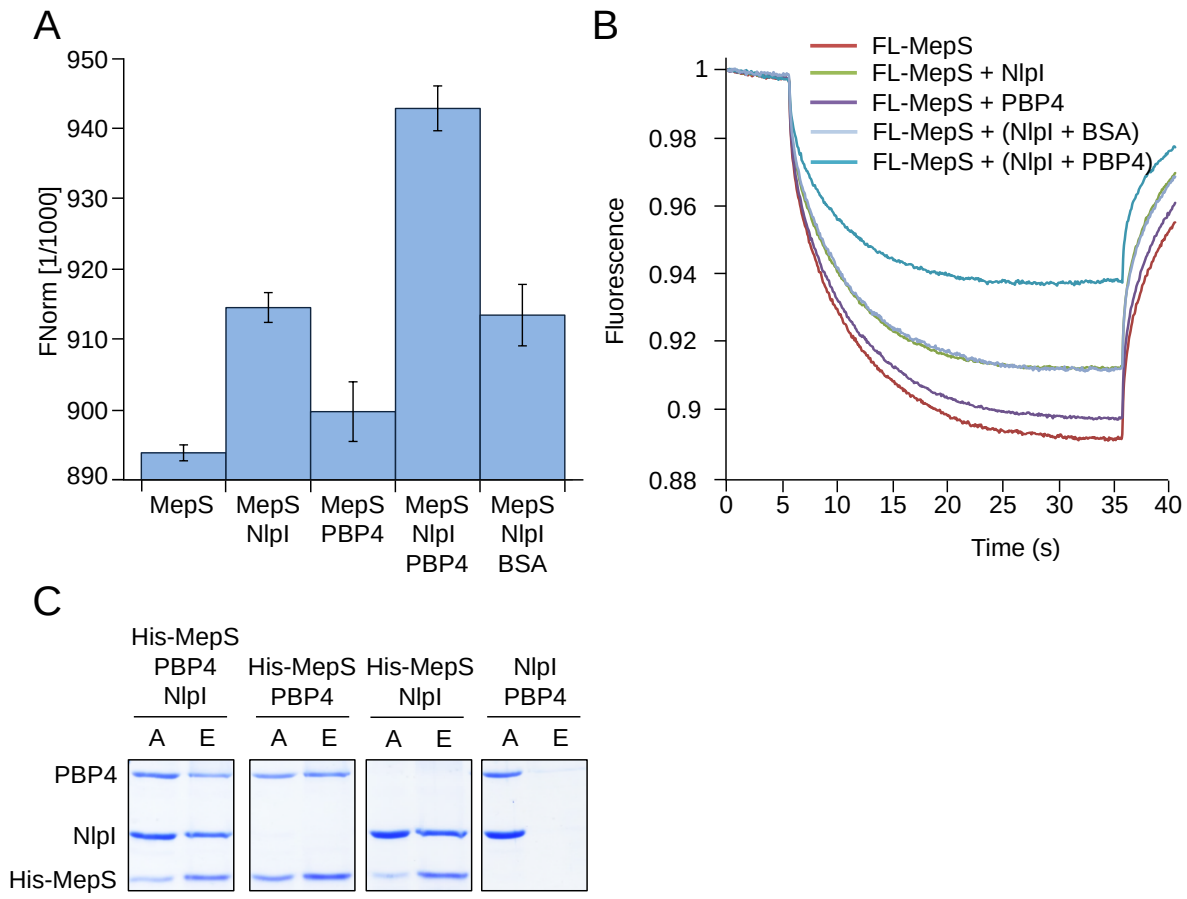

Figure 3.46 NlpI, MepS and PBP4 form a ternary complex

A. End-point normalised fluorescence (FNorm) showing the ternary complex of MepS, NlpI and PBP4. FL-MepS (62.5 nM) was measured either alone, or in the presence of NlpI (3 µM) or excess PBP4 (30 µM). The same concentrations were then used to pre-incubate NlpI with PBP4 before addition to FL-MepS. MST measurements were carried out with 20% LED power and 40% MST power. The values are the mean ± the standard deviation of three independent experiments. **B.** MST time traces of the experiments shown in A. The values are the mean of three independent experiments. **C.** An *in vitro* Ni^{2+} bead pull-down assay was used to show that His-MepS was able to retain both NlpI and PBP4 individually and at the same time. All proteins were used at 2 µM. A, applied sample taken prior to addition to beads; E, elution sample of bound proteins after washing. Proteins were separated by 12% SDS-PAGE and visualised by Coomassie-staining.

NlpI, MepS and PBP7

We used the same modified MST protocol to test the potential trimeric complex formation of MepS, NlpI and PBP7. FL-MepS and unlabelled NlpI were used at the same concentration as above; however, unlabelled NlpI was pre-incubated with unlabelled PBP7 (30 µM) prior to addition to FL-MepS, instead of PBP4.

The addition of NlpI (3 µM) to FL-MepS again caused a significant change in FNorm, indicative of an interaction (figure 3.47A). We observed no significant change upon the addition of PBP7 (30 µM), consistent with the regular MST protocol which showed that these proteins do not interact (figure 3.15A). Upon addition of NlpI saturated with PBP7, the observed change in FNorm was the same as with NlpI alone, showing that the presence of PBP7 bound to NlpI did not prevent the binding of NlpI to MepS (figure 3.47A/B).

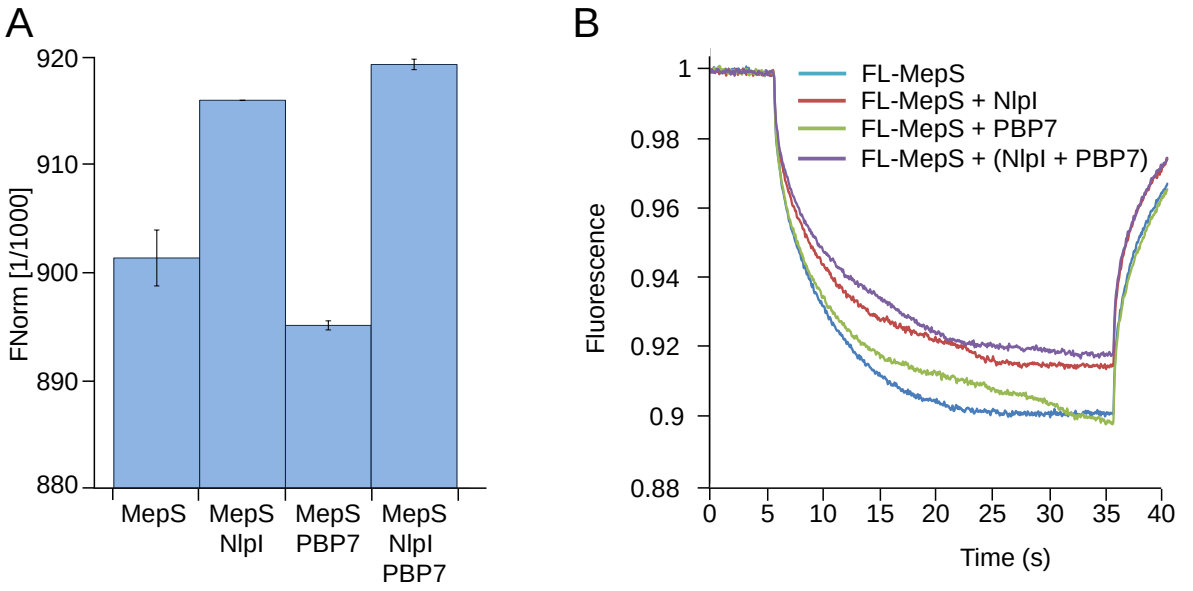

Figure 3.47 NlpI possesses different interaction sites for MepS and PBP7

A. End-point normalised fluorescence (FNorm) showing the presence of PBP7 does not prevent binding of NlpI to MepS. FL-MepS (62.5 nM) was measured either alone, or in the presence of NlpI (3 µM) or excess PBP4 (30 µM). The same concentrations were then used to pre-incubate NlpI with PBP7, before addition to FL-MepS. MST measurements were carried out with 20% LED power and 40% MST power. The values are the mean ± the standard deviation of three independent experiments. **B.** MST time traces of the experiments shown in A. The values are the mean of three independent experiments.

Larger complexes involving NlpI

Described and observed in this work are the interaction of NlpI with at least five EPases (PBP4, PBP7, MepS, MepM and MepA). In addition, work undertaken by Hamish Yau from the Vollmer group identified the interactions of Slt with four of the same EPases as NlpI (PBP4, PBP7, MepS and MepM) (Unpublished). Investigations are underway into the ability of NlpI and Slt to interact with their shared EPases in the presence of the other protein to determine preferential or competitive binding.

Using the Ni^{2+} bead pull-down assay, larger complexes than previously tested were attempted to observe direct or indirect interactions. Here, a five protein complex was tested using four unlabelled proteins, NlpI, PBP4, PBP7 and Slt, and one His-tagged, MepS.

Figure 3.48 shows that His-MepS was able to pull down NlpI, PBP4 and Slt. As there are shared interactions between all four of these proteins, we cannot say that MepS is interacting with all of these proteins simultaneously, but these data do infer that a large complex between these proteins is occurring *in vitro*. Large complexes, such as this have not been regularly observed, and this technique could be important for proteins with multiple direct or indirect interaction partners. For example, in this situation, PBP7 is not retained. More controls will need to be undertaken to determine whether PBP7 can be retained whilst one of the other proteins is not present and this would provide information on selective or preferential interactions of proteins with multiple interaction partners.

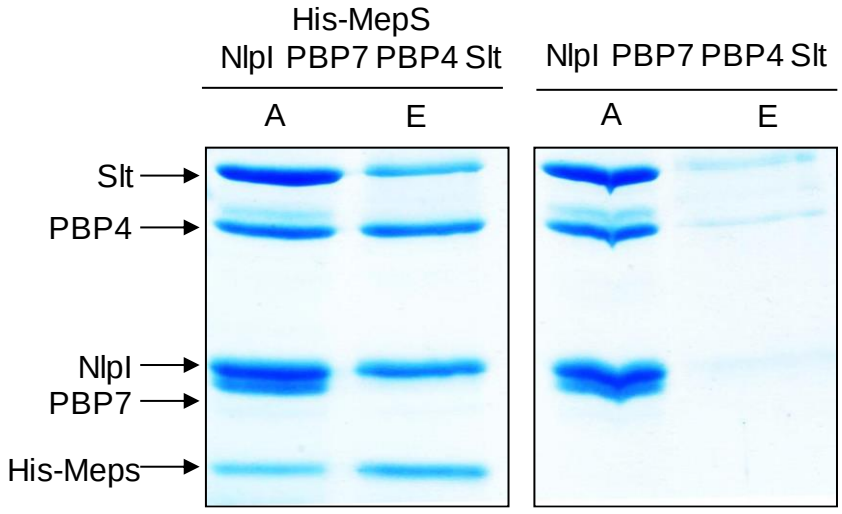

Figure 3.48 His-MepS retains PBP4, NlpI and Slt by *in vitro* Ni^{2+} bead pull-down

In vitro Ni^{2+} bead pull-down assay using His-MepS and untagged NlpI, PBP4, PBP7 and Slt. An applied sample was taken prior to addition to beads (A). Beads were washed and eluted and a sample taken (E). Proteins were separated by 12% SDS-PAGE and visualised by Coomassie staining.

3.5.9 Other NlpI interactions partners

Positive interactions

Characterised is this work are the shared interaction partners, PBP4 and PBP7, of NlpI, LpoA and PBP1A. We hypothesised therefore that NlpI may be capable of interacting directly with the core PG synthesis machinery during elongation.

Using MST we observed a weak interaction between NlpI and PBP1A (figure 3.49A) (section 2.5.1.7). FL-PBP1A (at amine residues) was used at a concentration of 41.5 nM and was titrated with two-fold serially diluted unlabelled NlpI from a concentration of 100 µM to 3.05 nM. The binding curve generated an apparent K_D of 1470 ± 138 nM.

Using an *in vitro* TPase assay we showed that NlpI had no effect on the activity of PBP1A and no effect on the stimulation of activity by LpoA (figure 5.47) (section 2.5.2.4).

We speculated that NlpI may interact exclusively with hydrolases possessing EPase activity. To test this we used the monofunctional CPases PBP6B and PBP5 (purified by Katharina Peters from the Vollmer group). Using *in vitro* cross-linking pull-down assays we confirm the absence of an interaction between His-NlpI and native PBP5 (figure 3.51C). However, His-NlpI was able to retain native PBP6B (figure 3.49B).

During an *in vitro* affinity chromatography search for potential NlpI interaction partners, our collaborators from the Typas group found EnvC and AmiC. These data infer that NlpI could have an additional role in the regulation of the activity of amidases.

Here we show the *in vitro* interaction between NlpI and EnvC using MST and a Ni^{2+} bead cross-linking pull-down assay (figure 3.49C/D). FL-NlpI (at amine residues) was used at a constant concentration of 166 nM. Unlabelled EnvC was two-fold serially diluted from a concentration of 10 µM to 0.305 nM and titrated with FL-NlpI. The resulting binding curve yielded an estimated K_D of 252 ± 47.5 nM. We confirmed this *in vitro* interaction by showing that His-NlpI retained untagged EnvC on Ni^{2+} beads after thorough washing (section 2.5.1.5).

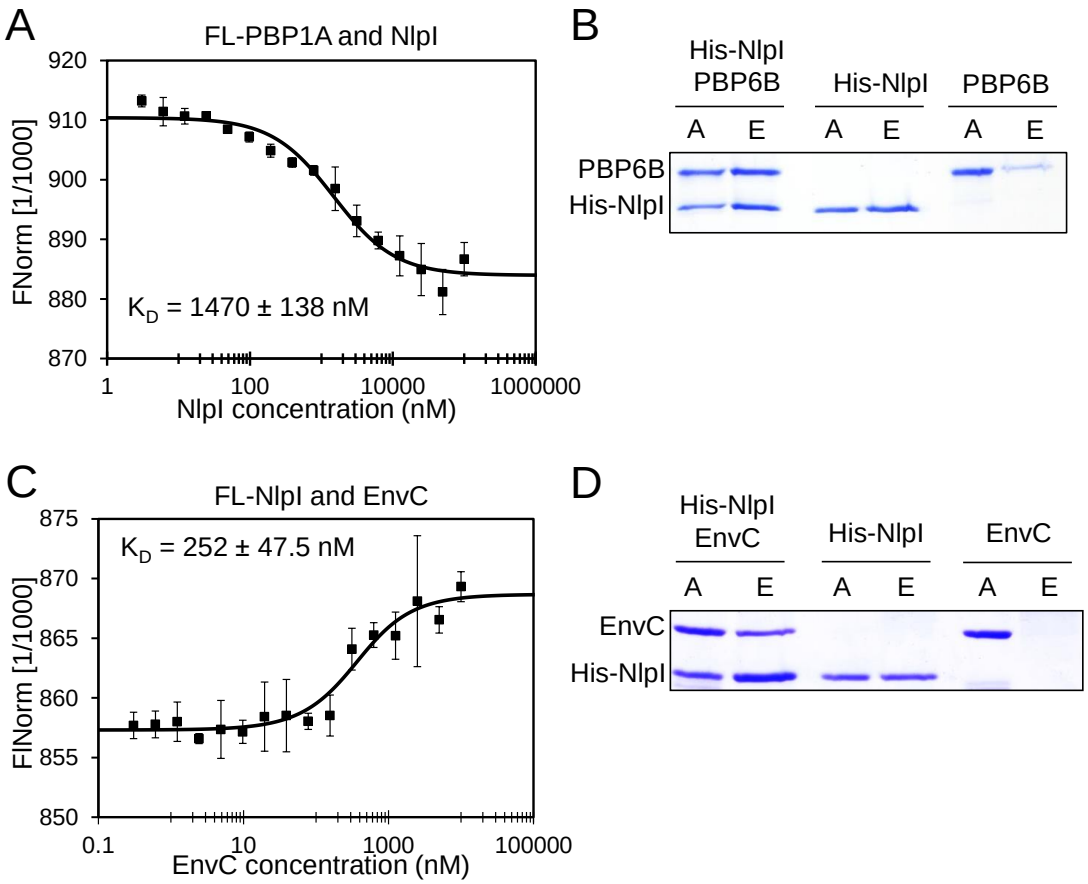

Figure 3.49 NlpI interacts with PBP1A, PBP6B and EnvC *in vitro*

A. MST showing the interaction between FL-PBP1A (at amine residues) at a constant concentration of 41.5 nM titrated with two-fold serially diluted unlabelled NlpI from a concentration of 100 µM – 0.35 nM. MST power 20%, LED power 80%. An apparent K_D of 1470 ± 138 nM was estimated using accompanying software. The values are the mean ± standard deviation of three independent experiments. Raw MST data are shown in figure 5.48. **B.** *In vitro* Ni^{2+} bead pull-down assay using His-NlpI and untagged PBP6B. An applied sample was taken prior to addition to beads (A). Beads were washed and eluted and a sample taken (E). Proteins were separated by 12% SDS-PAGE and visualised by Coomassie staining. **C.** MST of FL-NlpI, (at amine residues) at a concentration of 166 nM, titrated with two-fold serially diluted EnvC from a concentration of 10 µM – 0.305 nM. MST power 20%, LED power 80%. A K_D of 252 ± 47.5 nM was estimated using accompanying software. The values are the mean ± standard deviation of three independent experiments. Raw MST data are shown in figure 5.49. **D.** *In vitro* Ni^{2+} bead pull-down assay using His-NlpI and untagged EnvC. An applied sample was taken prior to addition to beads (A). Beads were washed and eluted and a sample taken (E). Proteins were separated by 12% SDS-PAGE and visualised by Coomassie staining.

Non-interacting proteins

After observing the interaction between NlpI and PBP1A, we tested an interaction between NlpI and LpoA. LpoA was fluorescently-labelled (at cysteine residues) and used at a concentration of 62.5 nM. Unlabelled NlpI was two-fold serially diluted from 100 µM to 3.05 nM and titrated with FL-LpoA (figure 3.50A). We also performed an *in vitro* Ni^{2+} pull-down assay using His-NlpI and native LpoA (figure 3.51A). Both assays concluded that there was no interaction between NlpI and LpoA.

In addition, NlpI did not interact with the soluble LT, Slt. FL-NlpI (at amine residues), at a concentration of 62.5 nM, was titrated with two fold serially diluted unlabelled Slt from 15 µM to 0.458 nM (figure 3.50B). We also performed an *in vitro* pull-down assay using His-Slt and native NlpI (figure 3.51B). In both assays we did not detect an interaction between NlpI and Slt.

NlpI also did not interact with LpoB. FL-NlpI (at amine residues), at a concentration of 62.5 nM, was titrated with two fold serially diluted LpoB from 50 µM to 1.526 nM to show no interaction (figure 3.50C).

Using *in vitro* Ni^{2+} bead pull-downs, we showed that there was no interaction between PBP5 and NlpI, using His-NlpI and thrombin-cleaved PBP5, purified by Katharina Peters from the Vollmer lab (figure 3.51C).

A deletion of *nlpI* and *pal* was shown to be synthetically lethal *in vivo* by Manuel Banzhaf (unpublished) implicating a functional relationship. However we not did not detect a direct interaction between the proteins by *in vitro* Ni^{2+} pull-down assay, using His-Pal and thrombin-cleaved NlpI (figure 3.51D).

Finally, we showed by an *in vitro* Ni^{2+} pull-down assay that there was no interaction between NlpI and CpoB. His-CpoB and thrombin-cleaved NlpI were used (figure 3.51E).

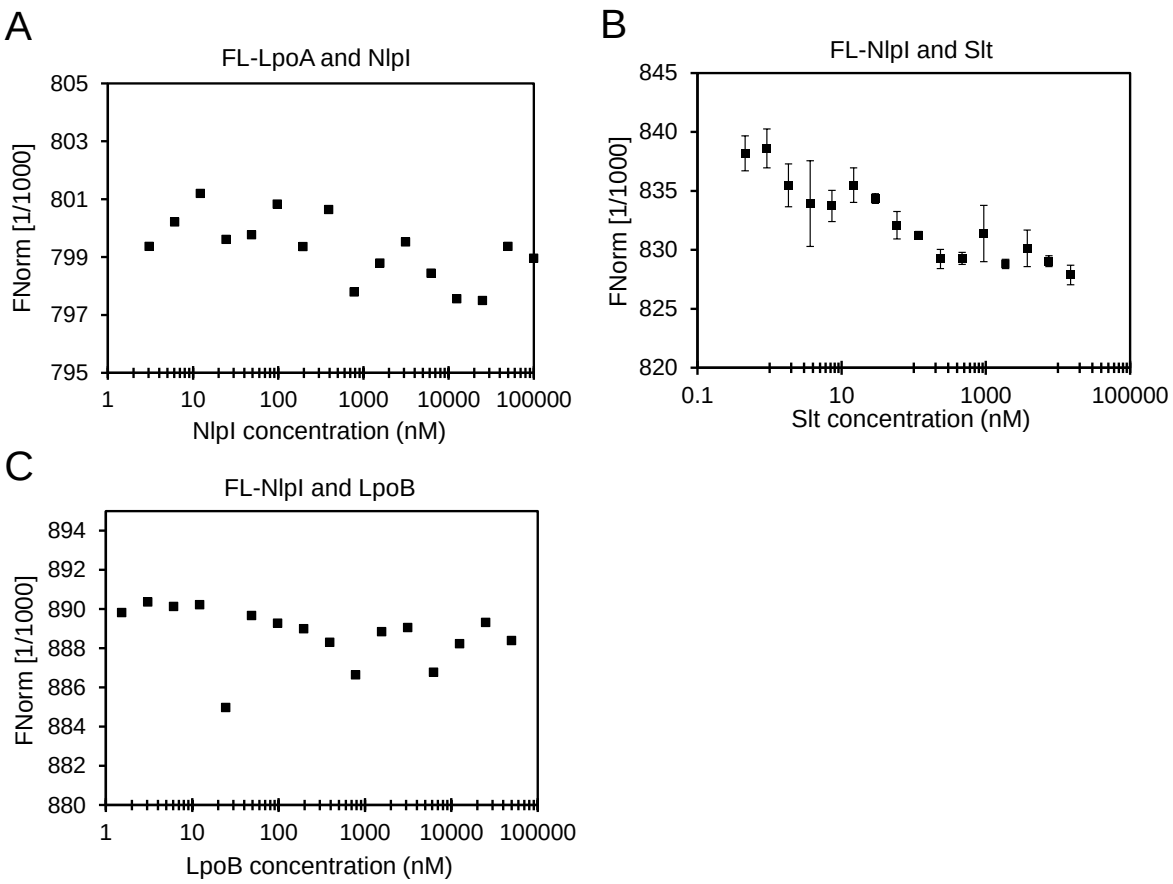

Figure 3.50 NlpI does not interact with LpoA, Slt or LpoB by MST

A. MST measurement of FL-LpoA (at cysteine residues) at 62.5 nM titrated with two-fold serially diluted unlabelled NlpI from 100 µM – 3.05 nM. MST power 40%, LED power 40%. **B.** MST measurement of FL-NlpI (at amine residues) at 62.5 nM titrated with two-fold serially diluted unlabelled Slt from 15 µM – 0.458 nM. MST power 40%, LED power 40%. **C.** MST measurement of FL-NlpI (at amine residues) at 62.5 nM titrated with two-fold serially diluted unlabelled LpoB from 50 µM – 1.526 nM. MST power 20%, LED power 40%. Raw MST data are shown in figures 5.50-5.52.

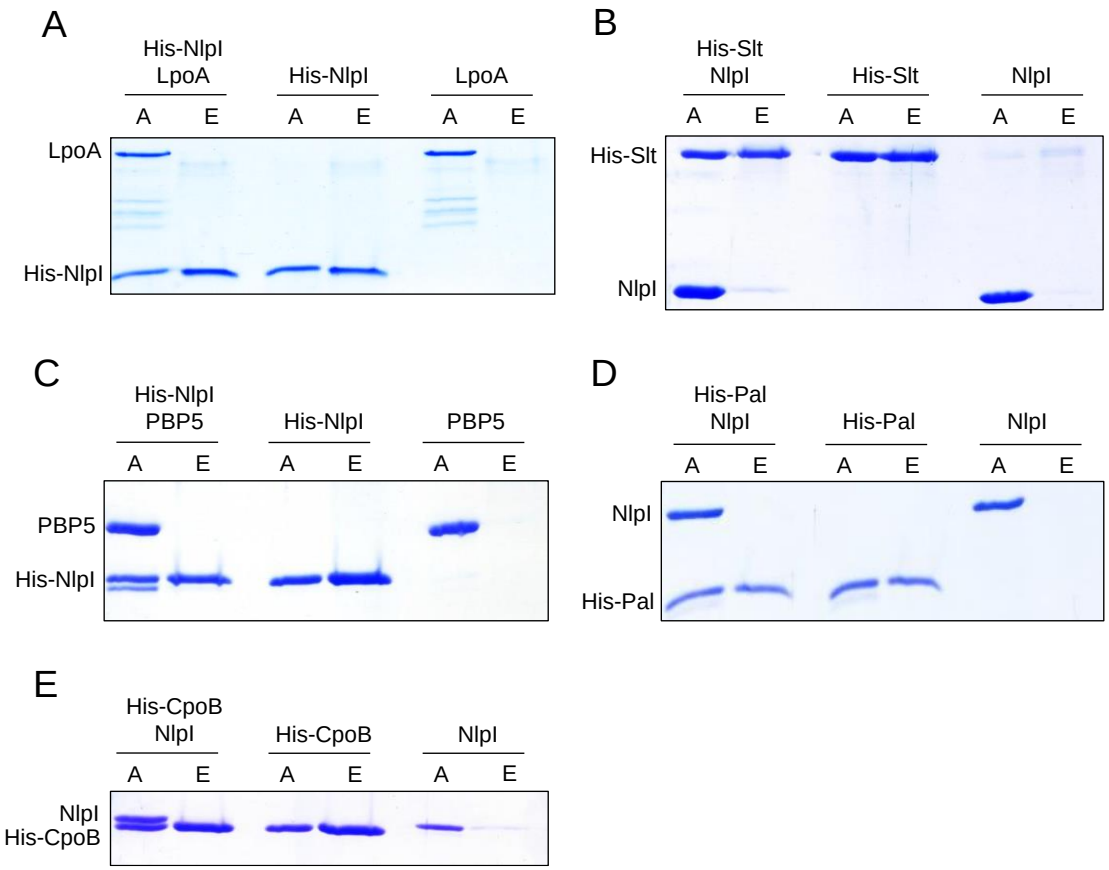

Figure 3.51 NlpI does not interact with LpoA, Slt, PBP5, Pal or CpoB by Ni^{2+} pull-down assay

A. *In vitro* Ni^{2+} bead pull-down assay using 2 µM of His-LpoA and untagged EnvC. A, applied sample taken prior to addition to beads; E, elution sample of bound proteins after washing. **B.** *In vitro* Ni^{2+} bead pull-down assay using 2 µM of His-Slt and untagged NlpI. **C.** *In vitro* Ni^{2+} bead pull-down assay using 2 µM of His-NlpI and untagged PBP5. **D.** *In vitro* Ni^{2+} bead pull-down assay using 2 µM of His-CpoB and untagged NlpI. Proteins were separated by 12% SDS-PAGE and visualised by Coomassie-staining.

3.5.10 Conclusions and discussions

The data presented in this section comprehensively characterised the role of New Lipoprotein I (NlpI), of previously debated cellular function, as a regulator of EPase activity. We have characterised the interactions of NlpI with five of the seven known PG EPases of *E. coli* and used MST to estimate the K_D value of each interaction. We showed that NlpI has differential effects on the activity of three of these EPases.

Oligomeric state of NlpI

After purification to homogeneity of the soluble form, we used AUC to determine the oligomeric state of NlpI in solution in collaboration with Alexandra Solovyova, Newcastle University. The results yielded one peak, corresponding to the estimated size of the dimeric form of the protein (~60 kDa). The published crystal structure predicted strong dimerisation between two large surfaces in a face-to-face formation. At the high concentrations used in AUC, we did not detect a monomeric form of NlpI. The AUC data showed a slight discrepancy between the predicted and the measured sedimentation velocities. We hypothesised that this was due to the dimer having a slightly more elongated shape than determined by crystallography, or an uncharacterised degree of flexibility between the monomers.

To determine the K_D of dimerisation, we used NlpI at much lower concentrations than required for AUC. Using MST we tested for the interaction between FL-NlpI, at 62.5 nM (predicted to be lower than the K_D for dimerisation), and serially diluted unlabelled NlpI. The binding curve generated an estimated K_D for dimerisation of 126 ± 9.1 nM. These MST data explain why no NlpI monomer was observed using AUC, and will provide a basis for the determination of stoichiometry in future interaction experiments.

NlpI is a novel regulator of endopeptidase activity

NlpI and PBP4

Our collaborators in Heidelberg used affinity chromatography to identify PBP4 as highly enriched after incubation of a combined *E. coli* membrane/periplasmic fraction with beads containing immobilised NlpI, compared to that of a control column. We confirmed the interaction by SPR which generated an equilibrium binding plateau. Using Scatchard analysis

by non-linear regression we estimated a K_D of 311 ± 46 nM. We further confirmed the *in vitro* interaction using MST, to generate an estimated K_D of 177 ± 49 nM. The dissociation constants calculated by the two methods closely correlate. In addition we used a Ni^{2+} bead cross-linking pull-down assay as a third method of confirming the *in vitro* interaction. Attempts have been made to observe the interaction *in vivo* using co-immunoprecipitation, but have been unsuccessful thus far.

Using a sacculi-based EPase activity assay we could show that, unlike the other interaction partners of PBP4 presented in this work (LpoA, PBP1A, PBP7 and MepA), NlpI is able to stimulate the activity of PBP4. We observe almost complete degradation of dimeric muropeptides by PBP4 in the presence of NlpI. We hypothesise that LpoA and PBP1A act to spatio-temporally coordinate PBP4 activity with ongoing PG synthesis, where NlpI acts to regulate this activity. It is possible that *in vitro* we only observe stimulation by NlpI where, *in vivo*, NlpI may be able to both stimulate and inhibit PBP4 activity when required. *In vivo* experiments are currently being undertaken by the Typas group regarding all of the EPases and NlpI.

In section 3.3.5 we showed that domain 3 is not an interaction site for LpoA or PBP1A. Using a Ni^{2+} bead pull-down assay and MST, we showed that PBP4ΔD3 does not interact with NlpI. These interaction and activity data correlate with the observed lack of activity upon deletion of domain 3. We speculate that the interaction between NlpI and PBP4 takes place primarily through domain 3 which causes a conformational change revealing or concealing the active site, thus regulating activity. As the conditions of the periplasm are not constant, NlpI may be bound to PBP4, via domain 3, to allow NlpI to alter the activity of PBP4 in response to these changing conditions.

Domain 3 of PBP4 may have a similar role as the regulatory α-helix of AmiB which is removed upon interaction with EnvC to allow activity (section 1.4.6). The mechanism of how and why domain 3 of PBP4 is essential for activity is not yet known. Co-crystallisation studies would help elucidate this function and have been undertaken in this project, however these have been unsuccessful so far, having only been able to obtain crystals of NlpI.

In the absence of domain 3, there is no interaction with NlpI, however the interaction between PBP4 and PBP1A and LpoA can still take place. Here we used a modified MST protocol to test whether PBP4 can interact with PBP1A and LpoA in the presence of excess NlpI. PBP1A is a shared interaction partner of PBP4 and NlpI, however the K_D for the interaction between NlpI and PBP1A is significantly higher (~1000 nM) than that of PBP4 and PBP1A (~60 nM).

This allowed us to use FL-PBP1A in the presence of a low concentration of PBP4 and an excess of NlpI without causing an interaction between NlpI and FL-PBP1A. We used 0.5 µM of unlabelled PBP4, which is within the bound state of the interaction observed for FL-PBP1A and PBP4, and 1 µM of NlpI, which is in excess of PBP4 but below the estimated K_D of interaction for PBP1A. We observed the binding of PBP4 to FL-PBP1A alone and in the presence of excess NlpI, supporting our hypothesis that PBP4 has different binding sites for its different interaction partners, which we predict to be domain 1 and/or 2 for PBP1A and domain 3 for NlpI.

This hypothesis is further supported using FL-LpoA and testing for interaction with PBP4 in the presence or absence of excess NlpI. The interaction between FL-LpoA (at cysteine residues) and PBP4 caused a concentration-dependent fluorescence enhancement, while LpoA does not interact with NlpI. We show again that the interaction between FL-LpoA and PBP4 caused a fluorescence enhancement, and that excess NlpI did not. The presence of excess NlpI also did not prevent the interaction of PBP4 and LpoA. Thus, these data support previous *in vitro* work in this project that infer that PBP4 interacts with LpoA and PBP1A via domain 1 and/or 2, (section 3.2.2.3 and 3.3.5) and interacts with NlpI via domain 3 (section 3.5.3.3).

NlpI and PBP7

We hypothesised that NlpI may have more than one interaction partner. We chose to firstly test one of the other members of the Class C PBPs, PBP7. We confirmed the interaction *in vitro* using a Ni^{2+} bead pull-down assay and MST. FL-PBP7 was titrated with serially diluted NlpI which generated an equilibrium binding event with an estimated K_D of 90 ± 8.9 nM, one of the strongest interactions observed in this work. However, when testing the interaction using FL-NlpI and unlabelled PBP7, the binding was no longer in equilibrium. We therefore applied the Hill model to estimate an apparent EC_{50} of 422 ± 25 nM, a significantly weaker interaction than before. Using this model, we also generated a Hill coefficient of 3.06, implying positive cooperativity. This indicates that the binding of PBP7 may cause a conformational change in NlpI leading to an increase in affinity for subsequent interactions with PBP7. This also suggests that NlpI may possess more than one PBP7 binding site. As NlpI was used as the fluorescently-labelled protein, it was below the concentration calculated for dimerisation. We speculate that the increased affinity for PBP7 observed for monomeric NlpI may be to prevent interactions with other EPases. In the cell, monomeric NlpI may exist at certain conditions in which an interaction with PBP7 is more favourable than the other

EPases. When NlpI is in its dimeric state it may be able to bind to all EPases simultaneously. We aim to thoroughly test the ability of NlpI to bind more than one EPase at the same time.

Unlike PBP4, NlpI had no effect on the EPase activity of PBP7 at all conditions tested. However, we should not exclude an effect on activity in the cell. It is also possible that PBP7 may not require regulation of activity, or that another interaction partner is involved. The role of NlpI here may be to coordinate EPase activity with the other EPases as part of a hydrolase/regulator complex, or activity may be only regulated when it is recruited to sites of ongoing PG synthesis.

NlpI and MepS

While inferred in recent publications [100,236], we present here the first evidence of the direct *in vitro* interaction between NlpI and MepS, a member of the NlpC/P60 peptidase superfamily. We showed the interaction using His-tagged MepS and untagged NlpI in a Ni^{2+} bead pull-down assay and MST, which we used to estimate a K_D of 145 ± 51.6 nM, an affinity which closely matches that of NlpI and PBP4.

Aramini *et al* (2008) used NMR spectroscopy and AUC to show that MepS exists as a monomer in solution. The high concentrations required for use as the serially diluted unlabelled ligand in MST means that NlpI is most likely in a dimeric state. We therefore initially hypothesised that MepS interacts with NlpI with a stoichiometry of 1:2.

We performed a saturation binding experiment by MST to test this hypothesis. We modified the MST protocol to estimate the concentration of NlpI required to saturate a constant concentration of FL-MepS. A narrow linear range of NlpI concentrations (0-300 nM) was added to a constant concentration of 125 nM FL-MepS and was analysed by MST. The linear range of NlpI reached a saturation plateau at 197.3 nM which corresponded to a stoichiometry of MepS to NlpI of 1:1.6. We predict that the ratio generated, being halfway between 1:1 and 1:2, is due to the presence of both monomeric and dimeric forms of NlpI present, monomeric at lower concentrations and dimeric at higher. Attempts to reverse this experiment using a constant concentration of FL-NlpI and a linear range of MepS have been unsuccessful thus far. Nevertheless, this adapted protocol is promising for investigating the stoichiometry of future interactions by MST.

The NMR structure of MepS predicted that the active site, while conserved within a putative substrate binding groove, is buried within the protein. We hypothesise this is the reason for

the low activity observed in the published data, and the lack of activity observed in this work. We predicted that the interaction of NlpI with MepS may cause a conformational change in such a way that the active site becomes more accessible for substrate and thus stimulate activity. When tested on intact sacculi, this was not the case at any of the conditions tested and NlpI did not affect activity. On muropeptides however, the presence of NlpI stimulated MepS activity at each condition tested, excluding high NaCl (300 mM) and low pH (pH 5.0), most obviously at 150 mM NaCl and pH 7.5. At present we do not know whether the binding of NlpI causes a conformational change in MepS, but efforts to co-crystallise the complex are planned. As discussed earlier, a recent publication by our collaborator [108] highlighted the role of NlpI in facilitating the proteolytic degradation of MepS. Our current hypothesis is that the effect on activity by NlpI is secondary to this regulation of degradation.

Phenotypically, we also confirmed the findings of [230] by showing that a deletion of *mepS* suppresses an *nlpI*$^-$ phenotype. We used growth curves of varying concentrations of imipenem, and a β-lactamase induction assay. The induction of β-lactamase relies on the turnover products of LTs and EPases (section 1.6). We show that in the absence of NlpI, cells are incapable of inducing a β-lactamase response upon imipenem stress (discussed in more detail in section 3.6). This implies that NlpI is involved in the *in vivo* activity of PG hydrolases. We show that there was no effect on β-lactamase induction upon deletion of *mepS*, which is unsurprising due to the redundant nature of the PG hydrolases. However, upon deletion of *mepS* in an *nlpI*$^-$ background, we observe suppression of this impaired induction. These data indicate that it is the unregulated activity of MepS that contributes to the impaired ability to induce β-lactamase in response to imipenem in the absence of NlpI, and perhaps the unregulated activity of the other EPases, although this has not been tested.

NlpI and MepM

In our lab so far we have been unsuccessful in the purification of MepH. However, we tested for the interaction between NlpI and MepM. Using His-MepM and native NlpI we showed an *in vitro* interaction by Ni^{2+} bead pull-down assay. By MST, we estimated a K_D of 152 ± 42.1 nM. This affinity is in close concordance with that of the four other hydrolase interaction partners of NlpI. The addition of unlabelled MepM to FL-NlpI (at amine residues) caused a concentration-dependent fluorescence enhancement, and the raw fluorescence values were used to estimate the dissociation constant.

NlpI inhibited the EPase activity of MepM on intact sacculi. As with the other EPases (excluding MepA), MepM activity was weaker at lower pH and at a higher concentration of NaCl, however, the inhibition by NlpI was observed at all conditions tested. Inhibition was most drastically observed at standard EPase reaction conditions (150 mM NaCl and pH 7.5).

NlpI and MepA

NlpI has now been shown to interact with four EPases at our standard pH 7.5 interaction conditions. MepA was the only EPase studied in this work to initially not interact with NlpI. The characterisation of the pH dependent activity and substrate binding ability of MepA in section 3.4 prompted us to test this interaction at pH 5.0. Using MST we observed an interaction with an estimated K_D of 140 ± 21.9 nM. In section 3.4 we concluded that the pH dependent activity of MepA could be another way of how the hydrolases of *E. coli* are regulated. We speculate that the redundancy of the hydrolases arises from differing optimal conditions and substrate specificities. Now we show the interaction between NlpI and MepA correlates with this pH dependency. The shared interactions of MepA and NlpI with PBP7, PBP4 and MepS at pH 7.5 suggests that MepA is also a part of this larger complex of hydrolases. However, when conditions are optimal for MepA activity, i.e. pH 5.0, this facilitates the interaction with NlpI. We observed no effect of NlpI on the activity of MepA at pH 5.0, however we hypothesise that *in vivo* NlpI may have a regulatory role.

Other NlpI interactions

NlpI and PBP1A

We investigated the possibility of NlpI interaction partners which do not possess EPase activity but exist within the multi-enzyme PG-synthesising complex. We firstly tested PBP1A, which shares at least three interaction partners with NlpI; LpoA, PBP4 and PBP7.

We confirmed an *in vitro* interaction using MST with FL-PBP1A and unlabelled NlpI to estimate an apparent K_D of 1470 ± 138 nM. This affinity is significantly weaker than any NlpI interaction partner identified so far. There is also no effect of NlpI on PBP1A activity, alone, or in the presence of LpoA. We have no further data as-of-yet regarding the importance of this interaction but hypothesise that it is yet another way of associating hydrolase activity to PG synthesis during cell elongation.

NlpI and EnvC

Our collaborators from the Typas group identified EnvC as a potential interaction partner of NlpI. We present here the *in vitro* interaction between NlpI and EnvC using a Ni^{2+} bead pull-down assay and MST, which was used to estimate a K_D of 252 ± 47.5 nM. The aberrant cell division phenotypes observed upon deletion of NlpI [228] could indicate a role in regulating amidase activity, which may be facilitated through an interaction with EnvC. Presently, we have no activity data regarding the effect of NlpI on the regulation of amidase activity by EnvC. Future work will investigate direct interactions between NlpI and the amidases AmiA and AmiB, which are regulated by EnvC, as well as AmiC which was also identified as a potential interaction partner by affinity chromatography. We hypothesise that NlpI could be a global regulator of hydrolase activity, regulating EPase activity during elongation and amidase activity during cell division.

NlpI and PBP6B

Using a Ni^{2+} bead pull-down assay we also observed an interaction between NlpI and PBP6B. No activity assays have been undertaken thus far, and the interaction has not been tested by another method. As PBP6B is a monofunctional CPase, it is possible that NlpI may regulate more than just EPase activity. PBP6B has been shown to be upregulated at pH 5.0 in comparison to pH 7.5, and although present and weakly active at pH 7.5, has higher activity at pH 5.0 (Peters *et al,*. 2016. *in press*). MepA may have a similar role for EPase activity at lower pH conditions and NlpI may interact and regulate both in the cell at these conditions.

NlpI has multiple EPase interaction sites

We tested for formation of ternary complexes *in vitro* using modified MST and Ni^{2+} pull-down protocols. These modified protocols could be used to infer whether a protein has one interaction site for multiple proteins, or that the binding of one protein prevents the binding of another. We tested if NlpI possesses multiple EPase interaction sites or is restricted to one interaction partner at a time. We have shown in this work that PBP4 and MepS do not interact by MST and that the bound state for the interaction between NlpI and MepS begins at ~1 µM. Unlabelled NlpI was pre-incubated with an excess of PBP4 and the pre-formed complex was tested for interaction by MST with FL-MepS. The interaction between MepS and NlpI-PBP4 takes place with a much larger thermophoretic movement than that of NlpI alone, indicative

of a larger complex binding to FL-MepS, causing a slower movement along the temperature gradient. Although no interaction was observed between MepS and PBP4 by MST, His-MepS retained native PBP4 in Ni^{2+} bead cross-linking pull-down assays. We hypothesise that the binding of NlpI to PBP4 may cause a conformational change in PBP4 to allow for a stronger interaction with MepS, or that the presence of NlpI strengthens this interaction and facilitates the formation of a trimeric complex. Using the Ni^{2+} bead cross-linking pull-down assay we show that His-MepS is able to retain PBP4 and NlpI separately, as observed previously, but could also retain both proteins simultaneously, complementing the MST data. We can therefore conclude that; MepS can interact with NlpI in the presence of excess PBP4, indicating that MepS and PBP4 do not share the same binding site on NlpI, and that NlpI, MepS and PBP4 can form a ternary complex.

Similarly, we observed that MepS and PBP7 do not interact, which allowed us to challenge the interaction between MepS and NlpI with excess PBP7. Using the same concentration of FL-MepS we see no indication of an interaction with PBP7. After pre-incubation of NlpI with excess PBP7, we still see the interaction between NlpI and MepS, thus inferring that NlpI possesses different interaction sites for MepS and PBP7. In contrast to the experiments using MepS, NlpI and PBP4, there was no cumulative increase in FNorm from FL-MepS upon addition of NlpI pre-incubated with PBP7. This could imply that while NlpI may have different interaction sites for MepS and PBP7, it is unable to interact with both proteins as a trimeric complex and may preferentially bind to FL-MepS, or, that the change in size/charge of FL-MepS upon addition of NlpI bound to PBP7 did not significantly alter the properties of FL-MepS compared to NlpI alone. We also aim to test the interaction of NlpI with EPases at different conditions, which could allow us to determine if NlpI conditionally binds to certain EPases.

Non-interacting proteins

Separate to this work and unpublished, Hamish Yau (Vollmer group) has shown that Slt is capable of interacting with four of the same EPases as NlpI (PBP4, PBP7, MepS and MepM). We show here that there is no direct interaction between NlpI and Slt. We hypothesise that, although we have seen no regulation of EPase activity by Slt, that it may also be a regulator of EPase activity, or localisation. It is possible, in the absence of one of NlpI or Slt, the other takes over as the primary interaction partner. Another model is that these hydrolases and regulators exist as a large complex by which the activity or localisation of these enzymes

could be tailored to the conditions of the cell, or what substrate is available. This could explain the robustness of the hydrolases and the lack of phenotype upon single gene deletions. The lack of interaction observed of NlpI with LpoB, Pal and CpoB, indicates that the hydrolase regulation of NlpI may be coordinated with the elongasome rather than the divisome. However, as discussed, the inferred interactions with the amidases may be evidence of an indirect and uncharacterised association to the divisome.

Final word

In this section we found that NlpI was able to interact with five of the seven known EPases of *E. coli* and differentially alter the activity of at least three (figure 3.52). We believe we have characterised the primary function of NlpI, whose cellular function is still debated, as a regulator of hydrolase activity and/or spatio-temporal localisation. The differential *in vitro* effects of NlpI on EPase activity suggests the ability to coordinate individual hydrolase activity at different stages of cell growth. The identification of the pH dependent interaction of NlpI and MepA is a prime example of this. While the other interaction partners of NlpI have lower activity at lower pH, in situations when the cell is in a low pH environment, NlpI may be able to 'choose' MepA as the primary active EPase. We have not shown conditional activity of the other EPases, but predict that there are conditions at which each will be most efficient at degrading PG, and that, like MepA, NlpI will be able to preferentially interact and regulate activity for each. The Typas group are currently testing the effect of NlpI on EPase activity *in vivo* and the next section details the attempts to phenotypically characterise the role of NlpI using the aforementioned β-lactamase induction assay. Through our collaboration with Tanneke den Blaauwen, University of Amsterdam, we are localising the EPases in the presence and absence of NlpI. In this section we have modified the established MST protocol for the observation of ternary interactions, to provide insight into the ability of one protein to interact with multiple proteins simultaneously. While we have identified no protein that prevents the interaction of another thus far, this assay could be used for the identification of proteins sharing interaction sites. Efforts are underway to study more potential trimeric complexes, particularly by Hamish Yau (Vollmer group). A summary of the interactions identified in this section and section 3.4 is shown in figure 3.52.

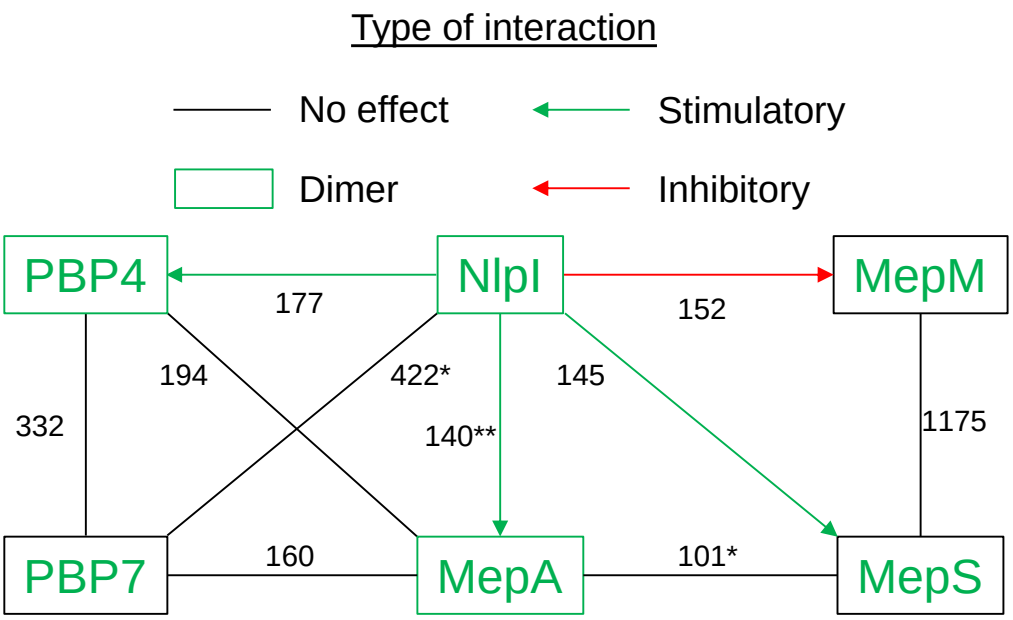

Figure 3.52 Interaction network of NlpI and the endopeptidases
Schematic to show the characterisation of novel interactions between NlpI and the PG hydrolases. K_D values are given in nanomolar. *Dissociation constant calculated using the Hill model as an EC_{50}. **Interaction only occurs at pH 5.0.

3.6 NlpI and the elongasome are required for correct β-lactamase induction

3.6.1 Introduction

The functional redundancy of the PG hydrolases complicates the *in vivo* analysis of protein interactions and activities. However, one of the few phenotypes observed upon a single deletion of PBP4 is the diminished induction of the β-lactamase AmpC in response to the broad-spectrum carbapenem, imipenem [112]. As discussed in section 1.6, AmpC induction in response to antibiotic stress is dependent on the amount of PG turnover products generated by EPases and LTs. We reasoned that proteins interacting with PBP4, and/or involved in the regulation of PBP4 activity, may have similar phenotypes and thus reveal the relevance of the interactions observed *in vitro*. To do so, we adapted the β-lactamase induction assay described in [224] and section 2.6.1 and tested multiple deletion and overexpression strains.

In doing so, we were able to optimise an assay for the future identification and characterisation of proteins involved in bacterial cell wall elongation, PG hydrolysis and PG hydrolysis regulation, and proteins involved either directly or indirectly with LT activity.

The strains in this section were obtained from the Keio collection available in the Vollmer group, or supplied by the Typas and Reddy laboratories. Prior to use in this assay all strains were transformed with the pJP1 plasmid, containing the *ampR/ampC* operon from *E. cloacae,* and subjected to growth curves to ensure a sub-lethal concentration of imipenem would be used (see table 5.2 for the list of strains used, growth curves not shown).

3.6.2 An intact elongasome is required for β-lactamase induction

The first strain tested was that of BW25113Δ*dacB* in comparison to WT BW25113. The method is as described in section 2.6.1.

Sanders *et al* observed a ~50% diminished β-lactamase induction in the absence of PBP4 [112] and we could reproduce this result (figure 3.53). Cells lacking PBP4 show an average fold difference over the control of 4.9 compared to a fold difference of 12.7 for WT. With the assay working as expected, we continued by testing the cells lacking the interaction partners of PBP4.

The first PBP4 interaction partner identified in this work was LpoA. In strains lacking LpoA, induction is as similarly diminished as cells lacking PBP4, with an average fold difference of 4.2 (figure 3.53). We continued by testing a strain lacking PBP1A and observed a complete inhibition in β-lactamase induction in response to imipenem (figure 3.53). The effect was

much more dramatic than in a deletion strain of PBP4. Cells lacking PBP1A had an average fold difference of 1.2. These data infer that the role of PBP1A in the induction of β-lactamase in response to imipenem is more important for the cell than that of PBP4. We speculated that a degenerate elongasome may actually be responsible for the impaired induction observed. A dysregulation of PG synthesis and hydrolysis through deletions in the core PG synthesis complex (PBP1A and LpoA) and/or PBP4 may alter the levels of the intracellular turnover products required for induction.

To test whether this effect is exclusive to the elongasome we performed the assay using a strain lacking PBP1B. We observed no significant changes in β-lactamase induction. A fold difference over the control of 9.9 was calculated (figure 3.53). In comparison to strains lacking components of the elongasome, cells were significantly less affected.

3.6.3 NlpI is required for β-lactamase induction

In the last section we characterised NlpI as an interaction partner of at least five EPases and a regulator of activity of at least three. As discussed, the turnover products of EPase activity are crucial for correct AmpC induction. We sought to use this β-lactamase assay to observe the intrinsic connection of NlpI and EPase activity and highlight the *in vivo* relevance of NlpI.

Prior to use in the β-lactamase induction assay, growth curves of each strain were taken at varying concentrations of imipenem. This is to ensure the concentration of imipenem used in the assay was sub-lethal. Figure 3.41 shows the growth curves of cells lacking NlpI. We observed that cells are more susceptible to imipenem, with growth showing a significant difference to WT after a 1 h exposure to 1 μg/ml of imipenem (figure 5.41). We showed that this growth impairment was due to an inability to induce an AmpC response (figure 3.53). Cells lacking NlpI produced a fold difference of 1.5. Conversely, in cells containing the overexpression plasmid pCL1920-NlpI, the average fold difference over the control was 24.2, 3.5 times that of WT cells containing the empty overexpression plasmid (BW27783-pCL1920) (figure 3.53). Using single deletions in the genes encoding two of the other NlpI interaction partners, MepS and MepM, we showed there to be no significant change in β-lactamase induction (figure 3.53). The tail-specific protease, Prc, cleaves the 12 C-terminal residues of NlpI and has been hypothesised to ‘activate’ NlpI [248]. However, a deletion or overexpression of Prc also had no effect on β-lactamase induction (figure 3.53).

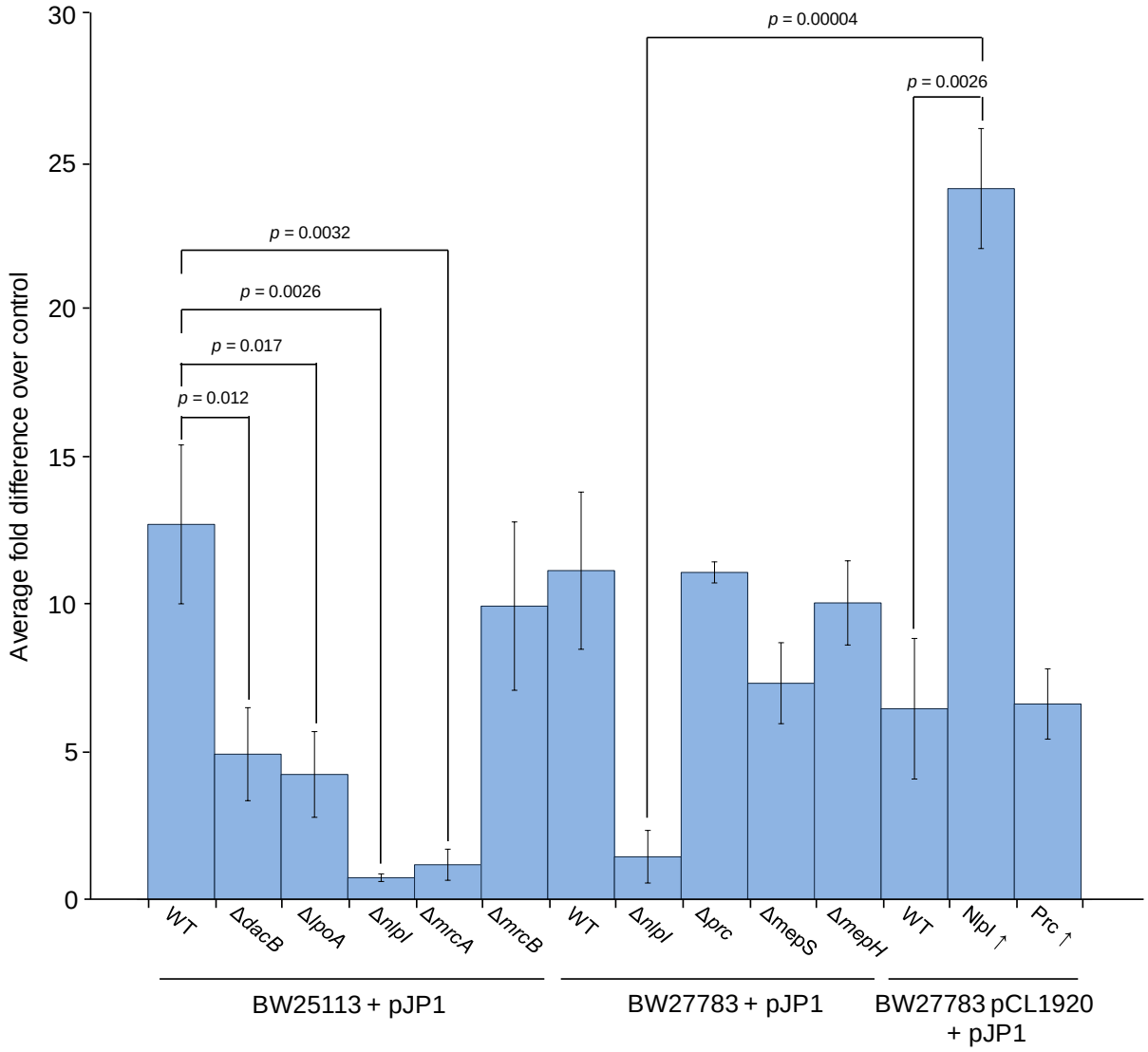

Figure 3.53 β-lactamase induction assay in response to imipenem

BW25113 strains were obtained from the Vollmer laboratory Keio collection.BW27783 strains were provided by the Reddy laboratory. The pCL1920 plasmid is an IPTG dependent overexpression plasmid. All strains were transformed with the pJP1 plasmid carrying the *ampR/ampC* operon from *E. cloacae*. Cells were exposed to sub-lethal concentrations (1 µg/ml) of imipenem. Cells were lysed by osmotic shock and β-lactamase induction measured using the chromogenic β-lactam nitrocefin. Hydrolysis of nitrocefin was measured using a spectrophotometer (555 nm) and the amount of nitrocefin hydrolysed per min per milligram of protein in the lysate was measured and compared to that of a control sample not exposed to imipenem. The purified β-lactamase Vim4, from *P. aeruginosa*, was used as a positive control. The fold difference was calculated and plotted. For overexpression strains (BW27783-pCL1920) 1 mM IPTG was used during the initial growth period.

3.6.4 Conclusions and discussion

We have adapted and optimised an *in vivo* assay, initially with the intention of providing relevance to the interaction partners of PBP4 characterised in this work. We continued by highlighting a potential secondary role of the elongasome as crucial for correct β-lactamase induction. We also provide *in vivo* relevance to the role of NlpI as a global regulator of PG hydrolase activity.

An intact elongasome is required for correct β-lactamase induction

We initially confirmed the assay as working optimally using a strain lacking PBP4 to replicate the data presented in [112], who showed cells lacking PBP4 were ~50% impaired in their ability to induce β-lactamase in response to imipenem. We proceeded by testing the interaction partners of PBP4 and discovered that cells lacking LpoA had a similarly poor induction response to that of cells lacking PBP4, with both mutant strains having ~60% impaired AmpC induction in comparison to WT. Contrary to the *in vitro* data, this indicates that LpoA may have a more important regulatory role when interacting with PBP4 in the cell. These data suggest that without LpoA regulating the activity of PBP4 the amount of turnover products is altered leading to the diminished induction observed. It is possible that the conditions used *in vitro* are not optimal to observe such an effect, for example we did not take into account the effect of periplasmic protein crowding.

However, when we analysed the induction response in cells lacking PBP1A we found a much more significant reduction in AmpC induction than observed in *dacB*$^{-}$ cells. We hypothesise therefore that PBP1A may play a more important role than PBP4 in β-lactamase induction in the cell.

This could be due to the strong interaction observed between PBP1A and PBP7 as well as PBP4, a deletion in PBP1A may lead to the unregulated activity of both PBP7 and PBP4 causing the larger effect observed. However, when Sanders *et al* published the data implicating PBP4 in the induction of β-lactamase, they showed there was no effect on hydrolysis of nitrocefin in strains lacking PBP7 and no cumulative change when both PBP4 and PBP7 were absent [112]. Of the mutant strains tested we found diminished induction in those associated with the elongasome; PBP1A, LpoA and PBP4. If β-lactamase induction relies on the amount of PG turnover products from EPase and LT activity, then maintaining the balance between PG hydrolysis and PG synthesis could be crucial to eliciting a successful response to β-lactam stress.

The divisome has recently been shown to have a secondary role in the coordination of membrane constriction through shared interactions with the Tol/Pal system [91]. We hypothesise β-lactamase induction in response to antibiotic stress may be a secondary role of the elongasome. As such, we tested the effect of a deletion in PBP1B which showed only a minor decrease in β-lactamase induction. We are continuing tests to confirm this hypothesis and, if successful, this assay could be modified to screen a large number of strains for the identification of novel members of the elongasome.

NlpI is required for correct β-lactamase induction

We show here that an *nlpI* mutant becomes susceptible to imipenem through an inability to induce a β-lactamase response. We have confirmed in this work the interactions of at least five EPases with NlpI. We hypothesise that the phenotype observed here is due to the unregulated activity of these EPases in the absence of NlpI. We showed that a strain overexpressing NlpI has a highly stimulated induction response, highlighting the role of NlpI in regulating EPase, and potentially LT, activity.

As previously mentioned, Hamish Yau (Vollmer group) has identified interactions between Slt and four of the same EPases that interact with NlpI (PBP4, PBP7, MepS and MepM). We hypothesise that in the absence of NlpI, not only is the activity of the EPases unregulated but, in addition, the activity of the other EPase interaction partners is also affected, for example Slt. We are yet to observe any regulatory effect of Slt on the EPases *in vitro*, or vice versa, and there is no direct interaction between NlpI and Slt. However, in the absence of NlpI the affinity of interaction between the EPases and the LTs could be altered, thus leading to more or less regulation of activity of both sets of enzymes. Thus, directly through the regulation of EPase activity, and indirectly through the activity of the LTs, a single deletion in NlpI could cause the phenotype presented here.

Final word

The data presented in this section described the characterisation of the *in vivo* relevance of some of the interactions identified in this project. In doing so we optimised a β-lactamase induction assay which highlighted the connections between the PG synthases and the PG hydrolases and potentially discovered a novel secondary function of the elongasome. We also

utilised this assay to show the importance of NlpI in the regulation of hydrolytic turnover products in a cellular environment.

Presently, we are designing a large scale screen of the Keio collection using a modified version of the plasmid used in this assay. We hypothesise that we will be able to use this assay to discover and characterise proteins involved with PG turnover and putative members of the elongasome, which could lead to the identification of novel antibiotic targets.

4 Discussion

The regulation of peptidoglycan hydrolysis in Escherichia coli

The data presented in this work significantly enhances our knowledge of how the potentially autolytic PG hydrolases are coordinated and controlled in *E. coli* and presumably other Gram-negative organisms. As many of the members of the PG-synthesising/hydrolysing proteins investigated in this work, including NlpI, are conserved among other Gram-negative organisms it is likely that some of the mechanisms can be transferred to other related species. However, as exemplified by the comparison between *E. coli* and *H. influenzae* LpoA, some of the proteins involved may have alternative primary roles.

Using combinations of state of the art *in vitro* and *in vivo* interaction assays we present the interactions of over 10 proteins participating in PG synthesis and hydrolysis as well as other cell envelope proteins. The methods of coordinating hydrolase activity in *E. coli*, discovered or elaborated upon in this project, can be summarised into four categories, which will be discussed and summarised below;

1. An interaction network associated to PG synthesis.
2. Conditional activity of hydrolases.
3. Hydrolase domains crucial for activity.
4. Regulation of activity by lipoproteins.

Hydrolase interaction network associated to PG synthesis

The high resolution structure of the N-terminal domain of the OM-anchored lipoprotein, LpoA was determined by NMR spectroscopy. In combination with SAXS and AUC of the full length protein, and modelling of the C-terminal domain based on the crystal structure of LpoA from *H. influenzae,* we present a full length structural model. It is predicted that LpoA is long enough to reach through pores in the PG layer to interact with the ODD domain of PBP1A. In comparison to *H. influenzae*, *E. coli* LpoA possesses C-terminal flexible 'wing'-like domains preventing structure determination by NMR spectroscopy. As $LpoA^{C}$ is sufficient for interaction and stimulation of PBP1A activity our hypothesis was that these domains could be interaction sites. However, we showed that these are not crucial for the *in vivo* interaction with PBP1A. Purification of LpoA versions lacking these domains have been unsuccessful which we hypothesise is due to intrinsic instability. Attempts to optimise the purification of these constructs are planned and we aim to use them to study the interaction and stimulation of PBP1A, and other LpoA interaction partners.

The ‘wing’-like domains of LpoA from *E. coli* are not present in *H. influenzae*. LpoA from both organisms and LpoB from *E. coli*, were tested for effects on the activity of PBP1A and PBP1B from both organisms. PBP1A from *H. influenzae* was as active as *E. coli* PBP1A when stimulated by its cognate LpoA. In contrast, the activity of PBP1B from *H. influenzae* has a very low level of TPase activity, alone or in the presence of any Lpo protein tested. There is no PBP stimulation by any non-cognate Lpo protein tested. The small size and slow generation time of *H. influenzae* in comparison to *E. coli* may explain why there is no requirement for stimulation and the low cross-linking activity of PBP1B. As LpoA is essential in *H. influenzae*, we predict a different primary role of LpoA in each organism. A CpoB-related function of *E. coli* LpoA has been described [91]. It is suggested that there is a partial redundancy between CpoB and LpoA in the tethering of the Tol-Pal system to the PG synthesis machinery for coordination with OM constriction during cell division. As PBP1A in *H. influenzae* is already as active as LpoA-stimulated PBP1A in *E. coli*, we hypothesise that the primary role of *H. influenzae* LpoA is this CpoB-related function, however, further experiments are required to address this hypothesis.

Continuing in *E. coli*, the *in vitro* interaction between LpoA and PBP1A was thoroughly investigated by SPR and MST. Using MST, a K_D of 852 ± 146 nM was determined. This affinity closely correlates with that of the interaction between LpoB and PBP1B which has a K_D of 810 ± 80 nM [75].

The NMR spectra of $LpoA^N$ revealed an elongated shape comprised exclusively of α-helices organised into canonical TPR motifs, between which are conserved residues. It was hypothesised that this domain could facilitate novel LpoA interaction partners.

Through a proteomics-based search for these proteins using $LpoA^N$ we discovered the functional relationship between LpoA and PBP4. The interaction sites between the two proteins likely include domain 1 and/or domain 2 of PBP4, and while both domains of LpoA can interact with PBP4, it is likely that $LpoA^C$ is the primary PBP4 interaction site. A direct *in vitro* and *in vivo* interaction between PBP4 and PBP1A was also discovered. It is $LpoA^C$ that interacts with PBP1A, and as stated above, we predict $LpoA^C$ is also primarily responsible for the interaction with PBP4. This could indicate that the three proteins interact as a trimeric complex. LpoA moderately inhibits the activity of PBP4 and stimulates the activity of PBP1A but there was no effect of PBP4 on PBP1A activity, or vice versa. It was concluded that these interactions may take place to recruit PBP4 to sites of ongoing PG synthesis by the core synthesis complex during elongation. Localisation studies will be required to test this hypothesis and whether this recruitment of PBP4 is exclusive to the elongation machinery.

PBP7 was also discovered to have direct interactions with LpoA, PBP1A, and PBP4. Again, we hypothesise that PBP7 is recruited as a space-making enzyme to facilitate the insertion of nascent PG, and whose activity may be coordinated with that of PBP4.

A direct interaction between two of the three recently discovered EPases, MepS and MepM was also observed, as was the interaction of MepS and PBP1A. No interactions between PBP4 and PBP7 with MepS or MepM have been observed and we hypothesise that MepS and MepM are recruited to the elongasome as a separate hydrolase complex to PBP7 and PBP4. Direct interactions between MepA and PBP4, PBP7 and MepS were also identified.

We have identified multiple direct interactions traversing four different groups of EPases; the Class C PBPs, PBP4 (also possessing CPase activity) and PBP7; the NlpC/P60 superfamily, MepS; the M23 LytM metallopeptidases, MepM; and the LAS family of metallopeptidases, MepA, with direct or indirect associations to the PG synthesis machinery. The data presented in this work suggests that the PG hydrolases of *E. coli* exist as large protein complexes of enzymes belonging to different protein families. We speculate that the hydrolases involved possess different substrate specificities, and different optimal conditions. The identification of the pH dependent activity of MepA supports this hypothesis and will be discussed below. To have a set of coordinated enzymes with the same cleavage site, but conditional activities and different substrate specificities, would provide the cell with a large degree of hydrolytic functional redundancy. This could explain why no single deletion of the *E. coli* hydrolases has a strong phenotype. The direct or indirect interactions of multiple hydrolases, between each other and the PG synthesis machinery, highlights a flexible yet well controlled PG hydrolase system for the safe insertion of nascent PG into the pre-existing layer.

Conditional activity of hydrolases

As alluded to above, conditional PG hydrolase activity is particularly highlighted in the case of MepA. We show that MepA is inactive on intact sacculi at pH 7.5, unlike the other EPases investigated in this work, whereas at pH 5.0, MepA is active. It was shown that this is due to an inability to bind to intact sacculi at pH 7.5.

It is speculated that this pH dependent hydrolase activity could be present in other protein families possessing hydrolase activity, for example the six redundant DD-CPases of *E. coli*. The monofunctional CPase PBP6B has recently been shown to be expressed in greater amounts at pH 5.0 than at pH 7.5 and to show more activity at pH 5.0 (Peters *et al.* 2016. *in press*). Conditional specificity has also been observed for the hydrolases possessing LT

activity, with MltA expressing optimal activity at pH 4-4.5 and at 30°C [249]. We therefore hypothesise that hydrolases across different families may have conditional specificity to allow efficient hydrolase activity at many different conditions.

Hydrolase domains crucial for activity

The amidases AmiB and AmiC are known to possess an α-helix which occludes the active site which prevents activity. Upon interaction with their cognate activators EnvC and NlpD, respectively, this α-helix is removed to allow activity. This is potentially a method of controlling aberrant hydrolase activity at sites other than at cell division.

Similarly, the biochemical investigation into the structure and activities of PBP4 identified the globular, non-catalytic domain 3 as crucial for activity, but not for substrate binding. Two possible explanations are that domain 3 acts to correctly position substrate for degradation, or, that without domain 3, PBP4 dimerises in such a way that substrate cannot be processed once bound. Interestingly, while domain 3 is not an interaction site for LpoA or PBP1A, which have little to no effect on activity, it is crucial for the interaction with NlpI, which stimulates activity *in vitro*. It is speculated that conformational changes in domain 3 may reveal or conceal more of the active site of PBP4 thus modulating activity. This, and a hypothesised complementary modulation of PBP4 activity by $LpoA^{N}$, is discussed in more detail below.

Regulation of activity by lipoproteins

There are currently two regulators of hydrolase activity in *E. coli* described in appreciable detail; EnvC and NlpD, the regulators of amidase activity during daughter cell separation. *E. coli* possesses ~30 hydrolases that have no known regulators of activity. Characterised in this work is the identification of NlpI, an OM-anchored lipoprotein, as a novel regulator of EPases in *E. coli*.

NlpI interacts with five of the seven known EPases of *E. coli*; PBP4, PBP7, MepS, MepM, and MepA, themselves linked by direct interactions with each other and the core PG synthesis complex during elongation. NlpI differentially affects the activity of PBP4, MepS and MepM *in vitro*. It was shown that NlpI possesses different binding sites for at least MepS, PBP4 and PBP7, being able to interact with each in the presence of excess concentrations of another, for example NlpI can still interact with MepS in the presence of PBP4. NlpI, MepS and PBP4 were also shown to form a ternary complex *in vitro*. It will be interesting to test if NlpI

preferentially binds to certain EPases at different conditions, for example the pH dependent interaction with MepA.

The first NlpI interaction partner confirmed was PBP4, which we continued to investigate by showing that it is domain 3 of PBP4 that is the main NlpI interaction site. As NlpI stimulates PBP4 activity *in vitro,* and domain 3 is essential for activity, it is hypothesised that the interaction causes a conformational change in domain 3 to alter its activity. In comparison to the interaction between PBP4 and LpoA where it is likely that domain 1 and /or 2 is the main LpoA interaction site. However, a potential modulatory role of $LpoA^N$ was identified, complementing that of NlpI; in the absence of domain 3, the K_D of the interaction between $LpoA^N$ and PBP4 decreases more than 50 fold. We speculate that these interactions could represent a putative modulation of PBP4 activity. NlpI may interact with domain 3 of PBP4 to stimulate activity by inducing a conformational change in domain 3, causing the affinity for $LpoA^N$ to increase in order to exert an inhibitory effect. This could be a novel method of modulating the potentially autolytic activity of PBP4 in response to the changing conditions of the cell. Using a modified version of the MST assay it was shown that the presence of excess NlpI does not prevent the interaction of PBP4 with PBP1A or LpoA. These data support the hypothesis that NlpI interacts with PBP4 primarily through domain 3 of PBP4 and that PBP1A/LpoA interact with PBP4 through domain 1 and/or 2.

Cells transformed with pJP1 and lacking NlpI are incapable of inducing a β-lactamase response when exposed to the antibiotic imipenem. These data support the *in vivo* regulation of EPase activity by NlpI, as well as potentially LT activity. More *in vivo* experiments are currently underway to observe the regulation of EPase activity by NlpI in the cellular environment. Localisation assays of the EPases in the presence and absence of NlpI are also underway in order to observe any spatio-temporal role of NlpI. As discussed above, we hypothesise that the hydrolases investigated in this work exist as a larger complex which can be recruited to sites of ongoing PG synthesis. We hypothesise that NlpI also exists as part of this complex and can differentially modulate the activity of the hydrolases when required. An example presented in this work is the pH dependent interaction of NlpI and MepA, whose activity is also pH dependent.

Differences in substrate specificity, and conditional optimal activity across the multiple hydrolase families present in this multi-enzyme complex, could provide the cell with the robustness required for growth at different conditions, and explain the high redundancy of the PG hydrolases. Some may be tailored to the digestion of intact sacculi, and some to the digestion of muropeptides, this would provide the cell with the tools required for the efficient

and complete breakdown and turnover of PG during growth. Others may be pH dependent, for example MepA, or more active at higher NaCl conditions. The role of NlpI in this complex may be to coordinate which hydrolases will be more or less active at which time. A schematic of all the interactions characterised in this work, as well as the effects on activity of these interactions, is summarised in figure 4.1 and table 4.1.

Summary

Höltje proposed that for the successful and safe enlargement of the bacterial cell wall in rod-shaped bacteria, PG synthases and hydrolases would be active within multi-enzyme complexes [57]. Since then, the identification of protein complexes specialised for the elongation and division phases of bacterial growth have been characterised [4,238]. More recently, prokaryotic cytoskeletal elements have been shown to spatio-temporally localise these complexes from the cytoplasm [23,238]. Later, it was discovered that PG synthesis is also regulated by OM-anchored lipoproteins; LpoA and LpoB [25,26]. While the mechanisms of PG synthesis have been studied in recent years, the molecular interplay with the PG hydrolases and how this activity is regulated remains poorly understood.

In this work we continued to dissect the known interaction between the major PG synthase during cell elongation, PBP1A and the OM-anchored regulator LpoA, identifying novel wing-like domains of LpoA through the high resolution NMR structure of $LpoA^N$ and subsequent modelling of the full length protein, drawing comparisons with LpoA from *H. influenzae*.

The search for novel LpoA interaction partners lead to the discovery of a potential trimeric complex consisting of a PG synthase (PBP1A) a PG hydrolase (PBP4) and a lipoprotein regulator (LpoA). This formed the basis of the search and discovery of a large number of direct and novel interactions between the PG synthases and hydrolases.

Four methods of controlling PG hydrolases in *E. coli* were concluded in this work; the identification of a network of interactions between the PG hydrolases and synthases providing support for the hypothesised multi-enzyme complexes for PG growth; pH dependent hydrolase activity, inferring conditional activity of PG hydrolases at different stages of the cell cycle; non-catalytic domains crucial for activity, but not for substrate binding, indicating intrinsic feedback within individual proteins; and the identification of a global regulator of EPase activity, NlpI.

Final word

The growth of the PG layer remains one of the most promising sources of novel antibiotic targets. This work provides major insights into the understanding of the regulation of peptidoglycan hydrolysis and its coordination with PG synthesis in *E. coli*. Improving the understanding of essential prokaryotic processes is paramount for the future identification of novel antibiotics, highlighted by the increasing prevalence of antibiotic resistant bacteria.

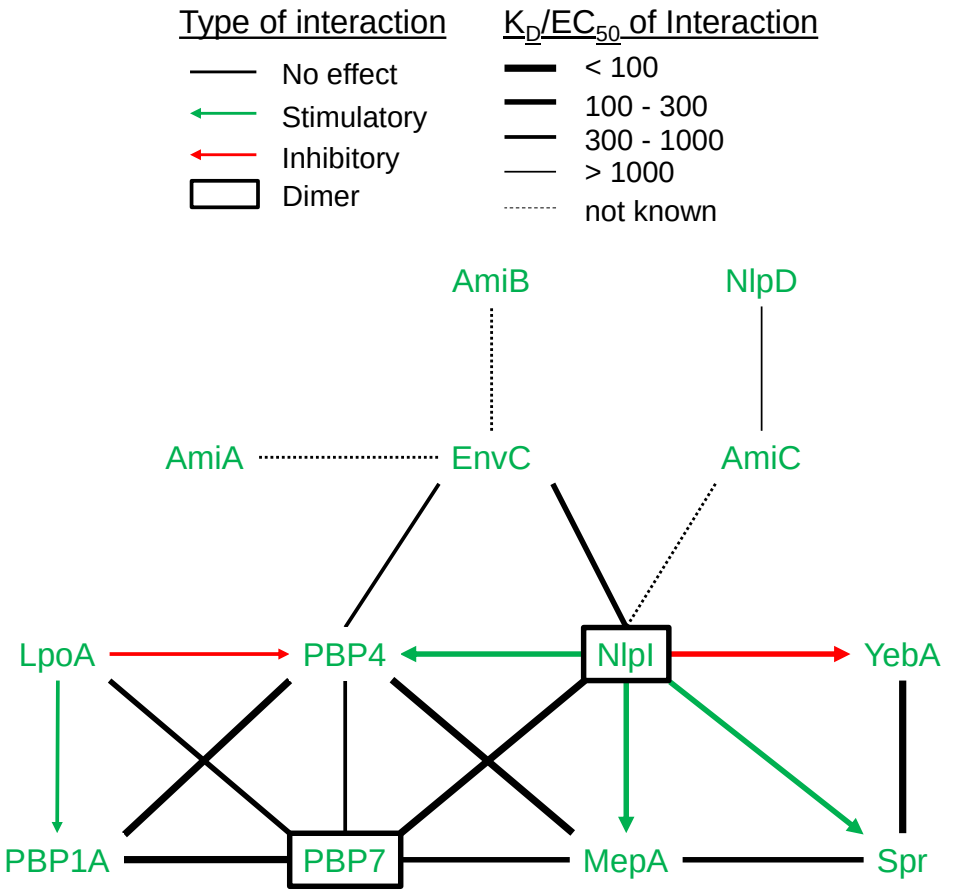

Figure 4.1 Network of interactions between the PG synthases, hydrolases and regulators

Summary of interactions and their affinities identified in this work, and by the Typas group which have not yet been tested *in vitro*. Interaction and K_D of NlpD and AmiC shown by [159].

Table 4.1 Project interaction summary

	PBP4	PBP4 ΔD3	LpoA	PBP1A	NlpI	NlpI ΔC11	Spr	PBP7	YebA	MepA	Slt	Pal	CpoB	EnvC	LpoB	PBP5	PBP6B
PBP4	M/A		M/P/S/C	M/P/S/C	M/P/S/A	P	M/P	M/P	M/P	M/P	M/P		P	M/P	P/C		
PBP4 ΔD3			M	M	M/P					M							
LpoA				M/S/C	M/P		M/P	M	P	M	M/P		P		P	P	
PBP1A					M		M	M/P									
NlpI					M/A		M/P	M/P/A	M/P	M/P	M/P/A	P	P	M/P	P	P	P
NlpI ΔC11							M/P										
Spr								M/P	M	M/P	M/P			M			
PBP7								A	M	M/P	M/P				M		
YebA										M	M/P						
MepA										M	M/P						
Slt											A			P	P		
Pal																	
CpoB																	
EnvC																	
LpoB																	
PBP5																	
PBP6B																	

	Positive interaction
	Contradictory results/needs repeating
	Negative interaction
	Not tested

M	Microscale thermophoresis
P	Ni-bead pull -downs
S	Surface Plasmon Resonance
A	Analytical Ultracentrifugation
C	*In vivo* co-immunoprecipitation

5 Appendix

5.1 Antibodies

Table 5.1 List of antibodies used in this project

Antibody	Working dilution	Source
α-LpoA	1 in 5000	Manuel Banzhaf[1]
α-PBP1A	1 in 5000	Manuel Banzhaf[1]
α-PBP1B	1 in 5000	Ute Bertsche[1]
α-PBP4	1 in 2000	This work
α-NlpI	1 in 5000	This work
α-MepA	1 in 5000	This work
α-MepS	1 in 2000	This work
α-MepM	1 in 5000	Astrid Schwaiger[1]
α-PBP7	1 in 5000	Hamish Yau[1]
Goat α-rabbit-HRP conjugated	1 in 10000	Sigma
TrueBlot™ α-rabbit	1 in 2000	eBioscience/Rockford

[1]Newcastle University, Vollmer group

5.2 Plasmids

Table 5.2 List of plasmids used in this project

Plasmid	Strain(s)	Resistance cassette	Remarks	Source
pET28-His-LpoA(sol)Δ1-27	BL21(DE3) DH5α	Kan	• N-terminal His-tag • Purification of full length His-LpoA(sol)	Katrin Beilhartz
pET28-His-LpoA^{N}	BL21(DE3) DH5α	Kan	• N-terminal His-tag • Purification of His-LpoA^{N}	Katrin Beilhartz
pET28-His-LpoA^{C}	BL21(DE3) DH5α	Kan	• N-terminal His-tag • Purification of His-LpoA^{C}	Katrin Beilhartz
pET28-His-LpoA (*H. influenzae*)	BL21(DE3) DH5α	Kan	• N-terminal His-tag • Purification of full length His-LpoA from *H. influenzae*	Manuel Banzhaf

pET28-His-LpoB(sol)Δ1-20	BL21(DE3) DH5α	Kan	• N-terminal His-tag • Purification of full length His-LpoB(sol)	[31]
pTK1A-His	MC1061	Kan	• N-terminal His-tag • Purification of full length His-PBP1A	Sylvia Liebscher
pET28-His-PBP1A (*H. influenzae*)	BL21(DE3) DH5α	Kan	• N-terminal His-tag • Purification of full length His-PBP1A from *H. influenzae*	Manuel Banzhaf
pDML924	BL21(DE3) DH5α	Kan	• N-terminal His-tag • Purification of full length His-PBP1B	[251]
pET28-His-PBP1B (*H. influenzae*)	BL21(DE3) DH5α	Kan	• N-terminal His-tag • Purification of full length His-PBP1A from *H. influenzae*	Manuel Banzhaf
pQE30-His-ODD	MC1061	Kan	• N-terminal His-tag • Purification of His-ODD of PBP1A	Athanasios Typas
pET21b-PBP4Δ1-60	BL21(DE3) DH5α	Amp	• Native • Purification of native PBP4	Manuel Pazos
pET21b-His-PBP4 Δ1-60	BL21(DE3) DH5α	Amp	• N-terminal His-tag • Purification of His- PBP4	Manuel Pazos
pET21b-PBP4 S62A Δ1-60	BL21(DE3) DH5α	Amp	• Native • Purification of native PBP4 active site mutant	Manuel Pazos
pBAD18-His-PBP4ΔD3	BL21(DE3) DH5α	Amp	• N-terminal His-tag • Purification of His- PBP4 lacking domain 3	Ann-Kristin Hov
pET21b-His-PBP4S62AΔ1-60	BL21(DE3) DH5α	Amp	• N-terminal His-tag • Purification of His-PBP4 active site mutant	Manuel Pazos

pET28-His-PBP7	BL21(DE3) DH5α	Kan	• N-terminal His-tag • Purification of His- PBP7	Ann-Kristin Hov
pET28-His-PBP7 S67A	BL21(DE3) DH5α	Kan	• N-terminal His-tag • Purification of His- PBP7 active site mutant	Manuel Banzhaf
pET28-His-EnvC	BL21(DE3) DH5α	Kan	• N-terminal His-tag • Purification of His- EnvC	Manuel Banzhaf
pJFK-MepA	MC1061	Kan	• Native • Purification of native MepA	Vollmer group strain collection
pET28-His-MepM	BL21(DE3) DH5α	Kan	• N-terminal His-tag • Purification of His- MepM	Manjula Reddy
pET28-His-MepM H314A	BL21(DE3) DH5α	Kan	• N-terminal His-tag • Purification of His- MepM active site mutant	Manjula Reddy
pET28-His-MepS	BL21(DE3) DH5α	Kan	• N-terminal His-tag • Purification of His- MepS	Manjula Reddy
pET28-His-MepS C68A	BL21(DE3) DH5α	Kan	• N-terminal His-tag • Purification of His- MepS active site mutant	Manjula Reddy
pCP20	DH5α	Cam/Amp	• Removal of FRT-flanked Kan resistance cassette in *E. coli* via yeast Flp recombinase	[234]
pJP1	MC1061	Kan	• a*mpR*/a*mpC* operon from E. cloacae	Vollmer group strain collection

5.3 Materials

5.3.1 Chemicals

30% Acrylamide (Rotipherese)	Roth
Acetic acid	Sigma
Agar	Fluka
Ammonium Peroxodisulphate (APS)	Serva
Amplex Red	Sigma
Bromphenol blue	Sigma
Bovine Serum Albumin	Pierce
Calcium Chloride	Sigma
Casein	VWR
Chloroform	Fisher
CNBr-activated sepharose	GE Healthcare
Coomassie Brilliant Blue R-250	Roth
D-amino acid oxidase	Sigma
DMSO	Sigma
DTSSP	Pierce/Thermo Scientific
DTT	Sigma
EDTA	Sigma
EGTA	Sigma
Ethanol	Fisher
Glycerol	Sigma
Glucose	Sigma
Glycine	Sigma
HEPES	VWR
Horseradish peroxidase	Sigma
Hydrochloric acid	Sigma
Imidazole	Sigma
Isopropanol	Sigma
Magnesium chloride	VWR
Lennox LB	Fisher Scientific

β-mercaptoethanol	Sigma
Methanol	Fisher
Methylene blue	Sigma
MilliQ H_2O	Millipore dispenser
Phosphoric acid	Sigma
Protease inhibitor cocktail (P8465)	Sigma
Rotiphorese	Roth
Rubidium chloride	Sigma
Sodium acetate	Sigma
Sodium azide	Merck
Sodium borate	Sigma
Sodium borohydride	Sigma
Sodium chloride	VWR
Sodium dihydrogenphosphate	VWR
di-Sodium orthophosphate	VWR
Sodium dodecyl sulphate	Melford
Sodium hydroxide	Sigma
Sodium phosphate	Sigma
TEMED	Sigma
Thrombin	Novagen
Triton X-100	Roche
Trizma™ base (Tris)	Sigma
Tryptone	VWR
Tween 20	Serva
Yeast extract	Deutshe Hefewerke

5.3.2 Antibiotics

Ampicillin	Sigma
Aztreonam	Sigma
Bocillin FL	Molecular probes
Chloramphenicol	Sigma
Imipenem monophosphate	Santa Cruz Biotechnology
Kanamycin	Sigma
Nitrocefin	Sigma
Streptomycin	Hoescht

5.3.3 Enzymes for PG analysis and assays

α-amylase (*Bacillus subtilis*)	Fluka
Cellosyl (*Streptomyces coelicolor*)	Hoescht
DNase (Bovine pancreatic)	Sigma
Pronase E (*Streptomyces grisens*)	Boehringer
Vim4 β-lactamase (*Pseudomonas aeruginosa*)	Adeline Derouaux

5.3.4 Molecular weight markers

PageRuler^{TM} prestained marker	Thermo Scientific
Spectra^{TM} high range marker	Thermo Scientific

5.3.5 Kits

Monolith protein labelling kit (red-malaimide)	Nanotemper
Monolith protein labelling kit (red-NHS)	Nanotemper
Pierce BCA protein assay kit	Thermo Scientific
ProteON^{TM} HP general amine coupling kit	Biorad
Genelute^{TM} HP plasmid midi-prep kit	Sigma
Zinc staining kit	BioRad

5.3.6 Other materials

Bioscale^{TM} Mini-CHT^{TM} hydroxyapatite cartridge (5 ml)	BioRad
Chemiluminescence (ECL) reagents	GE Healthcare
Dialysis cassettes MWc.o 6-8 kDa	Novagen
Dialysis tubing MWc.o 6-8 kDa	Spectrum labs
[^{14}C]-Glc*N*Ac lipid II	Eefjan Breukink
Dansyl-lipid II	Eefjan Breukink, Jules Phillipe
FloScint III liquid scintilant	Perkin Elmer
HisTrap HP (5 ml)	GE healthcare
HiTrap Q HP (5 ml)	GE healthcare
HiTrap SP HP (5 ml)	GE healthcare
Ni^{2+}-NTA superflow beads	QIAGEN
Nitrocellulose membrane	BioRad
ProteON^{TM} GLC sensorchip	BioRad
Protein G-coupled agarose	Pierce/Thermo Scientific
Superdex75 HiLoad 16/60	GE healthcare
Superdex75 10/300 GL	GE healthcare
Superdex200 HiLoad 16/60	GE healthcare
Superdex200 10/300 GL	GE healthcare
VivaSpin 6 columns (MWc.o 5 kDa)	Sartorius Stedim

5.3.7 *E. coli* strains

Table 5.3 List of *E. coli* strains used in this project

Strain	Property	Source
MC1061	Laboratory strain	[252]
BW25113	Keio laboratory strain	[239,240]
BL21(DE3)	Expression strain F- *ompT, dc hsdS* (rB- mB-) *gal* (λDE3	Novagen
XL1-Blue	Expression strain *recA1, endA1m gyrA96, thi-1, hsdR17, supE44, relA1, lac*	Stratagene
DH5α	Non-expression strain *huA2, lavU169, phoA, glnV44, φ80*	Invitrogen
BW25113Δ*dacB*	*dacB* deletion strain	[239,240]
BW25113Δ*lpoA*	*lpoA* deletion strain	[239,240]
CAG70778	BW25113. LpoA lacking wing 1 (Δ294-351)	Andrew Gray
CAG70779	BW25113. LpoA lacking wing 2 (Δ501-523)	Andrew Gray
CAG70780	BW25113. LpoA lacking wing 1 and wing 2 (Δ294-351 and Δ501-523)	Andrew Gray
CAG70169	BW25113. LpoA lacking TPR domain (Δ58-252)	Andrew Gray
CAG70777	BW25113. LpoA lacking the C-terminal domain (Δ257-679)	Andrew Gray
BW25113Δ*mrcA*	*mrcA* deletion strain	[239,240]
BW25113Δ*mrcB*	*mrcB* deletion strain	[239,240]
BW25113Δ*dacB*	*dacB* deletion strain	[239,240]
BW25113Δ*nlpI*	*nlpI* deletion strain	[239,240]
BW27783	Laboratory strain	Manjula Reddy
BW27783Δ*nlpI*	*nlpI* deletion strain	Manjula Reddy
BW27783Δ*prc*	*prc* deletion strain	Manjula Reddy
BW27783Δ*mepS*	*mepS* deletion strain	Manjula Reddy
BW27783Δ*mepM*	*mepM* deletion strain	Manjula Reddy

BW27783 pCL1920	Laboratory overexpression strain	Manjula Reddy
BW27783 pCL1920 NlpI	*nlpI* overexpression strain	Manjula Reddy
BW27783 pCL1920 Prc	*prc* overexpression strain	Manjula Reddy
BW25113 pJP1	Keio laboratory strain containing *ampR/ampC* of *E. cloacae*	This work
BW25113Δ*dacB* pJP1	*dacB* deletion strain containing *ampR/ampC* of *E. cloacae*	This work
BW25113Δ*lpoA* pJP1	*lpoA* deletion strain containing *ampR/ampC* of *E. cloacae*	This work
BW25113Δ*mrcA* pJP1	*mrcA* deletion strain containing *ampR/ampC* of *E. cloacae*	This work
BW25113Δ*mrcB* pJP1	*mrcB* deletion strain containing *ampR/ampC* of *E. cloacae*	This work
BW25113Δ*dacB* pJP1	*dacB* deletion strain containing *ampR/ampC* of *E. cloacae*	This work
BW25113Δ*nlpI* pJP1	*nlpI* deletion strain containing *ampR/ampC* of *E. cloacae*	This work
BW27783 pJP1	Laboratory strain containing *ampR/ampC* of *E. cloacae*	This work
BW27783Δ*nlpI* pJP1	*nlpI* deletion strain containing *ampR/ampC* of *E. cloacae*	This work
BW27783Δ*prc* pJP1	*prc* deletion strain containing *ampR/ampC* of *E. cloacae*	This work
BW27783Δ*mepS* pJP1	*mepS* deletion strain containing *ampR/ampC* of *E. cloacae*	This work
BW27783Δ*mepM* pJP1	*mepM* deletion strain containing *ampR/ampC* of *E. cloacae*	This work
BW27783 pCL1920 pJP1	Laboratory overexpression strain containing *ampR/ampC* of *E. cloacae*	This work
BW27783 pCL1920 NlpI pJP1	*nlpI* overexpression strain containing *ampR/ampC* of *E. cloacae*	This work
BW27783 pCL1920 Prc pJP1	*prc* overexpression strain containing *ampR/amp*C of *E. cloacae*	This work

5.3.8 Laboratory equipment

Agilent 1200 HPLC system	Agilent technologies
Autoclave	Astell
ÄKTA Prime^{+}	GE Healthcare
Avanti J-26 XP centrifuge	Beckman-Coulter
β-RAM model5 scintillation flow-cell	LabLogic

Developer	Konica SRX-101A
Digital sonifier	Branson
Epson perfection 3490 scanner	Epson
Gel tank, for SDS-PAGE	BioRad
ImageQuant LAS4000mini	GE Healthcare
J-810 spectropolarimeter	Jasco
Kern EG balance	Kern
Kern PFB balance	Kern
Mettler Toledo Classic plus balance	Mettler
FLUOstar Optima plate reader	BMG labtech
Micro 200R microfuge	Hettich
MilliQ PF plus water purification machine	Millipore
Monolith NT.115^{TM} series MST machine	Nanotemper technologies
Optima^{TM} ultracentrifuge	Beckman-Coulter
Optima^{TM} TLX ultracentrifuge	Beckman-Coulter
pH meter	Jenway
Prism microfuge	Labnet
ProteON^{TM} XPR36	BioRad
ScanVac SpeedVac system	UniEqzip
Sigma 3-16k centrifuge	Scientific Laboratory Supplies
Spectrophotometer	Biochrom Libra S22
Thermomixer	Eppendorf
Typhoon scanner	GE Healthcare
Water bath with thermostat	Clifton
Wet-Blot transfer chamber	BioRad

5.4 Supplementary figures

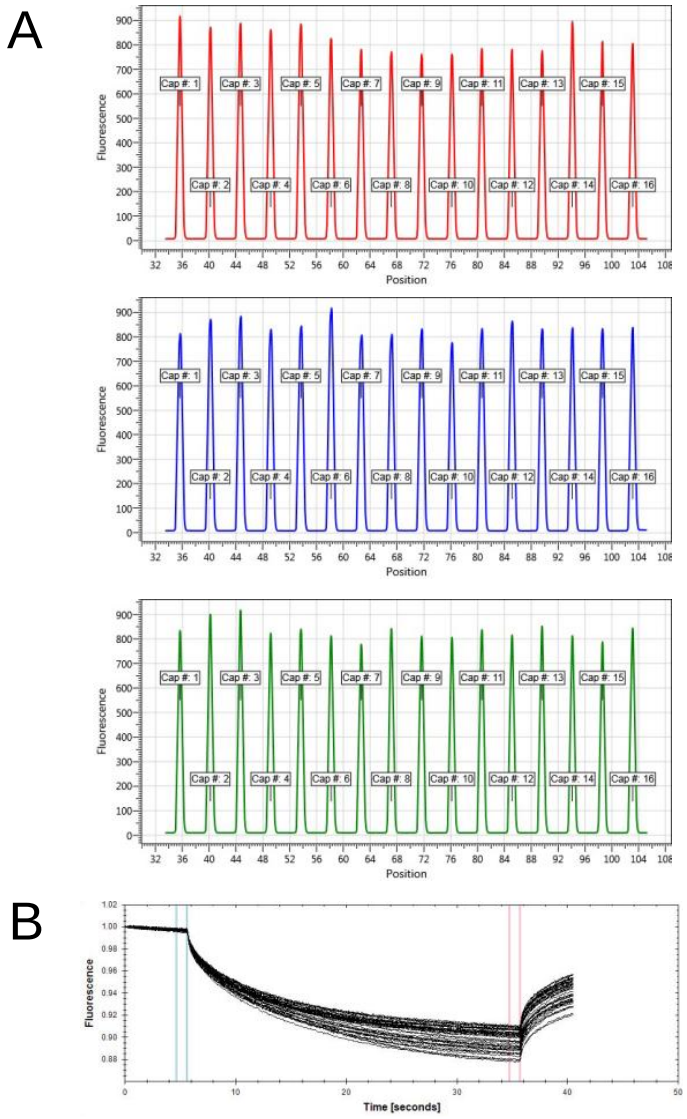

Figure 5.1 Raw MST data corresponding to figure 3.1B

A. Pre-experiment capillary scans of FL-PBP1A + LpoA. **B.** MST measurements were taken at 90% LED power and 20% MST power.

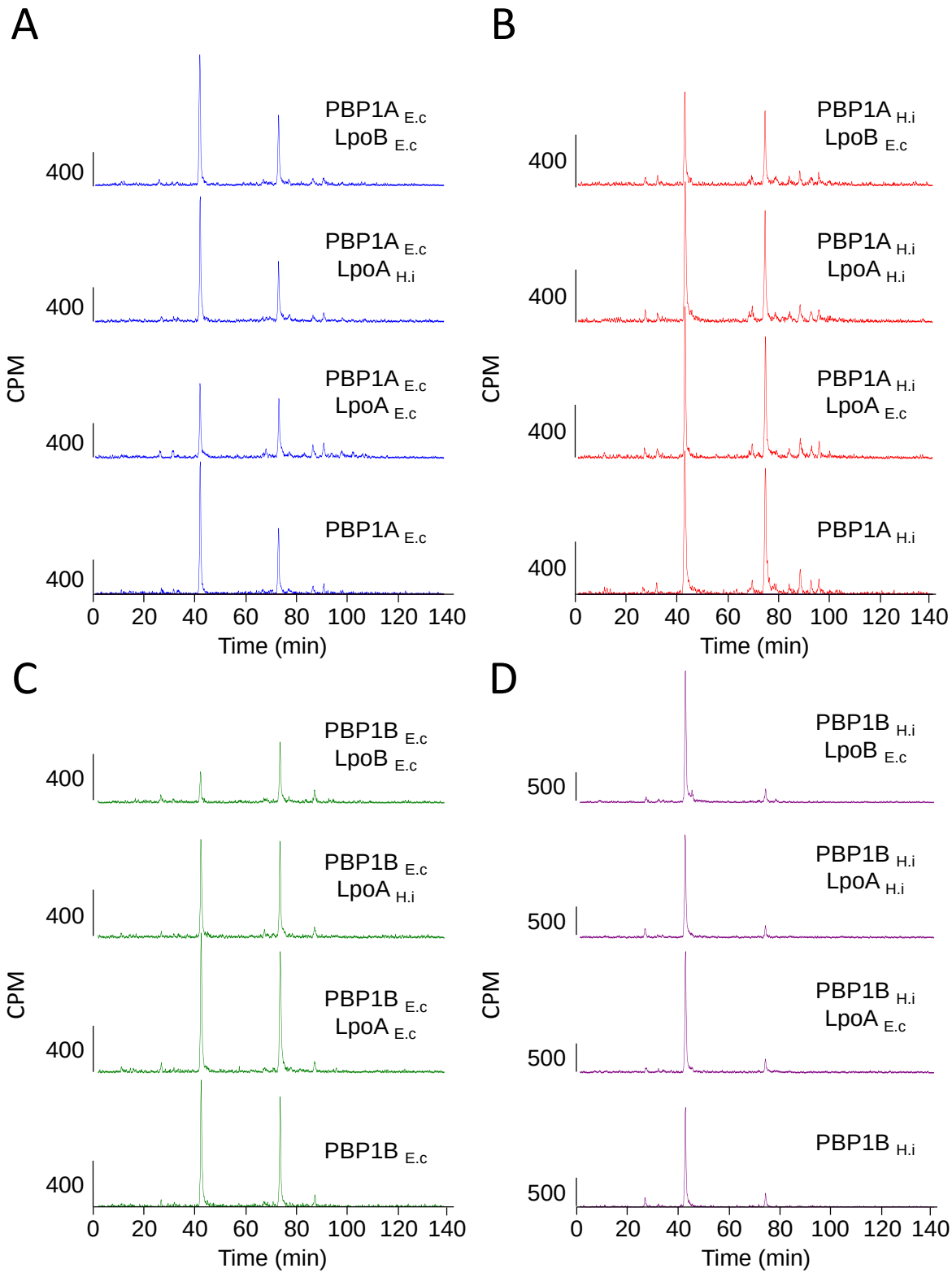

Figure 5.2 HPLC chromatograms corresponding to figure 3.7

Representative HPLC chromatograms corresponding to figure 3.7, showing counts per minute (CPM) against time (min). A; *E. coli* PBP1A + all Lpo proteins. B; *E. coli* PBP1B + all Lpo proteins. C; *H. influenzae* PBP1A + all LpoA proteins. C; *H. influenzae* PBP1B + all LpoA proteins.

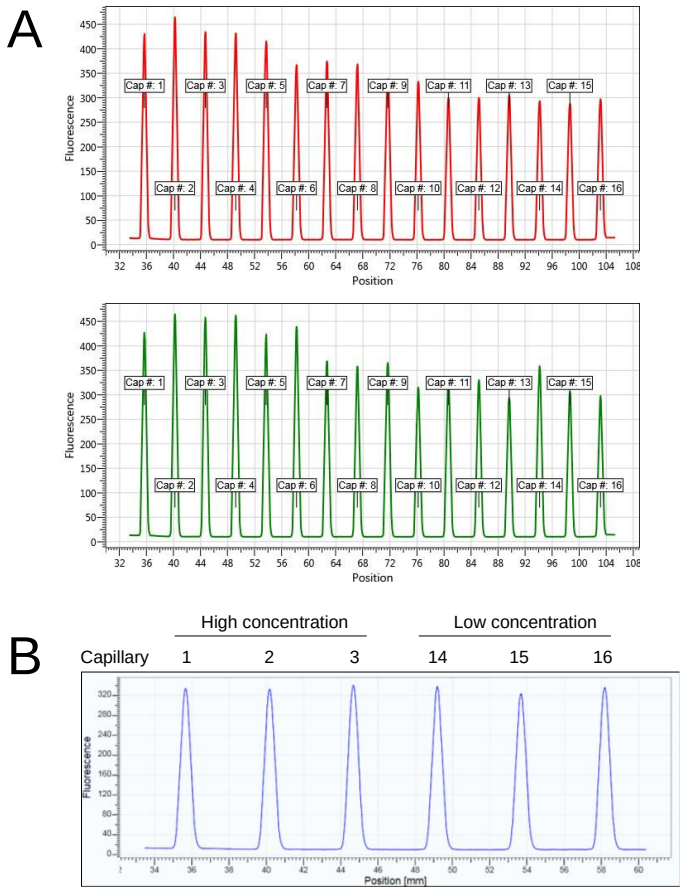

Figure 5.3 Raw MST data corresponding to figure 3.10B

A. Pre-experiment capillary scans of FL-LpoA + PBP4. **B.** Capillary scan after SDS-denaturation test of the three samples containing the highest concentration of unlabelled ligand and the three samples containing the lowest concentration. MST measurements were taken at 100% LED power and 20% MST power.

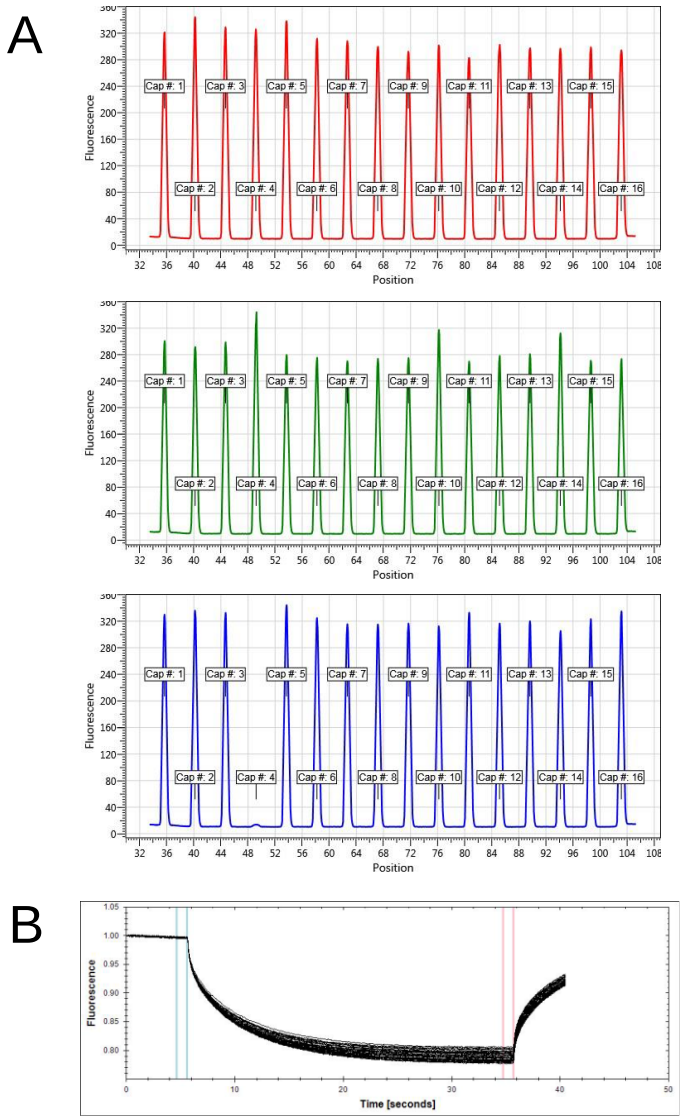

Figure 5.4 Raw MST data corresponding to figure 3.11B

A. Pre-experiment capillary scans of FL-LpoA + PBP4ΔD3 in triplicate. **B.** MST measurements were taken at 100% LED power and 20% MST power.

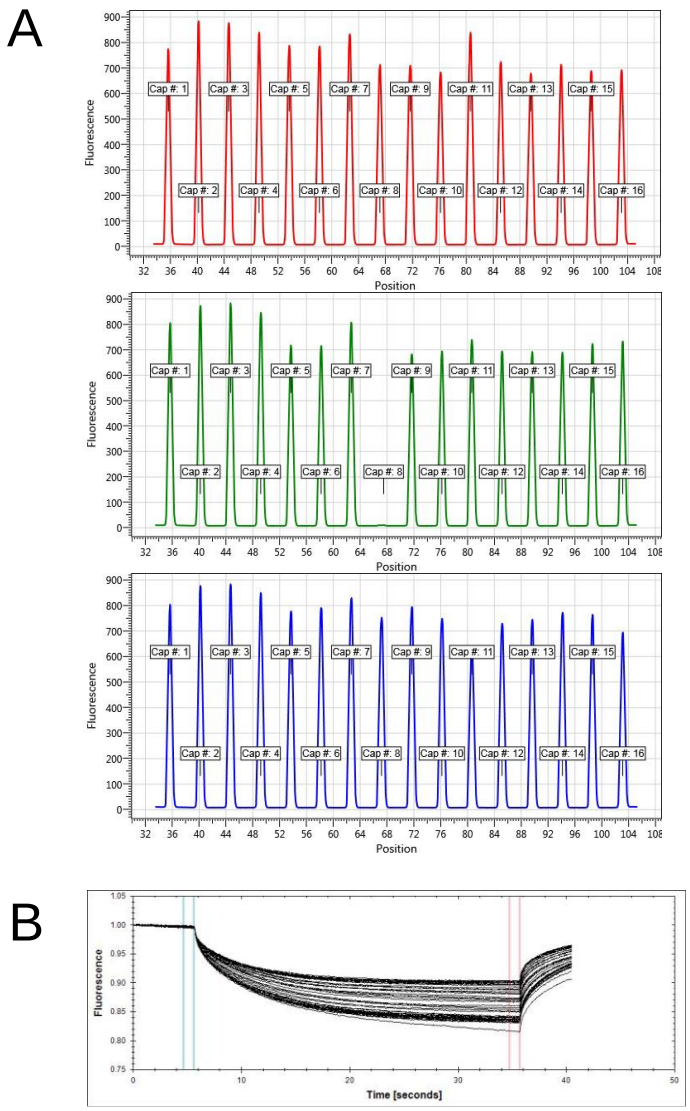

Figure 5.5 Raw MST data corresponding to figure 3.11C

A. Pre-experiment capillary scans of FL-LpoA^{C} + PBP4 in triplicate. **B.** MST measurements were taken at 20% LED power and 40% MST power.

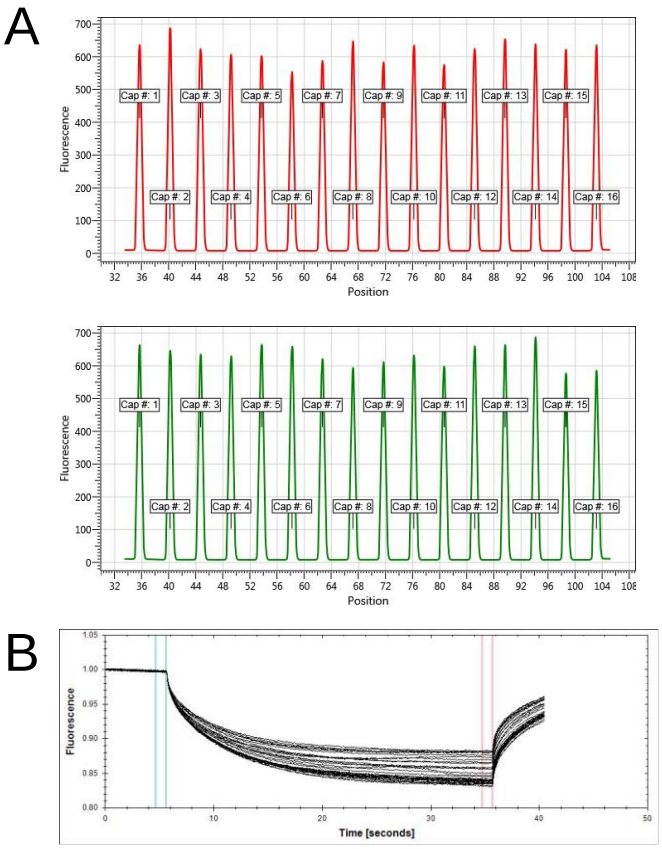

Figure 5.6 Raw MST data corresponding to figure 3.11D

A. Pre-experiment capillary scans of FL-LpoA^{C} + PBP4ΔD3 in triplicate. **B.** MST measurements were taken at 20% LED power and 40% MST power.

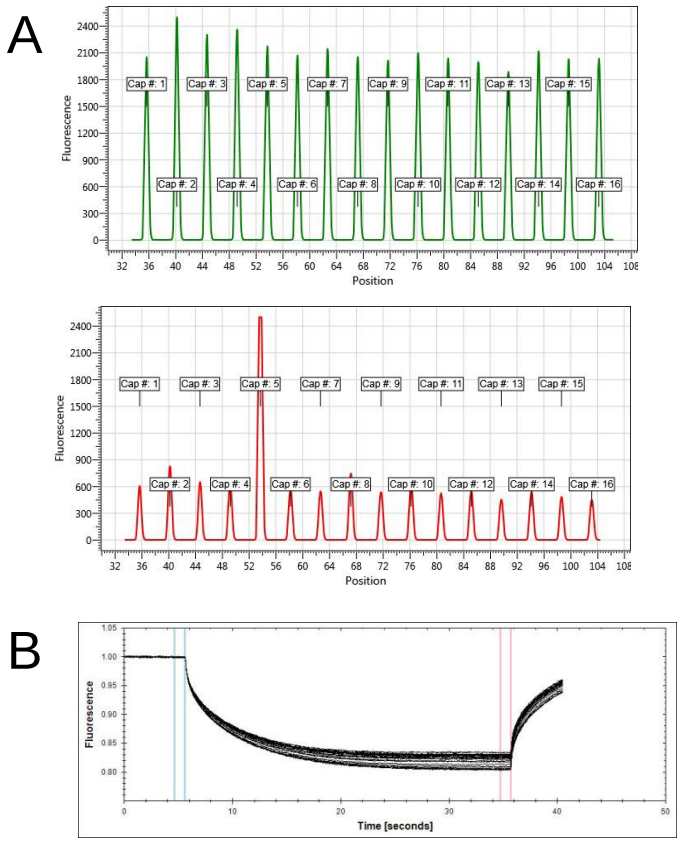

Figure 5.7 Raw MST data corresponding to figure 3.11E

A. Pre-experiment capillary scans of FL-LpoA^{N} + PBP4. **B.** MST measurements were taken at 20% LED power and 40% MST power.

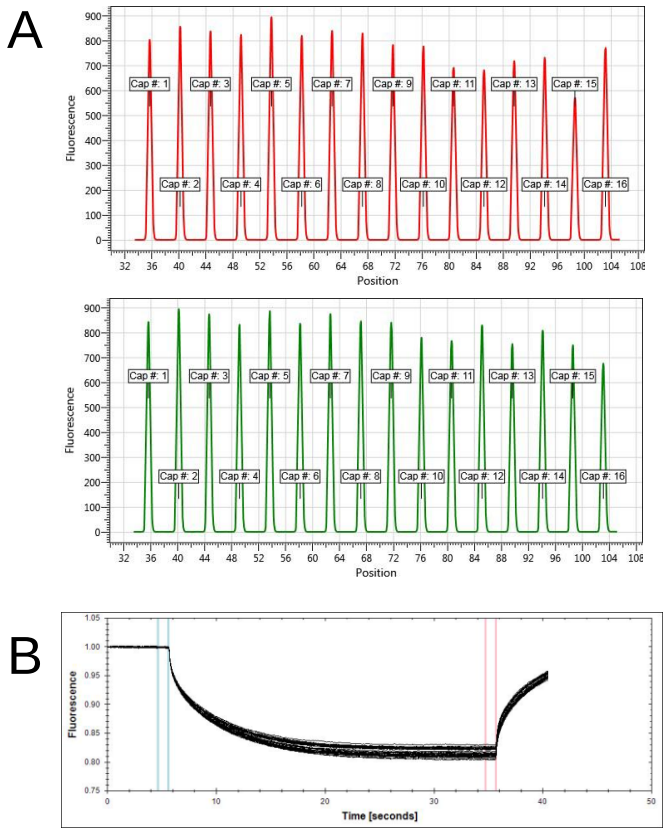

Figure 5.8 Raw MST data corresponding to figure 3.11F

A. Pre-experiment capillary scans of FL-LpoA^{N} + PBP4ΔD3 in duplicate. **B.** MST measurements were taken at 20% LED power and 40% MST power.

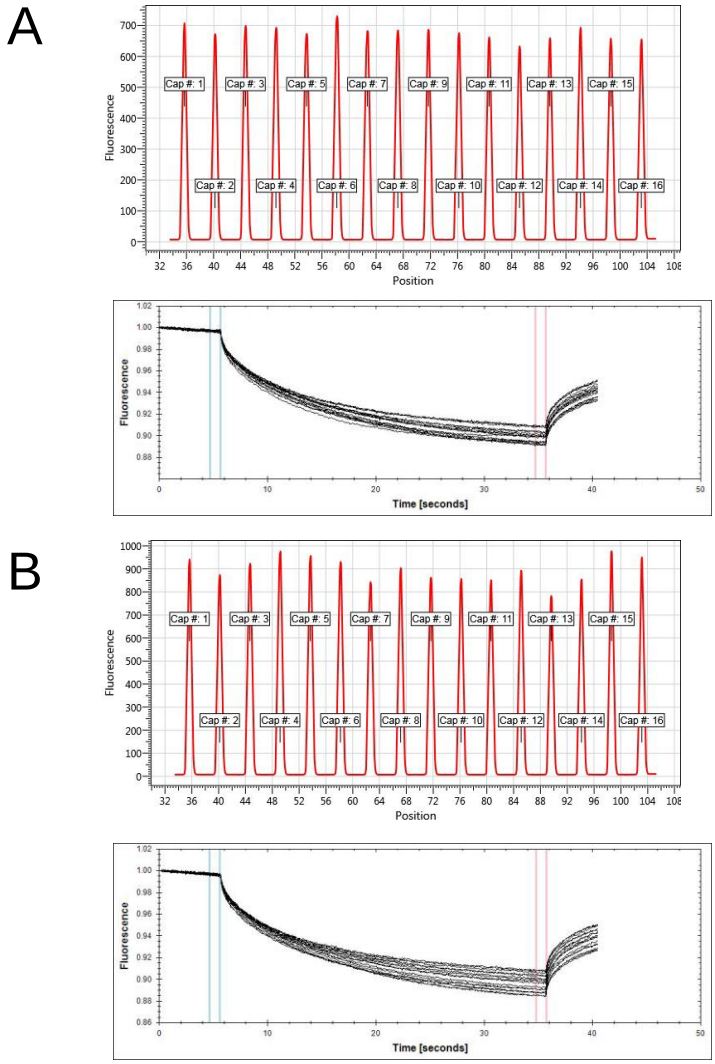

Figure 5.9 Raw MST data corresponding to figure 3.13B

A. Pre-experiment capillary scans of FL-PBP1A + PBP4 and MST timetrace taken at 20% MST power, 80% LED power. **B.** Repeat of the above.

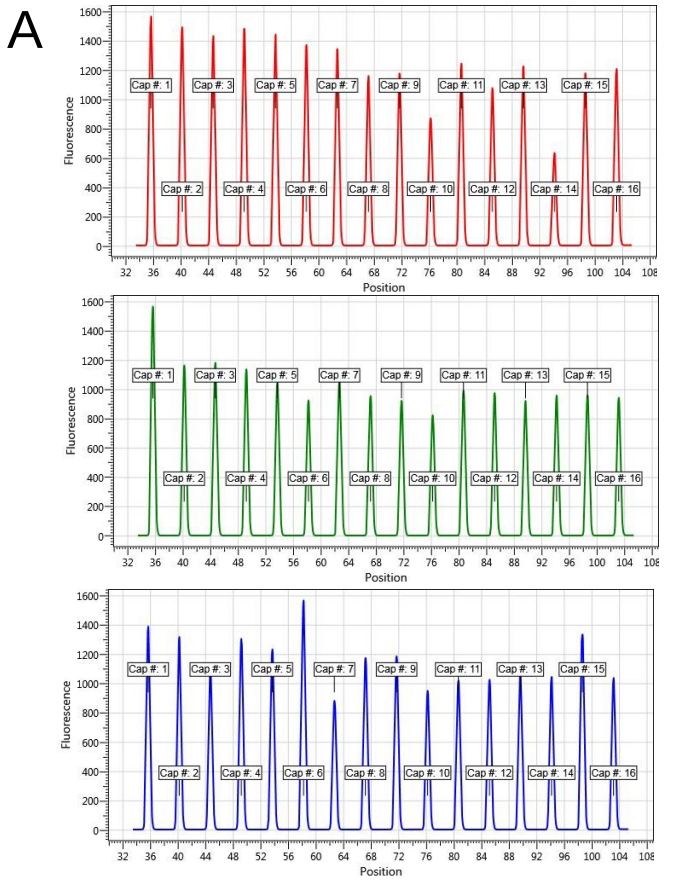

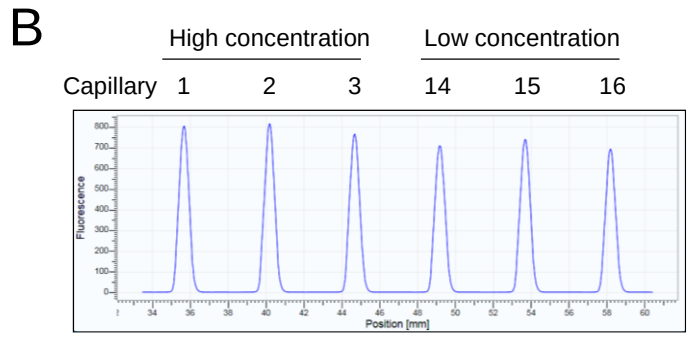

Figure 5.10 Raw MST data corresponding to figure 3.14A

A. Pre-experiment capillary scans of FL-PBP7 + LpoA in triplicate. **B.** Capillary scan after SDS-denaturation test of the three samples containing the highest concentration of unlabelled ligand and the three samples containing the lowest concentration. MST measurements were taken at 40% LED power and 20% MST power.

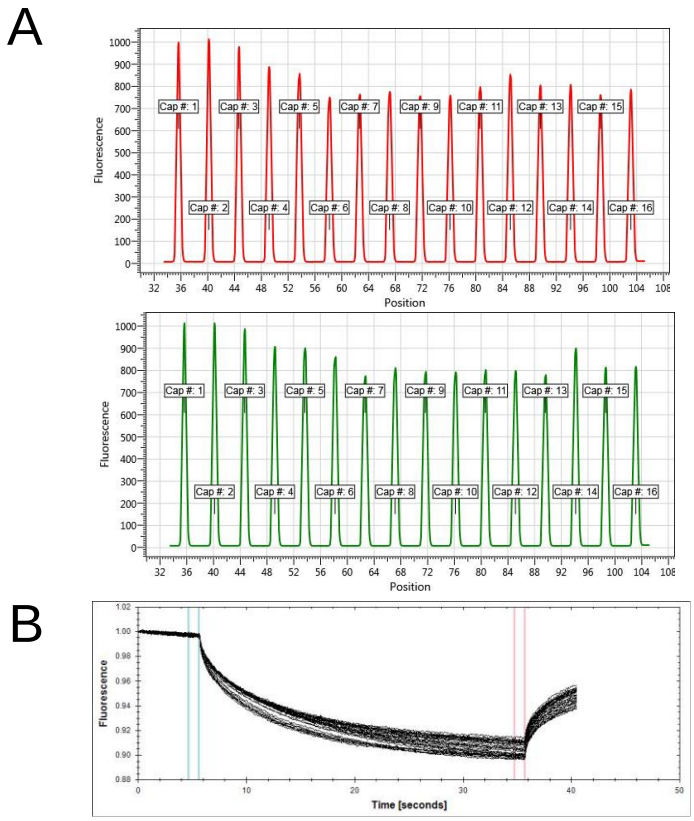

Figure 5.11 Raw MST data corresponding to figure 3.14B

A. Pre-experiment capillary scans of FL-PBP7 + PBP1A in duplicate. **B.** MST measurements were taken at 80% LED power and 20% MST power.

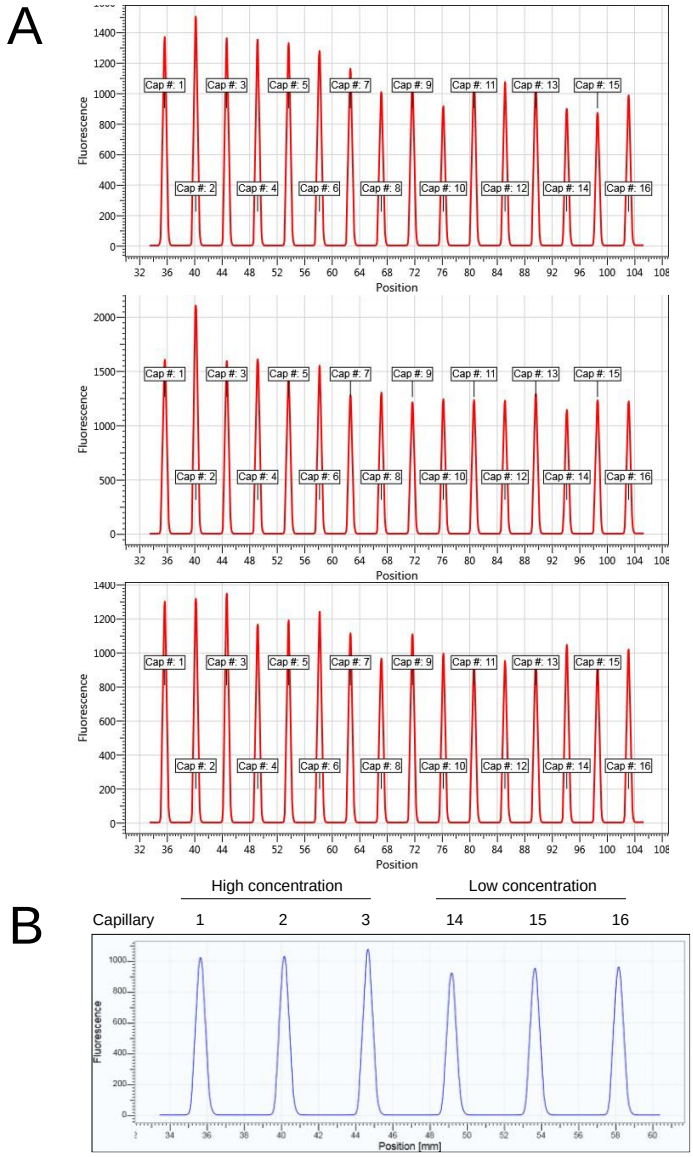

Figure 5.12 Raw MST data corresponding to figure 3.14C

A. Pre-experiment capillary scans of FL-PBP7 + PBP4 in triplicate. **B.** Capillary scan after SDS-denaturation test of the three samples containing the highest concentration of unlabelled ligand and the three samples containing the lowest concentration. MST measurements were taken at 40% LED power and 40% MST power.

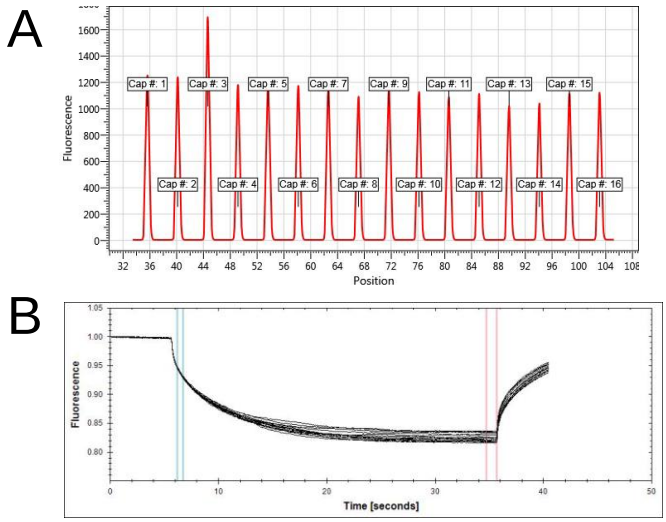

Figure 5.13 Raw MST data corresponding to figure 3.15A

A. Pre-experiment capillary scan of FL-MepS + PBP7. **B.** MST timetrace. MST measurements were taken at 40% LED power and 40% MST power.

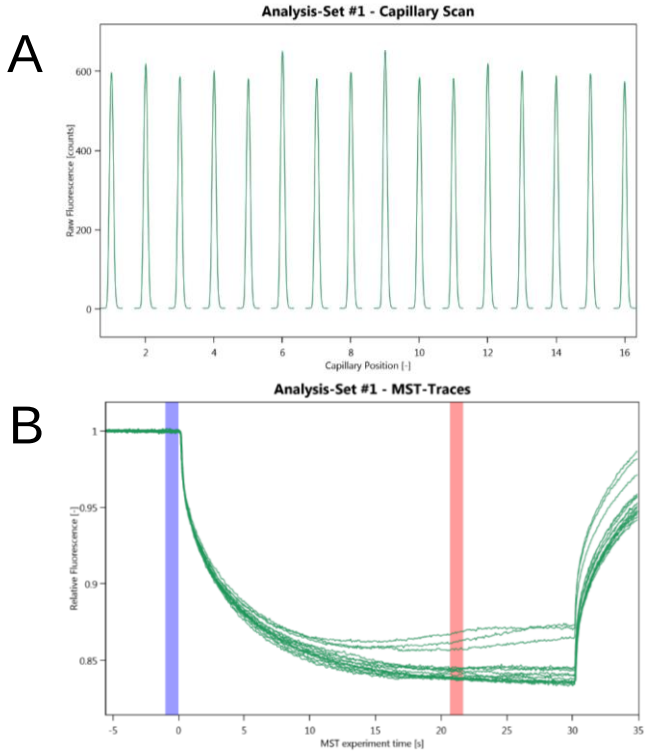

Figure 5.14 Raw MST data corresponding to figure 3.15B

A. Pre-experiment capillary scan of FL-MepM + PBP7. **B.** MST timetrace. MST measurements were taken at 40% LED power and 40% MST power.

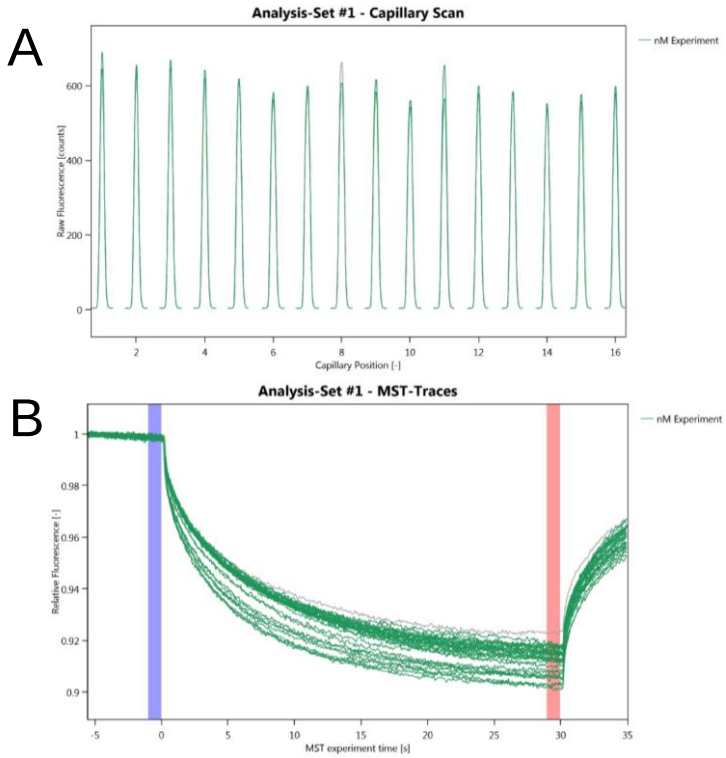

Figure 5.15 Raw MST data corresponding to figure 3.16A

A. Combined pre-experiment capillary scans of FL-MepM + MepS. **B.** MST timetrace. MST measurements were taken at 40% LED power and 20% MST power.

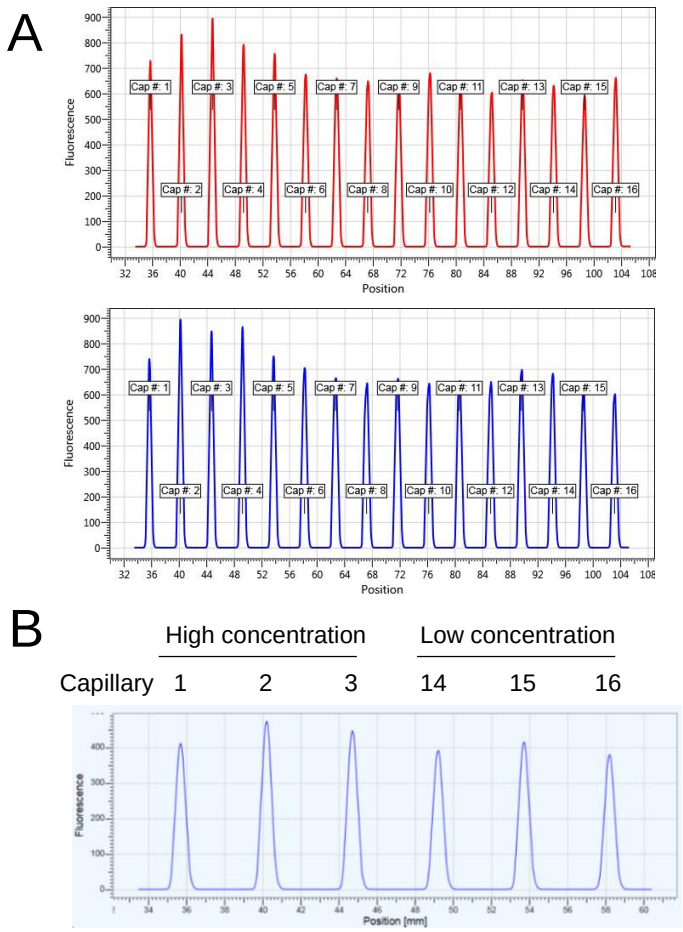

Figure 5.16 Raw MST data corresponding to figure 3.16B

A. Pre-experiment capillary scans of FL-PBP1A + MepS. **B.** Capillary scan after SDS-denaturation test of the three samples containing the highest concentration of unlabelled ligand and the three samples containing the lowest concentration. MST measurements were taken at 20% LED power and 40% MST power.

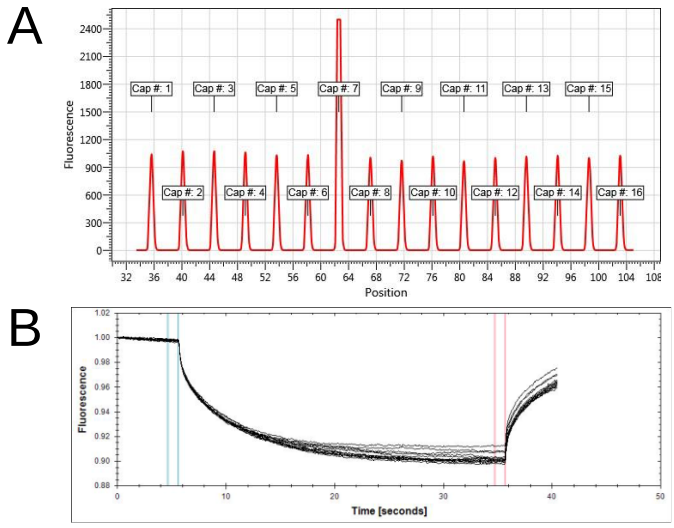

Figure 5.17 Raw MST data corresponding to figure 3.17A

A. Pre-experiment capillary scan of FL-MepS + LpoA. **B.** MST timetrace. MST measurements were taken at 40% LED power and 20% MST power.

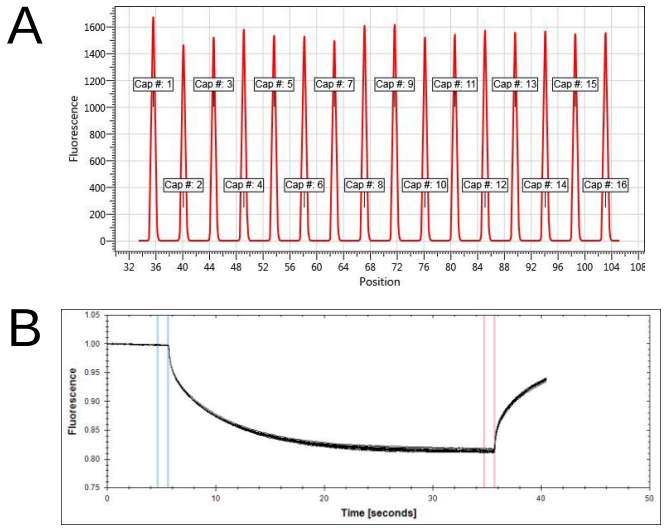

Figure 5.18 Raw MST data corresponding to figure 3.17B

A. Pre-experiment capillary scan of FL-MepS + PBP4. **B.** MST timetrace. MST measurements were taken at 40% LED power and 40% MST power.

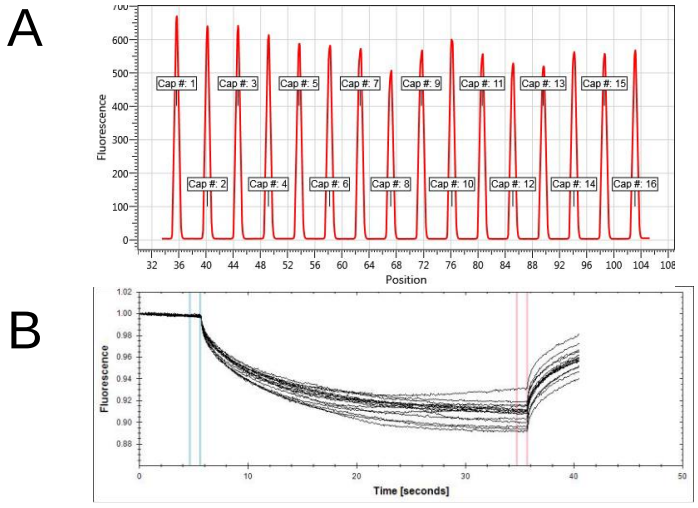

Figure 5.19 Raw MST data corresponding to figure 3.17D

A. Pre-experiment capillary scan of FL-MepS + EnvC. **B.** MST timetrace. MST measurements were taken at 40% LED power and 20% MST power.

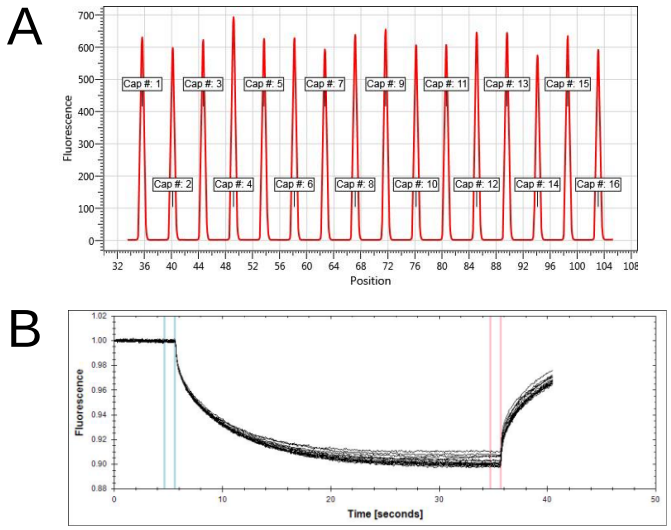

Figure 5.20 Raw MST data corresponding to figure 3.18A

A. Pre-experiment capillary scan of FL-MepM + PBP4. **B.** MST timetrace. MST measurements were taken at 20% LED power and 20% MST power.

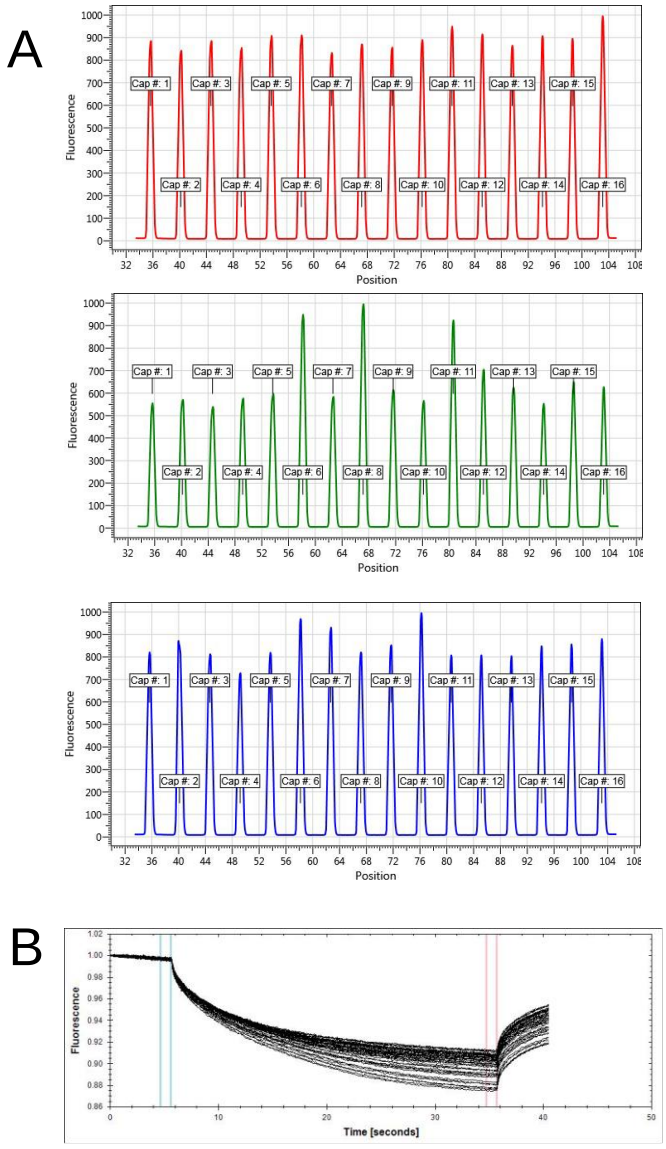

Figure 5.21 Raw MST data corresponding to figure 3.23

A. Pre-experiment capillary scans of FL-PBP1A + PBP4ΔD3. **B.** MST timetrace. MST measurements were taken at 80% LED power and 20% MST power.

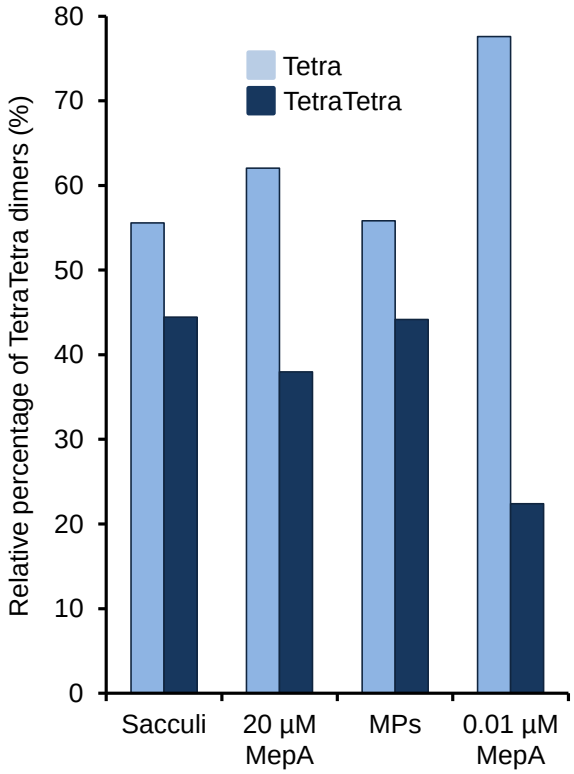

Figure 5.22 MepA activity on sacculi and muropeptides at pH 7.5

MepA was incubated o/n with intact sacculi (MC1061) at 20 µM, or for 90 min on isolated muropeptides (MPs) at 10 nM. The relative percentage of Tetra and TetraTetra-containing muropeptides after digestion was calculated and plotted. Assay was carried out at pH7.5 and 150 mM NaCl.

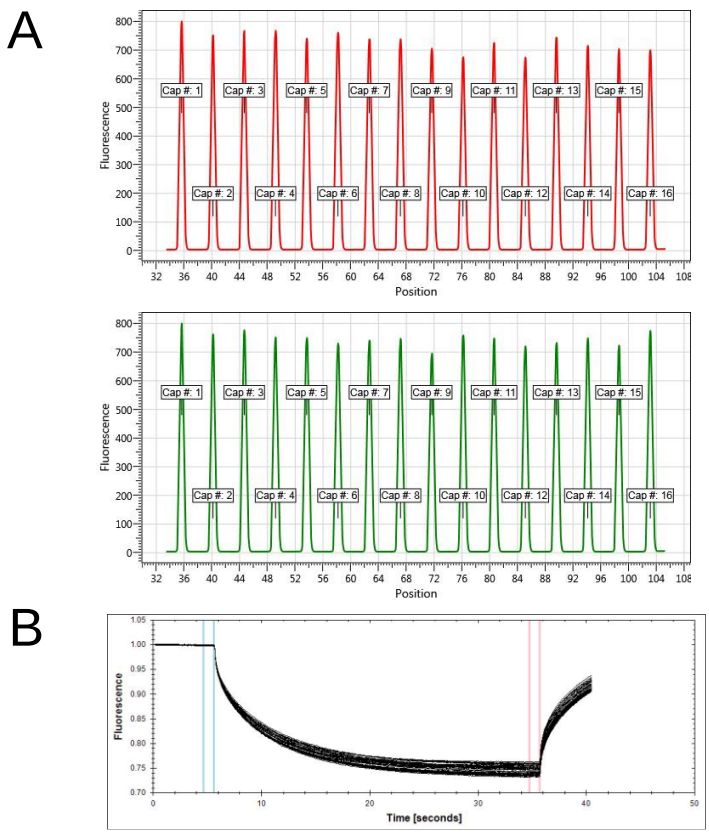

Figure 5.23 Raw MST data corresponding to figure 3.24A

A. Pre-experiment capillary scans of FL-MepA + PBP7. **B.** MST timetrace. MST measurements were taken at 40% LED power and 60% MST power.

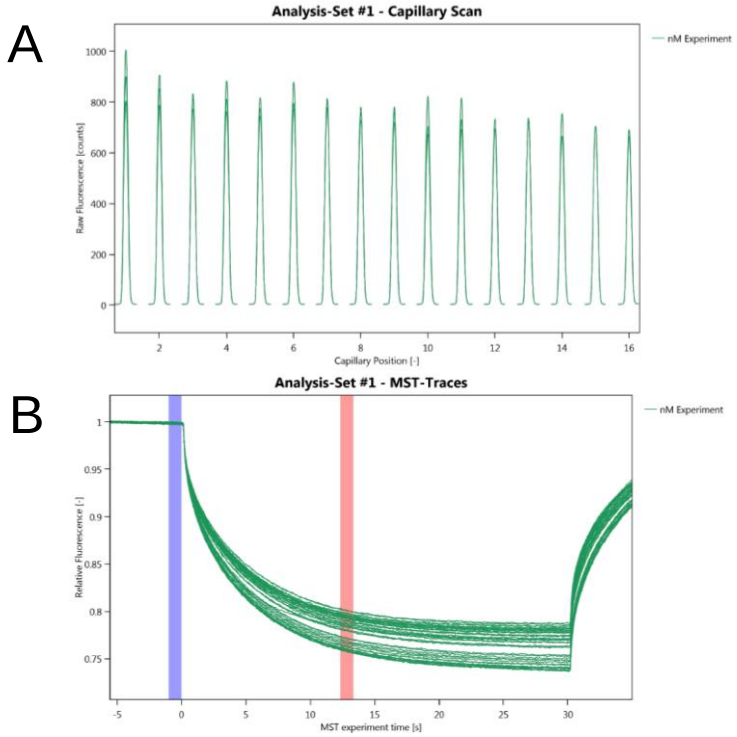

Figure 5.24 Raw MST data corresponding to figure 3.24B

A. Combined pre-experiment capillary scans of FL-MepA + PBP4. **B.** MST timetrace. MST measurements were taken at 40% LED power and 60% MST power.

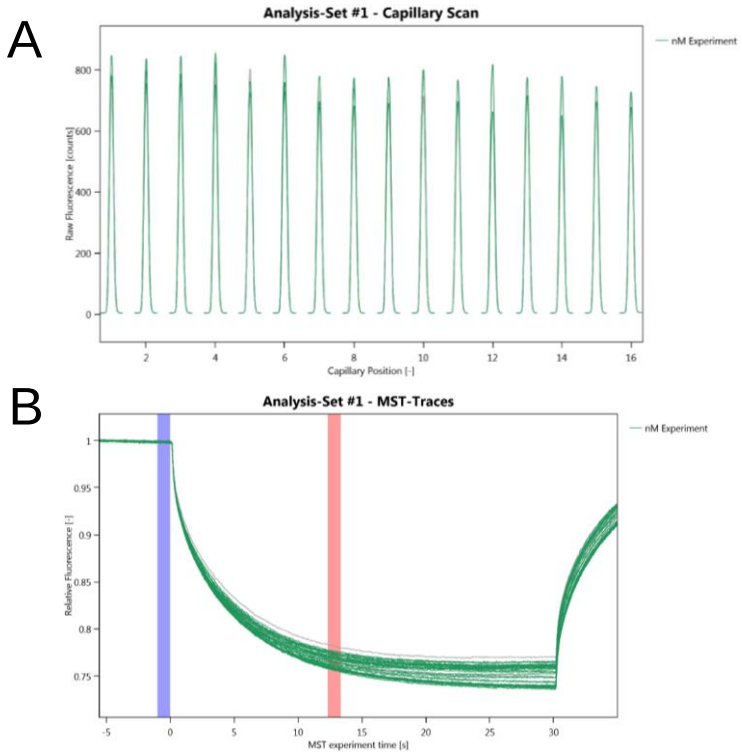

Figure 5.25 Raw MST data corresponding to figure 3.24C

A. Combined pre-experiment capillary scans of FL-MepA + MepS. **B.** MST timetrace. MST measurements were taken at 40% LED power and 60% MST power.

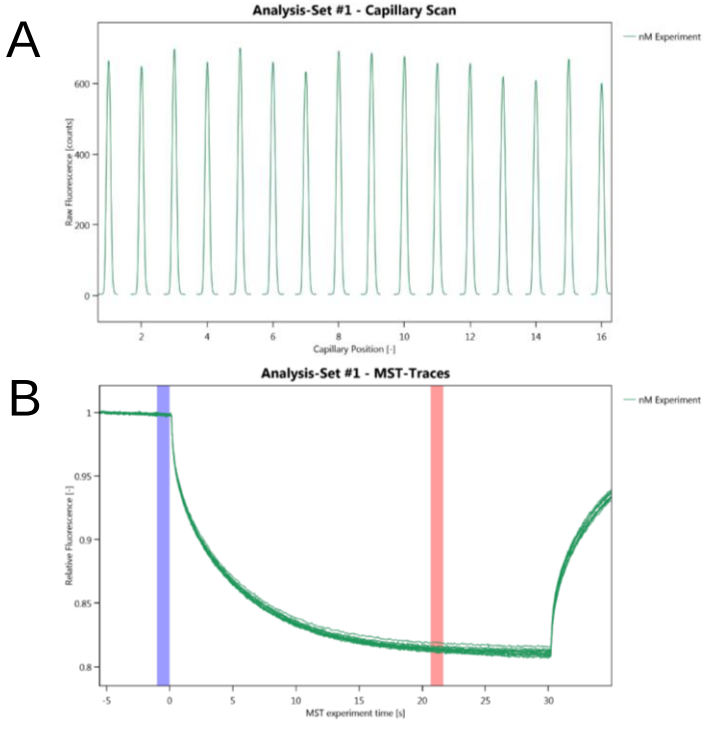

Figure 5.26 Raw MST data corresponding to figure 3.25C

A. Combined pre-experiment capillary scans of FL-MepA + MepM. **B.** MST timetrace. MST measurements were taken at 40% LED power and 60% MST power.

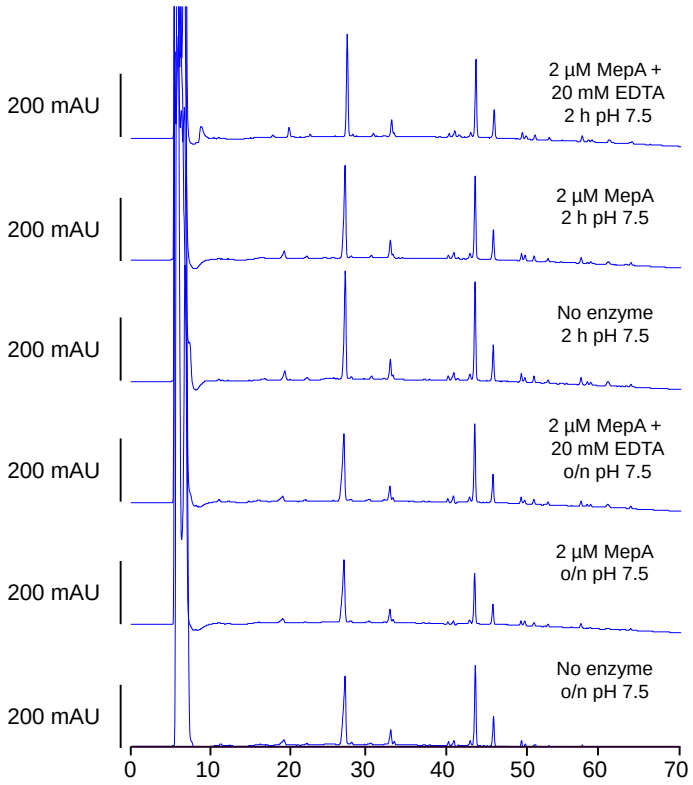

Figure 5.27 HPLC chromatograms corresponding to figure 3.26, pH 7.5

Representative HPLC chromatograms for pH 7.5 samples corresponding to figure 3.27 showing absorbance at 205 nm against time (min).

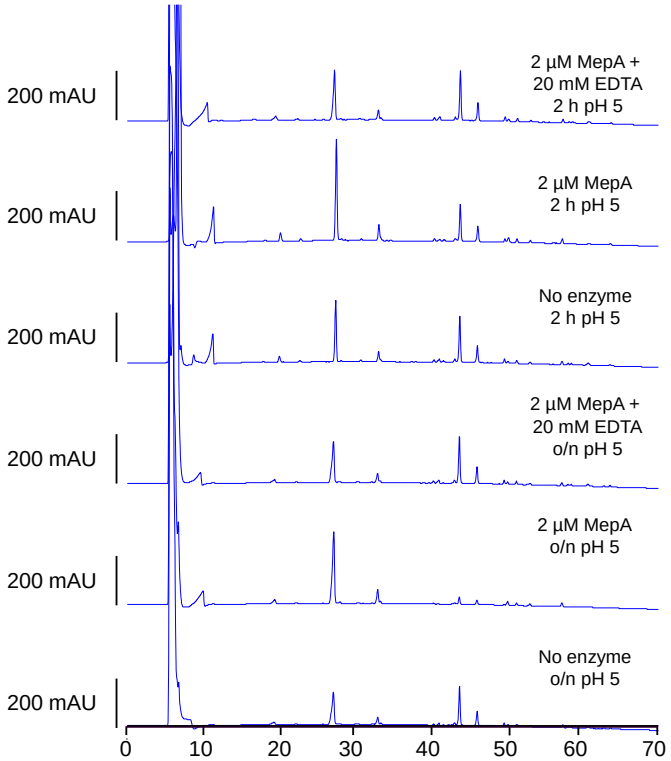

Figure 5.28 HPLC chromatograms corresponding to figure 3.27, pH 5.0

Representative HPLC chromatograms for pH 5.0 samples corresponding to figure 3.27 showing absorbance at 205 nm against time (min).

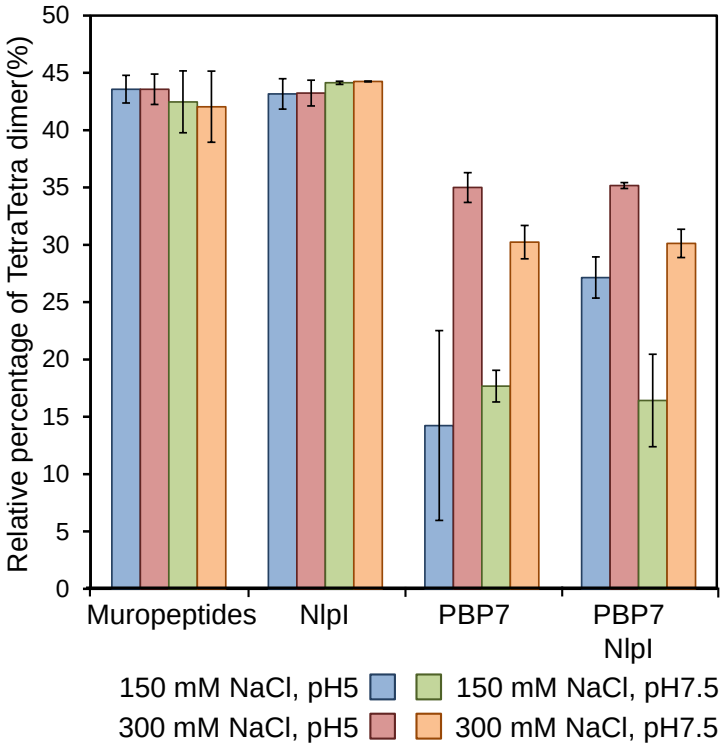

Figure 5.29 HPLC chromatograms corresponding to figure 3.35

Relative percentages of TetraTetra dimers of the total amount of Tetra-containing muropeptides at four different conditions corresponding to figure 3.36 showing absorbance at 205 nm against time (min). PBP7 (2 µM) was incubated with MC1061 muropeptides in the presence or absence of NlpI (4 µM) for 2 h.

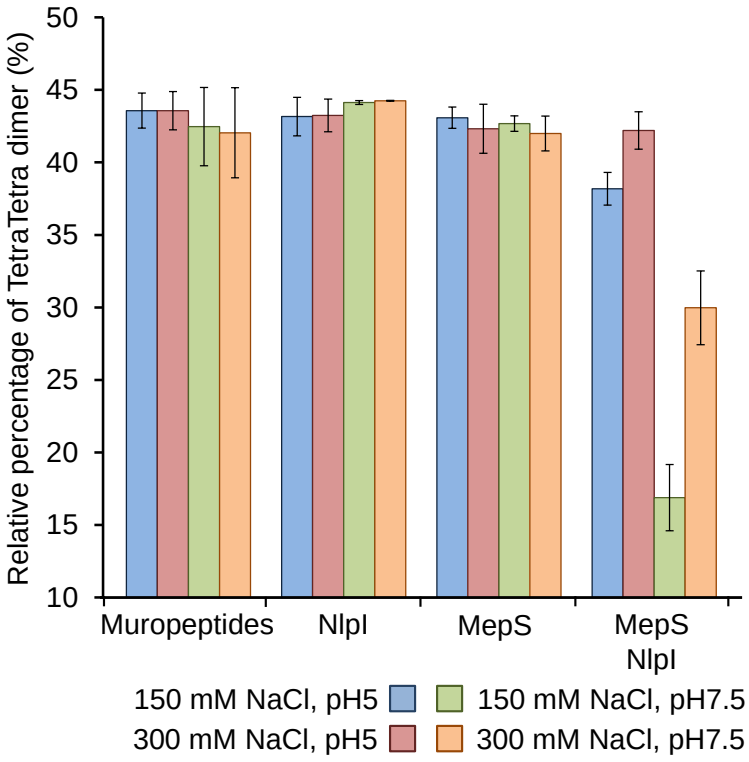

Figure 5.30 HPLC chromatograms corresponding to figure 3.40

Relative percentages of TetraTetra dimers of the total amount of Tetra-containing muropeptides at four different conditions corresponding to figure 4.39 showing absorbance at 205 nm against time (min). MepS (5 µM) was incubated with MC1061 muropeptides in the presence or absence of NlpI (10 µM) o/n.

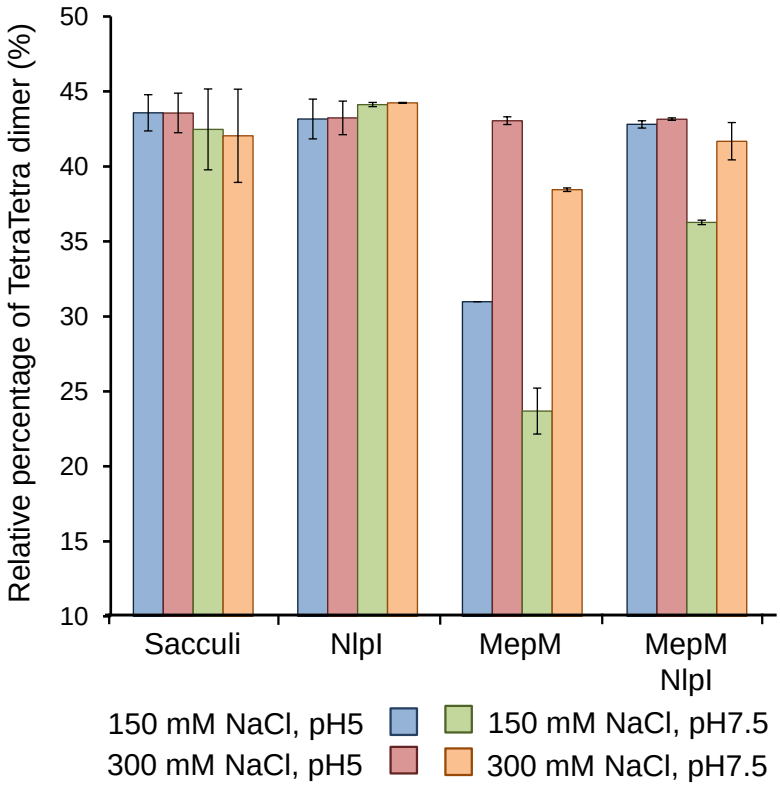

Figure 5.31 HPLC chromatograms corresponding to figure 3.43

Relative percentages of TetraTetra dimers of the total amount of Tetra-containing muropeptides at four different conditions corresponding to figure 4.42 showing absorbance at 205 nm against time (min). MepM (2 µM) was incubated with MC1061 sacculi in the presence or absence of NlpI (4 µM) for 4 h.

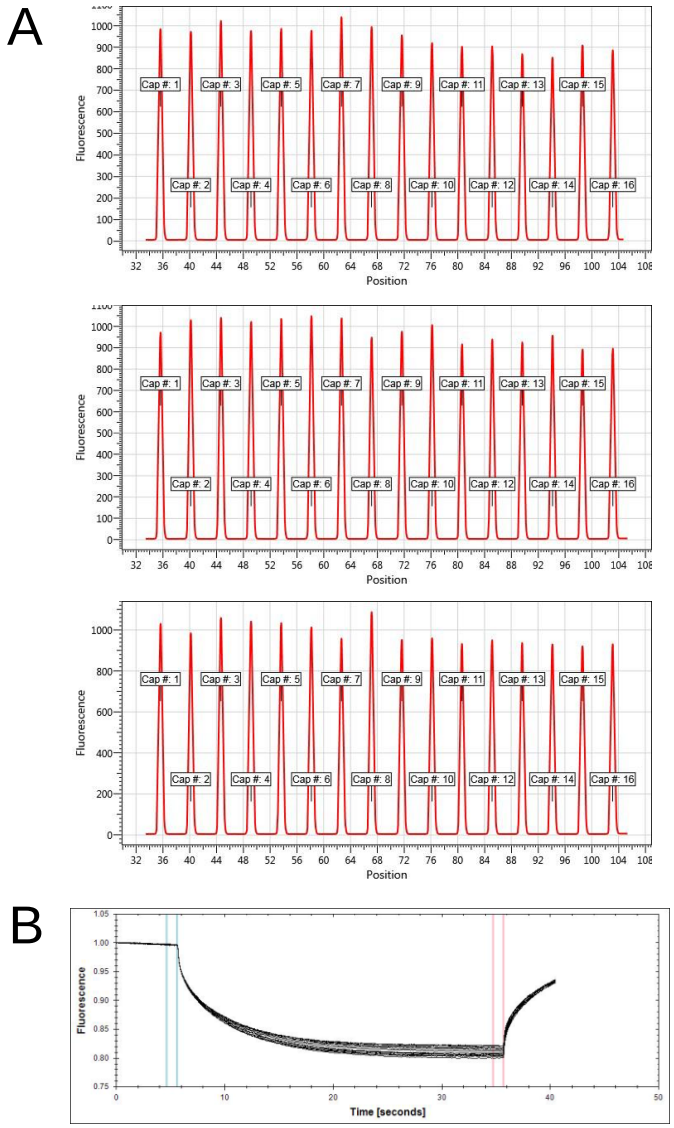

Figure 5.32 Raw MST data corresponding to figure 3.30

A. Pre-experiment capillary scans of FL-NlpI + NlpI. **B.** MST timetrace. MST measurements were taken at 50% LED power and 40% MST power.

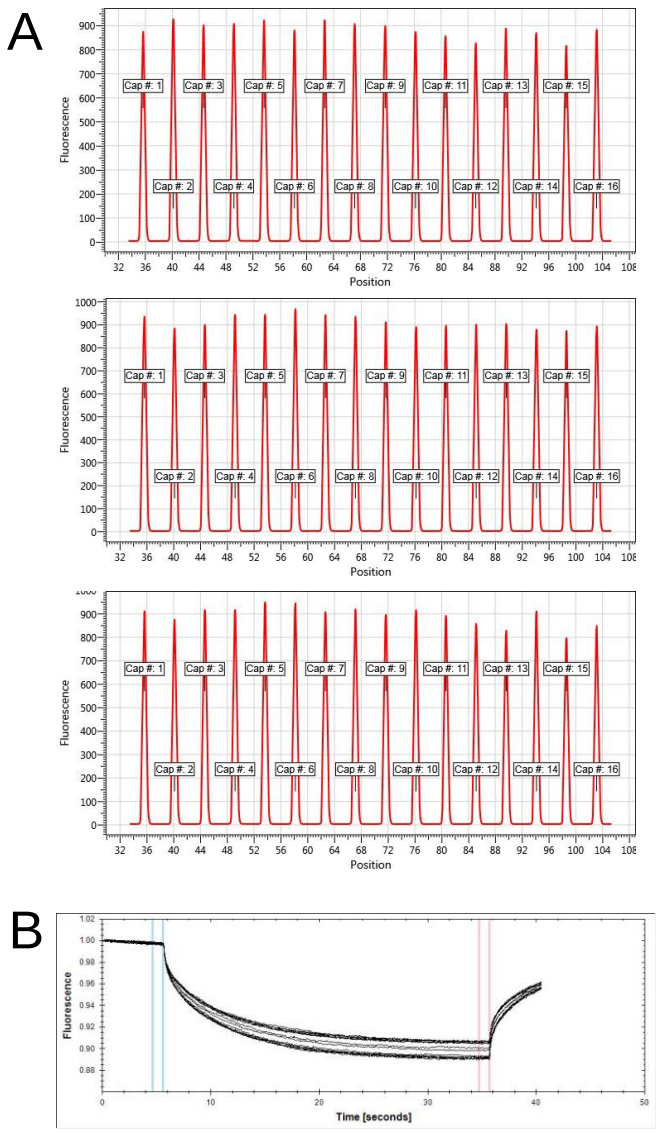

Figure 5.33 Raw MST data corresponding to figure 3.31C

A. Pre-experiment capillary scans of FL-NlpI + PBP4. **B.** MST timetrace. MST measurements were taken at 40% LED power and 20% MST power.

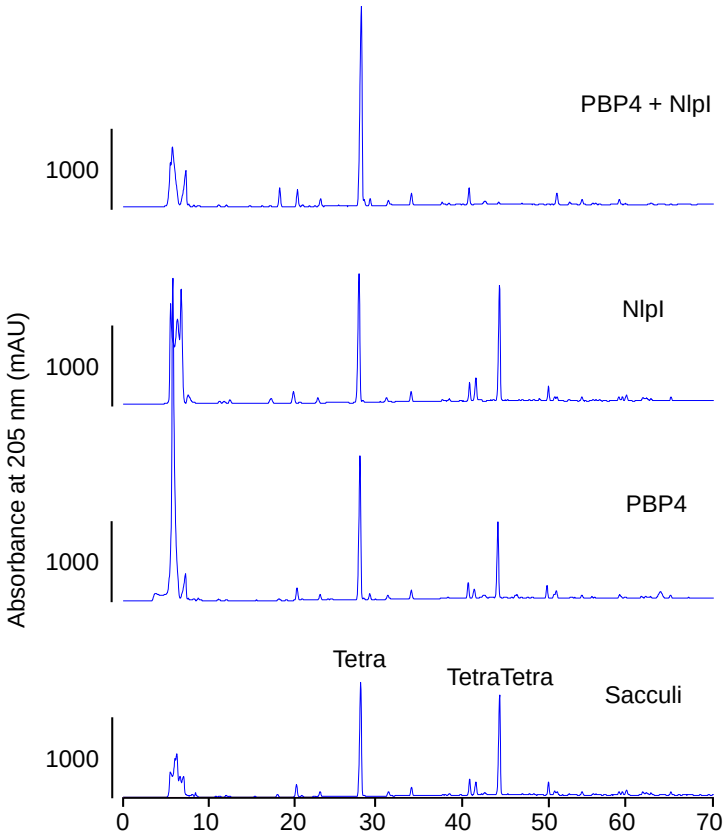

Figure 5.34 HPLC chromatograms corresponding to figure 3.32

Representative HPLC chromatograms for PBP4 (1 µm) on MC1061 sacculi in the presence or absence of NlpI (2 µm). Absorbance read at 205 nm shown against time (min).

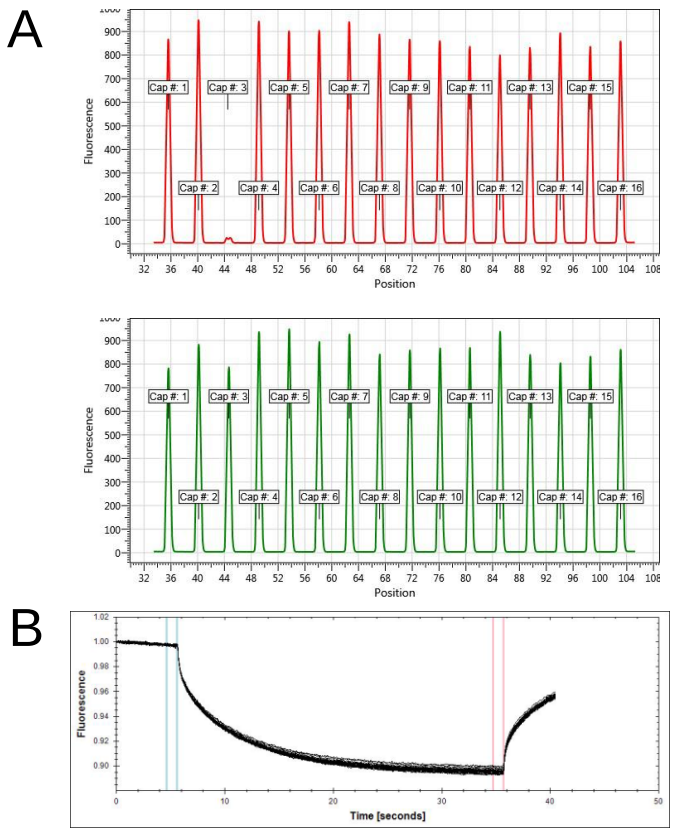

Figure 5.35 Raw MST data corresponding to figure 3.33B

A. Pre-experiment capillary scans of FL-NlpI + PBP4ΔD3. **B.** MST timetrace. MST measurements were taken at 40% LED power and 20% MST power.

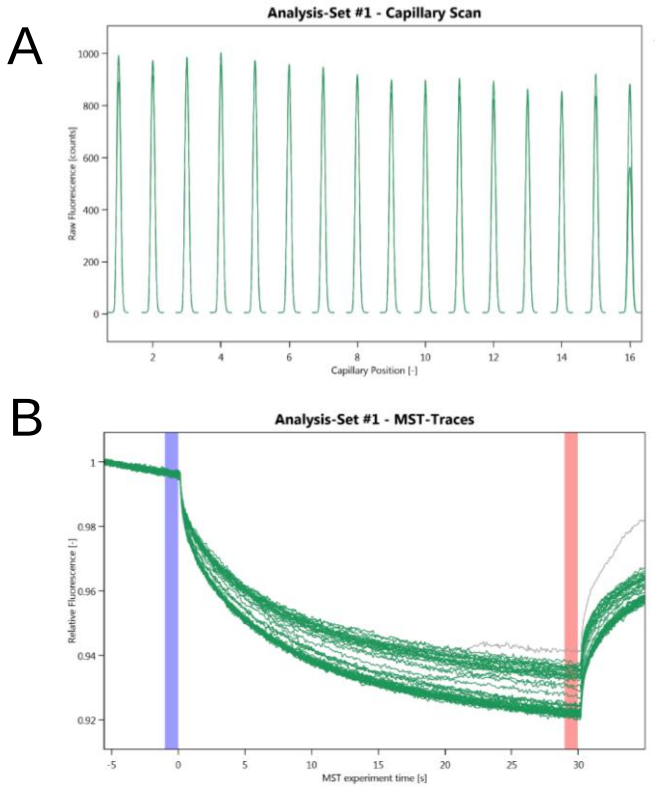

Figure 5.36 Raw MST data corresponding to figure 3.36B

A. Combined pre-experiment capillary scans of FL-NlpI + PBP7. **B.** MST timetrace. MST measurements were taken at 50% LED power and 10% MST power.

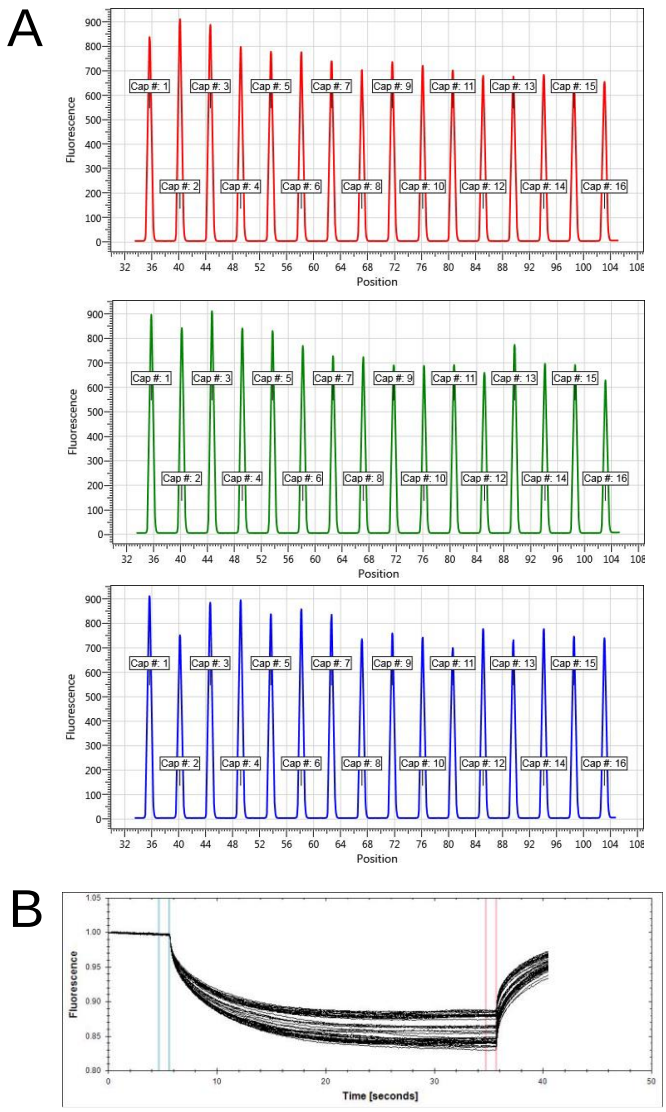

Figure 5.37 Raw MST data corresponding to figure 3.36C

A. Pre-experiment capillary scans of FL-PBP7 + NlpI. **B.** MST timetrace. MST measurements were taken at 40% LED power and 20% MST power.

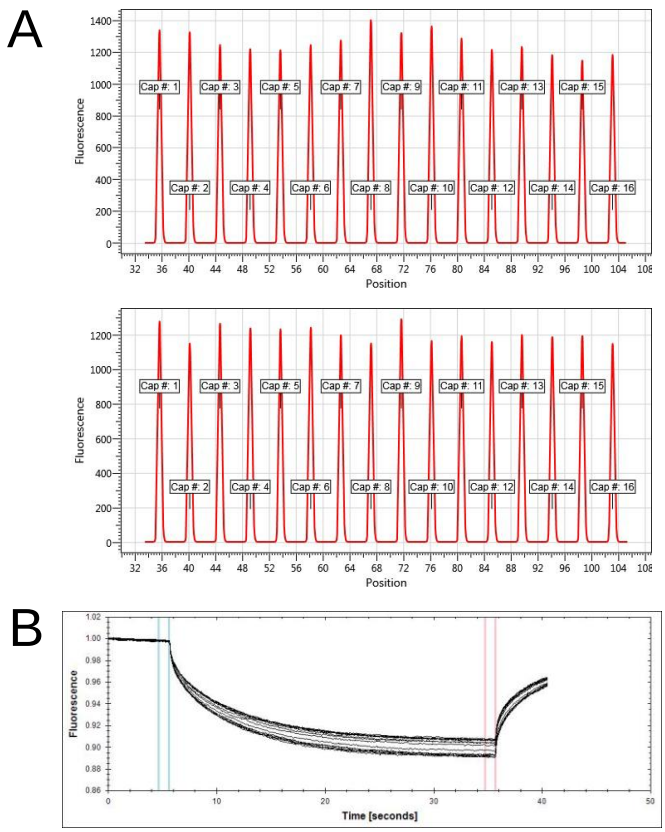

Figure 5.38 Raw MST data corresponding to figure 3.38B

A. Pre-experiment capillary scans of FL-MepS + NlpI. **B.** MST timetrace. MST measurements were taken at 20% LED power and 40% MST power.

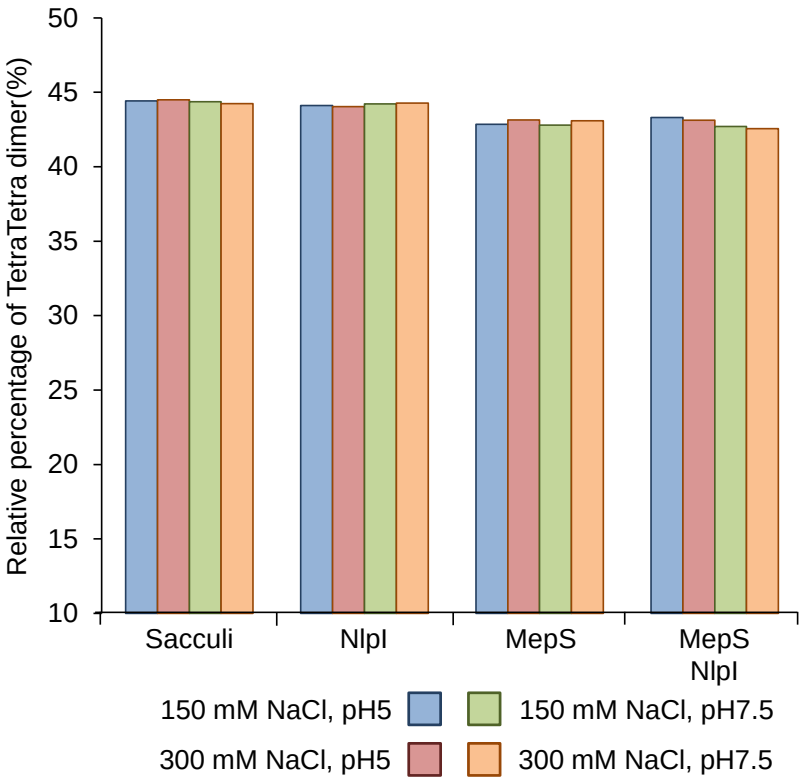

Figure 5.39 NlpI does not activate MepS activity on intact sacculi

Intact sacculi form the W/T *E. coli* strain, MC1061, was incubated o/n at 37°C with 5μM MepS alone or in the presence of 10 μM NlpI, at four different conditions. Samples were inactivated by boiling and centrifuged. The released muropeptide-containing supernatant was reduced with sodium borohydride and analysed by HPLC. The relative amounts of TetraTetra dimer were calculated as a percentage of the total number of Tetra-containing muropeptides.

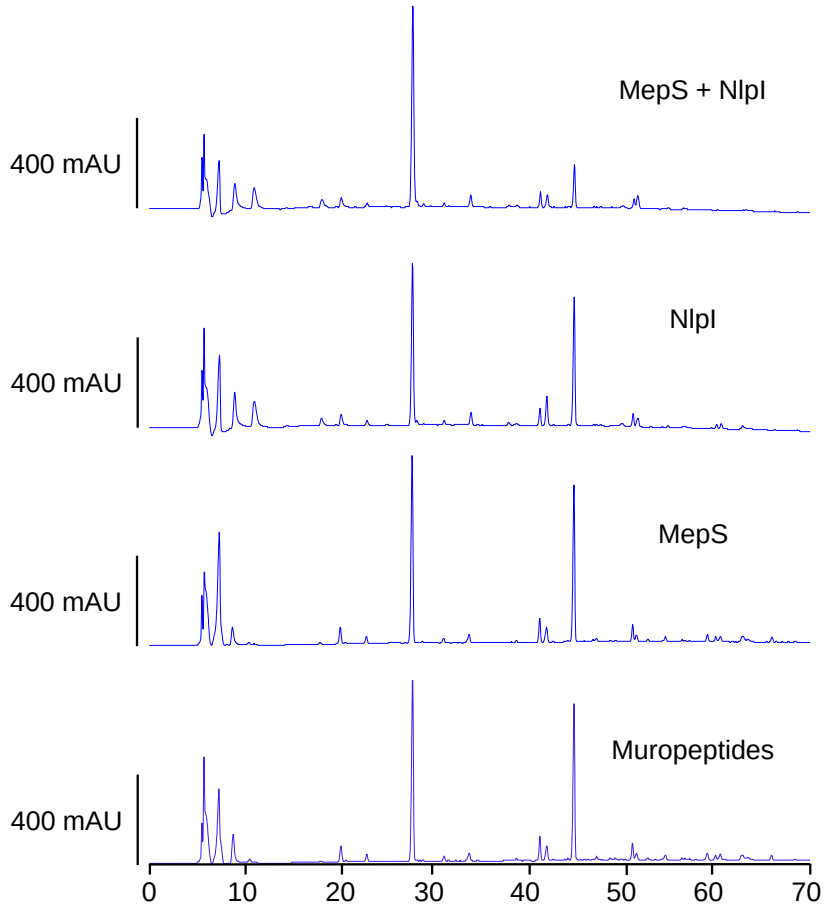

Figure 5.40 HPLC chromatograms corresponding to figure 3.40

Representative HPLC chromatograms for MepS (5 µm) on MC1061 muropeptides in the presence or absence of NlpI (10 µm). Absorbance read at 205 nm shown against time (min).

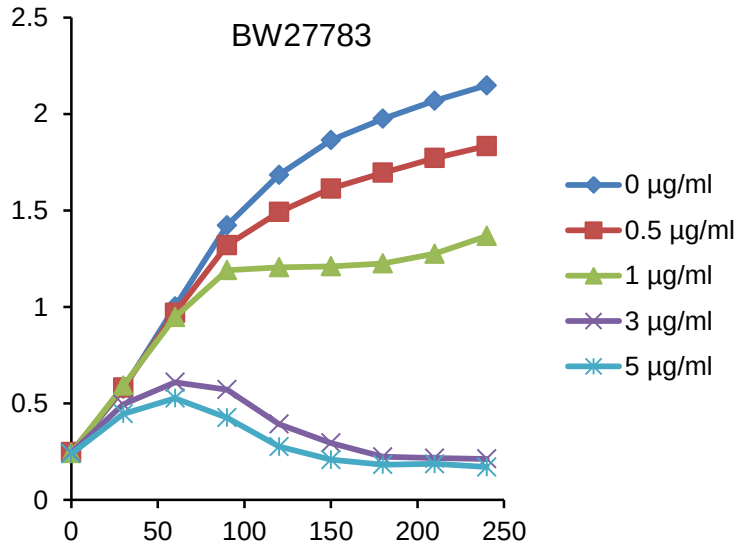

Figure 5.41 WT Growth curves corresponding to figure 3.41

BW27783 WT cells were grown to an OD_{578} of 0.2 before inoculation with varying concentrations of imipenem. Growth was monitored for 4 h every 30 min. Absorbance read at 578 nm shown against time (min).

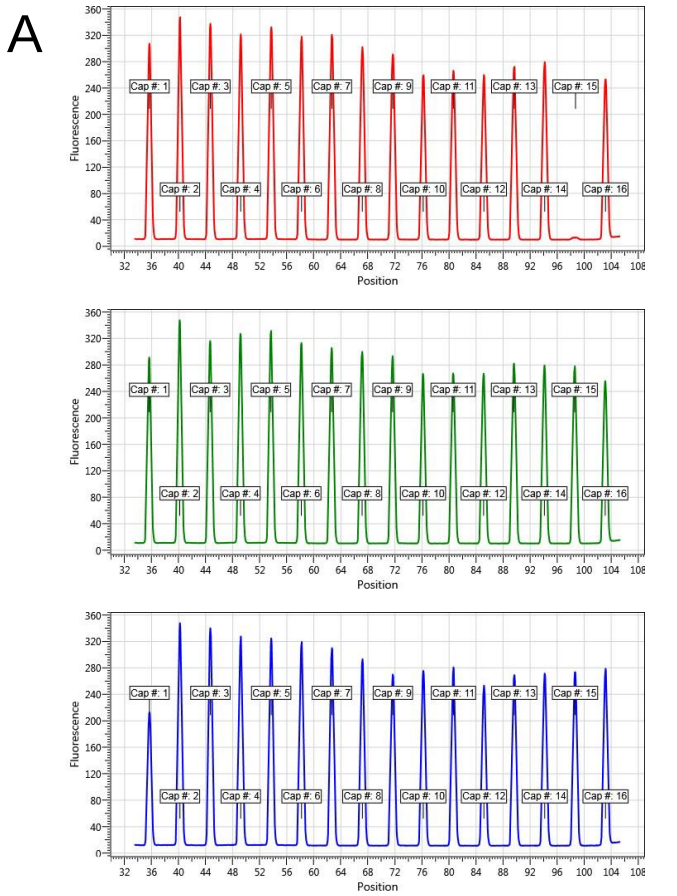

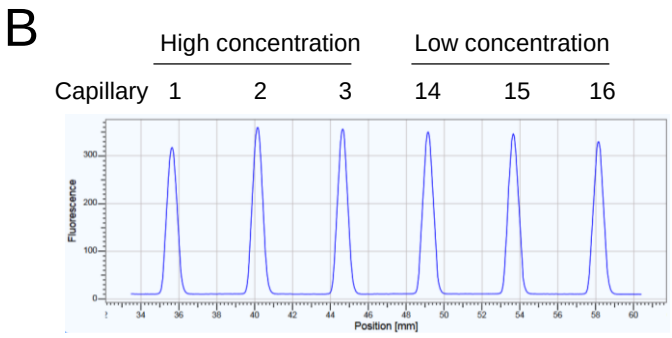

Figure 5.42 Raw MST data corresponding to figure 3.42B

A. Pre-experiment capillary scans of FL-NlpI + MepM. **B.** Capillary scan after SDS-denaturation test of the three samples containing the highest concentration of unlabelled ligand and the three samples containing the lowest concentration. MST measurements were taken at 100% LED power and 20% MST power.

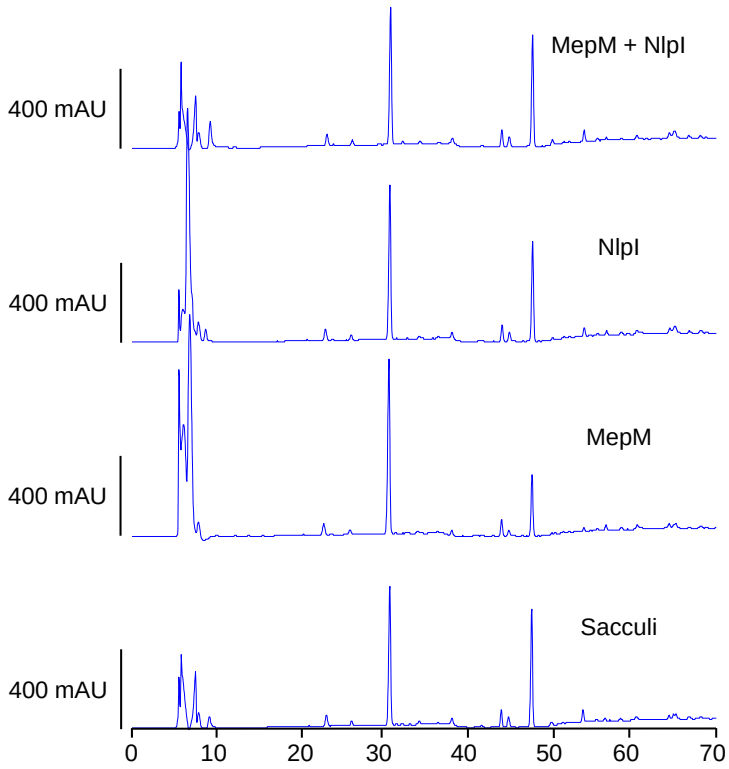

Figure 5.43 HPLC chromatograms corresponding to figure 3.43

Representative HPLC chromatograms for MepM (2 µM) on sacculi in the presence or absence of NlpI (4 µM). Absorbance read at 205 nm shown against time (min).

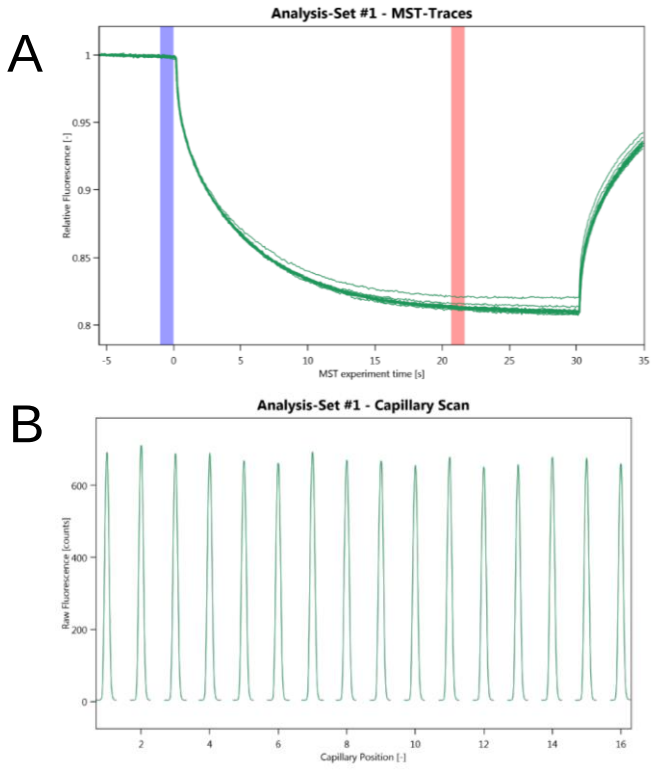

Figure 5.44 Raw MST data corresponding to figure 3.44B

A. Pre-experiment capillary scan of FL-MepA + NlpI at pH 7.5. **B.** MST timetrace. MST measurements were taken at 60% LED power and 60% MST power.

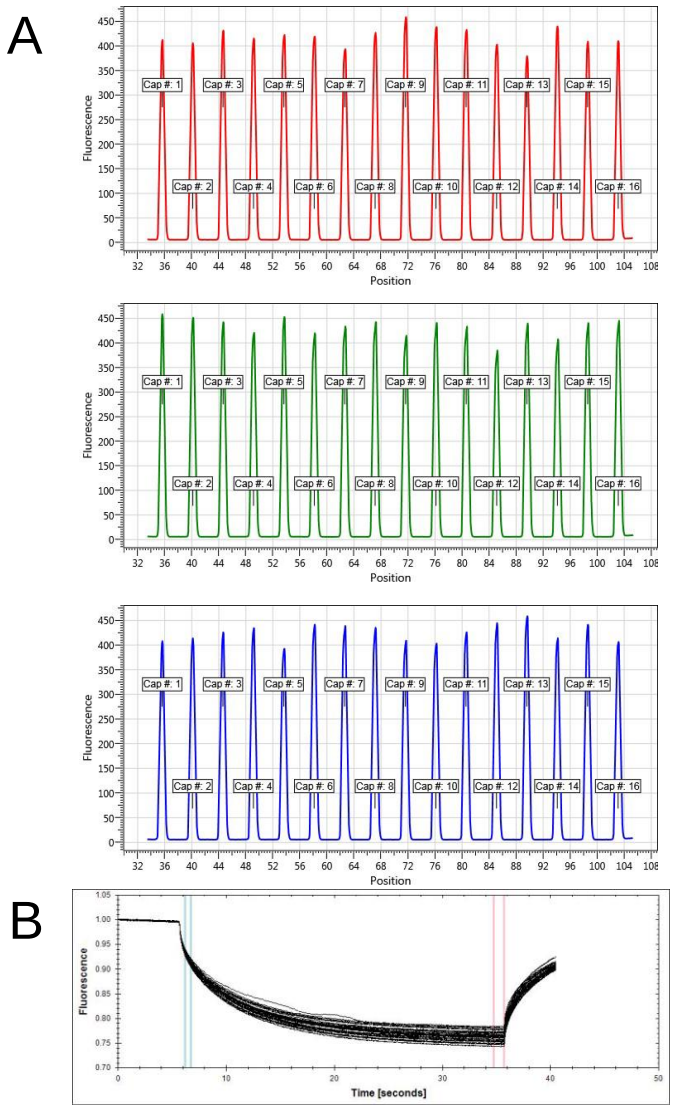

Figure 5.45 Raw MST data corresponding to figure 3.44A

A. Pre-experiment capillary scans of FL-MepA + NlpI at pH 5.0. **B.** MST timetrace. MST measurements were taken at 60% LED power and 60% MST power.

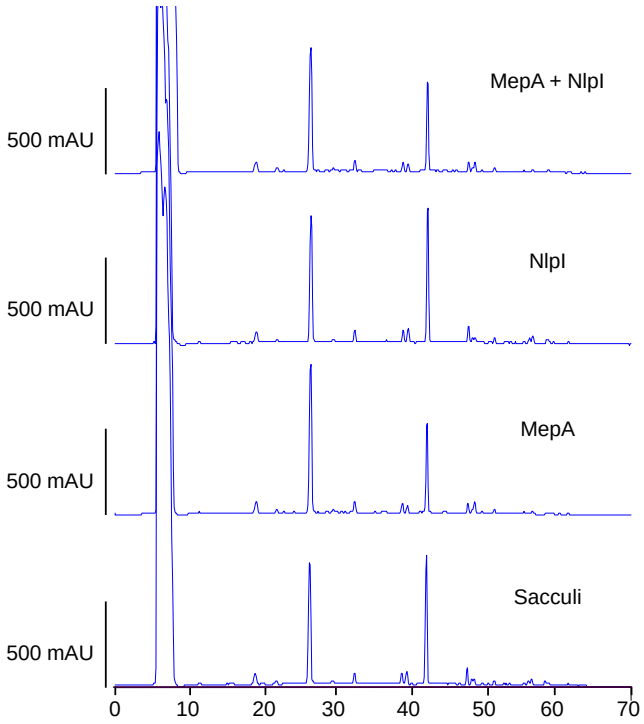

Figure 5.46 HPLC chromatograms corresponding to figure 3.45

Representative HPLC chromatograms for MepA (2 µM) in the presence or absence of NlpI (4 µM). Absorbance read at 205 nm shown against time (min).

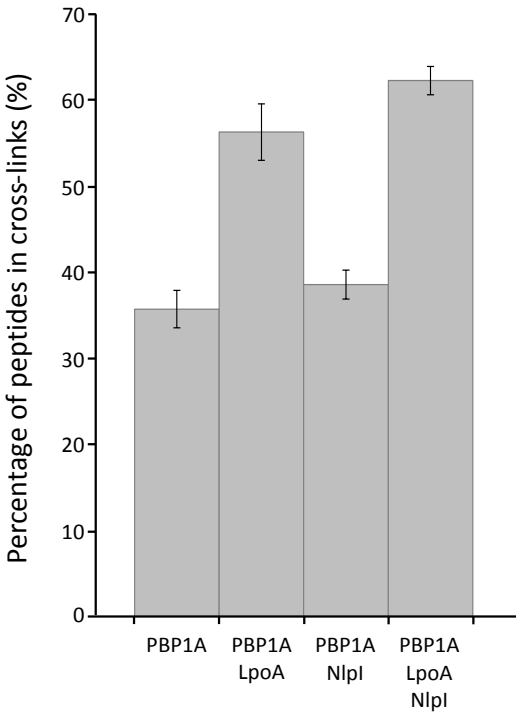

Figure 5.47 NlpI has no effect on the activity of PBP1A

The percentage of peptides in cross-links in PG made by PBP1A (0.5 µM) alone, in the presence of LpoA (2 µM), NlpI (2 µM) or both.

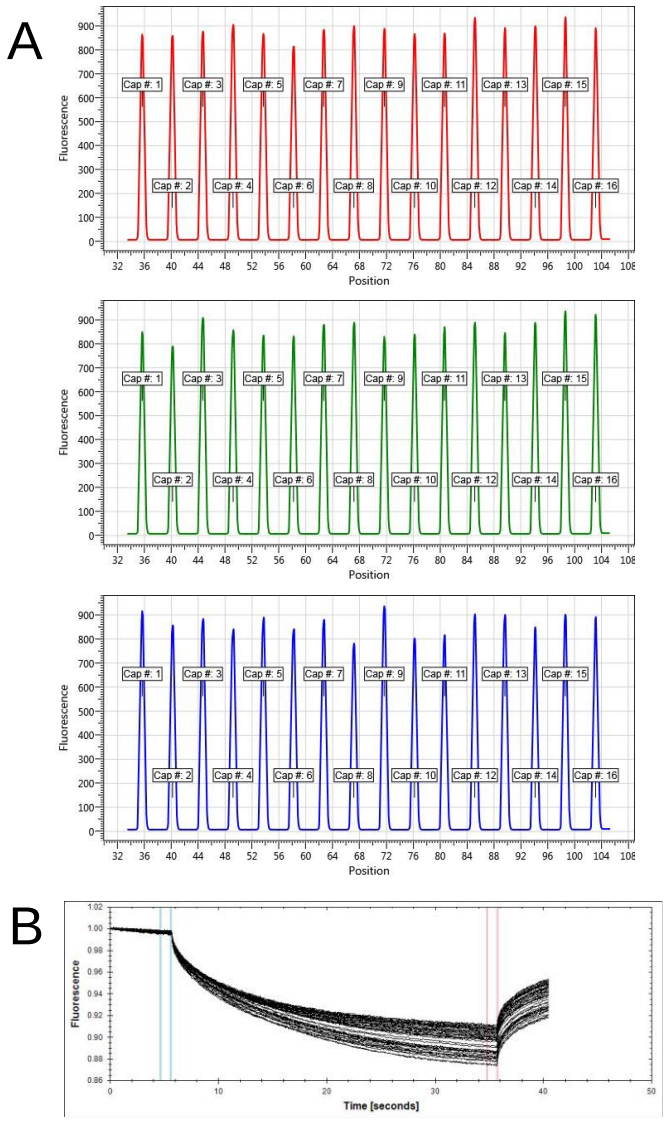

Figure 5.48 Raw MST data corresponding to figure 3.49A

A. Pre-experiment capillary scans of FL-PBP1A + NlpI. **B.** MST timetrace. MST measurements were taken at 80% LED power and 20% MST power.

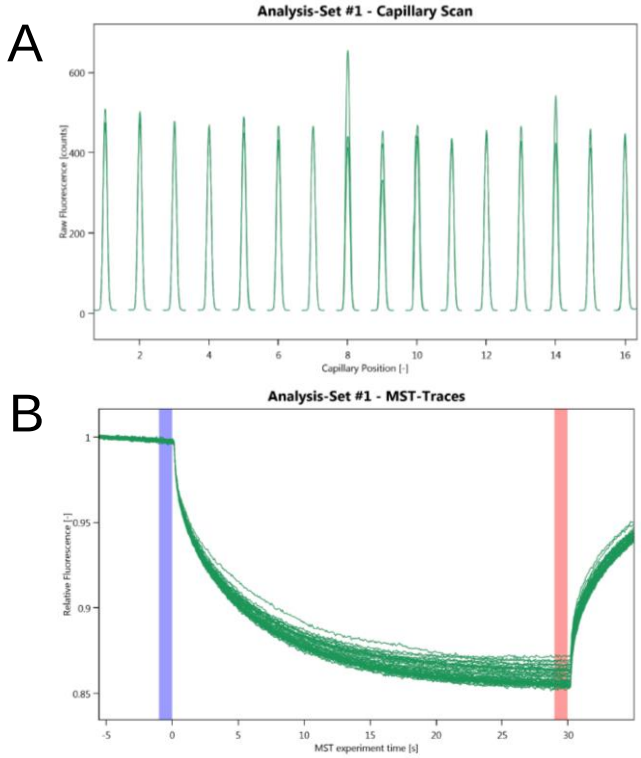

Figure 5.49 Raw MST data corresponding to figure 3.49C

A. Combined pre-experiment capillary scans of FL-NlpI + EnvC **B.** MST timetrace. MST measurements were taken at 80% LED power and 20% MST power.

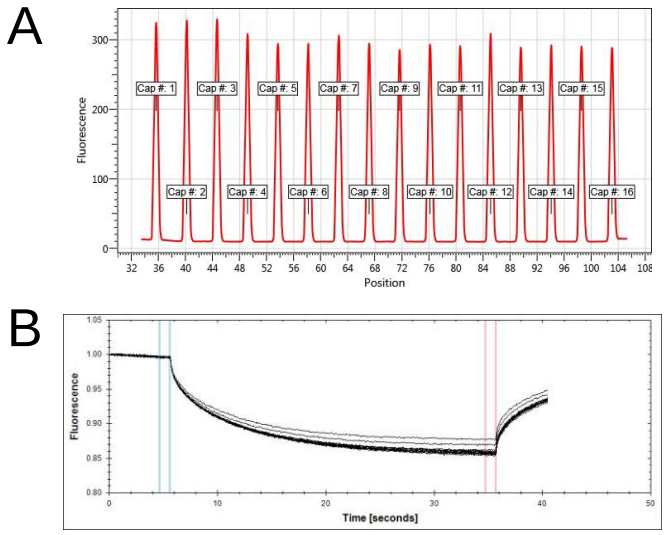

Figure 5.50 Raw MST data corresponding to figure 3.50A

A. Pre-experiment capillary scan of FL-LpoA + NlpI **B.** MST timetrace. MST measurements were taken at 100% LED power and 20% MST power.

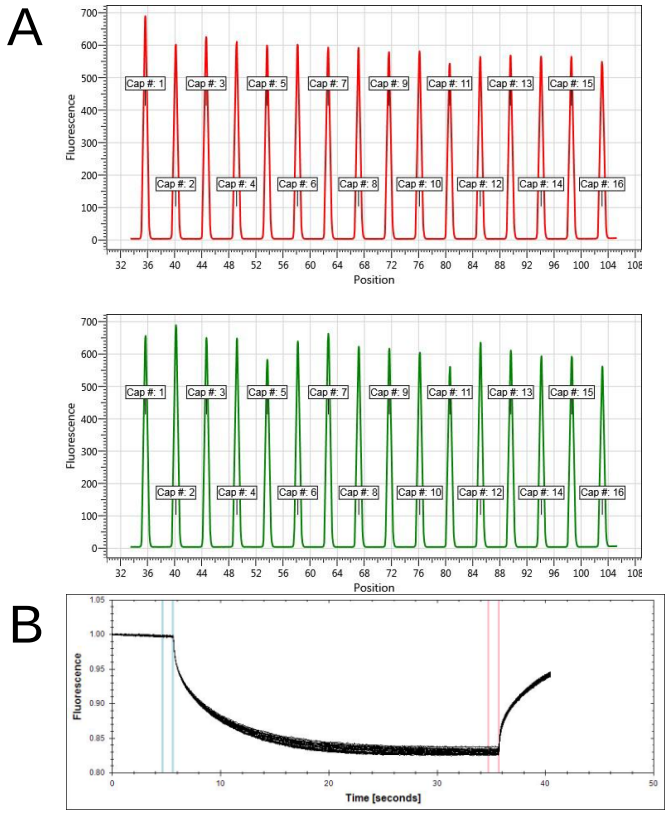

Figure 5.51 Raw MST data corresponding to figure 3.50B

A. Pre-experiment capillary scans of FL-NlpI + Slt. **B.** MST timetrace. MST measurements were taken at 40% LED power and 40% MST power.

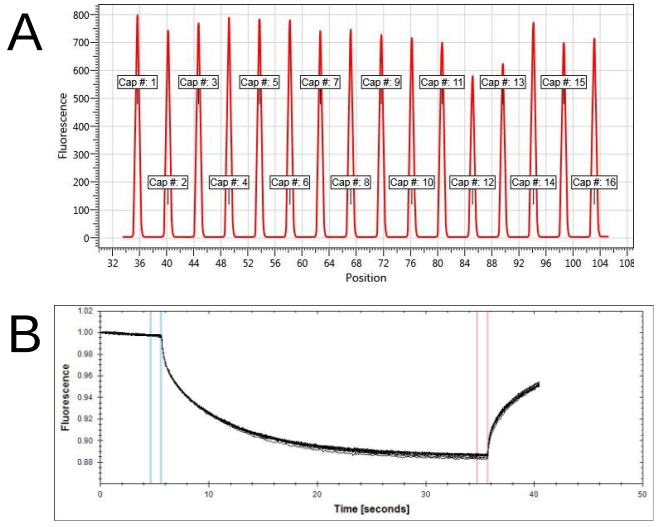

Figure 5.52 Raw MST data corresponding to figure 3.50C

A. Pre-experiment capillary scan of FL-NlpI + LpoB. **B.** MST timetrace. MST measurements were taken at 40% LED power and 20% MST power.

6 Publications

Jean N. L, Bougault C. M, Lodge A, Derouaux A, Callens G, Egan A. J. F, Ayala I, Lewis R. J, Vollmer W, and Simorre J-P. 2014. Elongated structure of the outer-membrane activator of peptidoglycan synthesis LpoA: implications for PBP1A stimulation. *Structure*. **22**:1047–54.

7 References

1. **Marr AG**, **Harvey RJ**, **Trentini WC**. 1966. Growth and division of *Escherichia coli*. *J. Bacteriol.* **91**: 2388–9.

2. **Donachie WD, Begg KJ VM**. 1976. Cell length, cell growth and cell division. *Nature* **264**: 328–33.

3. **Schleifer KH**, **Kandler O**. 1972. Peptidoglycan types of bacterial cell walls and their taxonomic implications. *Bacteriol. Rev.* **36**: 407–77.

4. **Egan AJF**, **Vollmer W**. 2013. The physiology of bacterial cell division. *Ann. N. Y. Acad. Sci.* **1277**: 8–28.

5. **Vollmer W**, **Blanot D**, **de Pedro M a**. 2008. Peptidoglycan structure and architecture. *FEMS Microbiol. Rev.* **32**: 149–67.

6. **Trachtenberg S**. 1998. Mollicutes—wall-less bacteria with internal cytoskeletons. *J. Struct. Biol.* **256**: 244–56.

7. **T. J. Silhavy, D. Kahne and SW**. 2010. The bacterial cell envelope. *Cold Spring Harb. Perspect. Biol.* **2**: 1–16.

8. **Tokuda H**. 2009. Biogenesis of outer membranes in Gram-negative bacteria. *Biosci. Biotechnol. Biochem.* **73**: 465–73.

9. **Weidenmaier C**, **Peschel A**. 2008. Teichoic acids and related cell-wall glycopolymers in Gram-positive physiology and host interactions. *Nat.Rev.Microbiol.* **6**: 276–87.

10. **Vollmer W**. 2008. Structural variation in the glycan strands of bacterial peptidoglycan. *FEMS Microbiol. Rev.* **32**: 287–306.

11. **Hadi T**, **Pfeffer JM**, **Clarke AJ**, **Tanner ME**. 2011. Water-soluble substrates of the peptidoglycan-modifying enzyme O-acetylpeptidoglycan esterase (Ape1) from Neisseria gonorrheae. *J. Org. Chem.* **76**: 1118–25.

12. **Gan L**, **Chen S**, **Jensen GJ**. 2008. Molecular organization of Gram-negative peptidoglycan. *Proc. Natl. Acad. Sci. U. S. A.* **105**: 18953–7.

13. **Vollmer W**, **Höltje JV**. 2004. The architecture of the murein (peptidoglycan) in gram-negative bacteria: Vertical scaffold or horizontal layer(s)? *J. Bacteriol.* **186**: 5978–87.

14. **Wilks JC**, **Slonczewski JL**. 2007. pH of the Cytoplasm and Periplasm of Escherichia coli : Rapid Measurement by Green Fluorescent Protein Fluorimetry □. **189**: 5601–7.

15. **Allison GE**, **Verma NK**. 2000. Serotype-converting bacteriophages Shigella flexneri.

Trends Microbiol. **8**: 17–23.

16. **Vollmer W**, **Seligman SJ**. 2010. Architecture of peptidoglycan: more data and more models. *Trends Microbiol.* **18**: 59–66.

17. **Vollmer W**, **Bertsche U**. 2008. Murein (peptidoglycan) structure, architecture and biosynthesis in Escherichia coli. *Biochim. Biophys. Acta* **1778**: 1714–34.

18. **Turner RD**, **Hurd AF**, **Cadby A**, **Hobbs JK**, **Foster SJ**. 2013. Cell wall elongation mode in Gram-negative bacteria is determined by peptidoglycan architecture. *Nat. Commun.* **4**: 1496.

19. **Harz H**, **Burgdorf K**, **Holtje J-V**. 1990. Isolation and Separation of the Glycan Strands from Murein of Escherichia co//' by Reversed-Phase High-Performance Liquid Chromatography. **128**: 120–8.

20. **Gmeiner J**, **Essig P**, **Martin HH**. 1982. Characterization of minor fragments after digestion of Escherichia coli murein with endo-N,O-diacetylmuramidase from Chalaropsis, and determination of glycan chain length. **138**: 109–12.

21. **Glauner B**, **Höltje J**, **Schwarz U**. 1988. The composition of the murein of Escherichia coli. *J. Biol. Chem.* **263**: 10088–95.

22. **Hughes R**. 1971. Autolysis of Bacillus cereus Cell Walls and Isolation of Structural Components. : 791–802.

23. **Ward J**. 1973. The chain length of the glycans in bacterial cell walls. : 395–8.

24. **Typas A**, **Banzhaf M**, **Gross C a.**, **Vollmer W**. 2012. From the regulation of peptidoglycan synthesis to bacterial growth and morphology. *Nat. Rev. Microbiol.* **10**: 123–36.

25. **Domínguez-Escobar J**, **Chastanet A**, **Crevenna AH**, **Fromion V**, **Wedlich-Söldner R**, **Carballido-López R**. 2011. Processive movement of MreB-associated cell wall biosynthetic complexes in bacteria. *Science* **333**: 225–8.

26. **van Teeffelen S**, **Wang S**, **Furchtgott L**, **Huang KC**, **Wingreen NS**, **Shaevitz JW**, **Gitai Z**. 2011. The bacterial actin MreB rotates, and rotation depends on cell-wall assembly. *Proc. Natl. Acad. Sci. U. S. A.* **108**: 15822–7.

27. **Garner E**, **Bernard R**, **Wang W**. 2011. Coupled, circumferential motions of the cell wall synthesis machinery and MreB filaments in B. subtilis. *Science (80-.).* **333**: 222–5.

28. **Jones LJ**, **Carballido-López R**, **Errington J**. 2001. Control of cell shape in bacteria:

helical, actin-like filaments in Bacillus subtilis. *Cell* **104**: 913–22.

29. **Bi E**, **Lutkenhaus J**. 1991. FtsZ ring structure associated with division in Escherichia coli. *Nature* **354**: 161–4.

30. **Aarsman MEG**, **Piette A**, **Fraipont C**, **Vinkenvleugel TMF**, **Nguyen-Distèche M**, **den Blaauwen T**. 2005. Maturation of the Escherichia coli divisome occurs in two steps. *Mol. Microbiol.* **55**: 1631–45.

31. **Typas A**, **Banzhaf M**, **van den Berg van Saparoea B**, **Verheul J**, **Biboy J**, **Nichols RJ**, **Zietek M**, **Beilharz K**, **Kannenberg K**, **von Rechenberg M**, **Breukink E**, **den Blaauwen T**, **Gross C a**, **Vollmer W**. 2010. Regulation of peptidoglycan synthesis by outer-membrane proteins. *Cell* **143**: 1097–109.

32. **Paradis-Bleau C**, **Markovski M**, **Uehara T**, **Lupoli TJ**, **Walker S**, **Kahne DE**, **Bernhardt TG**. 2010. Lipoprotein cofactors located in the outer membrane activate bacterial cell wall polymerases. *Cell* **143**: 1110–20.

33. **Badet B, Vermoote P, Haumont PY, Lederer F LF**. 1987. Glucosamine synthetase from Escherichia coli: purification, properties, and glutamine-utilizing site location. *Chem, W H J Biol* **26**: 1940–8.

34. **Mengin-Lecreulx D**, **van Heijenoort J**. 1994. Characterization of the glmU gene product as a Copurification of Glucosamine-1-Phosphate Acetyltransferase and N-Acetylglucosamine-1-Phosphate Uridyltransferase Activities of Escherichia coli : Characterization of the glmU Gene Product as a Bifunctional E. *J. Bacteriol.* **176**: 5788–95.

35. **Marquardt JL**, **Siegele DA**, **Kolter R**, **Walsh CT**. 1992. Cloning and sequencing of Escherichia coli murZ and purification of its product, a UDP-N-acetylglucosamine enolpyruvyl transferase. *J Bacteriol* **174**: 5748–52.

36. **Brown ED**, **Vivas EI**, **Walsh CT**, **Kolter R**. 1995. MurA (MurZ), the enzyme that catalyzes the first committed step in peptidoglycan biosynthesis, is essential in Escherichia coli. *J. Bacteriol.* **177**: 4194–7.

37. **Marquardt JL**, **Brown ED**, **Lane WS**, **Haley TM**, **Ichikawa Y**, **Wong CH**, **Walsh CT**. 1994. Kinetics, stoichiometry, and identification of the reactive thiolate in the inactivation of UDP-GlcNAc enolpyruvoyl transferase by the antibiotic fosfomycin. *Biochemistry* **33**: 10646–51.

38. **Bouhss A**, **Trunkfield AE**, **Bugg TDH**, **Mengin-Lecreulx D**. 2008. The biosynthesis of peptidoglycan lipid-linked intermediates. *FEMS Microbiol. Rev.* **32**: 208–33.

39. **Bouhss A**, **Dementin S**, **van Heijenoort J**, **Parquet C**, **Blanot D**. 2002. *Enzyme Kinetics and Mechanism Part F: Detection and Characterization of Enzyme Reaction Intermediates*. Elsevier.

40. **Wild J**, **Hennig J**, **Lobocka M**, **Walczak W**, **Klopotowski T**. 1985. Identification of the dadX gene coding for the predominant isozyme of alanine racemase in Escherichia coli K12. *MGG Mol. Gen. Genet.* **198**: 315–22.

41. **Zawadzke LE**, **Bugg TDH**, **Walsh CT**. 1991. Existence of two D-alanine:D-alanine ligases in Escherichia coli: cloning and sequencing of the ddlA gene and purification and characterization of the DdlA and DdlB enzymes. *Society* **30**: 1673–82.

42. **Doublet P**, **Van Heijenoort J**, **Bohin JP**, **Mengin-Lecreulx D**. 1993. The murI gene of Escherichia coli is an essential gene that encodes a glutamate racemase activity. *J. Bacteriol.* **175**: 2970–9.

43. **Born TL**, **Blanchard JS**. 1999. Structure/function studies on enzymes in the diaminopimelate pathway of bacterial cell wall biosynthesis. *Curr. Opin. Chem. Biol.* **3**: 607–13.

44. **Bouhss A**, **Crouvoisier M**, **Blanot D**, **Mengin-Lecreulx D**. 2004. Purification and characterization of the bacterial MraY translocase catalyzing the first membrane step of peptidoglycan biosynthesis. *J. Biol. Chem.* **279**: 29974–80.

45. **Barreteau H**, **Kovac A**, **Boniface A**, **Sova M**, **Gobec S**, **Blanot D**. 2008. Cytoplasmic steps of peptidoglycan biosynthesis. *FEMS Microbiol. Rev.* **32**: 168–207.

46. **Typas A**, **Banzhaf M**, **Gross C a**, **Vollmer W**. 2012. From the regulation of peptidoglycan synthesis to bacterial growth and morphology. *Nat. Rev. Microbiol.* **10**: 123–36.

47. **Sham L-T**, **Butler EK**, **Lebar MD**, **Kahne D**, **Bernhardt TG**, **Ruiz N**. 2014. MurJ is the flippase of lipid-linked precursors for peptidoglycan biogenesis. *Science (80-.).* **345**: 220–2.

48. **Mohammadi T**, **van Dam V**, **Sijbrandi R**, **Vernet T**, **Zapun A**, **Bouhss A**, **Diepeveen-de Bruin M**, **Nguyen-Distèche M**, **de Kruijff B**, **Breukink E**. 2011. Identification of FtsW as a transporter of lipid-linked cell wall precursors across the membrane. *EMBO J.* **30**: 1425–32.

49. **Perlstein DL**, **Zhang Y**, **Wang TS**, **Kahne DE**, **Walker S**. 2007. The direction of glycan chain elongation by peptidoglycan glycosyltransferases. *J. Am. Chem. Soc.* **129**: 12674–5.

50. **Höltje J V**. 1998. Growth of the stress-bearing and shape-maintaining murein sacculus of Escherichia coli. *Microbiol. Mol. Biol. Rev.* **62**: 181–203.

51. **Sauvage E**, **Kerff F**, **Terrak M**, **Ayala J a**, **Charlier P**. 2008. The penicillin-binding proteins: structure and role in peptidoglycan biosynthesis. *FEMS Microbiol. Rev.* **32**: 234–58.

52. **Ward JB**. 1984. Biosynthesis of peptidoglycan: points of attack by wall inhibitors. *Pharmacol. Ther.* **25**: 327–69.

53. **Roy R**, **Yang P**, **Kodali S**, **Xiong Y**. 2001. Direct interaction of a vancomycin derivative with bacterial enzymes involved in cell wall biosynthesis. *Chem. Biol.* **8**: 1095–106.

54. **van Heijenoort J**, **Gutmann L**. 2000. Correlation between the structure of the bacterial peptidoglycan monomer unit, the specificity of transpeptidation, and susceptibility to beta-lactams. *Proc. Natl. Acad. Sci. U. S. A.* **97**: 5028–30.

55. **Macheboeuf P**, **Contreras-Martel C**, **Job V**, **Dideberg O**, **Dessen A**. 2006. Penicillin binding proteins: key players in bacterial cell cycle and drug resistance processes. *FEMS Microbiol. Rev.* **30**: 673–91.

56. **Dmitriev B a**, **Toukach F V**, **Schaper K**, **Holst O**, **Rietschel ET**, **Ehlers S**. 2003. Tertiary Structure of Bacterial Murein : the Scaffold Model Tertiary Structure of Bacterial Murein : the Scaffold Model. *J. Bacteriol.* **185**: 3458–68.

57. **Höltje J-V**. 1993. "Three for one" — a Simple Growth Mechanism that Guarantees a Precise Copy of the Thin, Rod-Shaped Murein Sacculus of Escherichia coli. In *Bacterial Growth and Lysis-Metabolism and Structure of the Bacterial Sacculus - M. A. de Pedro, J.-V. Höltje, W. Löffelhardt*. p 419–26.

58. **Höltje J V**, **Heidrich C**. 2000. Enzymology of elongation and constriction of the murein sacculus of Escherichia coli. *Biochimie* **83**: 103–8.

59. **Höltje J**. 1996. Molecular interplay of murein synthases and murein hydrolases in Escherichia coli. *Microb Drug Resist.* **2**: 99–103.

60. **Huang KC**, **Mukhopadhyay R**, **Wen B**, **Gitai Z**, **Wingreen NS**. 2008. Cell shape and cell-wall organization in Gram-negative bacteria. *Proc. Natl. Acad. Sci. U. S. A.* **105**: 19282–7.

61. **Meisner J**, **Llopis PM**, **Sham L**, **Garner E**, **Bernhardt TG**, **Rudner DZ**. 2013. FtsEX is required for CwlO peptidoglycan hydrolase activity during cell wall

elongation in Bacillus subtilis. **89**: 1069–83.

62. **Li G-W**, **Burkhardt D**, **Gross C**, **Weissman JS**. 2014. Quantifying absolute protein synthesis rates reveals principles underlying allocation of cellular resources. *Cell* **157**: 624–35.

63. **Yousif SY**, **Broome-Smith JK**, **Spratt BG**. 1985. Lysis of Escherichia coli by beta-lactam antibiotics: deletion analysis of the role of penicillin-binding proteins 1A and 1B. *J. Gen. Microbiol.* **131**: 2839–45.

64. **Denome S a**, **Elf PK**, **Henderson T a**, **Nelson DE**, **Young KD**. 1999. Escherichia coli mutants lacking all possible combinations of eight penicillin binding proteins: viability, characteristics, and implications for peptidoglycan synthesis. *J. Bacteriol.* **181**: 3981–93.

65. **Lovering AL**, **Safadi SS**, **Strynadka NCJ**. 2012. Structural perspective of peptidoglycan biosynthesis and assembly. *Annu. Rev. Biochem.* **81**: 451–78.

66. **de Sousa Borges A**, **de Keyzer J**, **Driessen AJM**, **Scheffers D-J**. 2015. The Escherichia coli membrane protein insertase YidC assists in the biogenesis of penicillin binding proteins. *J. Bacteriol.* **197**: 1444–50.

67. **Born P**, **Breukink E**, **Vollmer W**. 2006. In vitro synthesis of cross-linked murein and its attachment to sacculi by PBP1A from Escherichia coli. *J. Biol. Chem.* **281**: 26985–93.

68. **Ghuysen J-M**. 1991. Serine β-lactamases and penicillin-binding proteins. *Annu. Rev. Microbiol.* **45**: 37–45.

69. **Goffin C**, **Ghuysen JM**. 1998. Multimodular penicillin-binding proteins: an enigmatic family of orthologs and paralogs. *Microbiol. Mol. Biol. Rev.* **62**: 1079–93.

70. **Banzhaf M**, **van den Berg van Saparoea B**, **Terrak M**, **Fraipont C**, **Egan A**, **Philippe J**, **Zapun A**, **Breukink E**, **Nguyen-Distèche M**, **den Blaauwen T**, **Vollmer W**. 2012. Cooperativity of peptidoglycan synthases active in bacterial cell elongation. *Mol. Microbiol.* **85**: 179–94.

71. **Sung M-T**, **Lai Y-T**, **Huang C-Y**, **Chou L-Y**, **Shih H-W**, **Cheng W-C**, **Wong C-H**, **Ma C**. 2009. Crystal structure of the membrane-bound bifunctional transglycosylase PBP1b from Escherichia coli. *Proc. Natl. Acad. Sci. U. S. A.* **106**: 8824–9.

72. **Lovering AL**, **de Castro LH**, **Lim D**, **Strynadka NC**. 2007. Structural insight into the transglycosylation step of bacterial cell-wall biosynthesis. *Science (80-.).* **315**: 1402–5.

73. **Yuan Y**, **Barrett D**, **Zhang Y**, **Kahne D**, **Sliz P**, **Walker S**. 2007. Crystal structure of a peptidoglycan glycosyltransferase suggests a model for processive glycan chain synthesis. *PNAS* **104**: 5348–54.

74. **Typas A**, **Banzhaf M**, **van den Berg van Saparoea B**, **Verheul J**, **Biboy J**, **Nichols RJ**, **Zietek M**, **Beilharz K**, **Kannenberg K**, **von Rechenberg M**, **Breukink E**, **den Blaauwen T**, **Gross C a**, **Vollmer W**. 2010. Regulation of peptidoglycan synthesis by outer-membrane proteins. *Cell* **143**: 1097–109.

75. **Egan AJF**, **Jean NL**, **Koumoutsi A**, **Bougault CM**, **Biboy J**, **Sassine J**, **Solovyova A**, **Breukink E**, **Typas A**, **Vollmer W**, **Simorre J-P**. 2014. Outer-membrane lipoprotein LpoB spans the periplasm to stimulate the peptidoglycan synthase PBP1B. *Proc. Natl. Acad. Sci.*

76. **Zijderveld C**, **Aarsman M**, **Blaauwen T Den**, **Nanninga N**. 1991. Penicillin-Binding Protein 1B of Escherichia coli Exists in Dimeric forms. *J. Bacteriol.* **173**: 5740–574.

77. **Schiffer G**. 1999. Cloning and Characterization of PBP 1C, a Third Member of the Multimodular Class A Penicillin-binding Proteins of Escherichia coli. *J. Biol. Chem.* **274**: 32031–9.

78. **Spratt BG**. 1975. Distinct penicillin binding proteins involved in the division, elongation, and shape of Escherichia coli K12. *Proc. Natl. Acad. Sci. U. S. A.* **72**: 2999–3003.

79. **Den Blaauwen T**, **Aarsman MEG**, **Vischer NOE**, **Nanninga N**. 2003. Penicillin-binding protein PBP2 of Escherichia coli localizes preferentially in the lateral wall and at mid-cell in comparison with the old cell pole. *Mol. Microbiol.* **47**: 539–47.

80. **Sykes RB**, **Bonner DP**. 1985. Discovery and development of the monobactams. *Rev. Infect. Dis.* **7**: Noe.

81. **Spratt BG**. 1977. Temperature-sensitive cell division mutants of Escherichia coli with thermolabile penicillin-binding proteins. *J. Bacteriol.* **131**: 293–305.

82. **Fraipont C**, **Alexeeva S**, **Wolf B**, **van der Ploeg R**, **Schloesser M**, **den Blaauwen T**, **Nguyen-Distèche M**. 2011. The integral membrane FtsW protein and peptidoglycan synthase PBP3 form a subcomplex in Escherichia coli. *Microbiology* **157**: 251–9.

83. **Sauvage E**, **Derouaux A**, **Fraipont C**, **Joris M**, **Herman R**, **Rocaboy M**, **Schloesser M**, **Dumas J**, **Kerff F**, **Nguyen-Distèche M**, **Charlier P**. 2014. Crystal structure of penicillin-binding protein 3 (PBP3) from Escherichia coli. *PLoS One* **9**: e98042.

84. **Han S**, **Caspers N**, **Zaniewski RP**, **Lacey BM**, **Tomaras AP**, **Feng X**, **Geoghegan KF**, **Shanmugasundaram V**. 2011. Distinctive attributes of beta-lactam target proteins in Acinetobacter baumannii relevant to development of new antibiotics. *J Am Chem Soc* **133**: 20536–45.

85. **Sainsbury S**, **Bird L**, **Rao V**, **Shepherd SM**, **Stuart DI**, **Hunter WN**, **Owens RJ**, **Ren J**. 2011. Crystal structures of penicillin-binding protein 3 from Pseudomonas aeruginosa: comparison of native and antibiotic-bound forms. *J. Mol. Biol.* **405**: 173–84.

86. **Derouaux A**, **Wolf B**, **Fraipont C**, **Breukink E**, **Nguyen-Distèche M**, **Terrak M**. 2008. The monofunctional glycosyltransferase of Escherichia coli localizes to the cell division site and interacts with penicillin-binding protein 3, FtsW, and FtsN. *J. Bacteriol.* **190**: 1831–4.

87. **Berardino M Di**, **Dijkstra A**, **Sttiber D**, **Keck W**, **Gubler M**. 1996. The monofunctional glycosyltransferase of Escherichia coli is a member of a new class of peptidoglycan-synthesising enzymes Overexpression and determination of the glycan-polymerising activity. **392**: 184–8.

88. **Egan AJF**, **Biboy J**, **van't Veer I**, **Breukink E**, **Vollmer W**. 2015. Activities and regulation of peptidoglycan synthases. *Philos. Trans. R. Soc. B Biol. Sci.* **370**: 20150031.

89. **Bertsche U**, **Kast T**, **Wolf B**, **Fraipont C**, **Aarsman MEG**, **Kannenberg K**, **von Rechenberg M**, **Nguyen-Distèche M**, **den Blaauwen T**, **Höltje J-V**, **Vollmer W**. 2006. Interaction between two murein (peptidoglycan) synthases, PBP3 and PBP1B, in Escherichia coli. *Mol. Microbiol.* **61**: 675–90.

90. **Lupoli TJ**, **Lebar MD**, **Markovski M**, **Bernhardt T**, **Kahne D**, **Walker S**. 2014. Lipoprotein Activators Stimulate Escherichia coli Penicillin-Binding Proteins by Di ff erent Mechanisms. **136**: 52–5.

91. **Gray AN**, **Egan AJF**, **Van't Veer IL**, **Verheul J**, **Colavin A**, **Koumoutsi A**, **Biboy J**, **Altelaar a FM**, **Damen MJ**, **Huang KC**, **Simorre J-P**, **Breukink E**, **den Blaauwen T**, **Typas A**, **Gross C a**, **Vollmer W**. 2015. Coordination of peptidoglycan synthesis and outer membrane constriction during Escherichia coli cell division. *Elife* **4**: 1–29.

92. **Gerding M a**, **Ogata Y**, **Pecora ND**, **Niki H**, **de Boer P a J**. 2007. The trans-envelope Tol-Pal complex is part of the cell division machinery and required for proper outer-membrane invagination during cell constriction in E. coli. *Mol. Microbiol.* **63**: 1008–

25.

93. **Krachler AM**, **Sharma A**, **Cauldwell A**, **Papadakos G**, **Kleanthous C**. 2010. TolA modulates the oligomeric status of YbgF in the bacterial periplasm. *J. Mol. Biol.* **403**: 270–85.

94. **Cascales E**, **Gavioli M**, **Sturgis JN**, **Lloubes R**. 2000. Proton motive force drives the interaction of the inner membrane TolA and outer membrane Pal proteins in Escherichia coli. *Mol. Microbiol.* **38**: 904–15.

95. **Jean NL**, **Bougault CM**, **Lodge A**, **Derouaux A**, **Callens G**, **Egan AJF**, **Ayala I**, **Lewis RJ**, **Vollmer W**, **Simorre J-P**. 2014. Elongated structure of the outer-membrane activator of peptidoglycan synthesis LpoA: implications for PBP1A stimulation. *Structure* **22**: 1047–54.

96. **Blatch GL**, **Lässle M**. 1999. The tetratricopeptide repeat: a structural motif mediating protein-protein interactions. *Bioessays* **21**: 932–9.

97. **Lupoli TJ**, **Lebar MD**, **Markovski M**, **Bernhardt T**, **Kahne D**, **Walker S**. 2014. Lipoprotein Activators Stimulate Escherichia coli Penicillin-Binding Proteins by Different Mechanisms. *J. Am. Chem. Soc.* **136**: 52–5.

98. **Akerley BJ**, **Rubin EJ**, **Novick VL**, **Amaya K**, **Judson N**, **Mekalanos JJ**. 2002. A genome-scale analysis for identification of genes required for growth or survival of Haemophilus influenzae. *Proc. Natl. Acad. Sci. U. S. A.* **99**: 966–71.

99. **Wong SM**, **Akerley BJ**. 2003. Inducible expression system and marker-linked mutagenesis approach for functional genomics of Haemophilus influenzae. *Gene* **316**: 177–86.

100. **Vijayalakshmi J**, **Akerley BJ**, **Saper M a**. 2008. Structure of YraM, a protein essential for growth of Haemophilus influenzae. *Proteins* **73**: 204–17.

101. **Goodell EW**, **Schwarz U**. 1985. Release of cell wall peptides into culture medium by exponentially growing Escherichia coli. *J. Bacteriol.* **162**: 391–7.

102. **Frirdich E**, **Gaynor EC**. 2013. Peptidoglycan hydrolases, bacterial shape, and pathogenesis. *Curr. Opin. Microbiol.* **16**: 767–78.

103. **Vollmer W**, **Joris B**, **Charlier P**, **Foster S**. 2008. Bacterial peptidoglycan (murein) hydrolases. *FEMS Microbiol. Rev.* **32**: 259–86.

104. **van Heijenoort J**. 2011. Peptidoglycan hydrolases of Escherichia coli. *Microbiol. Mol. Biol. Rev.* **75**: 636–63.

105. **Goodell EW**. 1985. Recycling of murein by Escherichia coli. *J. Bacteriol.* **163**: 305–10.

106. **Jacobs C**, **Huang LJ**, **Bartowsky E**, **Normark S**, **Park JT**. 1994. Bacterial cell wall recycling provides cytosolic muropeptides as effectors for beta-lactamase induction. *EMBO J.* **13**: 4684–94.

107. **Korat B**, **Mottl H**, **Keck W**. 1991. Penicillin-binding protein 4 of *Escherichia coli*: molecular cloning of the *dacB* gene, controlled overexpression, and alterations in murein composition. *Mol. Microbiol.* **5**: 675–84.

108. **Singh SK**, **Parveen S**, **SaiSree L**, **Reddy M**. 2015. Regulated proteolysis of a cross-link-specific peptidoglycan hydrolase contributes to bacterial morphogenesis. *Proc. Natl. Acad. Sci. U. S. A.* **112**: 10956–61.

109. **Gondré B**, **Flouret B**, **van Heijenoort J**. 1973. Release of D-alanyl-D-alanine from the precursor of the cell wall peptidoglycan by a peptidase of Escherichia coli K 12. *Biochimie.* **55**: 685–91.

110. **Lessard I a**, **Pratt SD**, **McCafferty DG**, **Bussiere DE**, **Hutchins C**, **Wanner BL**, **Katz L**, **Walsh CT**. 1998. Homologs of the vancomycin resistance D-Ala-D-Ala dipeptidase VanX in Streptomyces toyocaensis, Escherichia coli and Synechocystis: attributes of catalytic efficiency, stereoselectivity and regulation with implications for function. *Chem. Biol.* **5**: 489–504.

111. **Magnet S**, **Arbeloa A**, **Mainardi J**, **Hugonnet J**, **Fourgeaud M**, **Dubost L**, **Marie A**, **Delfosse V**, **Mayer C**, **Rice LB**, **Arthur M**. 2007. Specificity of L , D - Transpeptidases from Gram-positive Bacteria Producing Different Peptidoglycan Chemotypes. **282**: 13151–9.

112. **Sanders CC**, **Bradford P a**, **Ehrhardt a F**, **Bush K**, **Young KD**, **Henderson T a**, **Sanders WE**. 1997. Penicillin-binding proteins and induction of AmpC beta-lactamase. *Antimicrob. Agents Chemother.* **41**: 2013–5.

113. **Mottl H**, **Terpstra P**, **Keck W**. 1991. Penicillin-binding protein 4 of Escherichia coli shows a novel type of primary structure among penicillin-interacting proteins. *FEMS Microbiol. Lett.* **62**: 213–20.

114. **Kitano K**, **Williamson R**, **Tomasz A**. 1980. Murein hydrolase defects in the B-lactam tolerant mutants of Escherichia coli. *FEMS Microbiol. Lett.* **7**: 133–6.

115. **Kishida H**, **Unzai S**, **Roper DI**, **Lloyd A**, **Park S-Y**, **Tame JRH**. 2006. Crystal structure of penicillin binding protein 4 (dacB) from Escherichia coli, both in the native

form and covalently linked to various antibiotics. *Biochemistry* **45**: 783–92.

116. **Sauvage E**, **Herman R**, **Petrella S**, **Duez C**, **Bouillenne F**, **Frère J-M**, **Charlier P**. 2005. Crystal structure of the Actinomadura R39 DD-peptidase reveals new domains in penicillin-binding proteins. *J. Biol. Chem.* **280**: 31249–56.

117. **Sauvage E**, **Duez C**, **Herman R**, **Kerff F**, **Petrella S**, **Anderson JW**, **Adediran SA**, **Pratt RF**, **Frère JM**, **Charlier P**. 2007. Crystal Structure of the Bacillus subtilis Penicillin-binding Protein 4a, and its Complex with a Peptidoglycan Mimetic Peptide. *J. Mol. Biol.* **371**: 528–39.

118. **Clarke TB**, **Kawai F**, **Park S-Y**, **Tame JRH**, **Dowson CG**, **Roper DI**. 2009. Mutational analysis of the substrate specificity of Escherichia coli penicillin binding protein 4. *Biochemistry* **48**: 2675–83.

119. **Henderson TA**, **Templin M**, **Young KD**. 1995. Identification and Cloning of the Gene Encoding Penicillin- Binding Protein 7 of Escherichia coli. **177**: 2074–9.

120. **Dougherty TJ**, **Kennedy K**, **Kessler RE**, **Pucci MJ**, **Dougherty TJ**, **Kennedy K**, **Kessler RE**. 1996. Direct quantitation of the number of individual penicillin-binding proteins per cell in Escherichia coli . Direct Quantitation of the Number of Individual Penicillin-Binding Proteins per Cell in Escherichia coli † Downloaded from http://jb.asm.org/ on May. *J. Bacteriol.* **178**: 6110–5.

121. **Meberg BM**, **Paulson AL**, **Priyadarshini R**, **Young KD**. 2004. Endopeptidase Penicillin-Binding Proteins 4 and 7 Play Auxiliary Roles in Determining Uniform Morphology of Escherichia coli. *Society* **186**: 8326–36.

122. **Tina ROMEIS and Joachim-Volker HOLTE**. 1994. Penicillin-binding protein 7/8 of Escherichia coli is a DD-endopeptidase. *Aging (Albany. NY).* **224**: 597–604.

123. **Henderson TA**, **Dombrosky PM**, **Young KD**. 1994. Artifactual processing of penicillin-binding proteins 7 and 1b by the OmpT protease of Escherichia coli. *J. Bacteriol.* **176**: 256–9.

124. **Romeis T**, **Holtje J-V**. 1994. Specific Interaction of Penicillin-binding Proteins 3 and 7/8 with Soluble Lytic Transglycosylase in Escherichia coli. *J. Bacteriol.* **269**: 21603–7.

125. **Marcyjaniak M**, **Odintsov SG**, **Sabala I**, **Bochtler M**. 2004. Peptidoglycan amidase MepA is a LAS metallopeptidase. *J. Biol. Chem.* **279**: 43982–9.

126. **Firczuk M**, **Bochtler M**. 2007. Mutational analysis of peptidoglycan amidase MepA.

Biochemistry **46**: 120–8.

127. **Keck W**, **van Leeuwen AM**, **Huber M**, **Goodell EW**. 1990. Cloning and characterization of mepA, the structural gene of the penicillin-insensitive murein endopeptidase from Escherichia coli. *Mol. Microbiol.* **4**: 209–19.

128. **H, Engel, van Leeuwen A, Dijkstra A KW**. 1992. Enzymatic preparation of 1,6-anhydro-muropeptides by immobilized murein hydrolases from Escherichia coli fused to staphylococcal protein A. *Appl Microbiol Biotechnol.* **37**: 772–83.

129. **Singh SK**, **SaiSree L**, **Amrutha RN**, **Reddy M**. 2012. Three redundant murein endopeptidases catalyse an essential cleavage step in peptidoglycan synthesis of Escherichia coli K12. *Mol. Microbiol.* **86**: 1036–51.

130. **Bisicchia P**, **Noone D**, **Lioliou E**, **Howell A**, **Quigley S**, **Jensen T**, **Jarmer H**, **Devine KM**. 2007. The essential YycFG two-component system controls cell wall metabolism in Bacillus subtilis. *Mol. Microbiol.* **65**: 180–200.

131. **Aramini JM**, **Rossi P**, **Huang YJ**, **Zhao L**, **Jiang M**, **Maglaqui M**, **Xiao R**, **Locke J**, **Nair R**, **Rost B**, **Acton TB**, **Inouye M**, **Montelione GT**. 2008. Solution NMR structure of the NlpC/P60 domain of lipoprotein Spr from Escherichia coli: Structural evidence for a novel cysteine peptidase catalytic triad. *Biochemistry* **47**: 9715–7.

132. **Hara H**, **Abe N**, **Nakakouji M**, **Nishimura Y**, **Horiuchi K**. 2009. Overproduction of penicillin-binding protein 7 suppresses thermosensitive growth defect at low osmolarity due to an spr mutation of Escherichia coli. *Microb Drug Resist.* : 63–72.

133. **Finn RD**, **Tate J**, **Mistry J**, **Coggill PC**, **Sammut SJ**, **Hotz H**, **Ceric G**, **Forslund K**, **Eddy SR**, **Sonnhammer ELL**, **Bateman A**. 2008. The Pfam protein families database. **36**: 281–8.

134. **Uehara T**, **Dinh T**, **Bernhardt TG**. 2009. LytM-domain factors are required for daughter cell separation and rapid ampicillin-induced lysis in Escherichia coli. *J. Bacteriol.* **191**: 5094–107.

135. **Ercoli G**, **Tani C**, **Pezzicoli A**, **Vacca I**, **Martinelli M**, **Pecetta S**, **Petracca R**, **Rappuoli R**, **Pizza M**, **Norais N**, **Soriani M**, **Aricò B**. 2015. LytM proteins play a crucial role in cell separation, outer membrane composition, and pathogenesis in nontypeable Haemophilus influenzae. *MBio* **6**: 1–10.

136. **Ghosh AS**, **Chowdhury C**, **Nelson DE**. 2008. Physiological functions of D-alanine carboxypeptidases in Escherichia coli. *Trends Microbiol.* **16**: 309–17.

137. **Ghuysen JM**, **Frère JM**, **Leyh-Bouille M**, **Nguyen-Distèche M**, **Coyette J**. 1986. Active-site-serine D-alanyl-D-alanine-cleaving-peptidase-catalysed acyl-transfer reactions. Procedures for studying the penicillin-binding proteins of bacterial plasma membranes. *Biochem. J.* **235**: 159–65.

138. **Vega D**, **Ayala JA**. 2006. The DD-carboxypeptidase activity encoded by pbp4B is not essential for the cell growth of Escherichia coli. *Arch. Microbiol.* **185**: 23–7.

139. **Nicholas RA**, **Krings S**, **Tomberg J**, **Nicola G**, **Davies C**. 2003. Crystal structure of wild-type penicillin-binding protein 5 from Escherichia coli: Implications for deacylation of the acyl-enzyme complex. *J. Biol. Chem.* **278**: 52826–33.

140. **Potluri L**, **Karczmarek A**, **Verheul J**, **Piette A**, **Wilkin J-M**, **Werth N**, **Banzhaf M**, **Vollmer W**, **Young KD**, **Nguyen-Distèche M**, **den Blaauwen T**. 2010. Septal and lateral wall localization of PBP5, the major D,D-carboxypeptidase of Escherichia coli, requires substrate recognition and membrane attachment. *Mol. Microbiol.* **77**: 300–23.

141. **Jackson ME**, **Pratt JM**. 1987. An 18 amino acid amphiphilic helix forms the membrane-anchoring domain of the Escherichia coli penicillin-binding protein 5. *Mol. Microbiol.* **1**: 23–8.

142. **Pratt J**, **Jackson M**, **Holland I**. 1986. The C terminus of penicillin-binding protein 5 is essential for localisation to the E. coli inner membrane. *EMBO J.* **5**: 2399–405.

143. **Nelson DE**, **Ghosh AS**, **Paulson AL**, **Young KD**. 2002. Contribution of membrane-binding and enzymatic domains of penicillin binding protein 5 to maintenance of uniform cellular morphology of Escherichia coli. *J. Bacteriol.* **184**: 3630–9.

144. **Santos JM**, **Lobo M**, **Matos APA**, **De Pedro MA**, **Arraiano CM**. 2002. The gene bolA regulates dacA (PBP5), dacC (PBP6) and ampC (AmpC), promoting normal morphology in Escherichia coli. *Mol. Microbiol.* **45**: 1729–40.

145. **Priyadarshini R**, **Popham DL**, **Young KD**. 2006. Daughter cell separation by penicillin-binding proteins and peptidoglycan amidases in Escherichia coli. *J. Bacteriol.* **188**: 5345–55.

146. **Broome-smith JK**, **Ioannidis I**, **Edelman A**, **Spratt BG**. 1988. Nucleotide sequences of the penicillin-binding protein 5 and 6 genes of Escherichia coli. *Nucleic Acids Res.* **16**: 1988–1988.

147. **Baquero M**, **Bouzon M**, **Quintela JC**, **Ayala JA**, **Moreno F**. 1996. dacD , an Escherichia coli gene encoding a novel penicillin-binding protein (PBP6b) with DD-carboxypeptidase activity . dacD , an Escherichia coli Gene Encoding a Novel

Penicillin-Binding Protein (PBP6b) with DD -Carboxypeptidase Activity. *Am. Soc. Microbiol.* **178**: 7106–11.

148. **Gittins J**. 1994. Multiple mechanisms of membrane anchoring of Escherichia coli penicillin-binding proteins. *FEMS Microbiol. Rev.* **13**: 1–12.

149. **Gonzalez-Leiza SM**, **de Pedro MA**, **Ayala JA**. 2011. Amph, a bifunctional DD-endopeptidase and DD-carboxypeptidase of Escherichia coli. *J. Bacteriol.* **193**: 6887–94.

150. **Henderson TA**, **Young KD**, **Denome SA**, **Elf PK**. 1997. AmpC and AmpH, proteins related to the class C B-lactamases, bind penicillin and contribute to the normal morphology of Escherichia coli. *J. Bacteriol.* **179**: 6112–21.

151. **Metz R**, **Henning S**, **Hammes WP**. 1986. LD-Carboxypeptidase activity in Escherichia coil. *Arch. Microbiol.* **144**: 181–6.

152. **Beck BD**, **Park JT**. 1977. Basis for the observed fluctuation of carboxypeptidase II activity during the cell cycle in BUG 6, a temperature sensitive division mutant of Escherichia coli. *J. Bacteriol.* **130**: 1292–302.

153. **Templin MF**, **Ursinus A**, **Höltje JV**. 1999. A defect in cell wall recycling triggers autolysis during the stationary growth phase of Escherichia coli. *EMBO J.* **18**: 4108–17.

154. **Johnson JW**, **Fisher JF**, **Mobashery S**. 2013. Bacterial cell-wall recycling. *Ann. N. Y. Acad. Sci.* **1277**: 54–75.

155. **Das D**, **Hervé M**, **Elsliger MA**, **Kadam RU**, **Grant JC**, **Chiu HJ**, **Knuth MW**, **Klock HE**, **Miller MD**, **Godzik A**, **Lesley SA**, **Deacon AM**, **Mengin-Lecreulx D**, **Wilson IA**. 2013. Structure and function of a novel LD-Carboxypeptidase a involved in peptidoglycan recycling. *J. Bacteriol.* **195**: 5555–66.

156. **Lessard IA WC**. 1999. VanX , a bacterial D -alanyl- D -alanine dipeptidase : Resistance , immunity , or survival function ? **96**: 11028–32.

157. **Korndorfer IP**, **Danzer J**, **Schmelcher M**, **Zimmer M**, **Skerra A**, **Loessner MJ**. 2006. The Crystal Structure of the Bacteriophage PSA Endolysin Reveals a Unique Fold Responsible for Specific Recognition of Listeria Cell Walls. *J. Mol. Biol.* **364**: 678–89.

158. **Tomioka S**, **Nikaido T**, **Miyakawa T**, **Matsuhashi M**. 1983. Mutation of the N-acetylmuramyl-L-alanine amidase gene of Escherichia coli K-12. *J. Bacteriol.* **156**:

463–5.

159. **Rocaboy M**, **Herman R**, **Sauvage E**, **Remaut H**, **Moonens K**, **Terrak M**, **Charlier P**, **Kerff F**. 2013. The crystal structure of the cell division amidase amic reveals the fold of the AMIN domain, a new peptidoglycan binding domain. *Mol. Microbiol.* **90**: 267–77.

160. **Tsui H-CT**, **Zhao G**, **Feng G**, **Leung H-CE**, **Winkler ME**. 1994. The mutL repair gene of Escherichia coli K-12 forms a superoperon with a gene encoding a new cell-wall amidase. *Mol. Microbiol.* **11**: 189–202.

161. **Heidrich C**, **Templin MF**, **Ursinus A**, **Merdanovic M**, **Schwarz H**, **Pedro MA De**, **Holtje J-V**. 2001. Involvement of N -acetylmuramyl- L -alanine amidases in cell separation and antibiotic-induced autolysis of Escherichia coli. *Mol. Microbiol.* **41**: 167–78.

162. **Uehara T**, **Parzych KR**, **Dinh T**, **Bernhardt TG**. 2010. Daughter cell separation is controlled by cytokinetic ring-activated cell wall hydrolysis. *EMBO J.* **29**: 1412–22.

163. **Heidrich C**, **Ursinus A**, **Berger J**, **Schwarz H**, **H??ltje JV**. 2002. Effects of multiple deletions of murein hydrolases on viability, septum cleavage, and sensitivity to large toxic molecules in Escherichia coli. *J. Bacteriol.* **184**: 6093–9.

164. **Jacobs C**, **Joris B**, **Jamin M**, **Klarsov K**, **Beeumen J**, **Mengin-Lecreulx D**, **Heijenoort J**, **Park JT**, **Normark S**, **Frère J-M**. 1995. AmpD, essential for both ?-lactamase regulation and cell wall recycling, is a novel cytosolic N-acetylmuramyl-L-alanine amidase. *Mol. Microbiol.* **15**: 553–9.

165. **Holtje J V**, **Mirelman D**, **Sharon N**, **Schwarz U**. 1975. Novel Type of Murein Transglycosylase in Escherichia-Coli. *J. Bacteriol.* **124**: 1067–76.

166. **Thunnissen AM**, **Rozeboom HJ**, **Kalk KH**, **Dijkstra BW**. 1995. Structure of the 70-kDa soluble lytic transglycosylase complexed with bulgecin A. Implications for the enzymatic mechanism. *Biochemistry* **34**: 12729–37.

167. **Dietz H**, **Pfeifle D**, **Wiedemann B**. 1997. The signal molecule for β-lactamase induction in Enterobacter cloacae is the anhydromuramyl-pentapeptide. *Antimicrob. Agents Chemother.* **41**: 2113–20.

168. **von Rechenberg M, Ursinus A HJ**Affinity chromatography as a means to study multienzyme complexes involved in murein synthesis. *Microb Drug Resist.* **1996**: 155–7.

169. **Cho H**, **Uehara T**, **Bernhardt TG**. 2014. Beta-lactam antibiotics induce a lethal malfunctioning of the bacterial cell wall synthesis machinery. *Cell* **159**: 1310–1.

170. **Yunck R**, **Cho H**, **Bernhardt TG**. 2015. Identification of MltG as a potential terminase for peptidoglycan polymerization in bacteria. *Mol. Microbiol.* **99**: 700–18.

171. **Yang DC**, **Tan K**, **Joachimiak A**, **Bernhardt TG**. 2012. A conformational switch controls cell wall-remodelling enzymes required for bacterial cell division. *Mol. Microbiol.* **85**: 768–81.

172. **Hara H**, **Narita S**, **Karibian D**, **Park JT**, **Yamamoto Y**, **Nishimura Y**. 2002. Identification and characterization of the Escherichia coli envC gene encoding a periplasmic coiled-coil protein with putative peptidase activity. *FEMS Microbiol. Lett.* **212**: 229–36.

173. **Bernhardt TG**, **De Boer PAJ**. 2004. Screening for synthetic lethal mutants in Escherichia coli and identification of EnvC (YibP) as a periplasmic septal ring factor with murein hydrolase activity. *Mol. Microbiol.* **52**: 1255–69.

174. **de LE**, **Graham B**, **Phillips GJ**, **ten Hagen-Jongman CM**, **Oudega B**, **Luirink J**. 1999. Molecular characterization of Escherichia coli FtsE and FtsX. *Mol.Microbiol.* **31**: 983–93.

175. **Uehara T**, **Park JT**. 2007. An anhydro-N-acetylmuramyl-L-alanine amidase with broad specificity tethered to the outer membrane of Escherichia coli. *J. Bacteriol.* **189**: 5634–41.

176. **Aldea M**, **Hernandez-Chico C**, **Delacampa a G**, **Kushner SR**, **Vicente M**. 1988. Identification, Cloning, and Expression of Bola, an Ftsz- Dependent Morphogene of Escherichia-Coli. *J. Bacteriol.* **170**: 5169–76.

177. **Van den Ent F**, **Amos LA**, **Löwe J**, **Ent F Van Den**, **Amos LA**, **Lo J**. 2001. Prokaryotic origin of the actin cytoskeleton. *Nature* **413**: 39–44.

178. **Wachi M**, **Doi M**, **Okada Y**, **Matsuhashi M**. 1989. New mre genes mreC and mreD, responsible for formation of the rod shape of Escherichia coli cells. *J. Bacteriol.* **171**: 6511–6.

179. **Kruse T**, **Bork-Jensen J**, **Gerdes K**. 2005. The morphogenetic MreBCD proteins of Escherichia coli form an essential membrane-bound complex. *Mol. Microbiol.* **55**: 78–89.

180. **Van Den Ent F**, **Leaver M**, **Bendezu F**, **Errington J**, **De Boer P**, **L??we J**. 2006.

Dimeric structure of the cell shape protein MreC and its functional implications. *Mol. Microbiol.* **62**: 1631–42.

181. **Brunko P**. 1992. The procedure for marketing authorization for veterinary medicinal products derived from biotechnology in the European community. *Dev. Biol. Stand.* **79**: 11–5.

182. **Henriques AO**, **Glaser P**, **Piggot PJ**, **Moran Jr. CP**. 1998. Control of cell shape and elongation by the rodA gene in Bacillus subtilis. *Mol Microbiol* **28**: 235–47.

183. **Matsuzawa H**, **Hayakawa K**, **Sato T**, **Imahori K**. 1973. Characterization and genetic analysis of a mutant of Escherichia coli K-12 with rounded morphology. *J. Bacteriol.* **115**: 436–42.

184. **Takasesn I**, **Kunugitas K**, **Matsuzawa H**, **Asoh S**, **Ohta T**, **Spratt BG**, **Matsuhashis M**. 1986. Peptidoglycan Synthetic Activities in Membranes Escherichia coli caused by overproduction of penicillin-binding protein 2 and rodA protein. *Society* **261**: 7024–31.

185. **de Pedro M a**, **Donachie WD**, **Holtje J-V**, **Schwartz H**. 2001. Constitutive Septal Murein Synthesis in Escherichia coli with Impaired Activity of the Morphogenetic Proteins RodA and Penicillin-Binding Protein 2. **183**: 4115–26.

186. **van den Ent F**, **Johnson CM**, **Persons L**, **de Boer P**, **Löwe J**. 2010. Bacterial actin MreB assembles in complex with cell shape protein RodZ. *EMBO J.* **29**: 1081–90.

187. **Alyahya SA**, **Alexander R**, **Costa T**, **Henriques AO**, **Emonet T**, **Jacobs-Wagner C**. 2009. RodZ, a component of the bacterial core morphogenic apparatus. *Proc. Natl. Acad. Sci. U. S. A.* **106**: 1239–44.

188. **Mohammadi T**, **Karczmarek A**, **Crouvoisier M**, **Bouhss A**, **Mengin-Lecreulx D**, **Den Blaauwen T**. 2007. The essential peptidoglycan glycosyltransferase MurG forms a complex with proteins involved in lateral envelope growth as well as with proteins involved in cell division in Escherichia coli. *Mol. Microbiol.* **65**: 1106–21.

189. **Daniel R a**, **Errington J**. 2003. Control of cell morphogenesis in bacteria: two distinct ways to make a rod-shaped cell. *Cell* **113**: 767–76.

190. **Mukherjee A**, **Lutkenhaus J**. 1998. Dynamic assembly of FtsZ regulated by GTP hydrolysis. *EMBO J.* **17**: 462–9.

191. **Löwe J**, **Amos L a**. 1998. Crystal structure of the bacterial cell-division protein FtsZ. *Nature* **391**: 203–6.

192. **Hale C a**, **de Boer P a**. 1997. Direct binding of FtsZ to ZipA, an essential component

of the septal ring structure that mediates cell division in E. coli. *Cell* **88**: 175–85.

193. **Hale C a**, **de Boer P a**. 1999. Recruitment of ZipA to the septal ring of Escherichia coli is dependent on FtsZ and independent of FtsA. *J. Bacteriol.* **181**: 167–76.

194. **Ma X**, **Margolin W**. 1999. Genetic and functional analyses of the conserved C-terminal core domain of Escherichia coli FtsZ. *J. Bacteriol.* **181**: 7531–44.

195. **Pichoff S**, **Lutkenhaus J**. 2005. Tethering the Z ring to the membrane through a conserved membrane targeting sequence in FtsA. *Mol. Microbiol.* **55**: 1722–34.

196. **Szwedziak P**, **Wang Q**, **Freund SM V**, **Löwe J**. 2012. FtsA forms actin-like protofilaments. *EMBO J.* **31**: 2249–60.

197. **Yang DC**, **Peters NT**, **Parzych KR**, **Uehara T**, **Markovski M**, **Bernhardt TG**. 2011. An ATP-binding cassette transporter-like complex governs cell-wall hydrolysis at the bacterial cytokinetic ring. *Proc. Natl. Acad. Sci. U. S. A.* **108**: 1052–60.

198. **Corbin BD**, **Wang Y**, **Beuria TK**, **Margolin W**. 2007. Interaction between cell division proteins FtsE and FtsZ. *J. Bacteriol.* **189**: 3026–35.

199. **Wolf-watz H**, **Normark S**. 1976. Evidence for a Role of N-Acetylmuramyl-L-Alanine Amidase in Septum Separation in Escherichia coli. **128**: 580–6.

200. **Banzhaf M**, **van den Berg van Saparoea B**, **Terrak M**, **Fraipont C**, **Egan A**, **Philippe J**, **Zapun A**, **Breukink E**, **Nguyen-Distèche M**, **den Blaauwen T**, **Vollmer W**. 2012. Cooperativity of peptidoglycan synthases active in bacterial cell elongation. *Mol. Microbiol.* **85**: 179–94.

201. **Chen J**, **Beckwith J**. 2001. FtsQ, FtsL and FtsI require FtsK, but not FtsN, for co-localisation with FtsZ during *Escherichia coli* cell division. *Mol. Microbiol.* **42**: 395–413.

202. **Buddelmeijer N**, **Beckwith J**. 2004. A complex of the Escherichia coli cell division proteins FtsL, FtsB and FtsQ forms independently of its localization to the septal region. *Mol. Microbiol.* **52**: 1315–27.

203. **Mercer KLN**, **Weiss DS**. 2002. The Escherichia coli cell division protein FtsW is required to recruit its cognate transpeptidase, FtsI (PBP3), to the division site. *J. Bacteriol.* **184**: 904–12.

204. **Goehring NW**, **Robichon C**, **Beckwith J**. 2007. Role for the nonessential N terminus of FtsN in divisome assembly. *J. Bacteriol.* **189**: 646–9.

205. **Müller P**, **Ewers C**, **Bertsche U**, **Anstett M**, **Kallis T**, **Breukink E**, **Fraipont C**,

Terrak M, **Nguyen-Distèche M**, **Vollmer W**. 2007. The essential cell division protein FtsN interacts with the murein (peptidoglycan) synthase PBP1B in Escherichia coli. *J. Biol. Chem.* **282**: 36394–402.

206. **Ursinus A**, **Ent F Van Den**, **Brechtel S**, **Pedro D**, **Höltje J**, **Löwe J**, **Pedro M De**. 2004. Murein (Peptidoglycan) Binding Property of the Essential Cell Division Protein FtsN from Escherichia coli. *J. Bacteriol.* **186**: 6728–37.

207. **Peters NT**, **Dinh T**, **Bernhardt TG**. 2011. A Fail-safe mechanism in the septal ring assembly pathway generated by the sequential recruitment of cell separation amidases and their activators. *J. Bacteriol.* **193**: 4973–83.

208. **Lazzaroni JC**, **Vianney A**, **Popot JL**, **Bénédetti H**, **Samatey F**, **Lazdunski C**, **Portalier R**, **Géli V**. 1995. Transmembrane alpha-helix interactions are required for the functional assembly of the Escherichia coli Tol complex. *J. Mol. Biol.* **246**: 1–7.

209. **Fenton AK**, **Gerdes K**. 2013. Direct interaction of FtsZ and MreB is required for septum synthesis and cell division in Escherichia coli. *EMBO J.* **32**: 1953–65.

210. **van der Ploeg R**, **Verheul J**, **Vischer NOE**, **Alexeeva S**, **Hoogendoorn E**, **Postma M**, **Banzhaf M**, **Vollmer W**, **den Blaauwen T**. 2013. Colocalization and interaction between elongasome and divisome during a preparative cell division phase in Escherichia coli. *Mol. Microbiol.* **87**: 1074–87.

211. **Nanninga N**. 1991. Cell division and peptidoglycan assembly in Escherichia coli. *Mol Microbiol.* **5**: 791–5.

212. **Pedro MA De**, **Quintela JC**, **Höltje J V**, **Schwarz H**. 1997. Murein segregation in Escherichia coli. *Microbiology* **179**: 2823–34.

213. **Varma A**, **De Pedro MA**, **Young KD**. 2007. FtsZ directs a second mode of peptidoglycan synthesis in Escherichia coli. *J. Bacteriol.* **189**: 5692–704.

214. **Varma A**, **Young KD**. 2009. In Escherichia coli, MreB and FtsZ direct the synthesis of lateral cell wall via independent pathways that require PBP 2. *J. Bacteriol.* **191**: 3526–33.

215. **Thanedar S**, **Margolin W**. 2004. FtsZ exhibits rapid movement and oscillation waves in helix-like patterns in Escherichia coli. *Curr Biol.* **14**: 1167–73.

216. **Johnson JW**, **Fisher JF**, **Mobashery S**. 2013. Bacterial cell-wall recycling. *Ann. N. Y. Acad. Sci.* **1277**: 54–75.

217. **Park JT**. 1995. Why does Escherichia coli recycle its cell wall peptides? *Mol.*

Microbiol. **17**: 421–6.

218. **Lindberg F**, **Lindquist S**, **Normark S**. 1987. Inactivation of the *ampD* gene causes semiconstitutive overproduction of the inducible *Citrobacter freundii* β-lactamase. *J. Bacteriol.* **169**: 1923–8.

219. **Lindquist S**, **Weston-Hafer K**, **Schmidt H**, **Pul C**, **Korfmann G**, **Erickson J**, **Sanders C**, **Martin HH**, **Normark S**. 1993. AmpG, a signal transducer in chromosomal b-lactamase induction. *Mol. Microbiol.* **9**: 703–15.

220. **Cheng Q**, **Park JT**. 2002. Substrate specificity of the AmpG permease required for recycling of cell wall anhydro-muropeptides. *J. Bacteriol.* **184**: 6434–6.

221. **Cheng Q**, **Li H**, **Merdek K**, **Park JT**. 2000. Molecular Characterization of the B-N-Acetylglucosaminidase of Escherichia coli and Its Role in Cell Wall Recycling. *J. Bacteriol.* **182**: 4836–40.

222. **Uehara T**, **Park JT**. 2002. Role of the murein precursor UDP-N-acetylmuramyl-L-Ala-gamma-D-Glu-meso-diaminopimelic acid-D-Ala-D-Ala in repression of beta-lactamase induction in cell division mutants. *J. Bacteriol.* **184**: 4233–9.

223. **Jacobs Frere, J-M., and Normark, S. C**. 1997. Cytosolic intermediates for cell wall biosynthesis and degradation control inducible b-lactam resistance in Gram-negative bacteria. *Cell* **88**: 823–32.

224. **Kraft AR**, **Prabhu J**, **Ursinus A**, **Höltje J V**. 1999. Interference with murein turnover has no effect on growth but reduces beta-lactamase induction in Escherichia coli. *J. Bacteriol.* **181**: 7192–8.

225. **Goodell EW**, **Higgins CF**. 1987. Uptake of cell wall peptides by Salmonella typhimurium and Escherichia coli. *J. Bacteriol.* **169**: 3861–5.

226. **Park JT**. 1993. Turnover and recycling of the murein sacculus in oligopeptide permease- negative strains of Escherichia coli: Indirect evidence for an alternative permease system and for a monolayered sacculus. *J. Bacteriol.* **175**: 7–11.

227. **Park JT**, **Raychaudhuri D**, **Li H**, **Mengin-lecreulx D**, **Normark S**. 1998. MppA, a Periplasmic Binding Protein Essential for Import of the Bacterial Cell Wall Peptide L-Alanyl-y-D-Glutamyl-meso-Diaminopimelate. *J. Bacteriol.* **180**: 1215–23.

228. **Ohara M**, **Wu HC**, **Sankaran K**, **Rick PD**. 1999. Identification and characterization of a new lipoprotein, NlpI, in Escherichia coli K-12. *J. Bacteriol.* **181**: 4318–25.

229. **Tao J**, **Sang Y**, **Teng Q**, **Ni J**, **Yang Y**, **Tsui SK-W**, **Yao Y-F**. 2015. Heat shock

proteins IbpA and IbpB are required for NlpI-participated cell division in Escherichia coli. *Front. Microbiol.* **6**: 51.

230. **Schwechheimer C**, **Rodriguez DL**, **Kuehn MJ**. 2015. NlpI-mediated modulation of outer membrane vesicle production through peptidoglycan dynamics in Escherichia coli. *Microbiol. Open* **4**: 375–89.

231. **Hantke K**, **Braun V**. 1973. Covalent Binding of Lipid to Protein. Diglyceride and amide-linked fatty acid at the N-terminal end of the murein-lipoprotein of the Escherichia coli outer membrane. **296**: 284–96.

232. **Yonezawa H**, **Osaki T**, **Kurata S**, **Fukuda M**, **Kawakami H**, **Ochiai K**, **Hanawa T**, **Kamiya S**. 2009. Outer membrane vesicles of Helicobacter pylori TK1402 are involved in biofilm formation. *BMC Microbiol.* **9**: 197.

233. **Wilson CGM**, **Kajander T**, **Regan L**. 2005. The crystal structure of NlpI. A prokaryotic tetratricopeptide repeat protein with a globular fold. *FEBS J.* **272**: 166–79.

234. **Cherepanov PP**, **Wackernagel W**. 1995. Gene disruption in Escherichia coli: TcR and KmR cassettes with the option of Flp-catalyzed excision of the antibiotic-resistance determinant. *Gene* **158**: 9–14.

235. **Datsenko K a**, **Wanner BL**. 2000. One-step inactivation of chromosomal genes in Escherichia coli K-12 using PCR products. *Proc. Natl. Acad. Sci. U. S. A.* **97**: 6640–5.

236. **Cummings LJ**, **Snyder MA**, **Brisack K**. 2009. Protein chromatography on hydroxyapatite columns. *Methods Enzymol.* **463**: 387–404.

237. **Vollmer W**, **M von R**, **JV. H**. 1999. Demonstration of Molecular Interactions between the Murein Polymerase PBP1B, the Lytic Transglycosylase MltA, and the Scaffolding Protein MipA of Escherichia coli. *J. Biol. Chem.* **274**: 6726–34.

238. **Jerabek-Willemsen M**, **Wienken CJ**, **Braun D**, **Baaske P**, **Duhr S**. 2011. Molecular interaction studies using microscale thermophoresis. *Assay Drug Dev. Technol.* **9**: 342–53.

239. **Korsak D**, **Liebscher S**, **Vollmer W**. 2005. Susceptibility to antibiotics and ??-lactamase induction in murein hydrolase mutants of Escherichia coli. *Antimicrob. Agents Chemother.* **49**: 1404–9.

240. **O'Callaghan CH**, **Morris A**, **Kirby SM**, **Shingler AH**. 1972. Novel Method for Detection of -Lactamases by Using a Chromogenic Cephalosporin Substrate. *Antimicrob. Agents Chemother.* **1**: 283–8.

241. **Hayashi K**. 1975. A rapid determination of sodium dodecyl sulfate with methylene blue. **506**: 503–6.

242. **Kelley LA**, **Sternberg MJE**. 2009. Protein structure prediction on the Web: A case study using the Phyre server. *Nat. Protoc.* **4**: 363–71.

243. **Sharma UK**, **Dwarakanath P**, **Banerjee N**, **Town C**, **Balganesh TS**. 1995. Expression and characterization of the ponA (ORF I) gene of Haemophilus influenzae: Functional complementation in a heterologous system. *J. Bacteriol.* **177**: 6745–50.

244. **Tomioka S**, **Matsuhashi M**. 1978. Purification of penicillin-insensitive DD-endopeptidase, a new cell wall peptidoglycan-hydrolyzing enzyme in Escherichia coli, and its inhibition by deoxyribonucleic acids. *Biochem Biophys Res Commun.* **84**: 978–84.

245. **Keck W**, **Schwarz U**. 1979. Escherichia coli murein-DD-endopeptidase insensitive to beta-lactam antibiotics. *J. Bacteriol.* **139**: 770–4.

246. **Fallingborg J**. 1999. Intraluminal pH of the human gastrointestinal tract. *Dan. Med. Bull.* **46**: 183–96.

247. **Tseng Y**, **Wang S-W**, **Kim KS**, **Wang Y-H**, **Yao Y**, **Chen C-C**, **Chiang C-W**, **Hsieh P-C**, **Teng C-H**. 2012. NlpI facilitates deposition of C4bp on Escherichia coli by blocking classical complement-mediated killing, which results in high-level bacteremia. *Infect. Immun.* **80**: 3669–78.

248. **Tadokoro A**, **Hayashi H**, **Kishimoto T**, **Makino Y**, **Fujisaki S**, **Nishimura Y**. 2004. Interaction of the Escherichia coli Lipoprotein NlpI with Periplasmic Prc (Tsp) Protease. *J. Biochem.* **135**: 185–91.

249. **Ursinus A**, **Holtje J V.** 1994. Purification and properties of a membrane-bound lytic transglycosylase from Escherichia coli. *J. Bacteriol.* **176**: 338–43.

250. **den Blaauwen T**, **de Pedro M a**, **Nguyen-Distèche M**, **Ayala J a**. 2008. Morphogenesis of rod-shaped sacculi. *FEMS Microbiol. Rev.* **32**: 321–44.

251. **Terrak M**, **Ghosh TK**, **Van Heijenoort J**, **Van Beeumen J**, **Lampilas M**, **Aszodi J**, **Ayala JA**, **Ghuysen JM**, **Nguyen-Distèche M**. 1999. The catalytic, glycosyl transferase and acyl transferase modules of the cell wall peptidoglycan-polymerizing penicillin-binding protein 1b of Escherichia coli. *Mol. Microbiol.* **34**: 350–64.

252. **Casadaban MJ**, **Cohen SN**. 1980. Analysis of gene-control signals by DNA-fusion and cloning in Escherichia coli. *J. Mol. Biol.* **138**: 179–207.

253. **Baba T**, **Ara T**, **Hasegawa M**, **Takai Y**, **Okumura Y**, **Baba M**, **Datsenko KA**, **Tomita M**, **Wanner BL**, **Mori H**. 2006. Construction of Escherichia coli K-12 in-frame, single-gene knockout mutants: the Keio collection. *Mol. Syst. Biol.* **2**: 2006.0008.

254. **Yamamoto N**, **Nakahigashi K**, **Nakamichi T**, **Yoshino M**, **Takai Y**, **Touda Y**, **Furubayashi A**, **Kinjyo S**, **Dose H**, **Hasegawa M**, **Datsenko K a**, **Nakayashiki T**, **Tomita M**, **Wanner BL**, **Mori H**. 2009. Update on the Keio collection of Escherichia coli single-gene deletion mutants. *Mol. Syst. Biol.* **5**: 335.